

DEEP GEOLOGIC

REPOSITORY

FOR OPG's LOW & INTERMEDIATE LEVEL WASTE

Postclosure Safety Assessment (V1): Groundwater Modelling

July 2009

Prepared by:
J Avis, N Calder and R Walsh

NWMO DGR-TR-2009-06

Quintessa **INTERA**


SENE
SENE Consultants Limited

Note:

The Nuclear Waste Management Organization (NWMO) is managing the development of a Deep Geologic Repository for low and intermediate level radioactive waste, at the Bruce nuclear site, on behalf of Ontario Power Generation (OPG).

Nuclear Waste Management Organization

22 St. Clair Avenue East, Toronto, Ontario M4T 2S3 Canada
Toll Free: 1.866.249.6966
www.nwmo.ca

DEEP GEOLOGIC

REPOSITORY

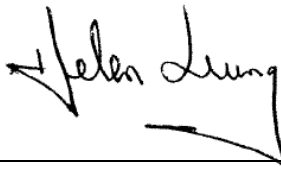
FOR OPG's LOW & INTERMEDIATE LEVEL WASTE

Preliminary

Postclosure Safety Assessment (V1): Groundwater Modelling

NWMO DGR-TR-2009-06

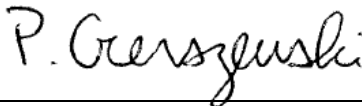
July 2009



Recommended by: _____ July 6, 2009

H. Leung
Section Manager, L&ILW Safety Assessment
NWMO

Date



Accepted by: _____ July 6, 2009

P. Gierszewski
Director, Repository Safety
NWMO

Date

DOCUMENT HISTORY

Title:	Postclosure Safety Assessment (V1): Groundwater Modelling		
Report Number:	NWMO DGR-TR-2009-06		
Revision:	0	Date:	6 th July 2009
Notes:	Initial release		
Prepared by:	J Avis, N Calder and R Walsh		
Reviewed by:	J Pickens (interim version) R Little and A Boardley (final version)		
Approved by:	 R Little Project Manager Quintessa Limited		

EXECUTIVE SUMMARY

Ontario Power Generation (OPG) is proposing to build a Deep Geologic Repository (DGR) for Low and Intermediate Level Waste (L&ILW) near the existing Western Waste Management Facility at the Bruce Site in the Municipality of Kincardine, Ontario. The Nuclear Waste Management Organization, on behalf of OPG, is currently preparing an Environmental Impact Statement (EIS) and Preliminary Safety Report (PSR) for the proposed repository.

The project involves investigation of the site's geological and surface environmental characteristics, conceptual design of the DGR, and safety assessment. The postclosure safety assessment (SA) evaluates the long-term safety of the proposed facility. It will provide the basis for a future version of the safety assessment that will support the EIS and the PSR.

This report describes analysis of the groundwater pathway for the Version 1 SA using detailed numeric groundwater flow and transport models. The models and results presented are based on existing site information and the repository conceptual design. The results provide information to direct and complement the Version 1 SA assessment modelling.

Models, Data and Simulation Cases

Conceptual models for groundwater flow in the geosphere were combined with details on the repository conceptual design and consensus descriptions of expected system evolution to create a high level description of the system to be modelled. Two compatible modelling approaches were developed to simulate performance of a saturated groundwater flow system and calculate the transport of a reference radionuclide (³⁶Chlorine, or Cl-36) from the repository to the surface environment. Cl-36 is an important radionuclide in the DGR waste because it is present in appreciable amounts, has a long half-life, and is soluble and mobile in groundwater.

These models focus on flow and transport within the lower permeability deep bedrock groundwater zone (the Ordovician sediments and below) and intermediate bedrock groundwater zone (the Silurian sediments from the Salina F unit shale down to the top of the Ordovician sediments). An additional model was designed to consider transport of Cl-36 within the shallow bedrock groundwater zone, consisting of primarily Devonian sediments. The shallow zone model also simulates uptake of contaminated groundwater in a water-supply well.

Groundwater flow for the base case model is assumed to be steady-state and possible impacts of repository gas generation such as delayed repository resaturation or repository pressurization are not included. The impact of variations in formation fluid density on groundwater flow is not explicitly assessed, and transient flow processes associated with observed underpressures in the Ordovician sediments are not incorporated in the base case model. Climate change and glaciation related impacts are also not addressed. The total Cl-36 inventory is assumed to be instantly dissolved in the repository water at the time of repository closure.

The groundwater models are implemented in the finite-element/finite-difference groundwater flow and contaminant transport code FRAC3DVS_OPG. The data used in preparing these models are documented in an associated report.

A series of calculation cases based on the Normal Evolution Scenario¹ were simulated. These include a base case and a number of sensitivity cases which address various areas of parameter and conceptual model uncertainty. In particular, the base case geosphere uses the low rock permeabilities derived from preliminary tests and analyses on DGR-1 and DGR-2 boreholes. An alternative model with even lower permeability geosphere is also considered, based on data from boreholes DGR-3 and DGR-4.

Additionally, four Disruptive Scenarios² are simulated which address: human intrusion into the repository by an exploration borehole; shaft seal failure; transport through an enhanced permeability vertical fault reactivated by an extreme earthquake event; and an inappropriately sealed exploration borehole.

Results and Analysis

Modelling of the Normal Evolution Scenario base case and sensitivity cases indicate the following.

- The rock mass and repository system forms a highly effective barrier to radionuclide transport.
- The lower-permeability alternative geosphere model results in a seven order of magnitude reduction in cumulative mass flow to the biosphere, compared to the base case geosphere.
- The shaft excavation disturbed zone (EDZ) provides a preferential pathway for advective transport of radionuclides. For the highest consequence Normal Evolution Scenario sensitivity case, nearly all transport to the biosphere occurs by this route. The EDZ has much less significant effect on the alternative lower-permeability geosphere results, where shaft sealing material properties are the controlling factor.
- If present, horizontal flow in the more permeable Silurian units will intercept vertical transport of contaminants up the shaft and shaft EDZ and prevent a portion of the contaminants from reaching the shallow bedrock groundwater zone.

Disruptive Scenario results can be summarized as follows.

- An inappropriately sealed exploration borehole would serve as a preferential conduit; however, it would have to be located very close to the repository footprint to have any impact on mass flow.
- An improperly abandoned exploration borehole that penetrates the repository would serve as a significant pathway for release of radionuclides. A significant fraction of the soluble inventory of the repository could reach the shallow bedrock groundwater zone within a period of 100 000 years after intrusion.

¹ The Normal Evolution Scenario describes the expected long-term evolution of the repository and site following closure.

² Disruptive Scenarios consider events that could lead to possible penetration of barriers and abnormal degradation and loss of containment. They are unlikely or “what if” cases that test the robustness of the DGR system.

- Severe shaft seal failure would result in similar consequences as an improperly abandoned exploration borehole, with most of the soluble repository inventory reaching the shallow bedrock groundwater zone within 30 000 years.
- Activation of a hypothetical vertical fault extending from the Pre-Cambrian basement to the shallow bedrock groundwater zone outside the site characterization area (c. 500 m) by a very large earthquake would not have a significant effect (about factor of ten) on radionuclide transport relative to the base case for the Normal Evolution Scenario.

Uncertainties

The conceptual model analysed assumes instant resaturation and ignores gas generation impacts. This is expected to be generally conservative. The implications of gas generation on repository evolution, and on radionuclide transport are considered in separate reports.

There are uncertainties with parameters that potentially have a large impact on results. Important uncertainties include the geosphere hydraulic conductivities (base case or lower-permeability case); parameterization of the shaft EDZ geometry and properties; and the characterization of hydraulic gradients in the more permeable Silurian units. The potential effects of these are illustrated with sensitivity cases.

Additional uncertainties in geosphere conceptual models will also affect results. Specifically, the time dependence and causal mechanisms for measured Cambrian overpressures and Ordovician underpressures are not completely understood. Furthermore, incorporation of glacial loadings in coupled hydromechanical models of the repository and geosphere system may provide additional insight into long-term system performance. However, the base case assumes the Cambrian pressure is retained indefinitely, such that there is a net upward hydraulic gradient through the repository system. The base case also assumes a steady-state flow system and ignores the effect of Ordovician underpressures, which would generally tend to direct hydraulic gradients towards the repository for extremely long time periods. These assumptions are expected to be generally conservative.

CONTENTS

	<u>Page</u>
EXECUTIVE SUMMARY	v
1. INTRODUCTION	1
1.1 PURPOSE AND SCOPE	2
1.2 REPORT OUTLINE	3
2. CONCEPTUAL MODELS	4
2.1 GEOSPHERE SYSTEM OVERVIEW.....	4
2.2 REPOSITORY LOCATION AND CHARACTERISTICS	7
2.3 NORMAL EVOLUTION AND DISRUPTIVE SCENARIOS	9
2.4 MODELLING APPROACH	11
2.4.1 3D Simplified (3DS) Model.....	11
2.4.2 2D Radial (2DR) Model.....	12
2.4.3 3D Simplified Upper (3DSU) Model.....	13
3. CALCULATION CASES	14
3.1 NORMAL EVOLUTION SCENARIO	15
3.2 DISRUPTIVE SCENARIOS	16
4. MODEL IMPLEMENTATION AND DATA	18
4.1 SOFTWARE CODES AND QUALITY ASSURANCE	18
4.2 DATA.....	18
4.2.1 Formation Properties	18
4.2.2 Shaft, Repository and Sealing Material Properties	24
4.2.3 Source Term and Radionuclide Properties.....	26
4.3 MODEL IMPLEMENTATION	27
4.3.1 Model Structure	27
4.3.2 Model Discretization and Property Assignment.....	32
4.3.3 Boundary and Initial Conditions.....	47
5. RESULTS FOR THE NORMAL EVOLUTION SCENARIO	49
5.1 Results Presentation	49
5.1.1 Flow Results	49
5.1.2 Transport Results	49
5.2 Reference Case (NE-RS1-F3 & NE-UG-RS1-F3)	50
5.2.1 NE-RS1-F3	51
5.2.2 NE-UG-RS1-F3.....	61
5.2.3 NE-RS1-3DSU	71
5.3 NE-NHG No Horizontal Flow in Silurian Case (NE-NHG-F3 & NE-NHG-F2)	71
5.3.1 NE-NHG-F3 Results	71
5.3.2 NE-NHG-F2 Results	76
5.3.3 2DR and 3DS Results Comparison.....	81
5.3.4 3DSU Results	83

5.4	NE-UG-NHG-F2 Updated Geosphere, No horizontal flow in Silurian, Transient Flow from environmental heads	88
5.4.1	Flow Results	88
5.4.2	Transport Results	91
5.5	NE-EDZ: Higher Conductivity in Shaft EDZ (NE-EDZ-F2 and NE-UG-EDZ-F2)	92
5.5.1	NE-EDZ-F2 Results	92
5.5.2	NE-UG-EDZ-F2 Results.....	97
5.6	NE-UG-RD1: Concrete seals through access and ring tunnel	101
5.6.1	Flow Results	101
5.6.2	Transport Results	102
6.	RESULTS FOR THE DISRUPTIVE SCENARIOS	104
6.1	HI-GR-F3: Exploration borehole intersecting the repository	104
6.1.1	Flow Results	104
6.1.2	Transport Results	107
6.2	SF-ES1: Failure of entire seal system (SE-ES1-F2 & SF-UG-ES1-F2)	110
6.2.1	SF-ES1-F2 Results	110
6.2.2	SF-UG-ES1-F2 Results	115
6.3	SF-US-F2: Failure of upper seal system	120
6.3.1	Flow Results	120
6.3.2	Transport Results	123
6.4	EE-BC-F3: Extreme Earthquake	125
6.4.1	Flow Results	125
6.4.2	Transport Results	127
6.5	OB-BC-F3: Open Borehole	130
6.5.1	Flow Results	130
6.5.2	Transport Results	133
7.	RESULTS ASSESSMENT AND COMPARISON	137
7.1	MODELLING APPROACH COMPARISON	137
7.2	CALCULATION CASE COMPARISONS	138
8.	UNCERTAINTIES AND ISSUES FOR FURTHER WORK	145
8.1	GEOSPHERE CONCEPTUAL MODEL UNCERTAINTY	145
8.2	MODELLING ASSUMPTIONS AND APPROACH	146
8.3	PARAMETER UNCERTAINTY	146
8.4	REPOSITORY DESIGN OPTIMIZATION	147
9.	SUMMARY AND CONCLUSIONS	148
	REFERENCES	150
	APPENDIX A: FRAC3DVS	153

LIST OF TABLES

	<u>Page</u>
Table 3-1: Groundwater modelling cases for the Normal Evolution Scenario	15
Table 3-2: Groundwater modelling cases for the Disruptive Scenarios	16
Table 4-1: Geological Units and Model IDs	19
Table 4-2: Relevant hydrogeological and transport properties for model units	21
Table 4-3: Hydraulic conductivities of Silurian and Ordovician units for UG updated (lower permeability) geosphere calculation cases	22
Table 4-4: Hydrogeological and transport properties for shaft, repository and EDZ materials ...	25
Table 4-5: Cross-sectional areas of combined shaft (Walke et al. 2009b).	28
Table 7-1: Summary of cumulative Cl-36 mass and peak Cl-36 mass flow for all calculation cases.....	142

LIST OF FIGURES

	<u>Page</u>
Figure 1.1: The DGR Concept at the Bruce Site	1
Figure 1.2: Document Structure for the Version 1 Postclosure Safety Assessment	2
Figure 2.1: Geological Stratigraphy at the DGR Site (Gartner Lee 2009b).....	5
Figure 2.2: Environmental head profile from DGR Site Investigation Boreholes based on May 2008 monitoring data.	6
Figure 2.3: Repository layout in UTM coordinate system.	7
Figure 2.4: Lithology and shaft sealing system (Walke et al. 2009b)	8
Figure 2.5: Conceptual illustration of the 3DS model of repository and shafts.	12
Figure 2.6: Conceptual illustration of the 2DR model of the repository and shaft.	13
Figure 4.1: Geologic layering in the 2DR and 3DS groundwater models.....	20
Figure 4.2: Vertical hydraulic conductivity for the base and updated geosphere (UG) calculation cases.....	23
Figure 4.3: Vertical cross-section of 2DR model.	28
Figure 4.4: Plan section of shaft above monolith in the 90° 2DR model.	29
Figure 4.5: Plan section through monolith and repository at the repository horizon in the 2DR model.	30
Figure 4.6: Plan outline of 3DS repository panels	31
Figure 4.7: Plan outline of 3DSU grid.....	32
Figure 4.8: Plan outline of inner portion of 2DR discretization.....	33
Figure 4.9: Detail of 2DR model property assignments.....	34
Figure 4.10: Detail of model repository (2DR model), access tunnel zone, monolith, shaft, and EDZ.....	35
Figure 4.11: Detail of asphalt waterstop system at Salina A0/Salina A1 (2DR model).	36
Figure 4.12: Detail of model repository (2DR model), access tunnel zone, monolith, shaft, EDZ, and lowest concrete bulkhead for the NE-EDZ case.	37
Figure 4.13: 3DS model vertical layout of repository, access tunnel zone, monolith, shaft sealing system, and EDZ properties.	38
Figure 4.14: 3DS model 3D layout of repository, access tunnel zone, monolith, shaft sealing system, and EDZ (transparent) properties.....	39
Figure 4.15: 3DS model plan section view of discretization of entire model domain. Darkest area has the finest discretization	40
Figure 4.16: 3DS model plan section view – repository detail.	40

Figure 4.17: 3DS model plan section view – ring tunnel detail.	41
Figure 4.18: 3DS model plan section view – shaft, EDZ and tunnel detail.....	41
Figure 4.19: 3DS NE-RD1 model plan section view	42
Figure 4.20: 3DS HI-GR model plan section view – borehole detail.	43
Figure 4.21: 3DS OB-BC model plan section view.	44
Figure 4.22: 3DS EE model plan section view – fault detail.	45
Figure 4.23: Plan and section of 3DSU mesh.	46
Figure 4.24: 3D view of reference case 3DSU model with boundary conditions.....	48
Figure 5.1: NE-RS1-F3 model head contours on a vertical slice through Grid Y=0.	52
Figure 5.2: NE-RS1-F3 model head contours in the vicinity of the repository on a vertical slice through Grid Y=0.....	52
Figure 5.3: NE-RS1-F3 model head contours in the vicinity of the repository on a horizontal slice through elevation -489 mASL.	53
Figure 5.4: NE-RS1-F3 model head contours in the vicinity of the monolith on a vertical slice through Grid Y=0.....	54
Figure 5.5: NE-RS1-F3 model head contours in the vicinity of the Silurian waterstop seals on a vertical slice through Grid Y=0.	54
Figure 5.6: NE-RS1-F3 advective velocity magnitude and vectors on a vertical slice through Grid Y=0.....	55
Figure 5.7: NE-RS1-F3 advective velocity magnitude and vectors in the repository and lower shaft on a vertical slice through Grid Y=0.....	55
Figure 5.8: NE-RS1-F3 advective velocity magnitude and vectors in the vicinity of the monolith on a vertical slice through Grid Y=0.....	56
Figure 5.9: NE-RS1-F3 advective velocity magnitude and vectors in the vicinity of the Silurian waterstop seals on a vertical slice through Grid Y=0.	56
Figure 5.10: NE-RS1-F3 advective velocity magnitude and vectors in the vicinity of the repository on a horizontal slice through elevation -490 mASL.	57
Figure 5.11: NE-RS1 CI-36 concentration at 50 000, 100 000, 500 000, and 1 000 000 years.	58
Figure 5.12: NE-RS1 CI-36 concentration isovolumes at 1 000 000 years.	59
Figure 5.13: NE-RS1 CI-36 concentration in plan section through Guelph and repository at 1 000 000 years.	59
Figure 5.14: NE-RS1-F3 total mass flow and cumulative mass transport.....	60
Figure 5.15: NE-RS1-F3 mass flow components.	60
Figure 5.16: NE-UG-RS1-F3 model head contours on a vertical slice through Grid Y=0.....	62
Figure 5.17: NE-UG-RS1-F3 model head contours in the vicinity of the repository on a vertical slice through Grid Y=0.....	62
Figure 5.18: NE-UG-RS1-F3 model head contours in the vicinity of the repository on a horizontal slice through elevation -489 mASL.....	63
Figure 5.19: NE-UG-RS1-F3 model head contours in the vicinity of the monolith on a vertical slice through Grid Y=0.....	64
Figure 5.20: NE-UG-RS1-F3 model head contours and advective velocity vectors in the vicinity of the Silurian waterstop seals on a vertical slice through Grid Y=0.	64
Figure 5.21: NE-UG-RS1-F3 advective velocity magnitude and vectors on a vertical slice through Grid Y=0.....	65
Figure 5.22: NE-UG-RS1-F3 advective velocity magnitude and vectors in the repository and lower shaft on a vertical slice through Grid Y=0.	65
Figure 5.23: NE-UG-RS1-F3 advective velocity magnitude and vectors in the vicinity of the monolith on a vertical slice through Grid Y=0.	66
Figure 5.24: NE-UG-RS1-F3 advective velocity magnitude and vectors in the vicinity of the Silurian waterstop seals on a vertical slice through Grid Y=0.	66

Figure 5.25: NE-UG-RS1-F3 advective velocity magnitude and vectors in the vicinity of the repository on a horizontal slice through elevation -490 mASL.67

Figure 5.26: NE-UG-RS1 CI-36 concentration at 50 000, 100 000, 500 000, and 1 000 000 years.68

Figure 5.27: NE-UG-RS1 CI-36 concentration isovolumes at 1 000 000 years.....69

Figure 5.28: NE-UG-RS1 CI-36 concentration in plan section through Guelph and repository at 1 000 000 years.69

Figure 5.29: NE-UG-RS1-F3 total mass flow and cumulative mass transport. All Salina F mass flows are below Y axis limits.....70

Figure 5.30: NE-UG-RS1-F3 mass flow components. All Salina F mass flows are below Y axis limits.....70

Figure 5.31: NE-NHG-F3 head contours on a vertical slice through Grid Y=0.....71

Figure 5.32: NE-NHG-F3 advective velocity magnitude and vectors in the shaft and seals in the vicinity of the S8 waterstop above the Guelph on a vertical slice through Grid Y=0.....72

Figure 5.33: NE-NHG-F3 CI-36 concentration at 50 000, 100 000, 500 000, and 1 000 000 years.73

Figure 5.34: NE-NHG-F3 CI-36 concentration isovolumes at 1 000 000 years.....74

Figure 5.35: NE-NHG-F3 total mass flow and cumulative mass transport.....75

Figure 5.36: NE-NHG-F3 mass flow components.75

Figure 5.37: NE-NHG-F2 head contours for the entire model domain.....76

Figure 5.38: NE-NHG-F2 advective velocity magnitude and vectors for the entire model domain.77

Figure 5.39: NE-NHG-F2 advective velocity magnitude and vectors in repository and lower shaft.77

Figure 5.40: NE-NHG-F2 advective velocity magnitude and vectors in vicinity of Silurian seals.....78

Figure 5.41: NE-NHG-F2 CI-36 concentration at 50 000, 100 000, 500 000, and 1 000 000 years.79

Figure 5.42: NE-NHG-F2 total mass flow and cumulative mass transport.....80

Figure 5.43: NE-NHG-F2 mass flow components.80

Figure 5.44: Comparison of NE-NHG-F3 and NE-NHG-F2 vertical fluid flux through shaft and EDZ.....81

Figure 5.45: Comparison of CI-36 mass flow results for the 3DS and 2DR NE-NHG models in the Shaft/EDZ system and in the rock mass.....82

Figure 5.46: NE-NHG-3DSU head contours for the entire model domain.83

Figure 5.47: NE-NHG-3DSU advective velocity magnitude and vectors for the entire model domain.84

Figure 5.48: NE-NHG-3DSU CI-36 concentration in horizontal plane through water-supply well at 1 000 000 years.85

Figure 5.49: NE-NHG-3DSU CI-36 concentration in horizontal plane through top of Salina G Formation at 1 000 000 years.....86

Figure 5.50: NE-NHG-3DSU CI-36 concentration on vertical plane through water-supply well and source at 1 000 000 years.86

Figure 5.51: Mass transport to Lake Huron and the pumping well for the 3DSU NE-NHG model.87

Figure 5.52: NE-UG-NHG-F2 transient hydraulic head versus time at R = 1000 m.88

Figure 5.53: NE-UG-NHG-F2 hydraulic head profiles at R = 1000 m.89

Figure 5.54: NE-UG-NHG-F2 head contours on a vertical slice at 1 000 000 years.90

Figure 5.55: NE-UG-NHG-F2 advective velocity magnitude and vectors in the vicinity of the repository at 1 000 000 years.90

Figure 5.56: NE-UG-NHG-F2 Cl-36 concentration at 50 000, 100 000, 500 000, and 1 000 000 years.	91
Figure 5.57: Mass transport results for the NE-UG-NHG-F2 model. Salina B and Salina F results are below Y axis limits.	92
Figure 5.58: NE-EDZ-F2 advective velocity magnitude and vectors in repository and lower shaft.	93
Figure 5.59: NE-EDZ-F2 advective velocity magnitude and vectors in vicinity of repository.	93
Figure 5.60: NE-EDZ-F2 advective velocity magnitude and vectors in vicinity of Silurian seals.	94
Figure 5.61: NE-EDZ-F2 Cl-36 concentration at 50 000, 100 000, 500 000, and 1 000 000 years.	95
Figure 5.62: NE-EDZ-F2 mass transport results. Note that the vertical axis limits differ from other mass flow figures.	96
Figure 5.63: NE-EDZ-F2 mass flow components.	96
Figure 5.64: NE-UG-EDZ-F2 advective velocity magnitude and vectors in repository and lower shaft.	97
Figure 5.65: NE-UG-EDZ-F2 advective velocity magnitude and vectors in vicinity of Silurian seals.	98
Figure 5.66: NE-UG-EDZ-F2 Cl-36 concentration at 50 000, 100 000, 500 000, and 1 000 000 years.	99
Figure 5.67: NE-UG-EDZ-F2 mass transport results. Note that the vertical axis limits differ from other mass flow figures.	100
Figure 5.68: NE-UG-EDZ-F2 mass flow components.	100
Figure 5.69: NE-UG-RD1-F3 advective velocity magnitude and vectors in the repository and lower shaft on a vertical slice through Grid Y=0.	101
Figure 5.70: NE-UG-RD1-F3 Cl-36 concentration at 50 000, 100 000, 500 000, and 1 000 000 years.	102
Figure 5.71: NE-UG-RD1-F3 total mass flow and cumulative mass transport.	103
Figure 5.72: NE-UG-RD1-F3 mass flow components.	103
Figure 6.1: HI-GR-F3 head contours on a vertical slice through Grid Y= 10.	104
Figure 6.2: HI-GR-F3 head contours in the vicinity of the repository on a vertical slice through Grid Y= 10.	105
Figure 6.3: HI-GR-F3 advective velocity magnitude and vectors on a vertical slice through Grid Y=10.	105
Figure 6.4: HI-GR-F3 advective velocity magnitude and vectors in the vicinity of the repository on a vertical slice through Grid Y=10.	106
Figure 6.5: HI-GR-F3 cumulative fluid flow gain and loss in the abandoned exploration borehole.	107
Figure 6.6: HI-GR-F3 Cl-36 concentration at 1 000, 10 000, 50 000, and 100 000 years.	108
Figure 6.7: HI-GR-F3 Cl-36 concentration isovolumes at 100 000 years.	108
Figure 6.8: HI-GR-F3 Cl-36 mass transport in the exploration borehole.	109
Figure 6.9: SF-ES1-F2 head contours for the entire model domain.	111
Figure 6.10: SF-ES1-F2 advective velocity magnitude and vectors for the entire model domain.	111
Figure 6.11: SF-ES1-F2 advective velocity magnitude and vectors in repository and lower shaft.	112
Figure 6.12: SF-ES1-F2 advective velocity magnitude and vectors in the vicinity of the Silurian seals.	112
Figure 6.13: SF-ES1 Cl-36 concentration at 1 000, 10 000, 50 000, and 100 000 years.	113
Figure 6.14: SF-ES1 Cl-36 total mass flow and cumulative mass transport.	114
Figure 6.15: SF-ES1-F2 mass flow components.	114

Figure 6.16: SF-UG-ES1-F2 head contours for the entire model domain.....	115
Figure 6.17: SF-UG-ES1-F2 advective velocity magnitude and vectors for the entire model domain.....	116
Figure 6.18: SF-UG-ES1-F2 advective velocity magnitude and vectors in repository and lower shaft.....	116
Figure 6.19: SF-UG-ES1-F2 advective velocity magnitude and vectors in the vicinity of the Silurian seals.....	117
Figure 6.20: SF-UG-ES1 CI-36 concentration at 50 000, 100 000, 500 000, and 1 000 000 years.....	118
Figure 6.21: SF-UG-ES1 CI-36 total mass flow and cumulative mass transport.....	119
Figure 6.22: SF-UG-ES1-F2 mass flow components.....	119
Figure 6.23: SF-US-F2 head contours for the entire model domain.....	120
Figure 6.24: SF-US-F2 advective velocity magnitude and vectors for the entire model domain.....	121
Figure 6.25: SF-US-F2 advective velocity magnitude and vectors in repository and lower shaft.....	121
Figure 6.26: SF-US-F2 advective velocity magnitude and vectors in the vicinity of the Silurian seals.....	122
Figure 6.27: SF-US-F2 CI-36 concentration at 50 000, 100 000, 500 000, and 1 000 000 years.....	123
Figure 6.28: SF-US-F2 CI-36 total mass flow and cumulative mass transport.....	124
Figure 6.29: SF-US-F2 mass flow components.....	124
Figure 6.30: EE-BC-F3 head contours on a vertical slice through Grid Y=0.....	125
Figure 6.31: EE-BC-F3 advective velocity magnitude and vectors on a vertical slice through Grid Y=0.....	126
Figure 6.32: EE-BC-F3 CI-36 concentration at 50 000, 100 000, 500 000, and 1 000 000 years.....	127
Figure 6.33: EE-BC-F3 CI-36 concentration isovolumes at 1 000 000 years.....	128
Figure 6.34: EE-BC-F3 CI-36 mass transport results.....	129
Figure 6.35: EE-BC-F3 mass flow components.....	129
Figure 6.36: OB-BC-F3 head contours on a vertical slice through Grid Y=0.....	130
Figure 6.37: OB-BC-F3 head contours on a plan section through the repository.....	131
Figure 6.38: OB-BC-F3 advective velocity magnitude and vectors on a plan section through the repository.....	132
Figure 6.39: OB-BC-F3 CI-36 concentration at 50 000, 100 000, 500 000, and 1 000 000 years.....	133
Figure 6.40: OB-BC-F3 CI-36 concentration at Guelph and repository elevations at 1 000 000 years.....	134
Figure 6.41: OB-BC-F3 CI-36 concentration isovolumes at 1 000 000 years.....	134
Figure 6.42: OB-BC-F3 CI-36 mass transport results.....	135
Figure 6.43: OB-BC-F3 mass flow components.....	135
Figure 7.1: CI-36 vertical mass transport across the Salina F MF plane and horizontal mass transport through permeable Silurian units (3DS only) for all Normal Evolution Scenario base case geosphere cases.....	138
Figure 7.2: CI-36 vertical mass transport across the Salina F MF plane and horizontal mass transport through permeable Silurian units (3DS only) for all Normal Evolution Scenario Updated Geosphere (NE-UG-) cases.....	139
Figure 7.3: CI-36 vertical mass transport across the Salina F MF plane and horizontal mass transport through permeable Silurian units (3DS only) for all Disruptive Scenario cases.....	140

Figure 7.4: Peak Cl-36 mass flow across the Salina F MF plane for all modelling cases. All UG case results except NE-UG-EDZ are below Y axis limit.....	143
Figure 7.5: Cumulative Cl-36 mass flow across the Salina F MF plane for all modelling cases. All UG case results except NE-UG-EDZ are below Y axis limit.....	143
Figure 7.6: Peak horizontal Cl-36 mass flow across the Silurian formations for all 3DS modelling cases. All UG case results are below Y axis limit.	144
Figure 7.7: Cumulative horizontal Cl-36 mass flow across the Silurian formations plane for all 3DS modelling cases. All UG case results except NE-UG-EDZ are below Y axis limit. ..	144

1. INTRODUCTION

Ontario Power Generation (OPG) is proposing to build a Deep Geologic Repository (DGR) for Low and Intermediate Level Waste (L&ILW) near the existing Western Waste Management Facility (WWMF) at the Bruce site in the Municipality of Kincardine, Ontario (Figure 1.1). The Nuclear Waste Management Organization (NWMO), on behalf of OPG, is currently preparing an Environmental Impact Statement (EIS) and Preliminary Safety Report (PSR) for the proposed repository.

The project involves investigation of the site's geological and surface environmental characteristics, conceptual design of the DGR, and safety assessment. The Version 1 postclosure safety assessment (SA) evaluates the long-term safety of the proposed facility and will provide the basis for a future version of the safety assessment that will support the final EIS and PSR.

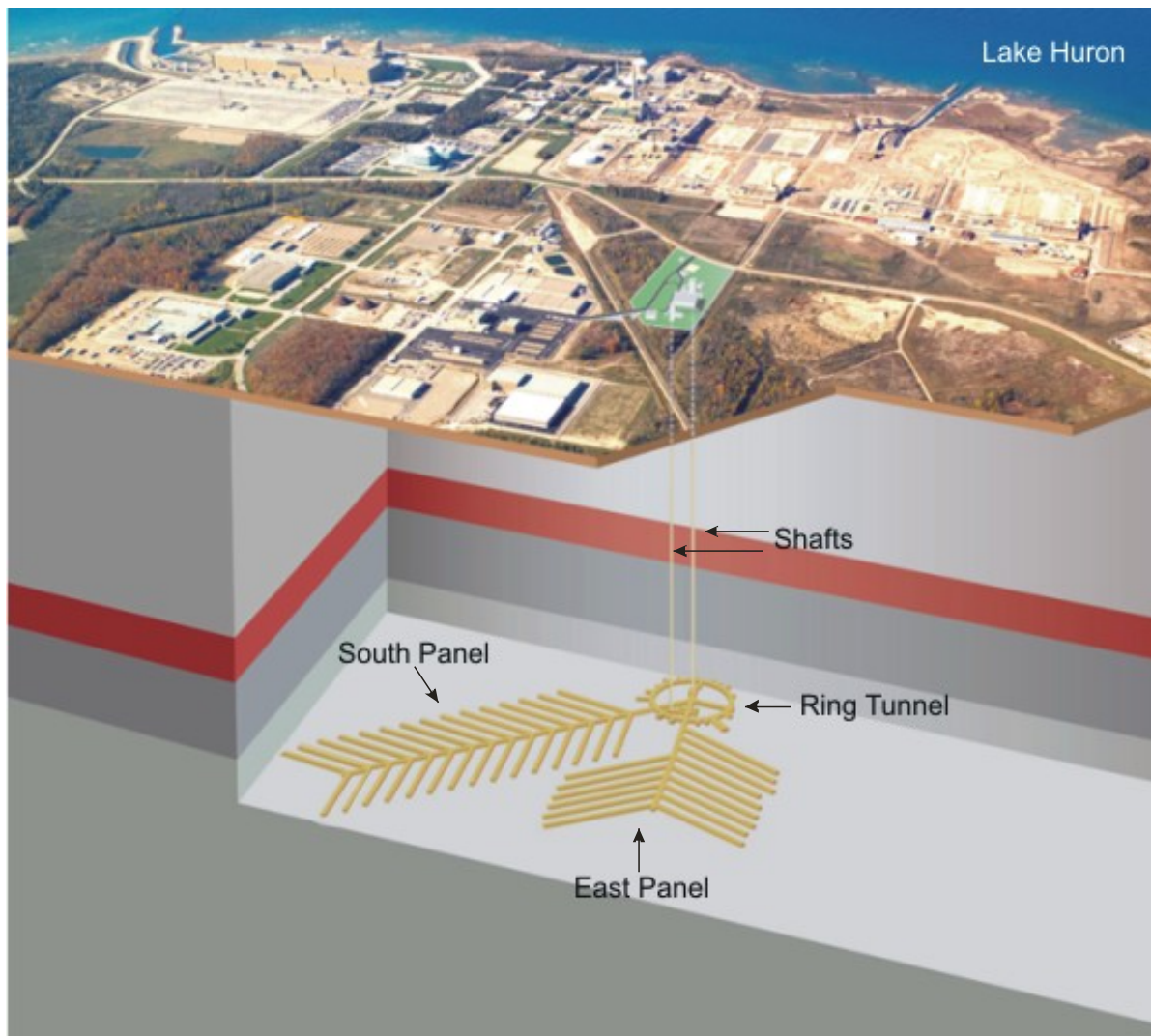


Figure 1.1: The DGR Concept at the Bruce Site

The Version 1 work builds upon a scoping assessment conducted by Quintessa in 2002 and 2003 (Penfold et al. 2003) and has been refined to take account of the revised waste inventory and repository design, and the greater understanding of the site that is being developed as the project proceeds.

This report (Groundwater Modelling) is one of a suite of documents that present the Version 1 SA studies (Figure 1.2), which also includes the Postclosure Safety Assessment report (Quintessa et al. 2009), the Normal Evolution Scenario Analysis report (Walke et al. 2009a), the Human Intrusion and Other Disruptive Scenarios Analysis report (Penfold and Little 2009), the System and Its Evolution report (Little et al. 2009), the Features, Events and Processes report (Garisto et al. 2009), the Data report (Walke et al. 2009b), and the Gas Modelling report (Calder et al. 2009).

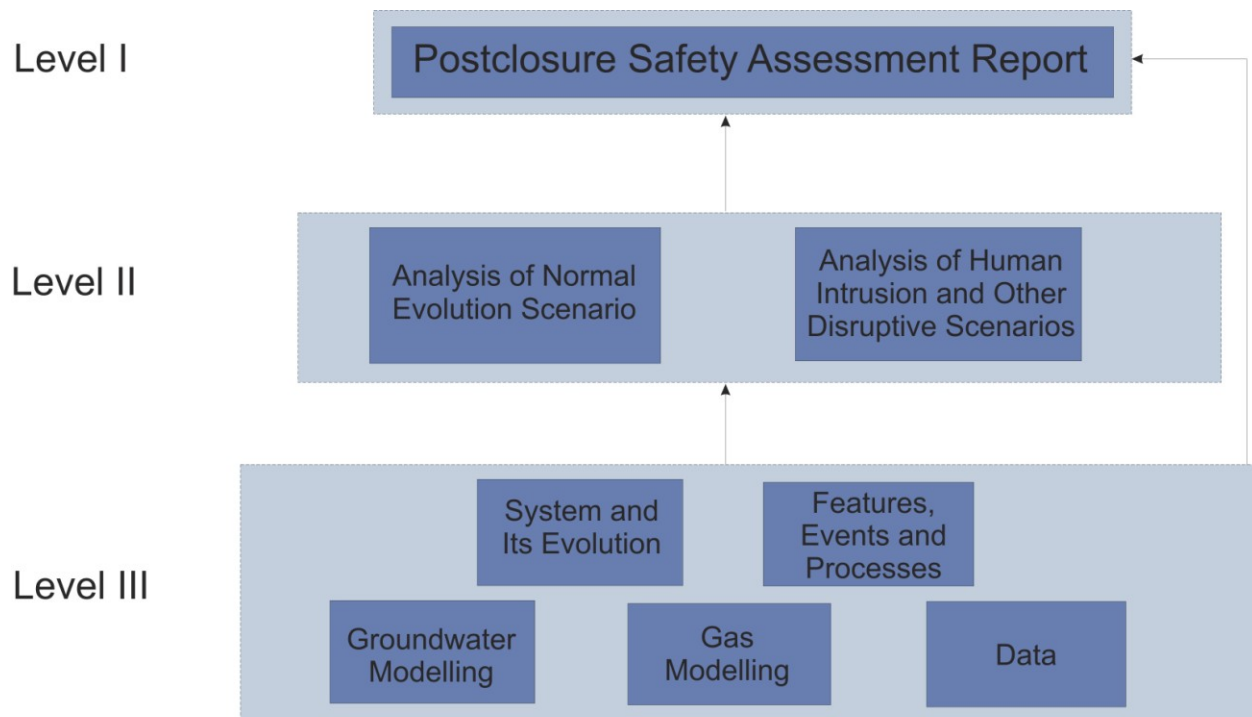


Figure 1.2: Document Structure for the Version 1 Postclosure Safety Assessment

1.1 PURPOSE AND SCOPE

This report describes numeric modelling work undertaken to estimate the flow of groundwater and the transport of radionuclides from the proposed repository to the accessible biosphere. The modelling was performed using groundwater flow and transport models that allow for detailed representation of repository and geosphere properties.

The detailed groundwater flow and transport models are expected to capture the most relevant aspects of overall system performance for a limited range of parameters (a normal or base case) and for a single radionuclide. Results from the detailed modelling provide input to the assessment modelling (Walke et al. 2009b; Penfold and Little 2009) and are also used to verify

the mathematically less complex models of groundwater flow and transport used in the assessment modelling. The assessment modelling describes the performance of the total system (repository, geosphere and biosphere) for all radionuclides, and calculates metrics that can be compared to regulatory standards, such as peak dose.

The detailed models were simulated for a base case set of parameters and initial conditions that approximate the Normal Evolution Scenario documented in Little et al. (2009) with the exception that glaciation cycle related impacts are not assessed. A number of calculation cases addressing sensitivity to Normal Evolution Scenario assumptions were also simulated, such as alternative geosphere boundary and initial conditions, engineered barrier system performance, and geosphere parameters. Additional calculation cases were defined to simulate possible disruptive scenarios. Results of calculation cases are compared to the base case to provide a quantitative assessment of scenario significance.

All simulations were performed for a single radionuclide, ³⁶Chlorine (Cl-36). Cl-36 has been identified as a primary contaminant of concern, being present in the waste inventory in sufficient quantity, having a long half life and being mobile.

Detailed modelling described in this report assumes fully saturated conditions and does not address the impact of gas generation from waste degradation and consequent two-phase (gas and water) flow through the repository system and geosphere. Detailed modelling of gas transport is described in Calder et al. (2009).

1.2 REPORT OUTLINE

The report is organised as follows:

- Section 2 describes the conceptual models of groundwater flow and transport and the approach used to create numeric models representing the conceptual models;
- Section 3 describes the defined calculation cases;
- Section 4 provides an overview of the data used in the numeric modelling and the implementation of the detailed numeric models;
- Section 5 presents results of modelling for the Normal Evolution Scenario calculation cases;
- Section 6 presents results for the Disruptive Scenarios calculation cases;
- Section 7 provides an overall comparison and assessment of the Normal Evolution and Disruptive Scenarios calculation cases;
- Section 8 describes uncertainties in modelling the scenarios and in the results, and enumerates issues for possible further consideration in subsequent version of the SA; and
- Section 9 provides overall conclusions on the detailed groundwater modelling results.

The report has been written for a technical audience that is familiar with the scope and objectives of the DGR project, the Bruce site, and the process of assessing the long-term safety of radioactive waste disposal.

2. CONCEPTUAL MODELS

This section of the report describes the overall conceptual model of the groundwater system at the Bruce site; the basic characteristics of the proposed repository and its relationship to the geosphere; and the modelling approaches selected to simulate the integrated repository and geosphere system.

2.1 GEOSPHERE SYSTEM OVERVIEW

As described in Little et al. (2009), groundwater flow at the Bruce site can be divided into four basic zones, delineated by stratigraphy. The stratigraphic column at the Bruce site is based on results from boreholes DGR-1 and DGR-2 described in Gartner Lee (2008a) and presented in Figure 2.1. The groundwater zones are:

1. Surficial deposits (overburden) groundwater zone – Local flow of fresh water providing precipitation driven recharge to the underlying shallow bedrock groundwater zone. The surficial zone is approximately 20 metres thick.
2. Shallow bedrock groundwater zone – The relatively high permeability sequence consisting of Devonian and Upper Silurian (to Salina G) sediments to an approximate depth of 185 metres below ground surface (mBGS), or an elevation of 0 metres above sea level (mASL). Groundwater in this zone is fresh to brackish and flow is primarily horizontal, driven by topographic features with discharge to Lake Huron. Hydraulic gradients in this zone are sufficiently high to create advective dominated flow.
3. Intermediate bedrock groundwater zone – The Silurian sediments from the Salina F down to the Manitoulin. Some zones of medium permeability exist in this sequence (Salina A2 evaporite, Guelph/Salina A0), but the formations are primarily low-permeability shales and dolostones, with some extremely low permeability anhydrite beds. Regional horizontal groundwater flow is expected to exist in the medium permeability units, albeit under very low horizontal gradients. Groundwater in the zone is saline to extremely saline (20 to 310 g L⁻¹). The intermediate zone is approximately 265 m thick (to an approximate depth of 450 mBGS, or an elevation of -265 mASL).
4. Deep bedrock groundwater zone - All stratigraphic units below the Manitoulin. Transport in the low-permeability Ordovician shale and limestone is expected to be diffusion dominated. Site characterization results (Figure 2.2) show elevated environmental heads in the Cambrian sandstones and underpressured conditions throughout the Ordovician sequence, indicating that the system is not in hydrodynamic equilibrium. Groundwater in the zone is extremely saline (150 to 350 g L⁻¹).

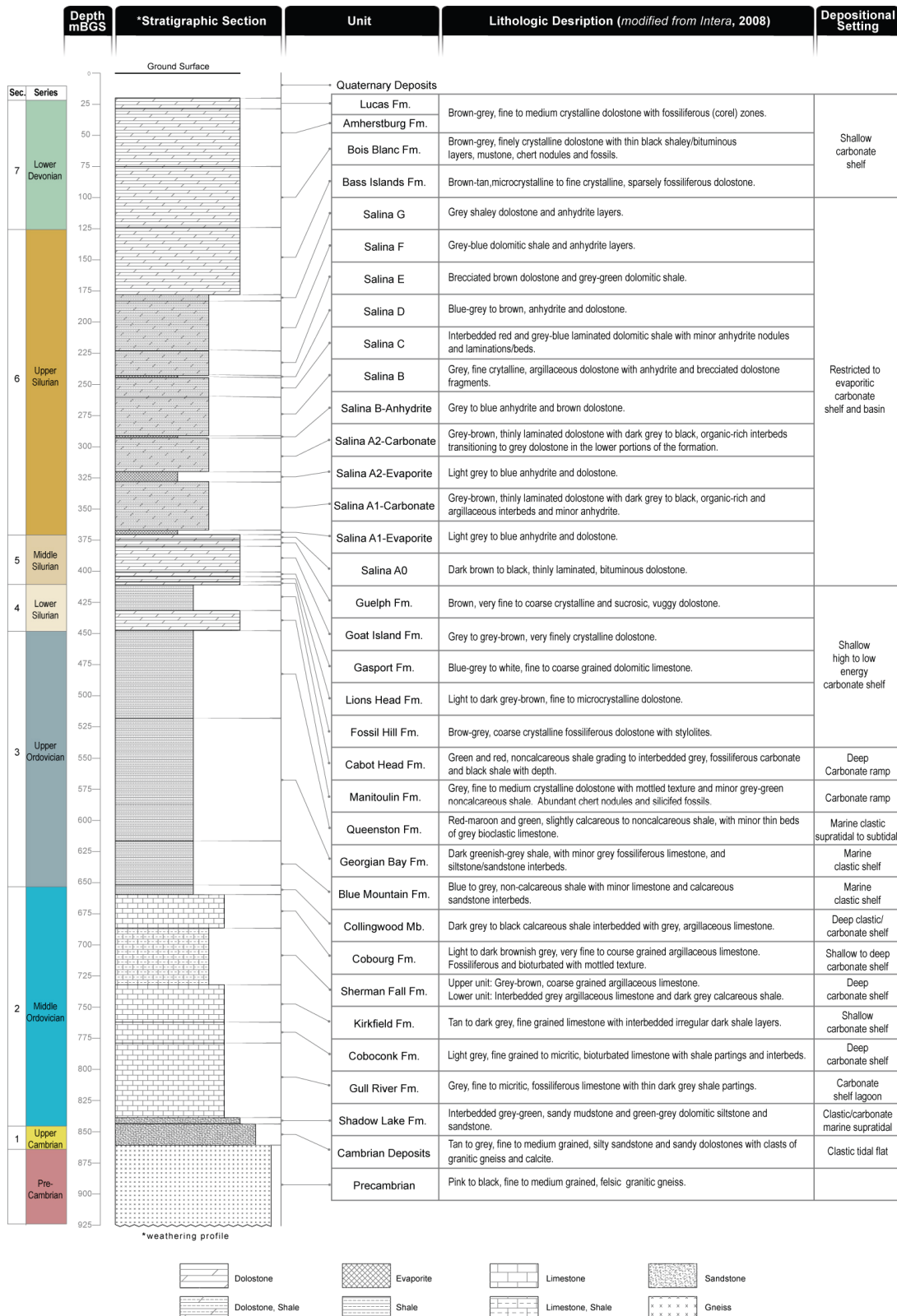


Figure 2.1: Geological Stratigraphy at the DGR Site (Gartner Lee 2009b)

There are significant uncertainties associated with hydrogeologic characterization of the intermediate and deep bedrock groundwater zones. Horizontal gradients in the more permeable intervals in the intermediate zones have not been determined at the site scale. Isolated zones of overpressure within the Silurian and Ordovician sediments shown in Figure 2.2 may represent the presence of a separate gas phase. The full extent of underpressures in the Ordovician sequences has yet to be determined, and the underlying cause of the non-equilibrium conditions is under investigation. The existence of the Cambrian overpressure is certain, however neither its cause nor time dependence are currently known.

However, all these features are indicative of a low vertical permeability host rock, and many of the uncertainties are essentially on "how low is low".

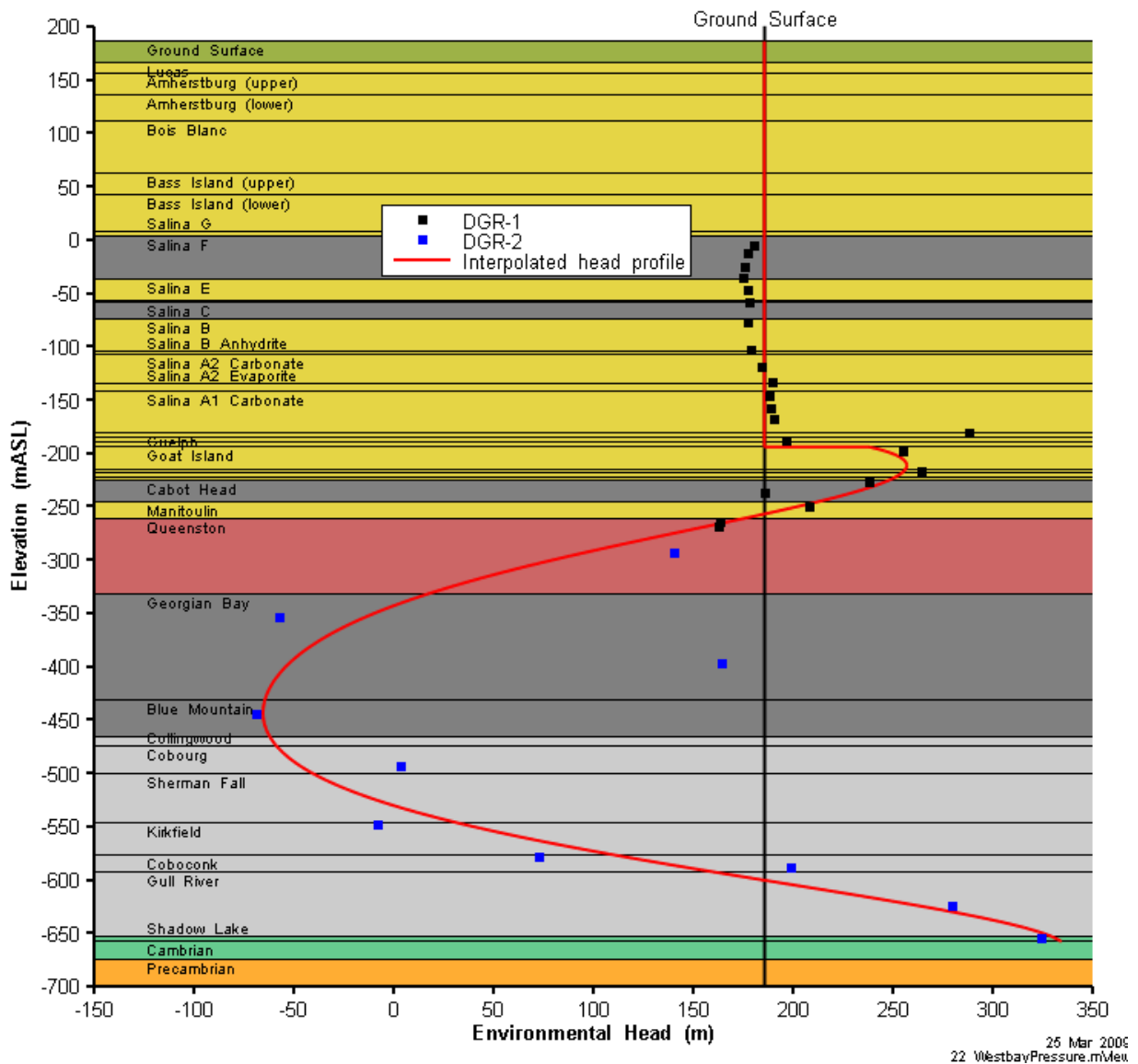


Figure 2.2: Environmental head profile from DGR Site Investigation Boreholes based on May 2008 monitoring data.

2.2 REPOSITORY LOCATION AND CHARACTERISTICS

The current repository design (adapted from Hatch, 2008) is shown in Figure 2.3 in relation to the site Universal Transverse Mercator (UTM) coordinate system. The figure also shows the location of current site characterization deep boreholes.

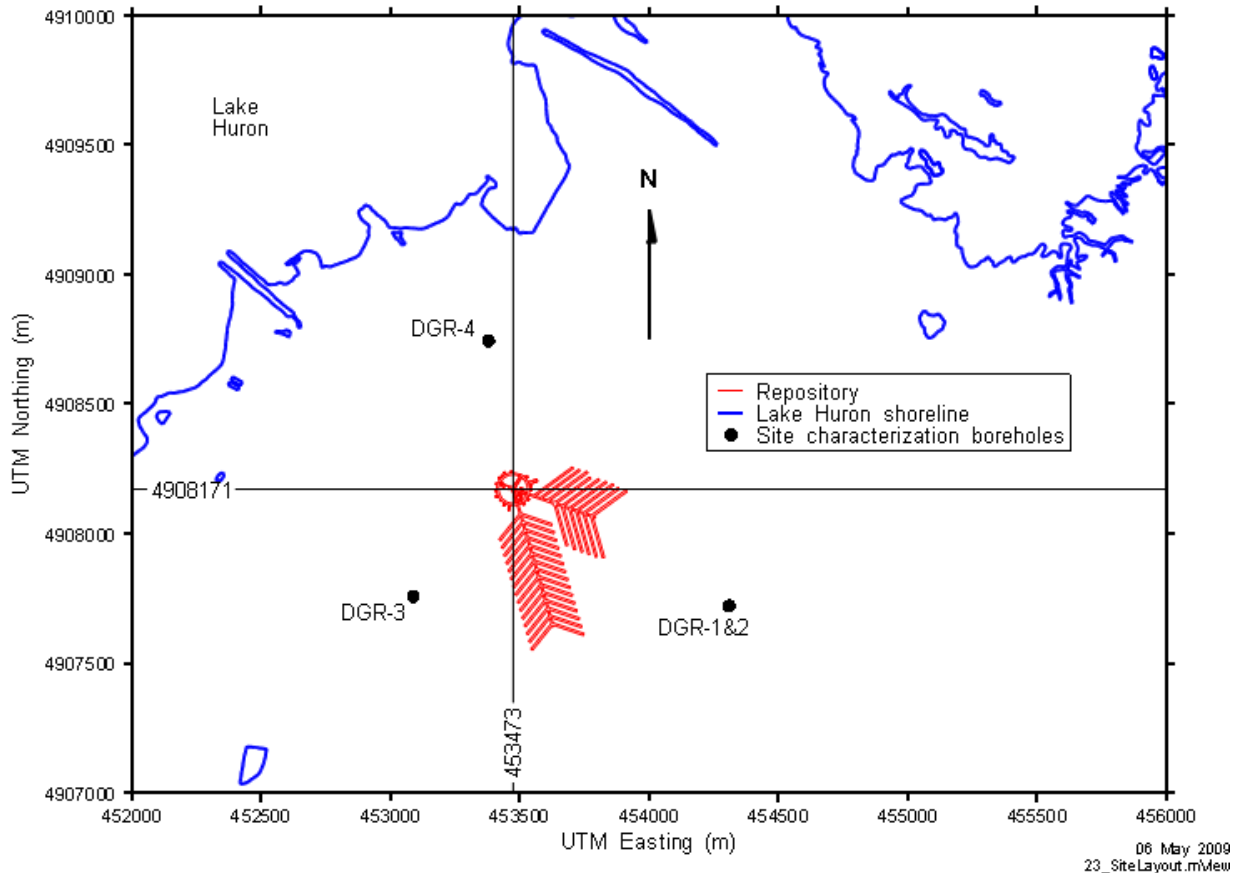


Figure 2.3: Repository layout in UTM coordinate system.

The repository design includes two waste emplacement panels (East and South) and two shafts; a main access shaft (8 m diameter at closure) and a smaller vent shaft (5.95 m diameter at closure). Both shafts are located within the area bounded by the 120 m diameter ring tunnel.

The repository is located at a depth of approximately 680 mBGS in the Cobourg Formation.

Hatch (2008) describes a post-closure shaft seal design consisting of compacted bentonite sand and asphalt waterstop seals separated by concrete bulkheads. The shaft sealing system isolates the repository from the biosphere by preventing groundwater and gas flow through the shafts and through the excavation damage zone (EDZ) surrounding each shaft. The EDZ is described in detail in Little et al. (2009). Within the EDZ, permeability of the rock mass will increase due to horizontal stress relaxation. The EDZ is conceptualized as consisting of two zones, an inner EDZ extending from the shaft wall to an additional radius equal to one half the shaft radius; and an outer EDZ extending an additional one half shaft radius beyond the inner

EDZ. The permeability of the inner EDZ is higher than the outer EDZ, reflecting increased stress relaxation in immediate proximity to the shaft.

A shaft seal design analysed in this report is described in Walke et al. (2009b) and is shown in Figure 2.4. The same sealing system is to be applied to both shafts. This design moves the location of some seals relative to the Hatch 2008 design to take advantage of newer information on site characteristics in order to improve overall system performance. It also includes cautious assumptions about the inner EDZ.

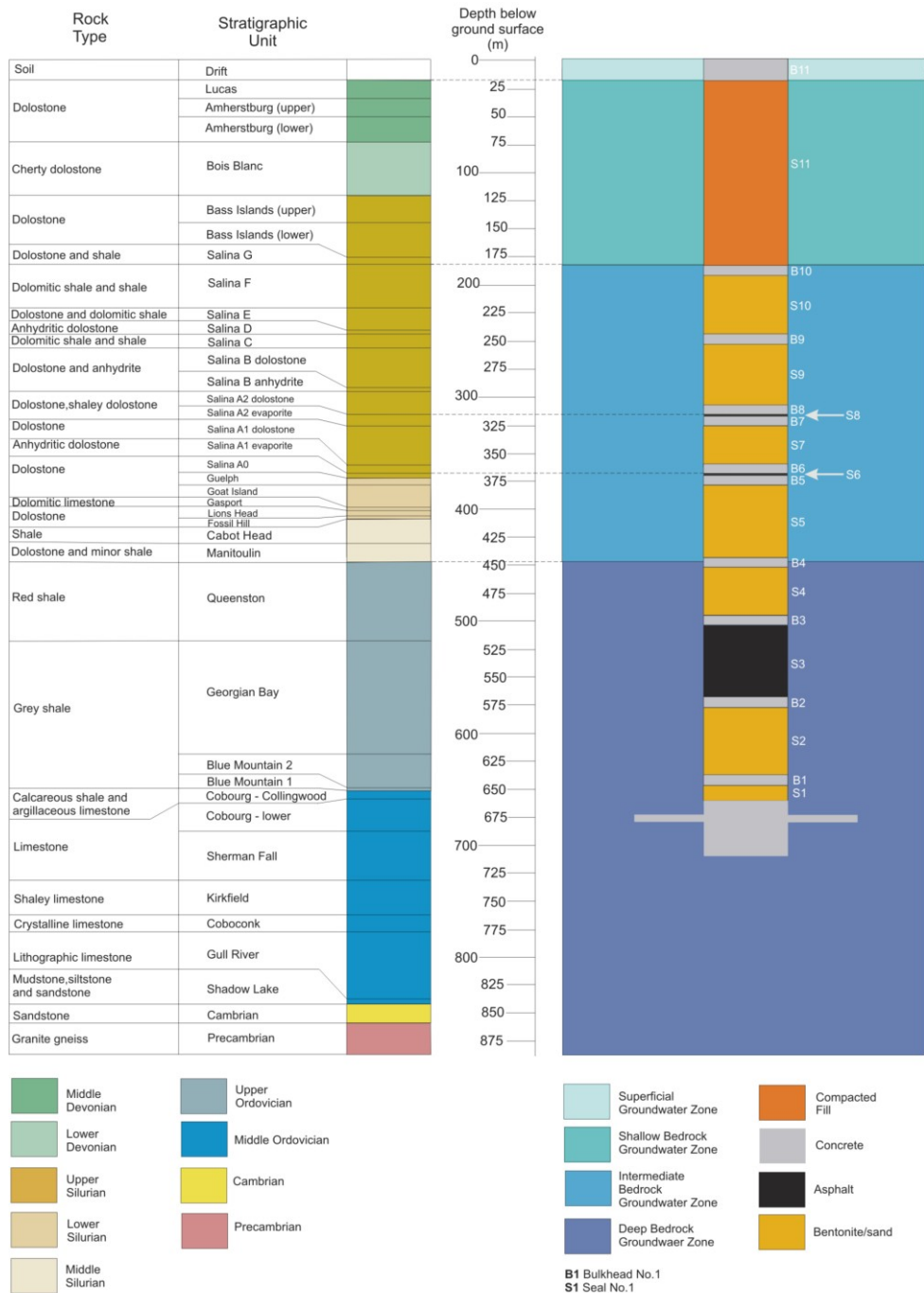


Figure 2.4: Lithology and shaft sealing system (Walke et al. 2009b)

2.3 NORMAL EVOLUTION AND DISRUPTIVE SCENARIOS

The Normal Evolution Scenario, described in detail in Little et al. (2009), is the consensus description of expected evolution of the geosphere and repository system as a function of time. It includes a detailed description of evolution of changes in the waste forms, repository conditions, geosphere evolution and climate conditions.

Ideally, a numeric model would incorporate all features, events, and processes (FEPs). However, limitations in numeric model capabilities preclude an all-inclusive approach. Consequently, the scenario must be simplified to address code limitations, while still considering key FEPs. The Normal Evolution Scenario implemented in the detailed groundwater modelling makes the following assumptions and simplifications.

1. Climatic impacts due to glaciation are not modelled. From a hydrogeologic modelling perspective, the impact of glaciation events can be extensive. Glacial advance and retreat provide large transient changes in mechanical and hydraulic loading of the geosphere. However, regional data and modelling indicate (Gartner Lee 2008a), and site characterization work is expected to confirm, that this hydraulic loading has little influence on the deep bedrock groundwater zone. The mechanical loading would reach the repository level, and the aggregate geomechanical impacts of multiple glacial cycles on the repository are included by making conservative assumptions about rockfall within the mined facility.
2. Repository resaturation is instantaneous at closure. Detailed gas modelling (Calder et al. 2009) indicates that the repository resaturation history is complex and the DGR might take in excess of a million years to resaturate. This resaturation history is conservatively ignored in the current modelling, and groundwater transport of radionuclides is assumed to commence immediately on repository closure. Advective transport of contaminated groundwater up the shaft and shaft EDZ system would likely not occur until the repository is fully saturated and repressurized.
3. For most modelling presented in this report, the flow system is assumed to be at steady-state, with vertical gradients driven by a constant head boundary condition at the Cambrian. One calculation case uses the current pressure profile as initial conditions and includes transient flow as the system repressurizes towards steady-state conditions. However, no further perturbations are applied to the system to simulate conditions which might cause further hydrodynamic disequilibrium. The steady-state flow system assumptions results in a prevailing upwards vertical gradient driven by the constant Cambrian head boundary condition. If the underpressures were incorporated in the analyses, the prevailing gradients within the Ordovician system would be towards the repository.
4. Contaminant release is instantaneous. The entire radionuclide inventory is assumed to dissolve in the saturated repository volume at time zero to derive initial concentrations in the repository. No solubility limitations or time varying release are incorporated. Actual contaminant release rates will depend upon repository resaturation, waste form degradation and dissolution processes. As mentioned previously, transport of a single unretarded radionuclide, Cl-36, is simulated in all modelling results presented in this report.

5. Groundwater is constant density. Preliminary site characterization results indicate that (as described in Section 2.1) extremely saline waters are found in the deep and intermediate systems. Ignoring salinity profiles simplifies the modelling approach and allows for use of steady-state models and in general is conservative. The effect of salinity gradients is partially included in the transient calculation case as initial head profiles are based on environmental heads which are compensated for fluid density. Furthermore, the Cambrian boundary condition heads used in the steady-state and transient modelling are based on the same density compensations. Modelling of salinity and variable density flow is important in systems with topographic driving forces for horizontal groundwater flow as increases in density with depth tend to decrease the depth of penetration of topographic induced heads and consequently moderates horizontal gradients, thus reducing transport. However, in the current local site system, where flow is primarily vertical due to the Cambrian overpressure and Ordovician underpressures, environmental head gradients already effectively incorporate the salinity profile.

Four Disruptive Scenarios were also identified in which various scenarios were considered in which the major geosphere barriers could be breached (Little et al. 2009). Briefly stated, the scenarios and their treatment in the detailed groundwater modelling are as follows.

- Human Intrusion – An exploration borehole penetrates the repository. The intrusion is assumed to occur once institution control over the site is no longer effective. A steady-state saturated flow system is assumed to be established immediately after the borehole intersects the repository. The borehole is poorly sealed, resulting in the loss of contaminants into permeable geosphere horizons above the repository.
- Severe Shaft Seal Failure – The shaft seals (including the EDZ) perform much poorer than expected, possibly due to poor installation undetected by quality assurance procedures and/or unexpected natural processes which results in more rapid and more extensive seal degradation. The scenario is modelled by setting the properties of all shaft-sealing materials to conservative values. In addition, the shaft seals do not intersect the EDZ and therefore do not impede flow through the EDZ. The EDZ permeability is assumed to be at the upper estimated value.
- Open Borehole – An exploration or monitoring borehole near, but not intersecting, the repository is not decommissioned properly. Standard practice is that exploration or water wells that are no longer to be used are sealed with bentonite or cement to prevent contamination of potable water supplies. If this step is improperly performed, the abandoned borehole can provide a preferential path for the migration of contaminated groundwater.
- Extreme Earthquake – An extreme seismic event causes the reactivation of a hypothetical fault in the vicinity of the repository, but outside the area assessed in detail by site characterization. An enhanced permeability vertical fault extending from the Cambrian to surface is assumed to reactivate at a location downgradient of the repository.

2.4 MODELLING APPROACH

The detailed groundwater flow and transport modelling presented in this report is for a model domain encompassing a several kilometre radius around the repository. This allows the modelling to focus on the impact of the repository on flow and transport, and to effectively represent the relatively small-scale features of the repository design such as shafts and shaft seals.

One effect of this limited domain is to require that regional flow processes be incorporated as boundary conditions. Regional flow modelling has been undertaken to support the Phase I site Geosynthesis (Sykes et al. 2008). Results of this modelling, and indications from site characterization, show that regional gradients and flow within the deep and intermediate bedrock groundwater zones are extremely low, and that transport within these zones is likely to be diffusion dominated. Consequently, the relatively small domain selected is appropriate for modelling transport in the vicinity of the repository. Vertical boundary conditions at the model's horizontal extents associated with low-permeability units were set to zero flow, while those for medium permeability Silurian units with specified gradients were set to fixed head, with the fixed head values adjusted to implement the specified gradient.

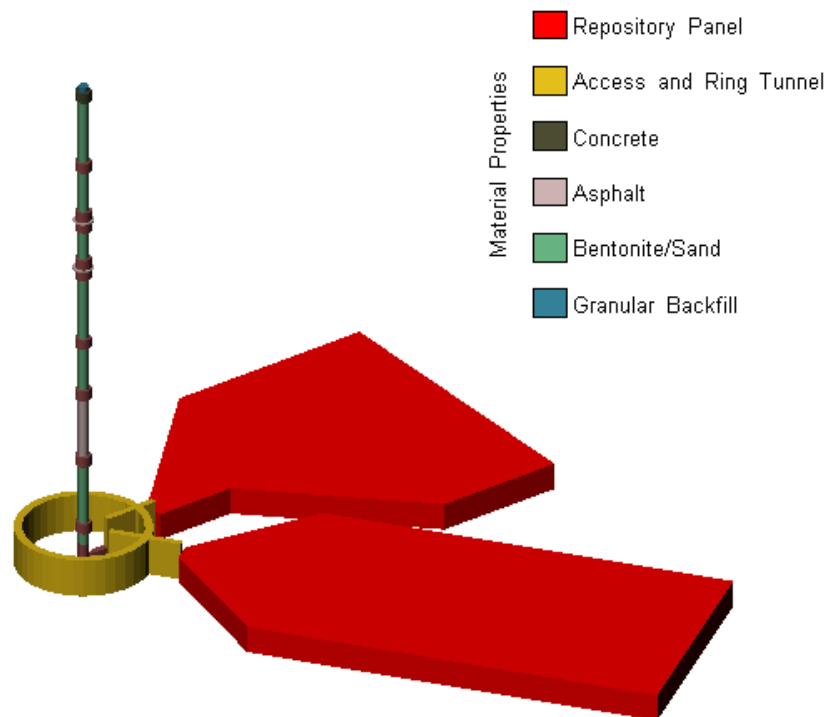
For the purposes of detailed groundwater modelling, the four groundwater zone system has been divided into two components:

1. an upper zone of high permeability horizontal advective zone consisting of the surficial sediments and shallow bedrock groundwater zone where flow is primarily horizontal (the superficial and shallow bedrock groundwater zones from Figure 2.4); and
2. a lower zone of generally low-permeability units where horizontal flow is restricted to a few medium-permeability units and the driving boundary conditions indicate vertical advective flow at very low velocities, with most transport in the rock mass being diffusion dominated (the intermediate bedrock and deep bedrock groundwater zones from Figure 2.4).

Of the two components, the lower zone is the more important and is the subject of the majority of modelling presented in this report. Two modelling approaches are used to simulate the calculation cases within this lower zone, whereas a single model is used to represent flow and transport in the upper zone.

2.4.1 3D Simplified (3DS) Model

The primary approach to modelling the lower zone consists of a fully three-dimensional model, denoted the Three-Dimensional Simplified, or 3DS, model. This model incorporates repository and geosphere characteristics in a spatially accurate sense, but with some simplification of repository features. A conceptual diagram of the 3DS model is shown in Figure 2.5. The repository panels are solid features and do not include individual galleries. The main and vent shafts have been combined to form a single shaft with total plan cross-sectional area equal to the sum of the areas of the main and vent shaft. This single shaft has been placed at the centre of the ring tunnel.



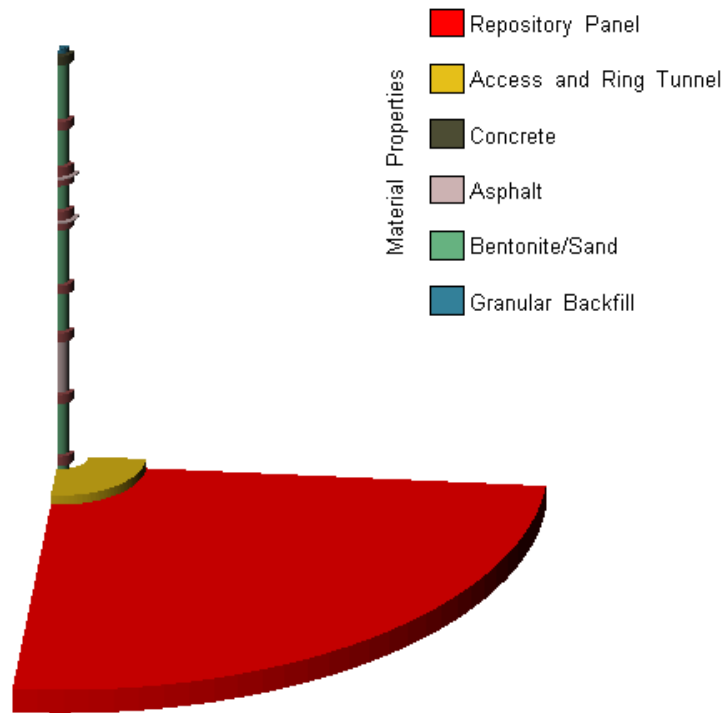
17 Mar 2009
25_3DS_Conceptual.mView

Figure 2.5: Conceptual illustration of the 3DS model of repository and shafts.

The geosphere is described as horizontal layers with properties varying on a formation basis. Horizontal formations are a minor simplification of actual stratigraphy given the restricted model domain and relatively shallow dip of formations at the Bruce site. Boundary conditions on the 3DS model are set to specify horizontal and vertical gradients across the model domain.

2.4.2 2D Radial (2DR) Model

The second approach used is denoted the Two-Dimensional Radial, or 2DR, model. In this model a two dimensional vertical axisymmetric grid is used to represent the repository and geosphere. Similar to the 3DS model, the main and vent shafts are combined to form a single aggregate shaft. The conceptualization of the repository and shaft in the 2DR model is shown in Figure 2.6



17 Mar 2009
26_2DRConcept.mView

Figure 2.6: Conceptual illustration of the 2DR model of the repository and shaft.

The 2DR model has significant computational advantages compared to the 3DS model as far fewer nodes are required to accurately discretize the system. However, the 2DR model is incapable of representing horizontal gradients across the model domain as all horizontal flow is relative to the central shaft. Furthermore, impacts of different spatial allocations of waste in the South or East panels cannot be represented.

2.4.3 3D Simplified Upper (3DSU) Model

The 3D Simple Upper (3DSU) model characterises the rock mass of the shallow bedrock groundwater system as completely isolated from the intermediate bedrock groundwater system. The goal of this model is to investigate the degree to which mass exiting at the top of the Salina F units (the top of the intermediate bedrock groundwater zone) will be captured by a downstream water-supply well or enter Lake Huron. The well is located approximated midway between the shaft and the Lake Huron shoreline and is consistent with the requirements of a small farm. Further well details are given in Section 4.3.1.3. Mass flow input rates of contaminants to the base of 3DSU model are derived from 3DS and 2DR model calculations.

3. CALCULATION CASES

Detailed groundwater modelling was performed for a number of parameter and conceptual model sensitivity cases. All models were derived from a base case characterization of the system, as follows:

- constant present-day climate conditions, no change in boundary condition during the assessment period;
- 1 000 000 year simulation period;
- stratigraphic, hydrogeologic, and transport properties as outlined in the Version 1 Safety Assessment Data report (Walke et al. 2009b);
- rockfall extends 20 m above repository and 30 m above central access and ring tunnels;
- EDZ zone with increased hydraulic conductivity (K) and porosity surrounding shaft and repository elements³;
- no shaft inner EDZ where concrete bulkheads are to be installed;
- higher hydraulic conductivity of concrete bulkheads in shallow aquifer zone due to presumed partial degradation;
- 140 m hydraulic head fixed boundary at the bottom of the modelled system (the top of the Cambrian geological unit);
- 0 m fixed head boundary at the top of the upper bedrock unit (the Lucas);
- no flow boundaries on all vertical model boundaries with the exception of a horizontal gradient of 0.002 in the Guelph/Salina A0 and Salina A2 evaporite units achieved by fixed head boundaries at the elevation of the units along the vertical boundaries;
- steady state, constant density water flow;
- saturated repository, tunnels, shaft, and EDZ;
- contaminant transport is assumed to start immediately after facility closure;
- Cl-36 transport, initial concentration in repository based on instantaneous dissolution of the Cl-36 inventory and repository void volume given in Walke et al. (2009b); and
- radioactive decay of Cl-36, no sorption in any formation.

Calculation cases were derived for the Normal Evolution scenario and for the four disruptive event scenarios. A common calculation case naming convention has been specified for the detailed groundwater, detailed gas and assessment modelling. The calculation case identifier is made up of the scenario (NE – normal evolution, HI - human intrusion, SF – shaft failure, EE – extreme earthquake, and OB - open borehole), additional identifiers describing the case (described below) and a suffix describing the model to be used (F2 – Groundwater 2DR, F3 – Groundwater 3DS, T – gas 2DR, A – assessment).

An additional modifier, -UG-, is used to indicate cases that are based on an “updated geosphere”. Recent preliminary site characterization information from boreholes DGR-3 and DGR-4 indicate that permeability in the Silurian and Ordovician sediments may be significantly lower than shown by DGR-1 and DGR-2 testing, which serves as the basis for the current permeability data as outlined in Walke et al. (2009b). These lower permeabilities will have significant impact on modelling results, and are therefore incorporated in the current

³ The shaft EDZ is described as two zones (Inner and Outer) while a single EDZ zone is defined for the repository and tunnels. All EDZ zones are isotropic and are parameterized with hydraulic conductivity calculated as a multiple on the associated intact rock vertical hydraulic conductivity.

assessment as an indicator of likely performance. However, until the preliminary DGR-3 and DGR-4 data are verified and accepted, the current base case permeability data will be used for most models. Hydraulic conductivity data for the updated geosphere are presented in Section 4.2.1.

3.1 NORMAL EVOLUTION SCENARIO

A number of parameter and conceptual model sensitivity cases have been developed to assess the impact of alternative likely parameterizations of the EDZ, engineered barrier systems, and geosphere. Table 3-1 describes the modelling cases for the Normal Evolution Scenario and the modelling approaches used to simulate those cases.

Table 3-1: Groundwater modelling cases for the Normal Evolution Scenario

Case ID	Case Description	Model
NE-RS1	Reference case parameters for groundwater modelling based on V1 inventory, R1 repository conceptual design and Phase I site characterization data, with immediate repository resaturation and no gas generation.	F3
NE-UG-RS1	NE-RS1 with updated geosphere data	F3
NE-NHG	NE-RS1 with no horizontal gradients in permeable Silurian sediments (Salina A2 evaporite, Guelph and Salina A0)	F2 and F3
NE-UG-NHG	NE-NHG with updated geosphere, transient flow from current pressure distribution	F2
NE-EDZ	As NE-NHG-F2, but hydraulic conductivity, K, for inner EDZ assumed to be four orders of magnitude (OM) greater than intact geosphere, and K for outer EDZ assumed to be two OM greater than intact geosphere. Interruption of EDZ by concrete bulkheads and asphalt waterstops is assumed to be ineffective.	F2
NE-UG-EDZ	NE-EDZ with updated geosphere	F2
NE-UG-RD1	NE-UG-RS1 with ring and access tunnels sealed with concrete.	F3

The groundwater reference case model (NE-RS1) specifies horizontal flow in the Guelph/Salina A0 and Salina A2 evaporite formations, and therefore can be modelled using the 3DS model only. The NE-NHG-F2 case is the reference case for the 2DR model and serves as the basis of comparison for other 2DR based cases.

Contaminant mass flow at a water supply well and mass flow loading to Lake Huron are calculated using the 3DSU model, with input mass flows developed by the NE-RS1-F3 and NE-NHG-F2 cases.

The NE-UG-NHG case is intended to assess the impact of the extant transient flow regime. This case assumes the gradual dissipation of the underpressure zone in the Ordovician with no future glaciation or erosion impacting the pressure distribution in the system. The hydraulic head in the Cambrian unit is assumed to remain constant over the duration of the simulation. The NE-EDZ and NE-UG-EDZ modelling cases examine the impact if the maximum shaft EDZ hydraulic conductivity estimates from Walke et al. (2009b) are applied (the hydraulic

conductivity of the EDZ around the repository emplacement rooms and tunnels remains the same as for the NE-RS1 and NE-UG-RS1 cases, i.e., three orders of magnitude higher than the horizontal conductivity of the host rock). Additionally, the NE-EDZ and NE-UG-EDZ cases assume that the concrete bulkheads and asphalt waterstops are ineffective in limiting the flow in the EDZ.

Modelling case NE-UG-RD1 examines the effect of sealing the access and ring tunnels with concrete, essentially extending the monolith out to the repository panels.

Diagrams illustrating the differing property assignments and discretizations for the various cases are presented in Section 4.3.2.

3.2 DISRUPTIVE SCENARIOS

Six calculation cases are considered for Disruptive Scenarios and are enumerated below in Table 3-2. These calculations simulate the Disruptive Scenarios previously described in Section 2.3.

Table 3-2: Groundwater modelling cases for the Disruptive Scenarios

Case ID	Case Description	Model
HI-GR	As NE-RS1-F3 but with an exploration borehole drilled from surface through to the repository and then terminated at repository depth. The borehole is assumed to be sealed with a fill material.	3DS
SF-ES1	As NE-NHG but with hydraulic properties of all seals, backfill and inner EDZ set to extreme values and seals not keyed into EDZ.	2DR
SF-UG-ES1	As SF-ES1 with updated geosphere data	2DR
SF-US	As SF-ES1 but with failure only for those seal system components located above the top of the Queenston shale.	2DR
EE-BC	As NE-RS1 but with a single enhanced permeability, reactivated fault 500 m down gradient from the repository.	3DS
OB-BC	As NE-RS1 but with a poorly sealed site characterization borehole located downgradient of the repository at the current location of site characterization borehole DGR-3.	3DS

Case HI-GR simulates an exploration borehole that is drilled from surface to intersect the middle of the East repository panel. The normal evolution 3DS model is modified to include a high conductivity borehole. In an actual scenario, this would result in a transient depressurization of the repository, possibly with extensive gas exposure if repository saturation was not complete. In the modelled scenario, the repository is already saturated, and is instantaneously depressurized and in steady state flow conditions. This simplification overlooks the initial high flow rates possible when the facility was first breached by the borehole. This initial flow would be driven by the compressibility of the fluid in the repository and the host rock. However, this initial release would be a small fraction of the total repository volume. The bulk of the mass in the repository would be transported up the borehole by advection over a longer timescale, which would be limited by the ability of the host rock to provide groundwater, with steady-state flow being a limiting case. The borehole is conservatively assumed to be filled with a high-conductivity material.

Case SF-ES1 simulates improper repository closure or other unexpected events that lead to very poor shaft seal performance. In this case, all shaft and seal materials are assigned an extremely high hydraulic conductivity. The SF-UG-ES1 case simulates the same sealing failure within the updated geosphere system. The SF-US case assumes the seal failure zone is restricted to the Silurian formations.

Case EE-BC is based on a modified NE-RS1-F3 model where a fault zone is incorporated 500 m downgradient of the repository. The fault is a one metre wide feature, which extends vertically from the top of the Cambrian to surface. Hydraulic conductivities within the fault are specified as a factor of 1000 higher than the surrounding rock mass.

Case OB-BC examines the effect of a poorly sealed site characterization borehole. The borehole is located several hundred metres downgradient of the facility and approximately 560 m from the shafts. The borehole extends from the top of the Cambrian through to ground surface. Borehole dimensions are consistent with current site characterization boreholes.

Diagrams illustrating the discretization used to implement the HI-GR, EE-BC, and OB-BC cases are presented in Section 4.3.2.2.

4. MODEL IMPLEMENTATION AND DATA

4.1 SOFTWARE CODES AND QUALITY ASSURANCE

All detailed groundwater modelling presented in this report has been performed using FRAC3DVS_OPG (Version R622, Build Date 2008 04 28 - 64-bit). FRAC3DVS_OPG is a successor code to FRAC3DVS (Therrien and Sudicky 1996). FRAC3DVS is a three-dimensional numeric model describing subsurface flow and solute transport. It has been previously used extensively by NWMO for flow and transport simulations relating to deep geologic repositories. FRAC3DVS_OPG is developed by Groundwater Simulations Group Incorporated and is currently undergoing quality assurance testing and documentation. Quality assurance data for FRAC3DVS_OPG is described in Appendix A.

Model pre- and post-processing has been performed using mView 4.02, a proprietary modelling support tool developed by Intera Engineering Ltd. Pre-processing procedures consist primarily of discretization and property assignment. Post-processing includes all summary calculations and visualizations. mView 4.00A has been qualified to Yucca Mountain Project (YMP) Software Quality procedures. Additional capabilities added to mView since the YMP qualification have been verified in compliance with Intera's internal, ISO 9001 compliant, software development procedure.

The detailed groundwater calculations have been conducted to standards specified in the Intera Engineering ISO9001 Registered Quality Management System. There is a specific Work Instruction (WI), Numeric Modelling, which describes model input file management and archiving using a version control system.

4.2 DATA

This section presents the rock property data from Walke et al. (2009b) and describes how the data are used to delineate model units

4.2.1 Formation Properties

Stratigraphy from Phase 1 of the Geoscientific Site Characterization at the Bruce DGR site, based on boreholes DGR-1 and DGR-2 serves as the basis for the assignment of properties to the layers of the numerical model. The geological model's horizontally layered stratigraphic units are described in Table 4-1. Stratigraphic nomenclature in Table 4-1 is taken from Walke et al. (2009b). The table column "Model ID" designates the material property name used for the geologic units in the detailed groundwater flow model. In the Model ID column, the text "_R" indicates that this is the property for the undisturbed rock mass, as distinguished from the property value used in the EDZ.

Table 4-1: Geological Units and Model IDs

Stratigraphic Unit	Hydro-stratigraphic Zone	Model ID	Top Elevation	
			mBGS	mASL
Drift	Surficial	N/A	0	186
Lucas	Shallow	Lucas_R	20	166
Amherstburg (upper)		AmherU_R	30	156
Amherstburg (lower)		AmherL_R	50	136
Bois Blanc		Bois_R	75	111
Bass Island (upper)		BassU_R	124	62
Bass Island (lower)		BassL_R	144	42
Salina G		SalinG_R	178	8
Salina F	Intermediate	SalinF_R	183	3
Salina E		SalinE_R	223	-37
Salina D		SalinD_R	243	-57
Salina C		SalinC_R	245	-59
Salina B		SalinB-2_R	260	-74
Salina B Anhydrite		SalinB-1_R	291	-105
Salina A2 Carbonate		SalinA2-2_R	293	-107
Salina A2 Evaporite		SalinA2-1_R	320	-134
Salina A1 Carbonate		SalinA1-2_R	328	-142
Salina A1 Evaporite		SalinA1-1_R	367	-181
Salina A0		SalinA0_R	371	-185
Guelph		Guelph_R	375	-189
Goat Island		Goat_R	380	-194
Gasport		Gasport_R	401	-215
Lions Head		Lions_R	404	-218
Fossil Hill		Fossil_R	408	-222
Cabot Head	Cabot_R	411	-225	
Manitoulin	Manitou_R	432	-246	
Queenston	Deep	Queen_R	448	-262
Georgian Bay		Georg_R	518	-332
Blue Mountain		Blue_R	649	-463
Collingwood		Colling_R	652	-466
Cobourg		Cobourg_R	660	-474
Sherman Fall		Sherm_R	687	-501
Kirkfield		Kirk_R	732	-546
Coboconk		Cobo_R	762	-576
Gull River		Gull_R	779	-593
Shadow Lake		Shadow_R	839	-653
Cambrian		N/A	844	-658
Precambrian		N/A	861	-675

The 3DS and 2DR numerical models extend from the top of the Salina G at a depth of 178 m (elevation 8 mASL) to the bottom of the Ordovician Shadow Lake Formation (Shadow_R) at a depth of 843 m (elevation -657.9 mASL), as shown in Figure 4.1. The 3DSU model extends from the top of the Lucas Formation (elevation 165.8 mASL) to the top of the Salina F shale.

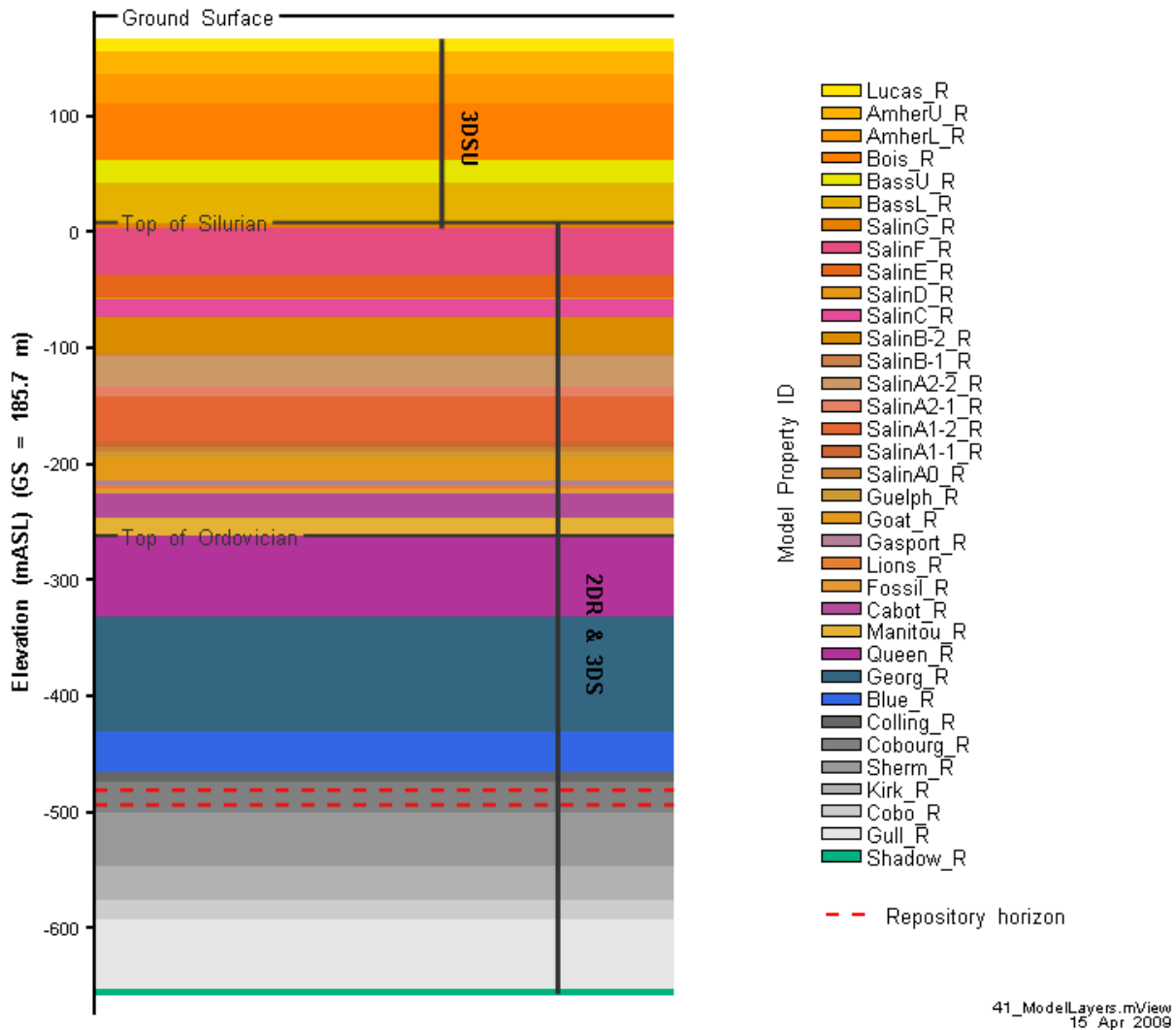


Figure 4.1: Geologic layering in the 2DR and 3DS groundwater models.

Hydrogeological and transport properties for each model unit are given in Table 4-2. FRAC3DVS calculates effective diffusivity from porosity, freewater diffusivity and tortuosity. Tortuosity values presented in Table 4-2 are those required to ensure that FRAC3DVS uses correct effective diffusivity. All values in Table 4-2 were derived from the Version 1 data report (Walke et al. 2009b).

For the majority of model units, vertical hydraulic conductivity values (K_z) were calculated from the horizontal hydraulic conductivity values (K_{xy}) by dividing K_{xy} by a factor of 10 representing a conservative anisotropy for the rock mass units. The Salina A1, Salina A2 and Salina B anhydrite/evaporate deposits do not have significant bedding and are presumed to be isotropic. Specific storage values presented in the table are calculated from rock compressibility and porosity. These values are used only for the transient NE-UG-NHG case.

Table 4-2: Relevant hydrogeological and transport properties for model units

Unit	Porosity (-)	K_{xy} ($m\ s^{-1}$)	K_z ($m\ s^{-1}$)	Specific Storage (m^{-1})	Horizontal Tortuosity (-)	Vertical Tortuosity (-)
Lucas_R	0.100	1.0E-06	1.0E-07	1.4E-06	0.100	0.100
AmherU_R	0.100	1.0E-06	1.0E-07	1.4E-06	0.100	0.100
AmherL_R	0.100	1.3E-07	1.3E-08	1.4E-06	0.100	0.100
Bois_R	0.100	1.0E-07	1.0E-08	1.4E-06	0.100	0.100
BassU_R	0.100	1.0E-04	1.0E-05	4.8E-06	0.100	0.100
BassL_R	0.100	1.0E-05	1.0E-06	4.8E-06	0.100	0.100
SalinG_R	0.080	1.0E-07	1.0E-08	4.5E-07	0.093	0.093
SalinF_R	0.030	2.9E-12	2.9E-13	3.7E-06	0.038	0.025
SalinE_R	0.080	9.7E-12	9.7E-13	3.7E-06	0.046	0.046
SalinD_R	0.030	9.7E-12	9.7E-13	4.5E-07	0.046	0.046
SalinC_R	0.080	4.7E-12	4.7E-13	3.7E-06	0.038	0.025
SalinB-2_R	0.080	2.5E-12	2.5E-13	1.9E-05	0.046	0.046
SalinB-1_R	0.080	2.5E-12	2.5E-12	4.5E-07	0.046	0.046
SalinA2-2_R	0.080	1.3E-10	1.3E-11	9.1E-07	0.046	0.046
SalinA2-1_R	0.080	8.5E-09	8.5E-09	4.5E-07	0.046	0.046
SalinA1-2_R	0.080	9.7E-13	9.7E-14	7.0E-07	0.046	0.046
SalinA1-1_R	0.080	9.7E-13	9.7E-13	4.5E-07	0.046	0.046
SalinA0_R	0.080	1.3E-08	1.3E-09	7.0E-07	0.046	0.046
Guelph_R	0.080	1.3E-08	1.3E-09	7.0E-07	0.093	0.093
Goat_R	0.080	1.9E-11	1.9E-12	7.0E-07	0.046	0.046
Gasport_R	0.080	1.9E-11	1.9E-12	7.0E-07	0.046	0.046
Lions_R	0.080	1.9E-11	1.9E-12	7.0E-07	0.046	0.046
Fossil_R	0.080	1.9E-11	1.9E-12	7.0E-07	0.046	0.046
Cabot_R	0.030	9.7E-13	9.7E-14	3.0E-05	0.038	0.025
Manitou_R	0.010	2.9E-12	2.9E-13	3.1E-06	0.038	0.038
Queen_R	0.085	5.5E-12	5.5E-13	5.3E-06	0.040	0.020
Georg_R	0.089	1.3E-11	1.3E-12	8.4E-06	0.057	0.013
Blue_R	0.087	9.7E-12	9.7E-13	2.6E-05	0.013	0.009
Colling_R	0.015	2.0E-11	2.0E-12	1.7E-06	0.060	0.013
Cobourg_R	0.015	2.0E-11	2.0E-12	1.1E-06	0.060	0.013
Sherm_R	0.008	1.6E-11	1.6E-12	2.5E-06	0.125	0.125
Kirk_R	0.020	4.1E-11	4.1E-12	1.1E-06	0.050	0.050
Cobo_R	0.020	5.4E-11	5.4E-12	1.1E-06	0.050	0.050
Gull_R	0.015	3.6E-11	3.6E-12	1.1E-06	0.030	0.030
Shadow_R	0.010	8.0E-12	8.0E-13	1.7E-06	0.050	0.050

For the purposes of flow and advective-dispersive transport modelling, relevant porosities from Walke et al. (2009b) were used. Longitudinal dispersivities for all 2DR and 3DS model units were set to 10 m, as approximately several percent of the expected plume size over the performance period. Transverse dispersivities for the 2DR and 3DS models are set at 10% of longitudinal dispersivity, or 1 m. Dispersivities in the Devonian system for the 3DSU model are set at 100 m (longitudinal) and 10m (transverse) to reflect the larger transport distance.

The updated geosphere (all UG cases) hydraulic conductivities (DGR 2009) are presented in Table 4-3. All other parameters remain the same as for the reference case.

Table 4-3: Hydraulic conductivities of Silurian and Ordovician units for UG updated (lower permeability) geosphere calculation cases.

Unit	Kxy (m s ⁻¹)	Kz (1) (m s ⁻¹)
SalinG_R	1.0E-07	1.0E-08
SalinF_R	6.0E-14	6.0E-15
SalinE_R	6.0E-13	6.0E-14
SalinD_R	6.0E-13	6.0E-14
SalinC_R	7.0E-13	7.0E-14
SalinB-2_R	7.0E-13	7.0E-14
SalinB-1_R	7.0E-13	7.0E-13
SalinA2-2_R	5.0E-10	5.0E-11
SalinA2-1_R	7.0E-08	7.0E-08
SalinA1-2_R	8.0E-11	8.0E-12
SalinA1-1_R	1.0E-12	1.0E-12
SalinA0_R	8.0E-11	8.0E-12
Guelph_R	3.0E-08	3.0E-09
Goat_R	2.0E-12	2.0E-13
Gasport_R	2.0E-12	2.0E-13
Lions_R	2.0E-12	2.0E-13
Fossil_R	2.0E-12	2.0E-13
Cabot_R	2.0E-13	2.0E-14
Manitou_R	2.0E-13	2.0E-14
Queen_R	2.0E-14	2.0E-15
Georg_R	3.0E-14	3.0E-15
Blue_R	3.0E-14	3.0E-15
Colling_R	2.0E-14	2.0E-15
Cobourg_R	1.0E-14	1.0E-15
Sherm_R	2.0E-14	2.0E-15
Kirk_R	9.0E-15	9.0E-16
Cobo_R	3.0E-12	3.0E-13
Gull_R	1.0E-12	1.0E-13
Shadow_R	8.0E-12	8.0E-13

Note:

1. Same anisotropy as for Table 4-2.

K_z values for the reference case and UG cases are shown graphically in Figure 4.2. As described previously, UG case hydraulic conductivities are significantly lower than base case within the Ordovician sequence. Within the Silurian formations they are lower in some case, and higher in others. The most significant differences are increased permeabilities within the sequence from the Guelph upwards to the Salina A2 evaporite, with the exception of the Salina A0, which is not considered a high-permeability unit in the UG cases.

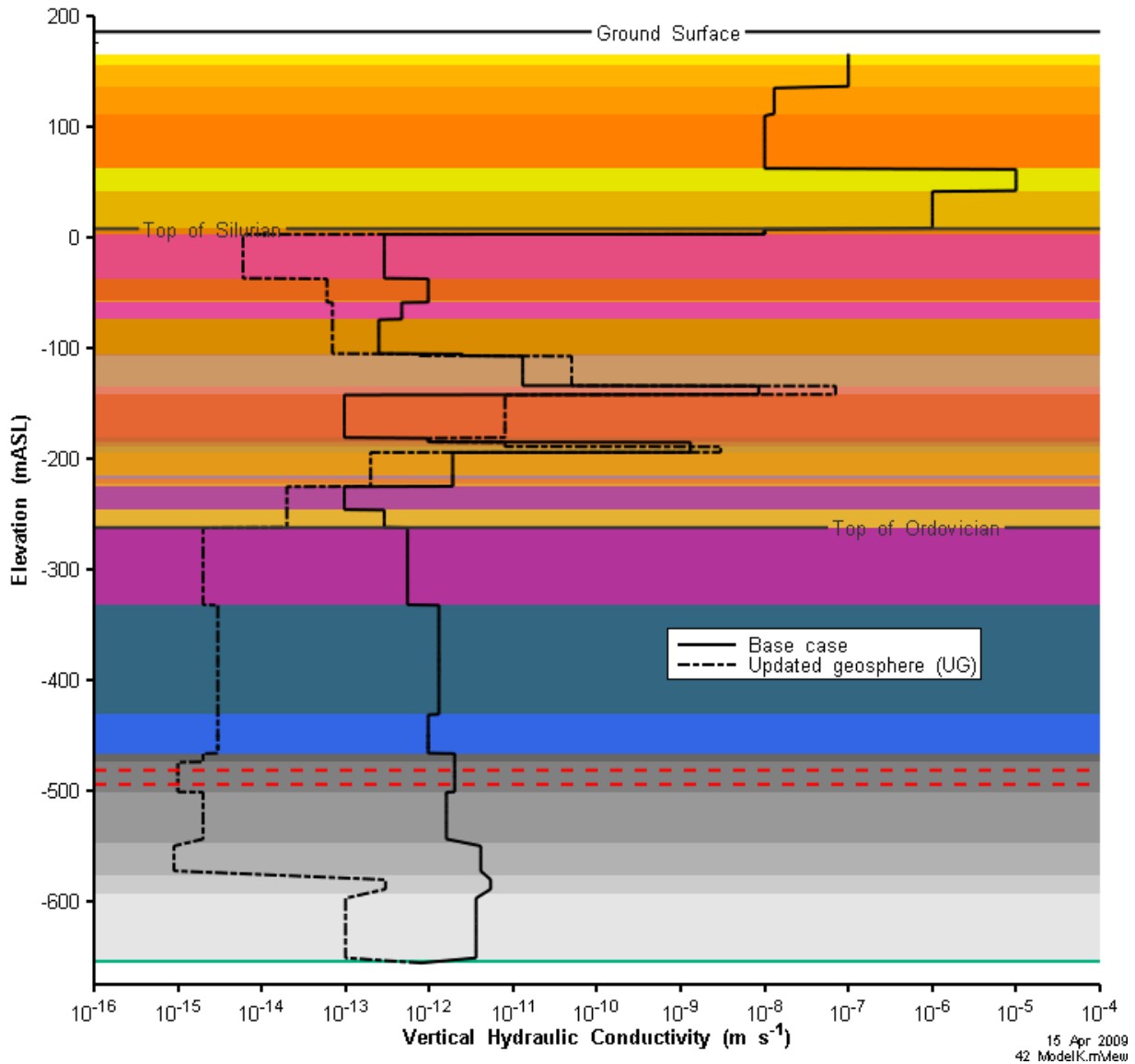


Figure 4.2: Vertical hydraulic conductivity for the base and updated geosphere (UG) calculation cases.

For the EE1 disruptive case, a new group of material properties were defined (Shadow_E through Lucas_E) with hydraulic conductivities three orders of magnitude higher than for the associated rock mass unit. These were used to define the fault properties. All other material properties for the fault (_E) materials are the same as the corresponding rock mass (_R).

4.2.2 Shaft, Repository and Sealing Material Properties

The repository, main access shaft, the ventilation shaft, and their associated sealing systems form the engineered portion of the modelled system. For these components of the model, there is no directionality to the material and the vertical and horizontal hydraulic conductivity are equal. Model IDs in this section are shown in bold text to make them easily distinguishable.

The repository is located in the Cobourg (Cobourg_R) unit, with the bottom of the repository at an elevation of -494.2 mASL. The repository is conceptually divided into two components, the emplacement tunnels (**repository**) and access and ring tunnels (**access**), each with slightly different properties. The porosity used for the repository is calculated from the ratio of the total void volume of tunnels (access and waste disposal) as calculated in Walke et al. (2009b) to the total volume assigned to the **repository** model property (including rockfall volume). This calculation ignores the small porosity of the rock in the room pillars and above the repository. Concrete volumes on floors, walls, and ceilings are also included in the calculation.

The resulting calculated porosity of the **repository** zone is 0.061 for the 2DR G1 model and 0.065 for the 3DS BC model. Differences between 3DS and 2DR model are due to slightly different volumes assigned to repository material types in each discretization. The porosity of the **access** material group is calculated similarly by assuming that the access tunnels are initially empty and rock mass porosity is negligible. The calculated access tunnel porosity is largely a reflection of post-rockfall porosity, where the initial void volume is dispersed across the volume extending to the top of the rockfall zone. The porosity of the **access** material group was calculated as 0.184 for the 2DR G1 model and 0.264 for the 3DS model.

The EDZ surrounding the monolith, access and ring tunnels, and the repository (referred to as **repoEDZ**) is assumed to have uniform and isotropic properties. Hydraulic conductivity of the **repoEDZ** is 1000 times higher than the Cobourg rock mass horizontal hydraulic conductivity. The dimensions of this EDZ zone are described in more detail in Section 4.3.1.1.

The shafts are divided into two zones, based on the sealing system for the shaft:

1. a primary seal extending through the Deep and Intermediate Bedrock Groundwater Zones, from the repository in the Cobourg (Cobourg_R) to the top of the Salina F (SalinaF_R) unit;
2. a secondary seal extending from the top of the primary seal to ground surface.

The primary seals are backfilled with a series of compacted bentonite/sand seals (**bento_sand**), separated by concrete bulkheads. The primary seal also contains a section of asphalt (**asphalt**) and two asphalt waterstops separated by concrete bulkheads. The secondary seal is backfilled with compacted crushed rock obtained from excavation of the shaft, labelled **backfill** (see Figure 2.4). Above 0.2 mASL, the sealing plan also calls for the concrete liner to remain in place. This liner is in the zone where concrete degradation is expected to be more likely (see Walke et al. 2009b), and before closure this liner will have been

in service for 50 – 100 years under operational conditions. Thus, it has been assumed in this model that the liner will not be a significant hydraulic barrier, and the liner is not included in the model, and is treated as EDZ material in the Salina G portions of the 2DR and 3DS model. The shaft is not included in the 3DSU model, where several formation hydraulic conductivities are of similar magnitude to shaft backfill material.

At the base of the shaft, a concrete monolith extends approximately 20 m beyond the edge of the shaft along the access and ring tunnels. Within the Hatch (2008) design, slightly different monolith sizes are used for the vent and main shaft. The geometric simplifications in the 2DR and 3DS model do not allow representation of this level of detail. The impact on simulated performance of different monolith sizes will be negligible. The composition of the concrete for the monolith and concrete bulkheads in the Deep and Intermediate Bedrock Groundwater Zones within the shaft have not yet been specified, and are assigned general low-permeable concrete properties and designated as **concrete_lower**. The last two concrete bulkheads above -10 mASL are conservatively assumed to have degraded slightly and therefore have somewhat higher permeabilities (Walke et al. 2009b), and are designated **concrete_shallow**.

The shaft has an inner and outer EDZ, with separate model properties defined for each geologic unit intersected by the shaft. EDZ property identifiers (IDs) are identical to the geologic unit IDs, with the “R” in the model ID replaced by an “I” for the inner EDZ and an “O” for the outer EDZ. For example, the Cobourg unit has rock, inner EDZ and outer EDZ model property IDs, labelled respectively as Cobourg_R, Cobourg_I and Cobourg_O. The inner EDZ (_I) extends from the shaft to an additional 0.5*(shaft radius) distance. The outer EDZ (_O) extends a further 0.5*(shaft radius) from the end of the inner EDZ.

Hydrogeological and transport properties for these materials are given in Table 4-4. Values for bentonite/sand, asphalt, backfill, and concrete are taken from Walke et al. (2009b). In actual fact the repository will have a very high hydraulic conductivity as it is primarily void space. However, numeric issues associated with permeability contrasts required that a nominal permeability is present for the code to execute successfully. A value of 10^{-6} m s^{-1} was chosen as an acceptable value that would not materially impact flow or transport results.

Table 4-4: Hydrogeological and transport properties for shaft, repository and EDZ materials

Unit	Porosity (-)	K (m s^{-1})	Specific Storage (m^{-1})	Tortuosity (-)
repository	0.061 (2DR) 0.065 (3DS)	1.0E-06	1.2E-05	1.00
access	0.184 (2DR) 0.264 (3DS)	1.0E-06	1.3E-05	1.00
repoEDZ	0.030	2.0E-08 (BC) 1.0E-11 (UG)	1.7E-06	0.06
bento_sand	0.300	1.0E-11	6.7E-06	0.33
asphalt	0.020	1.0E-12	3.6E-06	0.01
backfill	0.300	1.0E-04	1.2E-04	1.00
concrete_lower	0.150	1.0E-11	1.5E-06	0.02
concrete_shallow	0.250	1.0E-08	2.0E-06	0.50

Due to the large number of geologic units, and consequently the large number of inner and outer EDZ material types, Table 4-4 does not provide the properties for each EDZ material. Except for vertical hydraulic conductivity and porosity, EDZ properties are identical to rock mass properties given in Table 4-2.

Within the EDZ it is assumed that material properties are isotropic: vertical and horizontal hydraulic conductivity are identical. In the base case presented in this report the inner EDZ has an isotropic hydraulic conductivity 100 times greater than the associated rock mass vertical hydraulic conductivity, and the outer EDZ has an isotropic hydraulic conductivity 10 times greater. Inner EDZ porosity is twice the rock mass porosity and outer EDZ porosity is equal to that of the associated rock mass. For example, the Cobourg unit inner EDZ has a vertical hydraulic conductivity of 2.0×10^{-10} m/s and a porosity of 0.03, and the Cobourg unit outer EDZ has a vertical hydraulic conductivity of 2.0×10^{-11} m/s and a porosity of 0.015.

Differences in porosity for the 2DR and 3DS repository and access tunnel properties are due to the impact of different geometric simplifications, which lead to different volumes of model discretization being assigned **repository** and **access** property types. Porosities are calculated to adjust the model volumes to the correct void volumes as presented in Walke et al. (2009b). Differences in effective diffusivity are as a consequence of the different porosities.

For the NE-EDZ sensitivity case, the inner EDZ and outer EDZ conductivity are 10 000 and 100 times the rock mass vertical conductivity, respectively.

For the SF-ES1 disruptive event case, the shaft below the Salina G unit is assumed filled with a sand/granular material with a conductivity of 10^{-7} m s⁻¹ and a porosity of 0.40. Above the Salina F, the upper shaft backfill material conductivity is 10^{-4} m s⁻¹ with a porosity of 0.30.

The boreholes in the HI-GR and OB-BC cases are assumed to have been filled with a material with hydraulic conductivity of 10^{-4} m s⁻¹ and a porosity of 0.30.

4.2.3 Source Term and Radionuclide Properties

The reference radionuclide Cl-36 source term was defined by specifying an initial concentration for all repository elements. The initial concentration was calculated by assuming that the entire radionuclide inventory of Cl-36 is instantly dissolved at time 0 years. The inventory activity of Cl-36 was converted to a mass and divided by the void volume of the repository in the numeric model (Table 4-4) to obtain the initial concentration. The design by Hatch (2008) calls for placing intermediate level waste (ILW) (with some low level waste) in the east panel and low level waste (LLW) in the south panel. The activity of Cl-36 in ILW is much higher than in LLW (Walke et al. 2009b). For this reason, the initial distribution of Cl-36 in the 3DS model is almost entirely within the east panel, as this is where ILW will be placed.

According to Walke et al. (2009b), the Cl-36 activity is 3.93×10^7 Bq in the LLW to be deposited in the South panel and 1.13×10^{12} Bq in the predominantly ILW to be deposited in the East panel. These values were converted to masses of 3.21×10^{-5} kg and 0.922 kg respectively. For the 2DR models these masses were summed and distributed over the entire repository zone, yielding an initial concentration of 3.09×10^{-3} g m⁻³. For the 3DS models, the initial chlorine mass was distributed in the South and East panels according to the planned distribution of waste as outlined above. The calculated initial concentrations in the South and East panels are 1.87×10^{-7} g m⁻³ and 7.30×10^{-3} g m⁻³, respectively, for all cases.

Two additional parameters are needed to define the transport and decay of Cl-36. According to Walke et al. (2009b) the half life of Cl-36 is 301 000 years. A free water diffusion coefficient of $1.0\text{E-}9 \text{ m}^2/\text{s}$ was assigned. Material tortuosities are adjusted to yield calculated effective diffusion coefficients as specified in Walke et al. (2009b). Sorption of Cl-36 is not considered significant.

4.3 MODEL IMPLEMENTATION

This section presents the structure, discretization, property assignments, boundary conditions, and initial conditions for the three different models previously described in Section 2.4.

4.3.1 Model Structure

The detailed groundwater models use three different representations of the physical system. The 2DR and 3DS models both incorporate the shafts and EDZ in the overall system. For the 2DR and 3DS models, the model domain extends from the top of the Salina G Formation (at 8 mASL or approximately 178 mBGS) down to the top of the Cambrian sandstone at an elevation of -674.9 mASL (or 843.7 mBGS). The choice of the Cambrian sandstone as the lower boundary was dictated by a requirement to simulate pressurised conditions within this unit. In both the 3DS and 2DR models, the geology is represented as a flat “layer cake” system.

4.3.1.1 2DR Model

The 2DR model provides a dimensionally simplified representation and computationally efficient model of the system. The 2DR model cannot account for lateral advective flow. All flow is radial, vertical, or a combination of the two. This means that this model is not suitable for any conceptual model that includes horizontal gradients or a water abstraction well (unless the well is located at the centre of the repository shaft). For such problems a 3D model is required. The advantage of the 2DR model is that it allows a much greater mesh resolution than the 3D model, leading to significantly improved computational performance and the ability to assess the impact of much smaller features of the repository sealing system and rock formations.

The engineered components of the repository are simplified to comply with the radial model concept. The two shafts (Main and Ventilation) are merged into a single shaft that combines the cross-sectional area of both shafts in Walke et al. (2009b), which is based on the Hatch (2008) repository design. The repository is modelled as a radial segment of appropriate angle, thickness and volume. Figure 4.3 is a vertical cross-section of the conceptual model, showing all major components except the rock mass.

The repository design contains a central ring tunnel system with the access tunnels and emplacement panels to the south and east radiating outward from the centre of this ring at an offset of approximately 55° (see Figure 2.3).

In a 2DR model, only a very thin slice of the repository is modelled. Subsequently the flows crossing this slice are multiplied by the ratio of the slice area to the total required area to get the total flow and the mass transport from the repository. It is possible to distribute the repository area over any angle, depending on the conceptual model. Given the repository design, with the main and ventilation shafts close together and two repository panels radiating outward, a 90° 2DR model is appropriate.

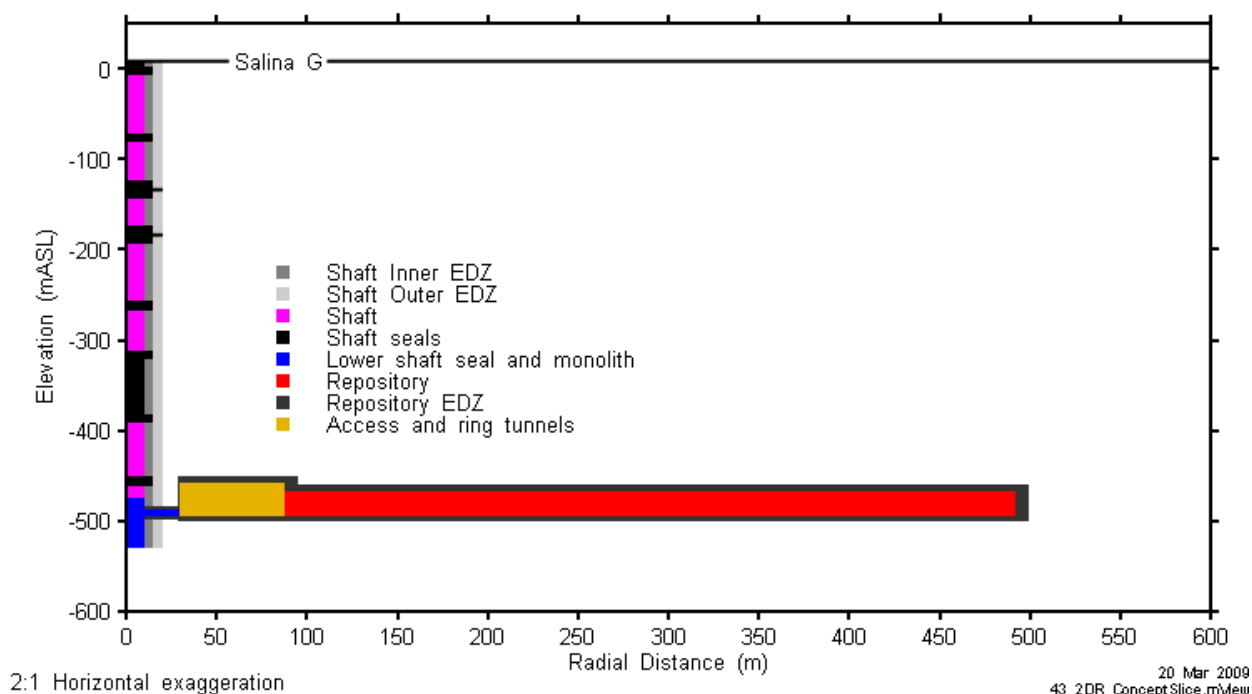


Figure 4.3: Vertical cross-section of 2DR model.

In the 2DR model, the repository area is distributed over 90 degrees and the combined shaft is located at the corner of the model (See Figure 4.4). The combined shaft represents the effective combined response of the Main and Ventilation Shafts. Table 4-5 shows the cross-sectional areas of the combined shaft and shaft EDZ. EDZ radii are defined in terms of the shaft radius (R_{shaft}), with the inner EDZ extending from the shaft wall to a radius of $1.5 R_{shaft}$, and the outer EDZ extending from $1.5 R_{shaft}$ to $2.0 R_{shaft}$. The shaft area and the inner and outer EDZ areas are combined to obtain the shaft dimensions for the model. The combined shafts are represented as a wedge (see Figure 4.4). This approximation is reasonable because flow in the shafts for all steady-state cases will largely be vertical, driven by the Cambrian overpressure at the bottom of the model domain.

Table 4-5: Cross-sectional areas of combined shaft (Walke et al. 2009b).

Shaft	Shaft radius	Inner EDZ Radius	Outer EDZ Radius	Shaft Area	Inner EDZ Area	Outer EDZ Area
	m	m	m	m ²	m ²	m ²
Main shaft	4.00	6.00	8.00	50.3	62.8	88.0
Vent shaft	3.00	4.50	6.00	28.3	35.3	49.5
Combined shaft	5.00	7.50	10.00	78.5	98.2	137.4
Combined shaft 90° wedge	10.00	15.00	20.00	78.5	98.2	137.4

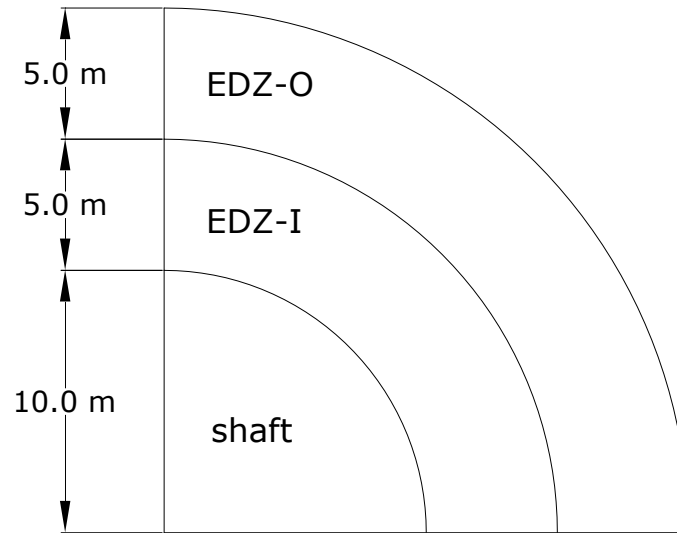


Figure 4.4: Plan section of shaft above monolith in the 90° 2DR model.

In the repository plan, there is a concrete “monolith” at the base of each shaft extending approximately 20.0 m beyond the edge of the shaft, shown at elevation -490 mASL in Figure 4.3. In the model, the areas of the two monoliths are not combined, as horizontal flow and transport in the monolith and in the EDZ surrounding the monolith are the relevant processes. Combining the two monoliths (as was done for the shaft components) would increase the horizontal path length from the access and ring tunnel system to the shaft. As a conservative simplification the combined monolith uses the 20 m distance rather than the corrected (larger) combined distance. In the 2DR model the monolith still extends 20.0 m beyond the edge of the combined shaft (see Figure 4.5). The monolith EDZ extends 4 m beyond the monolith into the surrounding rock on all sides.

The closure plan for the access and ring tunnels calls for using these tunnels to dispose of concrete debris from the shaft liner removal and to dispose of all used equipment. However, there will still be open space, and for the reference case it is assumed that there is 30 m of roof collapse above the top of the access tunnel (see Appendix A of the System and its Evolution report, Little et al. 2009), and that this collapse occurs immediately after closure. Consequently, the tunnels will be filled with rubble, with a very high effective permeability. These tunnels have been modelled simply as a high permeability and porosity zone with properties as described in Table 4-4. The thickness of the quarter ring representing the access tunnel zone is based on the average distance between the edge of the repository and the centre of the ring tunnel. For this model, the EDZ on all sides of the access and ring tunnels extends 7 m into the surrounding rock (Walke et al. 2009b).

For the repository itself the volume of the two repository panels has been calculated (including access tunnels, emplacement rooms, and pillars) and, using an average repository height of 6.7 m (Walke et al. 2009b) plus 20 m of rockfall (less than the ring tunnel because the rooms are partially filled with waste packages- see Appendix A of the System and its Evolution report, Little et al. 2009). This volume has been distributed in a quarter ring outside the access tunnel zone. This means that the path length from the repository and the repository EDZ to the shaft is somewhat shorter than the actual path length in the repository as planned. The repository

EDZ extends 7 m beyond the repository zone into the surrounding rock. A plan section of the model representation of the repository is shown in Figure 4.5.

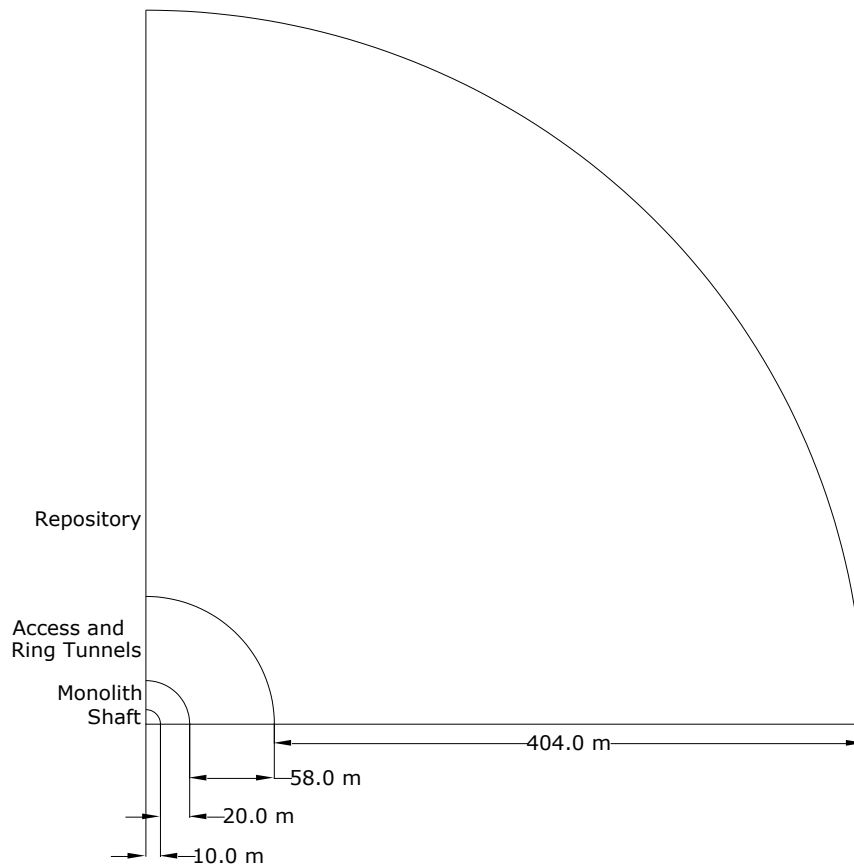


Figure 4.5: Plan section through monolith and repository at the repository horizon in the 2DR model.

4.3.1.2 3DS Model

As described in Section 2.4.1, the 3DS model is intended to model the repository footprint with greater fidelity to the Hatch 2008 design. The model includes separate repository panels and the ring tunnel. However, the main and vent shaft design is simplified with both planned shafts being represented with a single modelled shaft, located at the centre of the ring tunnel. Another simplification in this model is that the individual emplacement rooms are not explicitly represented, but rather they are combined with the repository pillars in a repository panel unit. Thus, the repository panels are modelled as two volumes, which roughly approximate the plan outline of the repository as shown in Figure 4.6. This approach simplifies the modelling process by reducing the required level of discretization, while not significantly compromising the modelling capacities of the model. Shaft, tunnel and repository EDZ parameters are the same as previously described for the 2DR model.

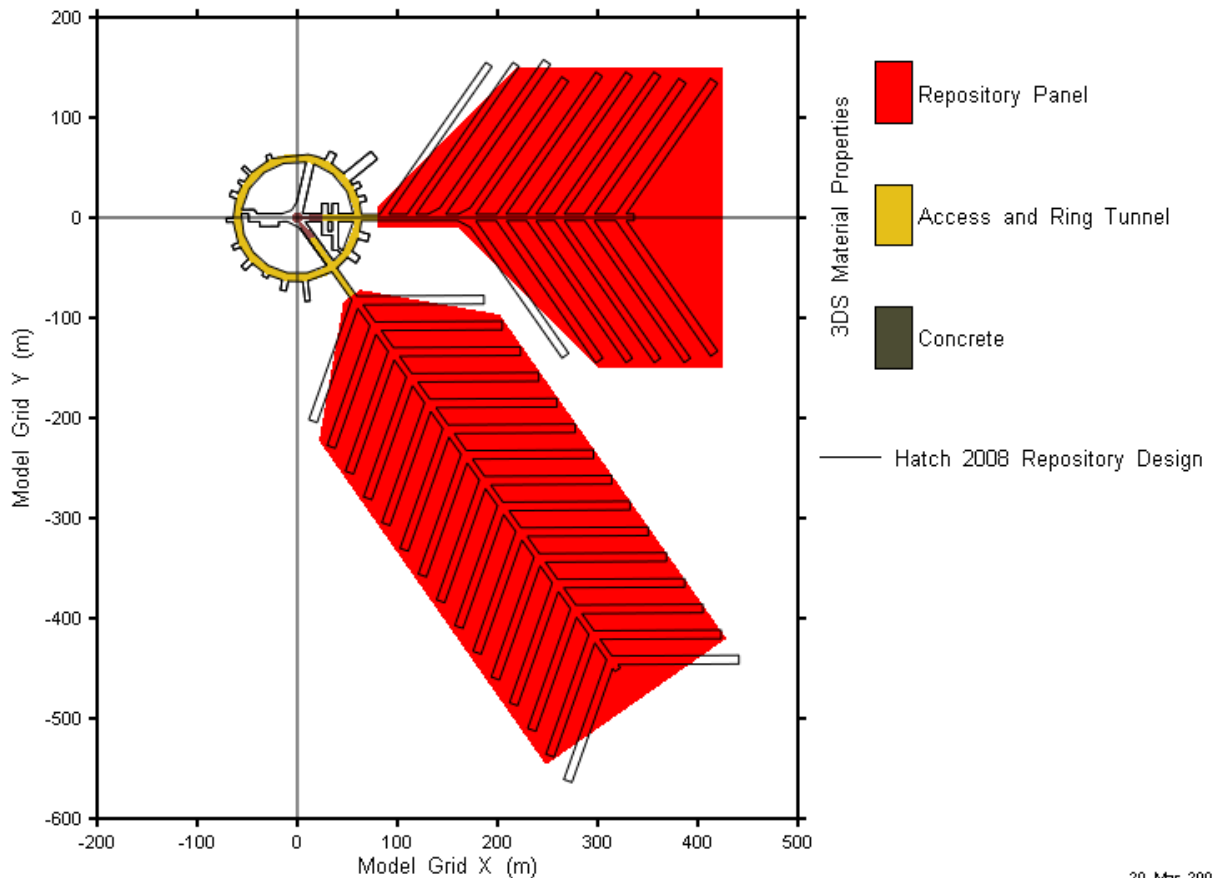


Figure 4.6: Plan outline of 3DS repository panels

Note that Figure 4.6 uses a modelling coordinate system with its origin at the centre of the ring tunnel and a positive X axis extending along the main access tunnel for the East Panel. This modelling coordinate system will be used in all further 3DS figures for this report.

4.3.1.3 3DSU Model

The 3DSU model characterises the rock mass of the shallow bedrock groundwater system as completely isolated from the intermediate bedrock groundwater zone. The goal of this model is to investigate how mass exiting at the top of the Salina F units (the top of the intermediate bedrock groundwater zone) will be captured by a downstream drinking water well or enter Lake Huron. This highly simplified conceptual model of the shallow bedrock groundwater system includes the Salina G and the Devonian units only (Lucas, Amherstburg, Bois Blanc, and Bass Island).

The system to be modelled is represented in plan as a rectangle with sides parallel and perpendicular to the prevailing head gradient and is conceptually oriented on the Bruce site as shown in Figure 4.7. While the exact lake margin will change with time, it is conservatively assumed that any mass flow leaving the model boundary is transferred quickly to the lake.

The dimensions of the model are 1700 m long (parallel to gradient) and 1200 m wide (perpendicular to gradient).

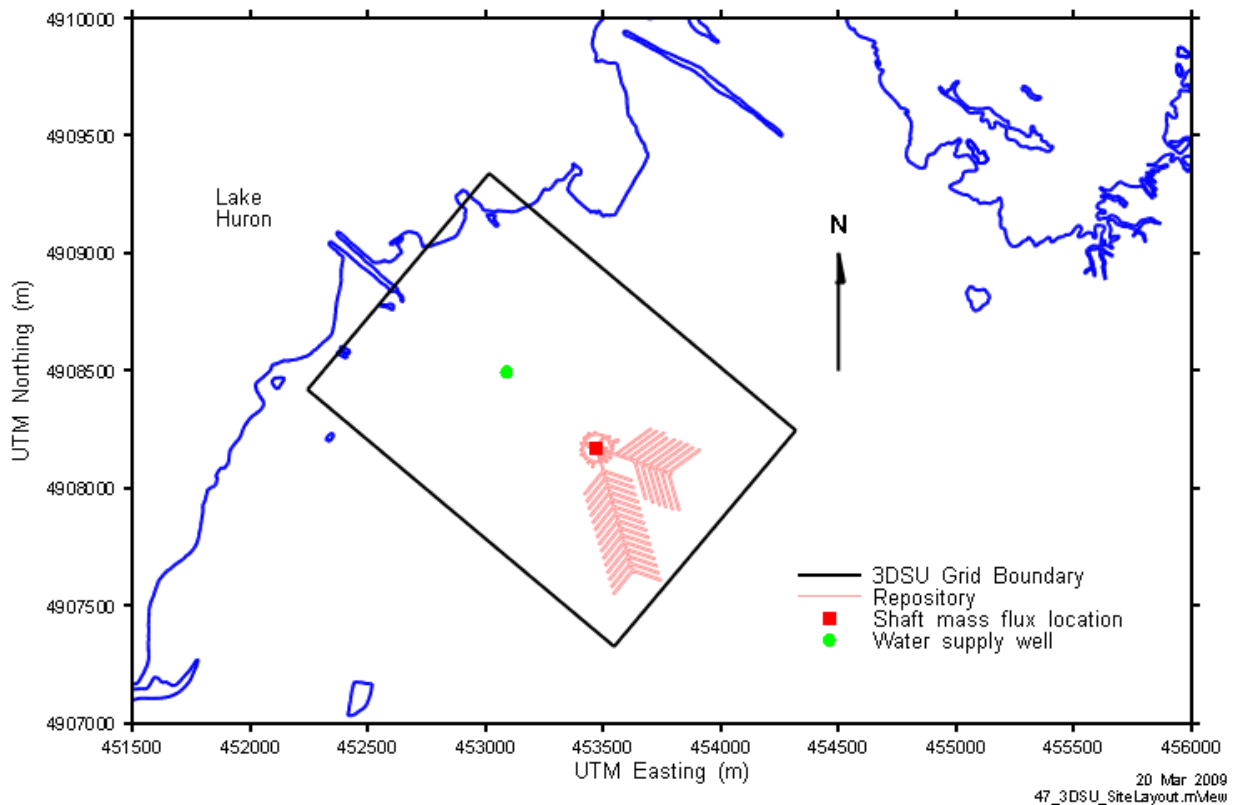
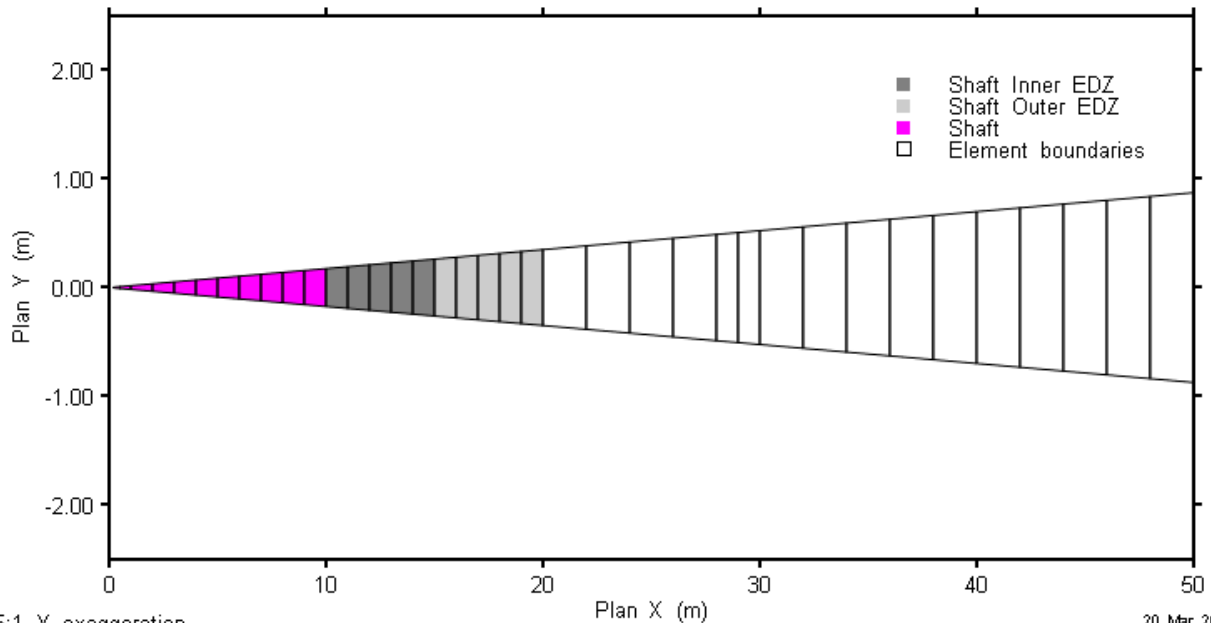


Figure 4.7: Plan outline of 3DSU grid

4.3.2 Model Discretization and Property Assignment

4.3.2.1 2DR Model

In plan section, the 2DR grid is constructed of a radial slice of 4-sided elements. The one element thick slice is then projected vertically to obtain an array of 6-sided elements. The total included angle of 0.0349 radians (2.0 degrees) represents 1/45th of a quarter circle. Flows from the model must be multiplied by a factor of 45 to obtain the total flow from the system. Figure 4.8 is a horizontal slice of discretization above the monolith, showing property assignments for the shaft itself and the inner and outer shaft EDZ.



5:1 Y exaggeration

20 Mar 2006
48 2DR ConceptPlan.mxd

Figure 4.8: Plan outline of inner portion of 2DR discretization

Vertically, the model is divided into 429 layers. The model grid spans the formations from the top of the Cambrian (-657.9 mASL) to the top of the Salina G unit (8 mASL), as shown in Figure 4.9. Note that discretization is not shown in the figure as it would completely obscure property assignments at the figure scale.

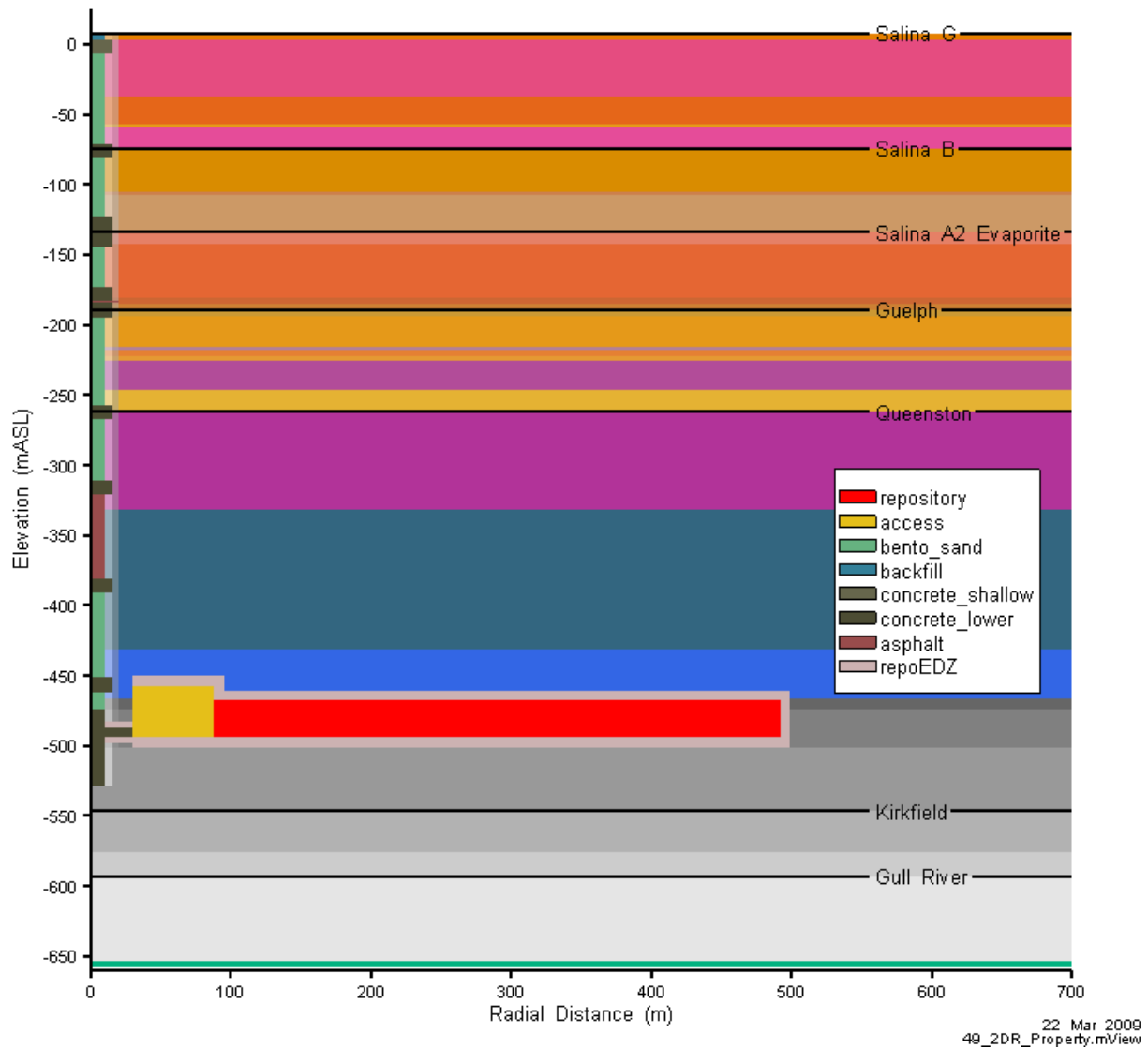


Figure 4.9: Detail of 2DR model property assignments.

Vertical discretization is refined at various elevations to resolve repository and seal features.

Horizontally, the mesh is finest within about 30 m of the shaft centre, to resolve the shaft, the inner and outer EDZ, and the concrete monolith. The discretization remains relatively fine past the end of the repository, beyond which the mesh size increases. The 2DR model is discretized with a total of 196 radial increments of progressively increasing size out to an external boundary radius of 3000 m. The horizontal and vertical discretization results in a mesh with approximately 169 000 nodes and 84 000 elements.

Figure 4.10 and Figure 4.11 show details of the discretization at the shaft monolith and at the asphalt waterstop seal located at the bottom of the Salina A1.

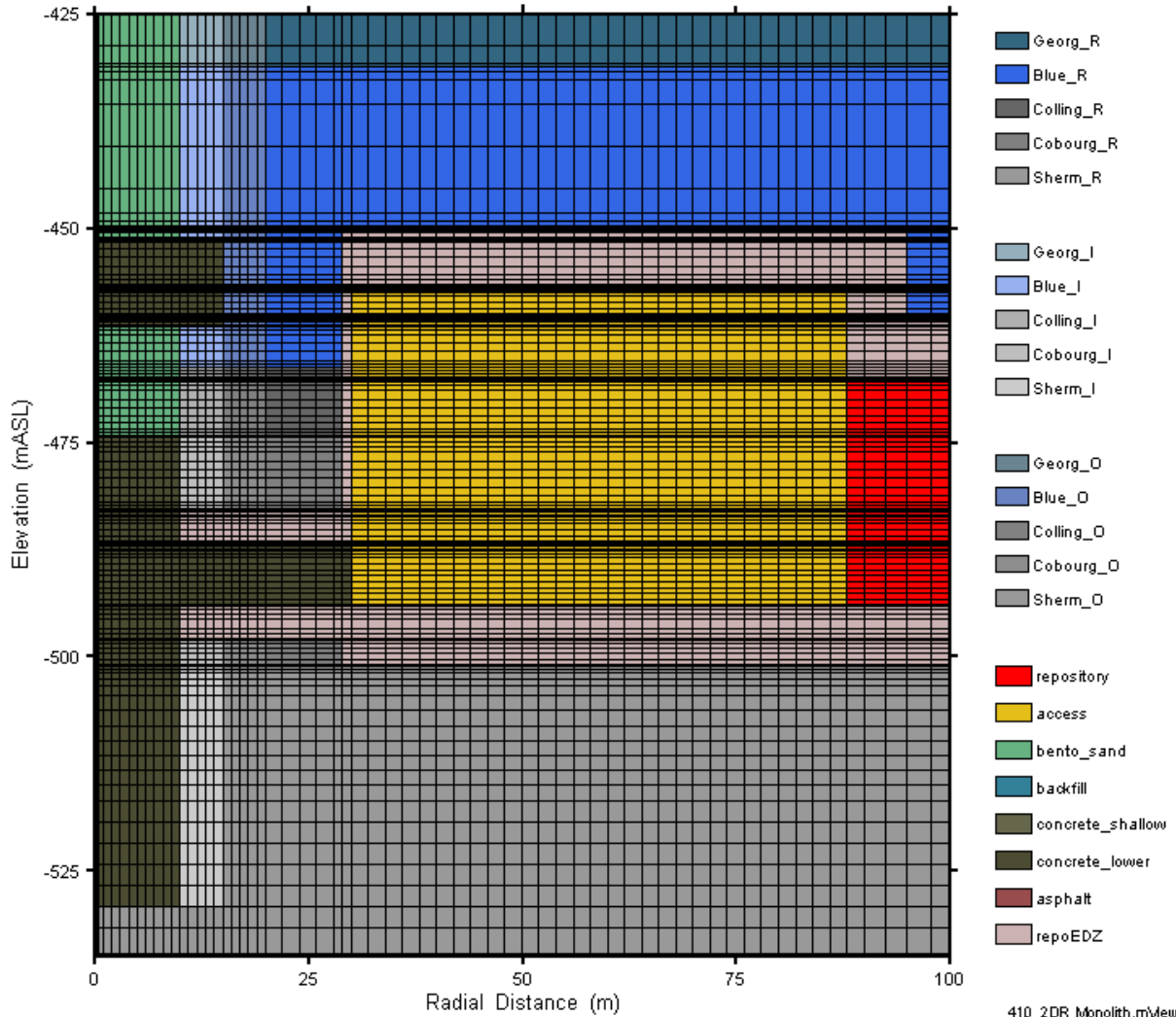


Figure 4.10: Detail of model repository (2DR model), access tunnel zone, monolith, shaft, and EDZ.

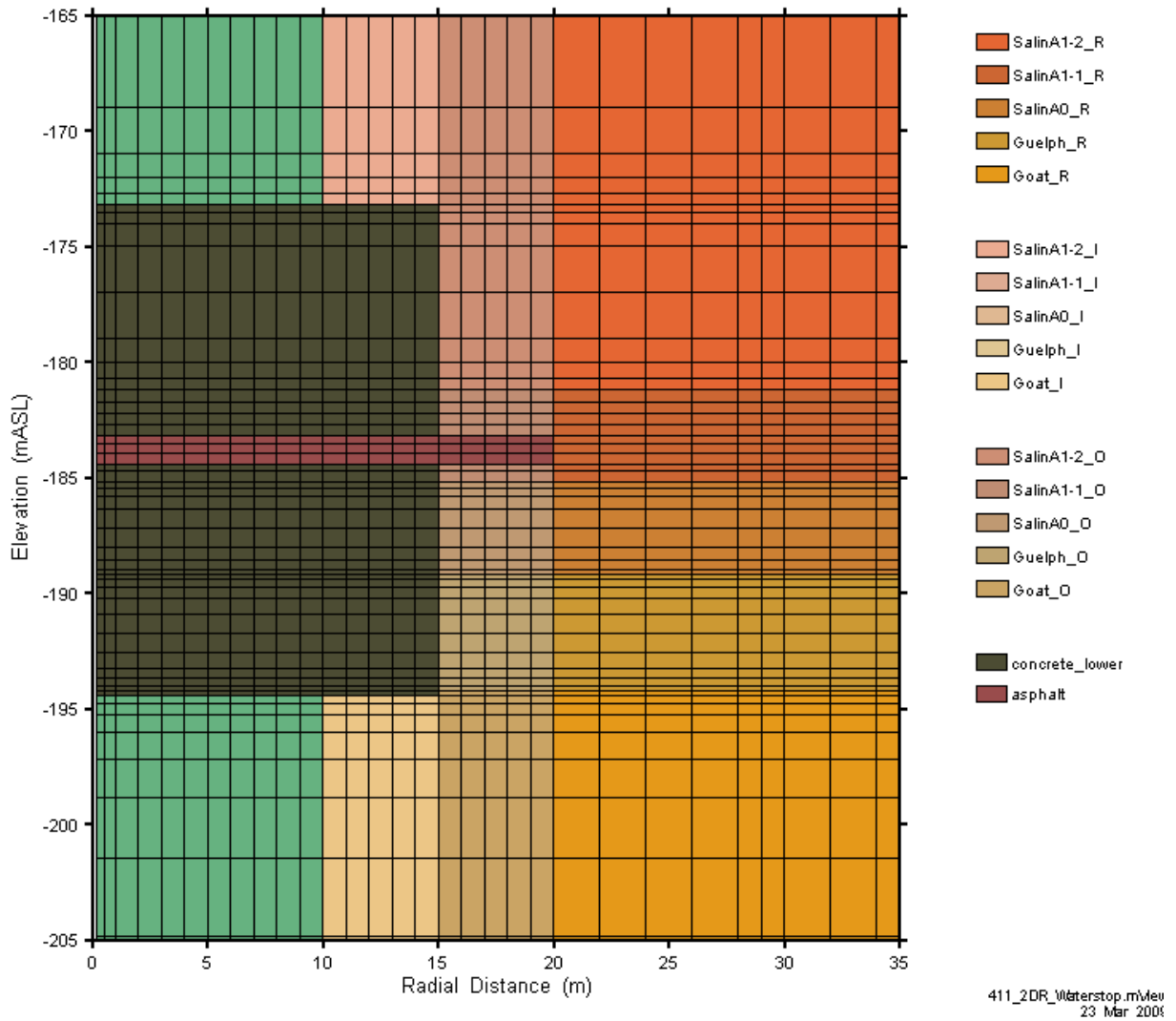


Figure 4.11: Detail of asphalt waterstop system at Salina A0/Salina A1 (2DR model).

Shaft seal discretization and property assignment for the NE-EDZ case (increased EDZ permeability, ineffective shaft seals) is shown in Figure 4.12.

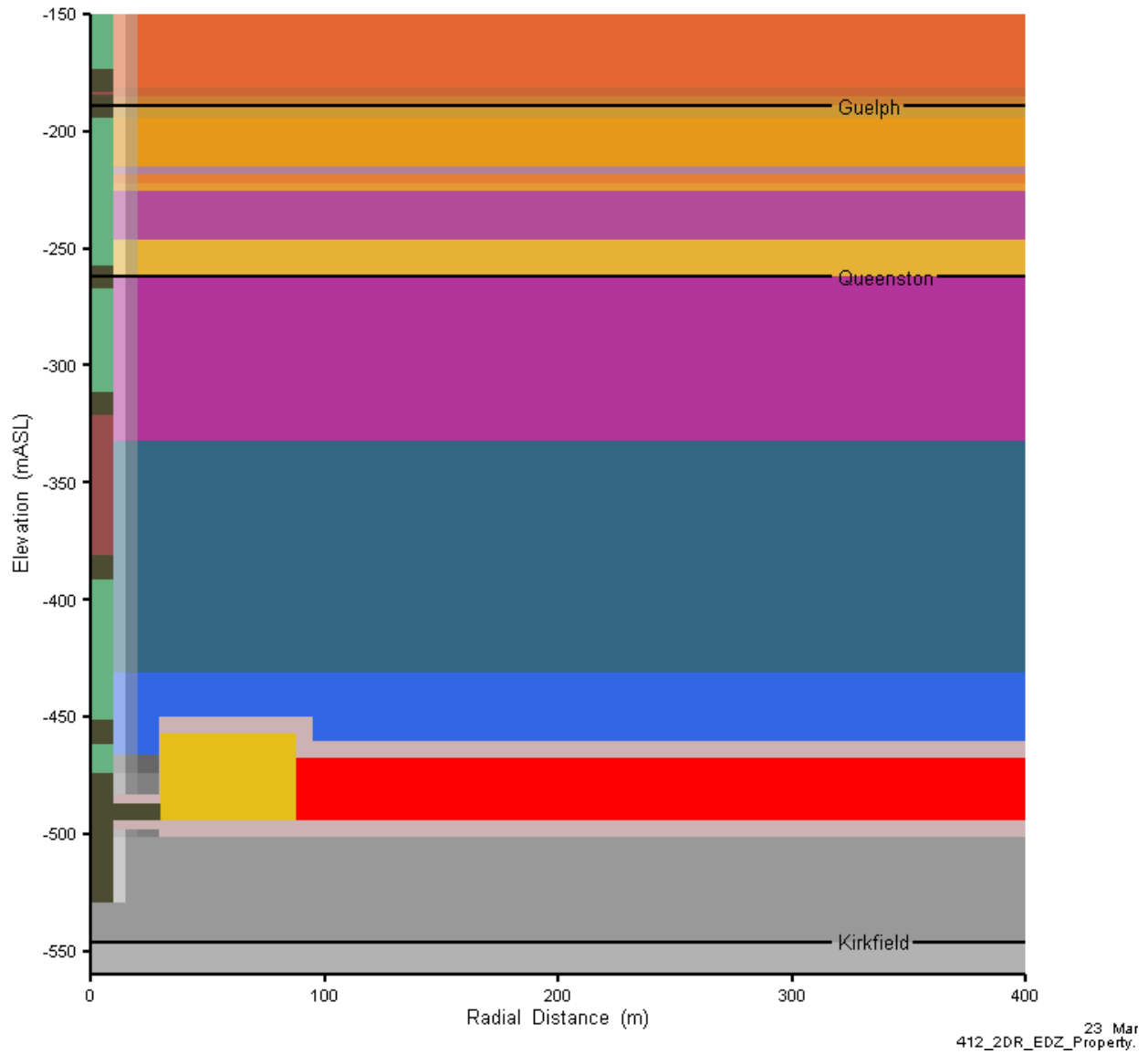


Figure 4.12: Detail of model repository (2DR model), access tunnel zone, monolith, shaft, EDZ, and lowest concrete bulkhead for the NE-EDZ case.

4.3.2.2 3DS Model

Vertical discretization of the 3DS model is similar to the 2DR model, but with a reduced number of layers to increase computational tractability. Differences are also found in property assignments as the 3DS model includes the ring tunnel and access tunnels in a spatially correct fashion. Figure 4.13 shows property assignments on a vertical slice through the shaft and East panel at Y = 0 m.

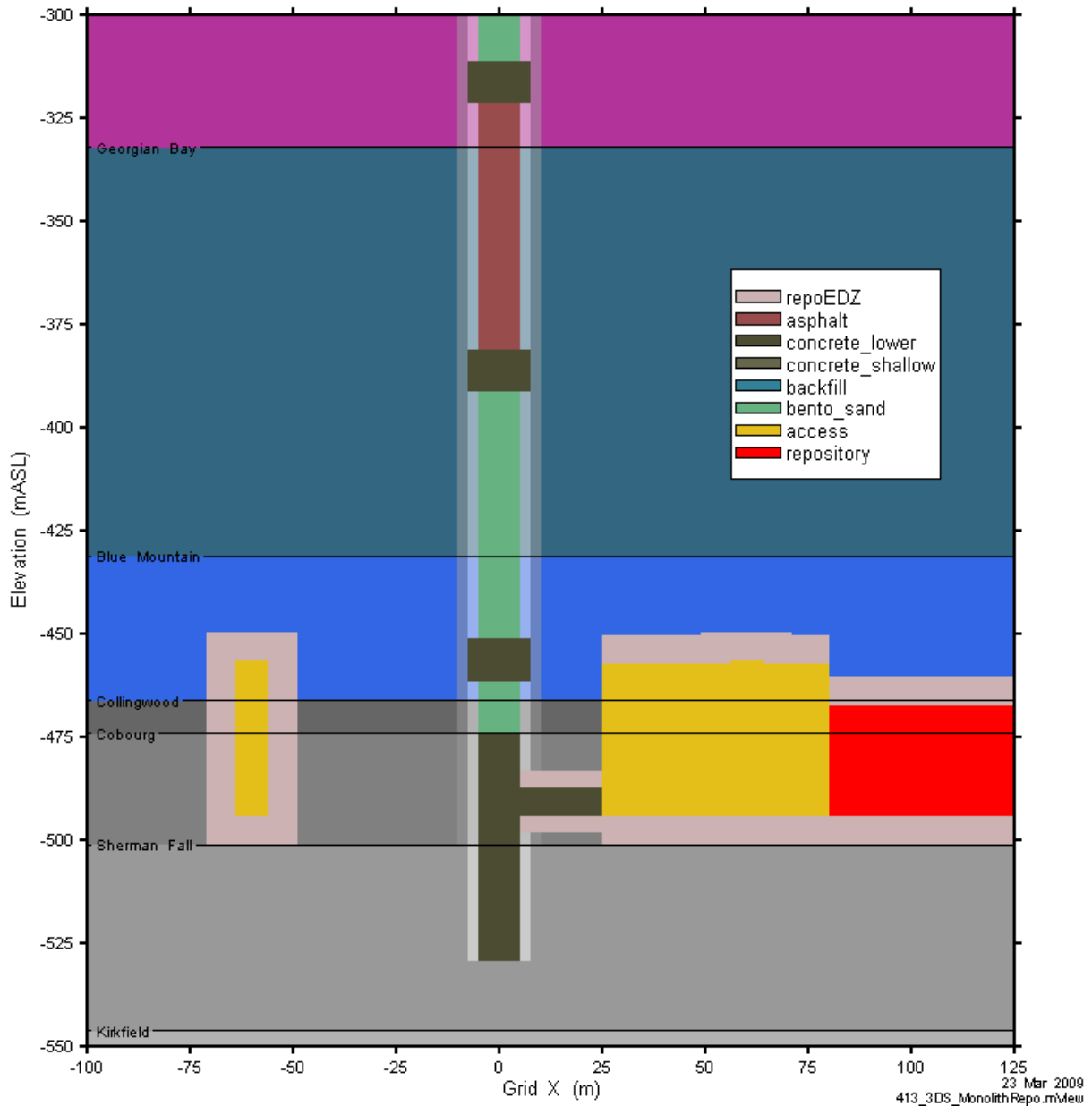


Figure 4.13: 3DS model vertical layout of repository, access tunnel zone, monolith, shaft sealing system, and EDZ properties.

Figure 4.14 is a three-dimensional illustration of the 3DS repository and property assignment. In this figure the EDZ surrounding the shaft, repository, and access tunnels is shown as transparent.

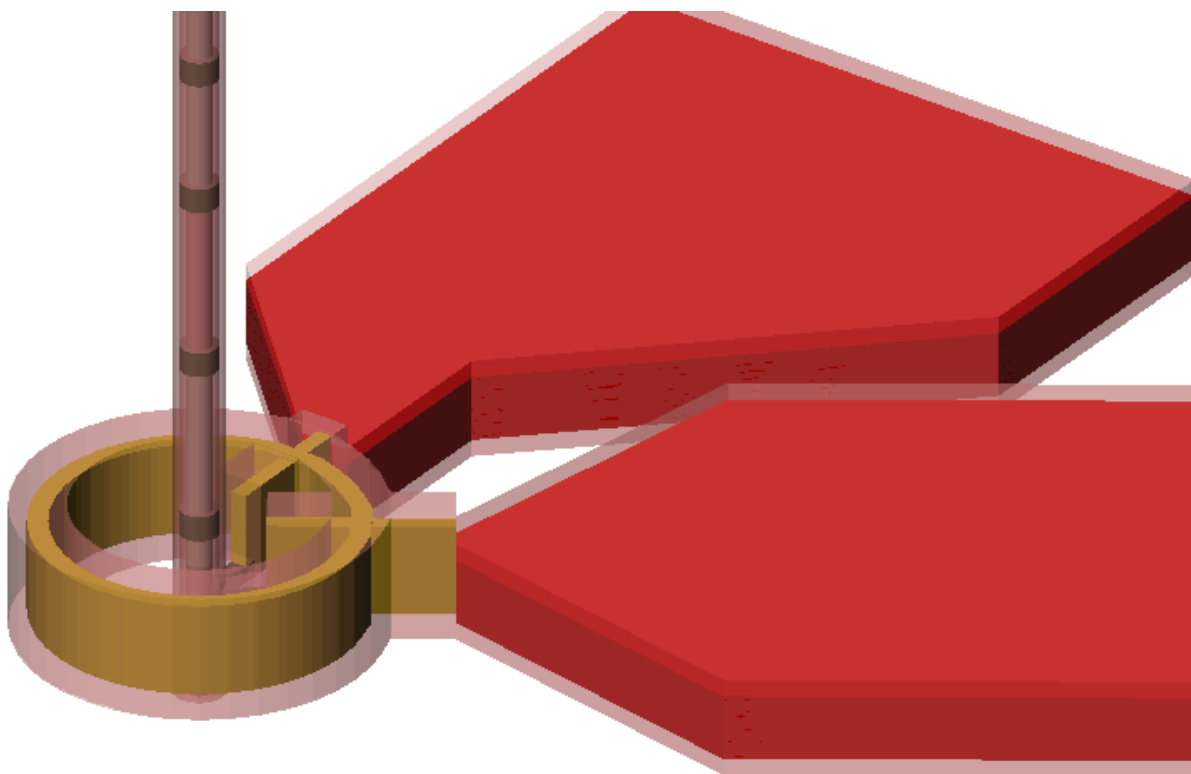
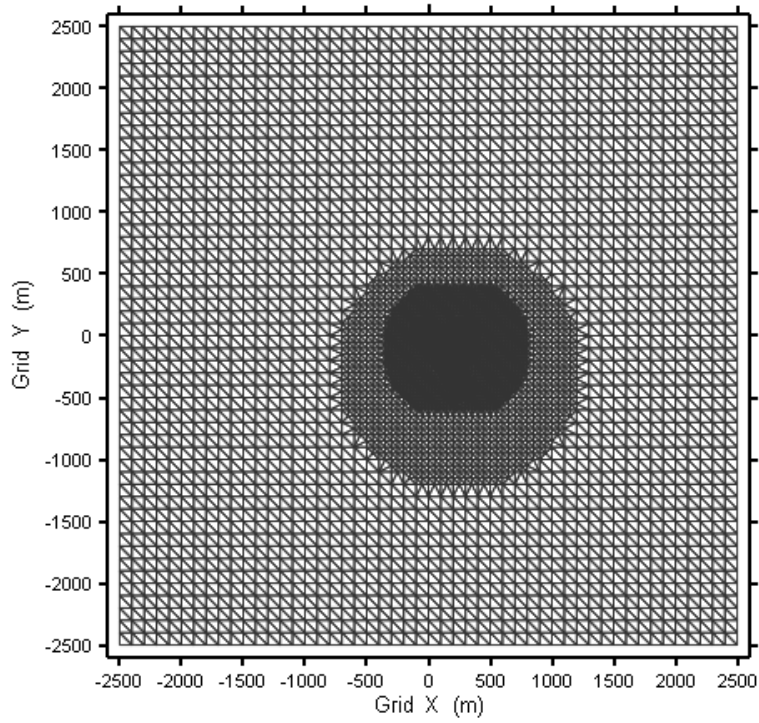


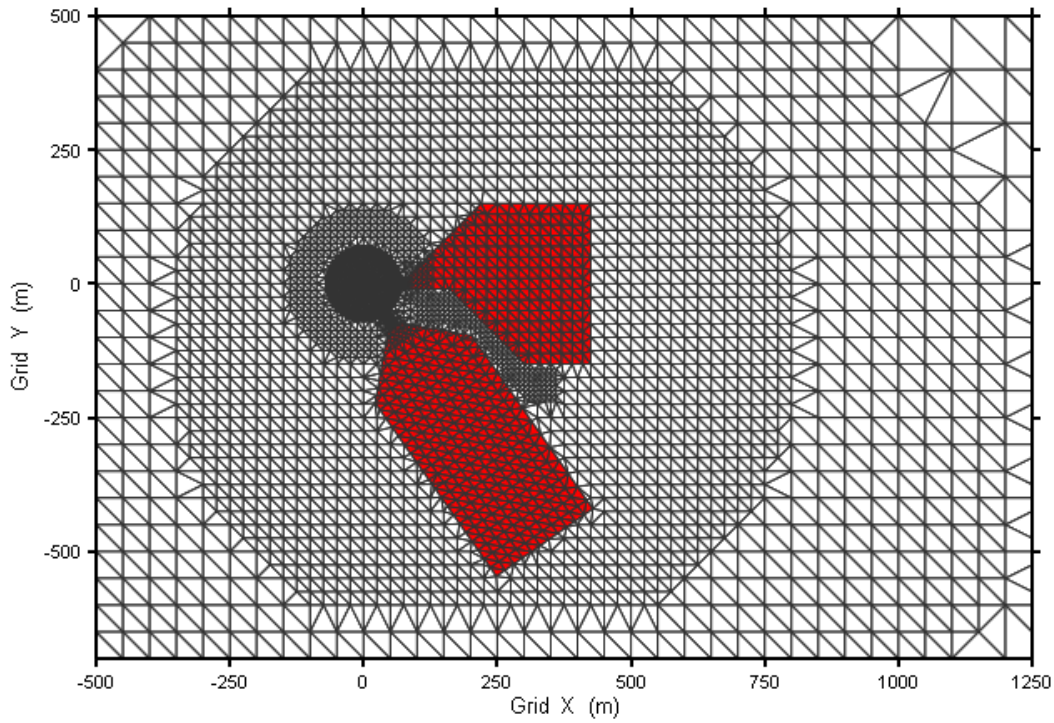
Figure 4.14: 3DS model 3D layout of repository, access tunnel zone, monolith, shaft sealing system, and EDZ (transparent) properties.

The 3DS model differs significantly from the 2DR model in plan section discretization. The 3DS model uses a triangular finite-element approach to provide high spatial resolution within the vicinity of the repository. The sequence of figures below (Figure 4.15 to Figure 4.18) shows the discretization in increasing levels of detail.



23 Mar 2009
415 18 3DS Plan.mView

Figure 4.15: 3DS model plan section view of discretization of entire model domain. Darkest area has the finest discretization



23 Mar 2009
415 18 3DS Plan.mView

Figure 4.16: 3DS model plan section view – repository detail.

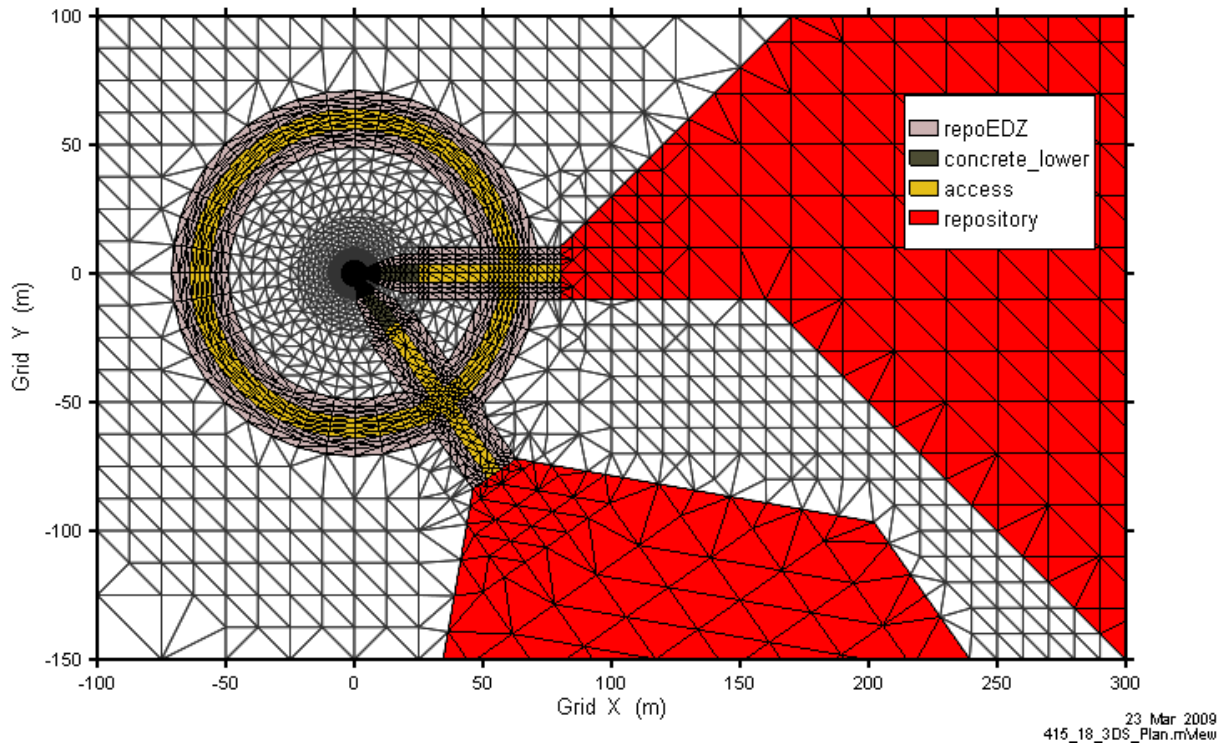


Figure 4.17: 3DS model plan section view – ring tunnel detail.

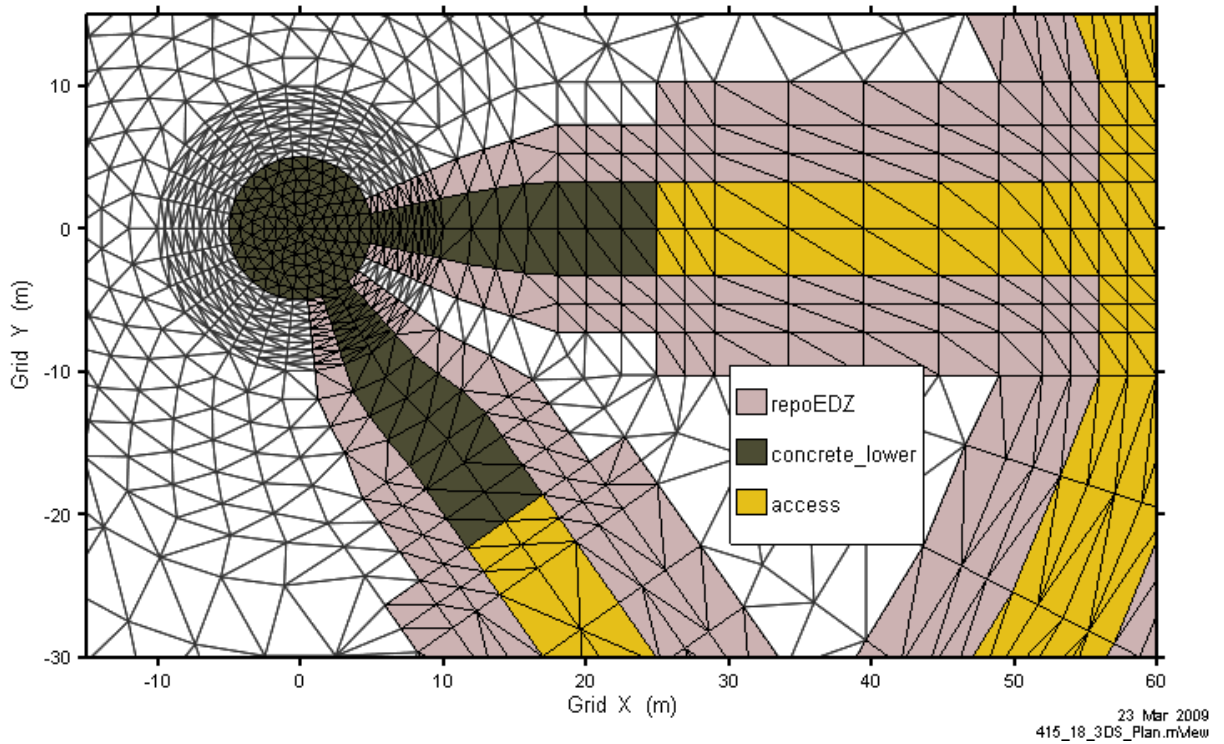


Figure 4.18: 3DS model plan section view – shaft, EDZ and tunnel detail.

The plan view discretization contains 6883 nodes and 13 564 elements. There are 306 layers in the model, yielding approximately 2 100 000 nodes and 4 100 000 elements.

The NE-UG-RD1 calculation case uses different property assignments within the repository access tunnels, as shown in Figure 4.19. In this case the access tunnels and ring tunnels are filled with concrete and the EDZ surrounding the tunnels is reduced to 4 m thick to reflect the effect of the additional support provided by the concrete, consistent with the EDZ surrounding the monolith.

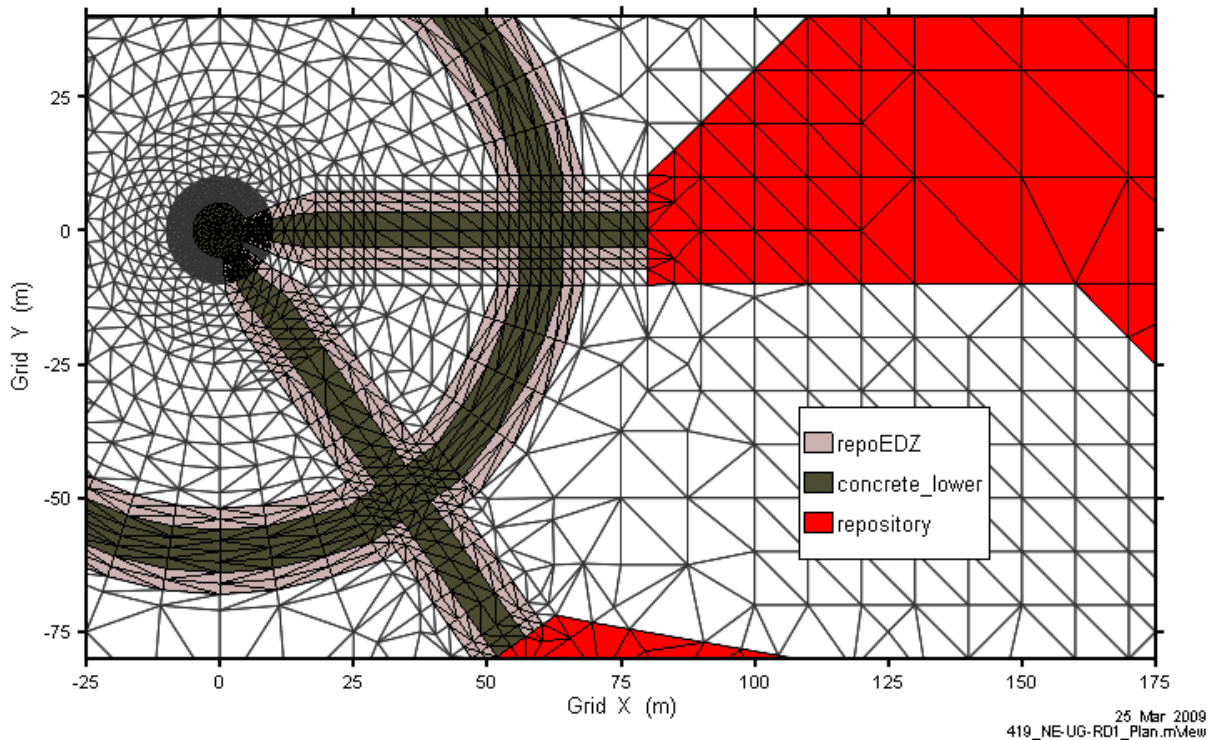


Figure 4.19: 3DS NE-RD1 model plan section view

The Disruptive Scenario HI-GR, OB-BC and EE-BC cases use variants on the 3DS model grid. For the HI-GR case, a borehole intersects the approximate centre of the East panel. The borehole is implemented as a sequence of high conductivity line elements extending from the top of the repository to the top of the model. The line element properties are consistent with a 16.5 cm (6.5 inch) diameter borehole, filled with relatively high conductivity material similar to the shaft backfill described in Table 4-4. Additional discretization, shown in Figure 4.20 as the round zone in the middle of the East panel, is included to minimize numeric errors associated with the steep concentration gradients expected near the borehole.

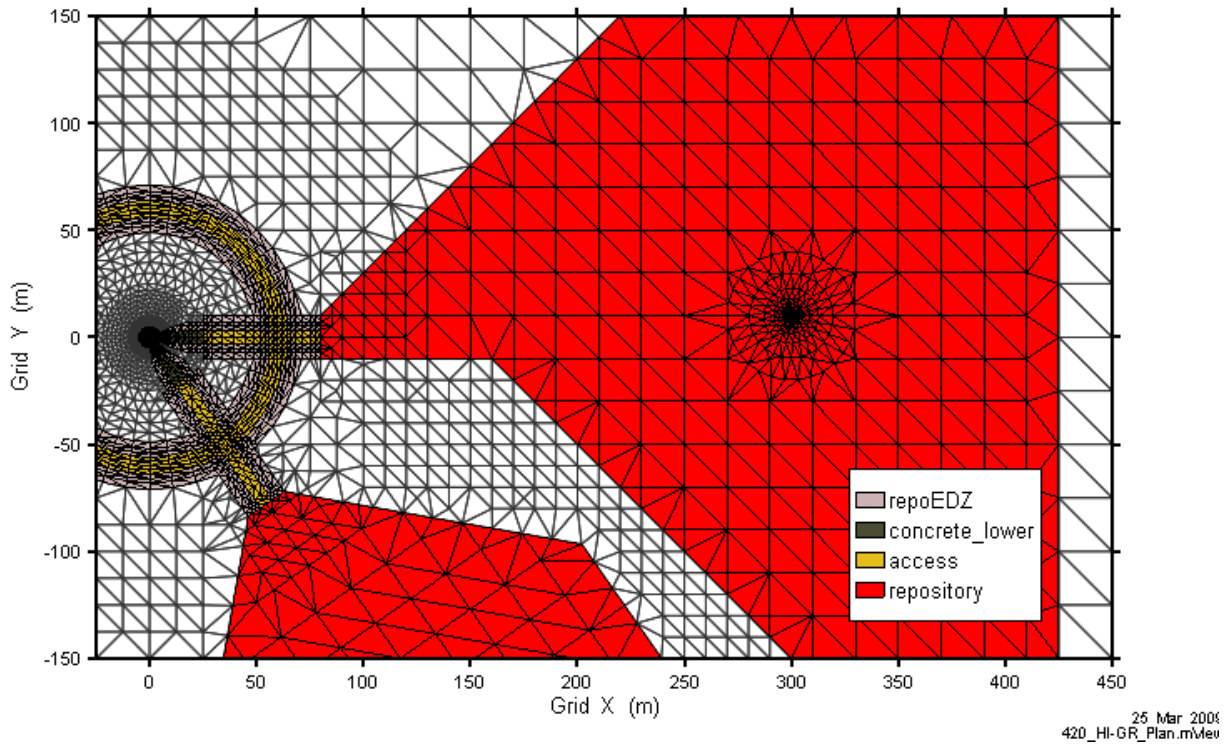
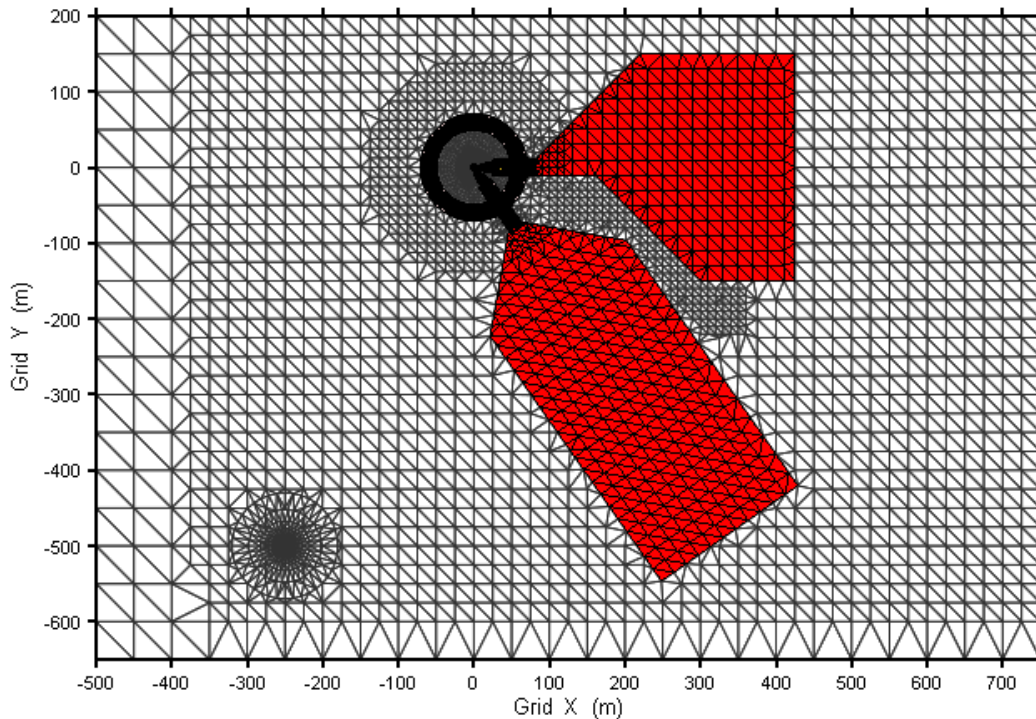


Figure 4.20: 3DS HI-GR model plan section view – borehole detail.

Similar discretization is used for the OB-BC case (Figure 4.21), with the borehole located at the approximate location of current site characterization borehole DGR-3. In this case the line elements extend through the entire model. The line element properties are consistent with a 14.25 cm (5.625 inch) diameter borehole, filled with high permeability material. Actual closure plans for DGR-3 have not yet been developed, but would involve closure with much lower conductivity material (bentonite or cement) than used in this conservative case.



25 Mar 2009
421_OB-BC_Plan.mView

Figure 4.21: 3DS OB-BC model plan section view.

In the EE-BC case a vertical fault is incorporated in the grid at $X = -500\text{m}$, as shown in Figure 4.22. The fault extends through the entire model domain in the Y and Z directions and is one metre thick in the X direction. As described in Section 4.2.1, a new group of material properties were defined (Shadow_E through Amherst_E) with vertical hydraulic conductivities three orders of magnitude higher than for the associated rock mass unit. Porosity values in the fault are the same as the associated rock mass unit.

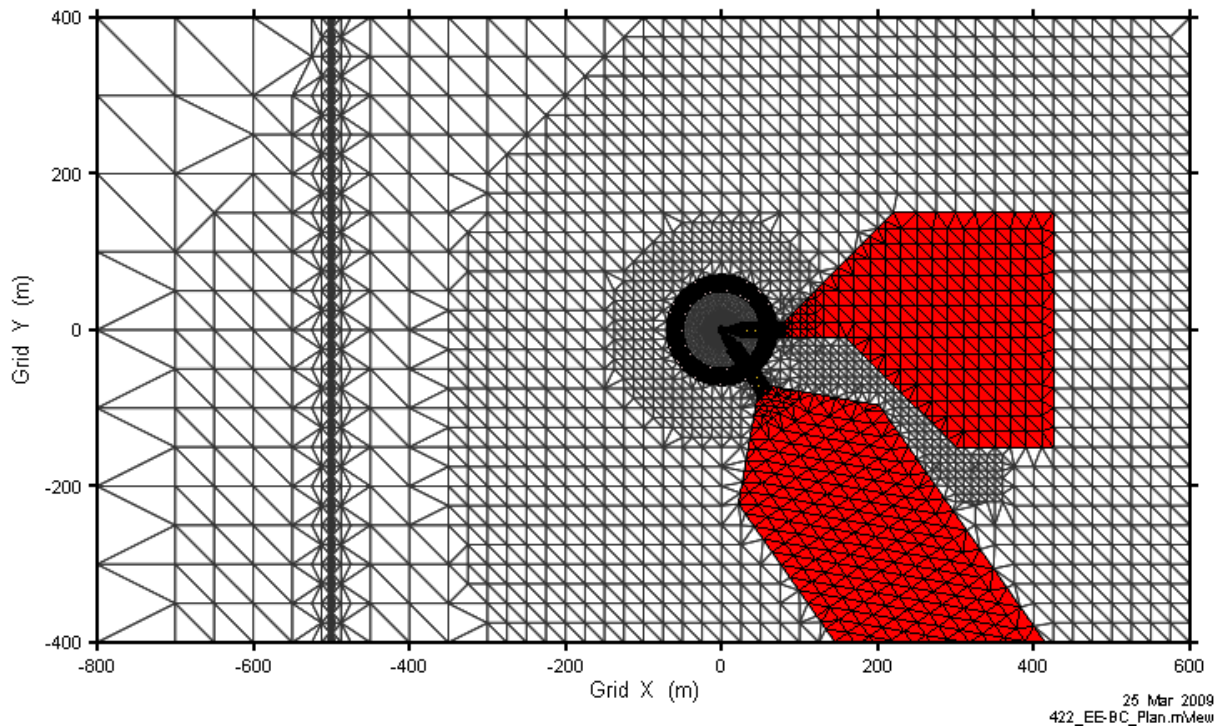
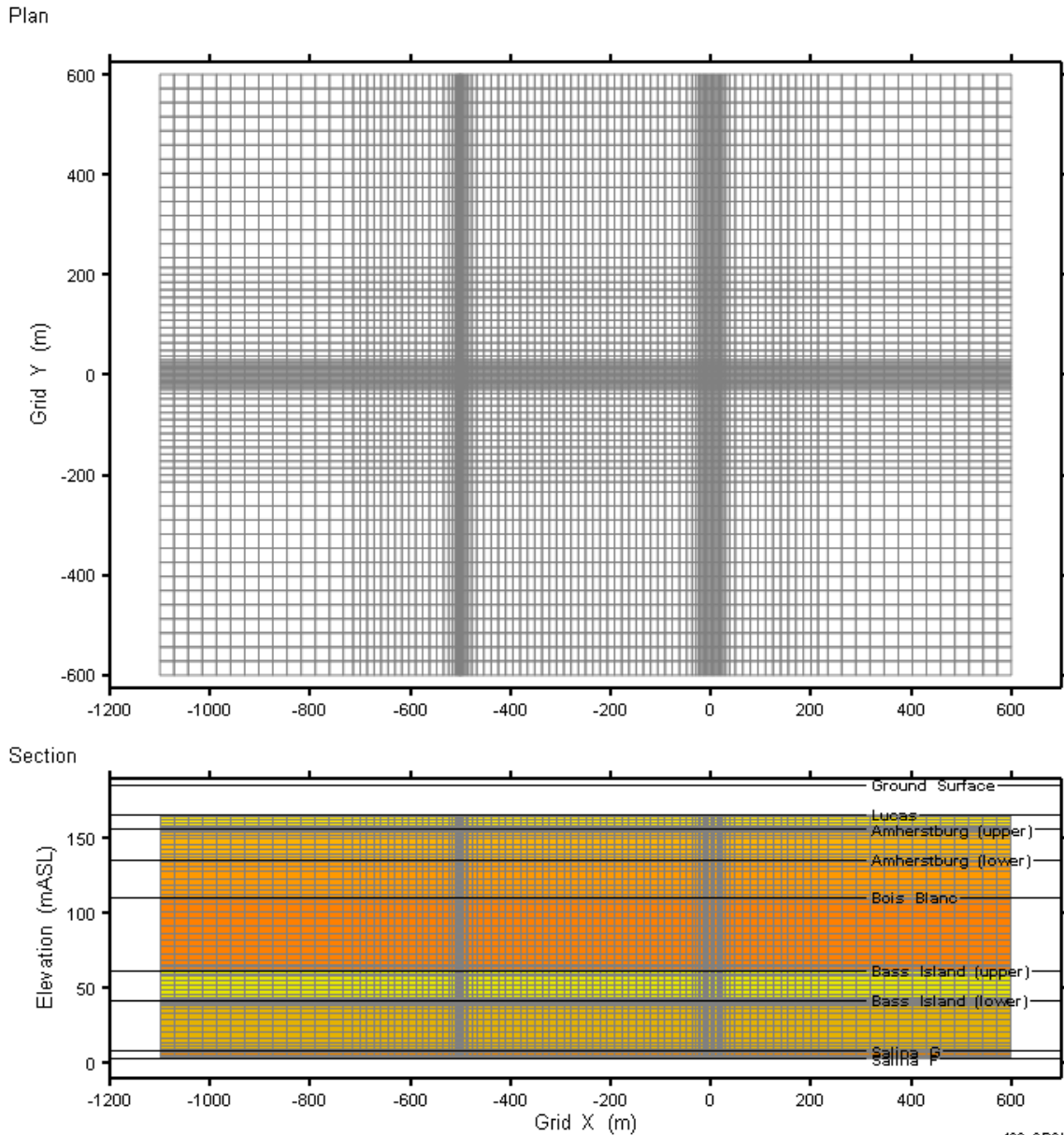


Figure 4.22: 3DS EE model plan section view – fault detail.

4.3.2.3 3DSU Model

The 3DSU model spans the formations from the top of the Salina F unit (2.7 mASL) to the top of the Lucas unit (165.7 mASL). The 3DSU model is made up of hexahedral elements. The model is refined in the vicinity of the source zone and the extraction well to resolve steep concentration fronts and drawdown. Grid size varies between a minimum of approximately 4 m and a maximum of approximately 30 m. As described in section 4.3.1.3, the dimensions of the model are 1700 m long, 1200 m wide, and 163 m thick. The resulting mesh, shown in Figure 4.23, has approximately 585 000 nodes and 565 000 elements in 72 layers.



Vertical exaggeration = 3:1

423_3DSU_Grid.mView
25 Mar 2009

Figure 4.23: Plan and section of 3DSU mesh.

4.3.3 Boundary and Initial Conditions

4.3.3.1 2DR and 3DS Models

Both the 2DR and 3DS models have fixed head boundary conditions on the top and bottom layers of the model, defining a vertical gradient in the system. All modelling cases apply a 140 m total change in head, with the top model surface (at 8 mASL) having a defined head of 0 m, and the bottom surface (at -657.9 mASL) having a defined head of 140 m. The value of zero at the top of the Salina G assumes no substantial vertical gradients in the Devonian system. The value of 140 m represents the environmental head calculated from measured Cambrian overpressures, presented previously in Figure 2.2.

The 2DR model cannot account for lateral advective flow in the model domain. All flow is radial, vertical, or a combination of the two. The external boundary at $R = R_{\max}$ (where $R_{\max} = 3000$ m) is zero-flow. External transport boundaries are zero mass flux.

All 3DS models except for NE-NHG and NE-UG-NHG incorporate horizontal flow in the permeable Salina units (the Guelph/Salina A0 and Salina A2 evaporite). In these units, constant head boundary conditions are imposed to achieve a specified gradient of 0.002. The gradient is oriented in the Grid X direction with flow from left to right. Actual gradients at the Bruce site are not known at this time, but will be determined as further site characterization data becomes available. Boundary condition heads are calculated by first simulating the steady-state flow field with zero flow boundaries, and then modifying the calculated heads in the permeable units to force the required gradient. Equal values (5m) of head are added to nodes on the left grid boundary (at $X = 2500$ m) and subtracted from nodes on the right side (at $X = -2500$ m) for the permeable units.

Zero flow vertical boundary conditions are specified for all other units, and for all units for the NE-NHG and NE-UG-NHG cases.

Initial head conditions for the transient NE-UG-NHG case were derived from the head elevation relationship presented previously in Figure 2.2.

4.3.3.2 3DSU Model

The 3DSU model imposes a horizontal head gradient of 0.003 (Walke et al. 2009b) over the entire model domain. This corresponds to a head differential of 5.2 m over the 1700 m length. The bottom, top, and Grid Y side boundaries are no-flow.

The source, which represents the top of the combined main and vent shafts, is located 1100 m upstream of the lake boundary at Grid X = 0. The source is defined as a specified mass flux boundary, with the flux rate based on the total mass exiting the Salina F unit in the 2DR or 3DS model. As outlined in Walke et al. (2009b) the reference case well location is 500 m downstream of the shaft, and the bottom of the well is at elevation 105.7 mASL (80 mBGS). The well is screened over the interval from 40 to 80 mBGS and has an abstraction rate of $2871 \text{ m}^3 \text{ a}^{-1}$.

Figure 4.24 shows the location of 3DSU model boundary conditions, well, and source.

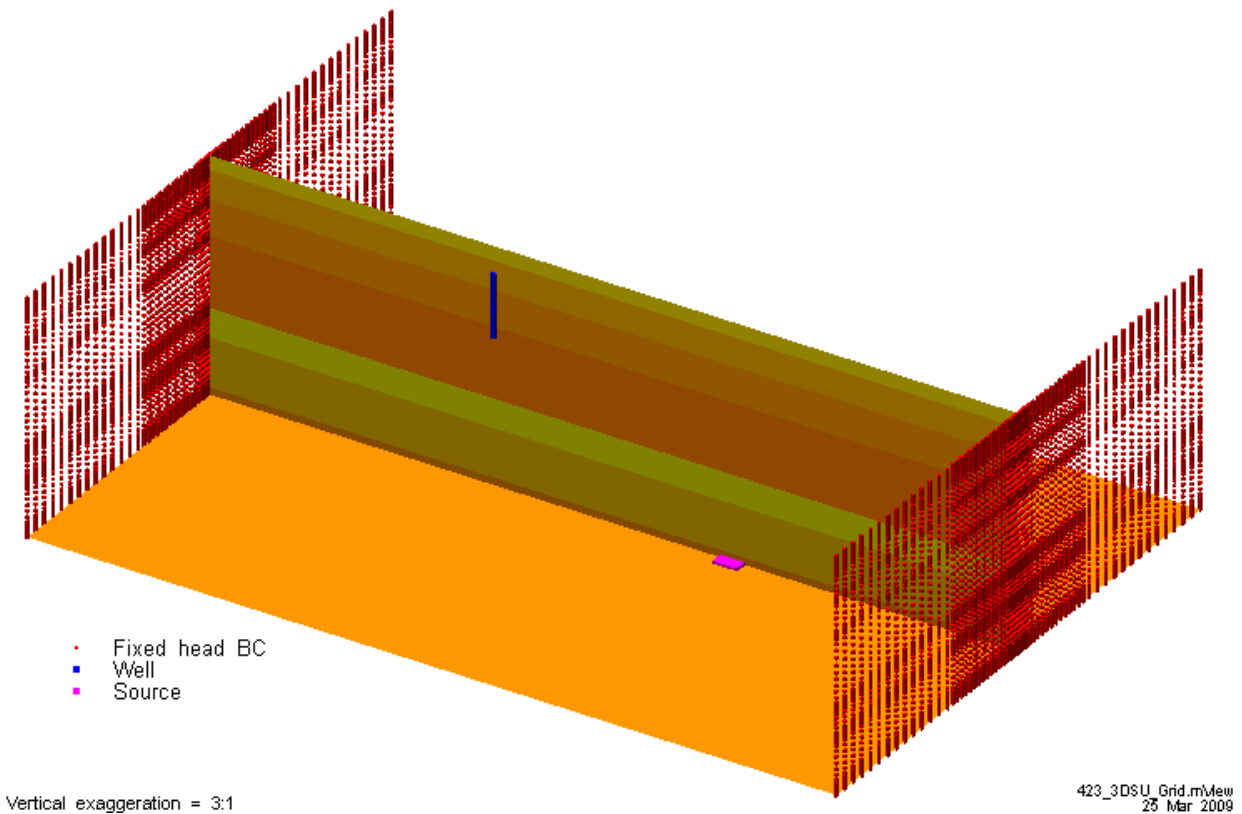


Figure 4.24: 3D view of reference case 3DSU model with boundary conditions.

5. RESULTS FOR THE NORMAL EVOLUTION SCENARIO

The 2DR and 3DS reference case models were run for a 1 000 000 year assessment period with steady-state flow or transient flow, depending on the calculation case. The radionuclide of interest was Cl-36 with an initial mass of 0.922 kg in the repository (see Section 4.2.3).

5.1 Results Presentation

Results are presented in graphical format using a variety of visualization approaches. Where possible, results presentations are limited to the data ranges that are physically relevant. However, in some cases it is necessary to present very low results to allow effective comparison of different case results.

5.1.1 Flow Results

Flow results are reported largely through the use of hydraulic head and advective linear velocity contour plots.

Hydraulic head ranges and contours are adjusted to best display the data being presented. For example, vertical cross-section plots of the entire model domain will generally show a hydraulic head range of 0 to 140 m with contours at 5 m intervals, while horizontal cross-sections at the repository horizon may show a range of several metres with a sub-metre contour interval.

Advective linear velocities are generally mapped to a logarithmic colour scale over the range from 10^{-2} to 10^{-6} m a⁻¹. Values outside this range are portrayed with the colour associated with maximum or minimum as appropriate. Some figures will have an expanded range if necessary. For most advective velocity figures presented in this report, velocity vectors are shown only for those regions where velocities exceed 10^{-4} m a⁻¹ (i.e., at least 100 m of advective transport in 1 Ma). In general, the vector length is scaled by log velocity, however the scaling factor varies depending upon figure scale, and vector lengths should be regarded as a qualitative indication only.

5.1.2 Transport Results

Transport results are reported through the use of both two-dimensional and three-dimensional Cl-36 concentration contour plots and Cl-36 mass transport flows across defined control planes.

Contour plots of Cl-36 concentrations are generally limited to concentrations exceeding 10^{-7} g m⁻³. Although the deep and intermediate groundwaters are saline and not drinkable, as a benchmark it is noted that a Cl-36 concentration of 10^{-7} g m⁻³ in drinking water yields a dose of approximately 10^{-7} Sv a⁻¹ or 0.1 μSv a⁻¹, (based on an ingestion rate of 2.3 L d⁻¹ and a dose coefficient of 9.3×10^{-10} Sv Bq⁻¹ from the Data report, Walke et al. 2009b). Concentrations at and below this level would have no significant impact.

Mass flow results indicate the mass of contaminant passing through a hypothetical plane or area. Mass flow results are reported directly as flows in g a^{-1} and as cumulative mass based on integrated flows. Cumulative mass presentations are not adjusted for radioactive decay after the mass has been accumulated at the plane.

Three horizontal mass transport planes have been defined at:

1. -262.2 mASL, the interface between the Queenston and Manitoulin units (denoted Ordovician MF on figures);
2. -107.2 mASL, the interface between the Salina A2 carbonate unit and the Salina B anhydrite unit (denoted Salina B MF); and
3. 2.8 mASL, the interface between the Salina F and Salina G units (denoted Salina F MF).

The Ordovician plane results indicate the effectiveness of the main geologic barrier, the Ordovician shales and limestones. The Salina F MF plane results are indicative of mass flow to the accessible and potable shallow bedrock groundwater zone, while the Salina B results can be used as an indicator of mass flow into the permeable Silurian zones. The difference between Salina B and Ordovician results allows assessment of the impact of any diversion of groundwater flow by the more permeable Guelph/Salina A0 and Salina A2 evaporite.

At each elevation, the mass transport planes are divided into two regions representing the shaft and the EDZ (denoted EDZ), and the rest of the model domain (denoted Rock). Where appropriate, the mass flow rates in the EDZ and Rock are combined to obtain the total mass flow across the model plane.

The 3DS model results also include two vertical mass transport planes transecting the Guelph/Salina A0 (denoted Guelph MF) and the Salina A2 evaporite (denoted Salina A2 MF) at a distance 100m downgradient of the shaft. These planes capture horizontal mass flow in the permeable Silurian units.

Most mass flow plots are limited to mass flow exceeding $10^{-10} \text{ g a}^{-1}$. Assuming a mass flow of Cl-36 of this magnitude was captured by a water supply well pumping $2871 \text{ m}^3 \text{ a}^{-1}$ (the reference case well abstraction rate from Data report, Walke et al. 2009b), this mass flow would yield an average concentration of $3.5 \times 10^{-14} \text{ g m}^{-3}$, corresponding to a dose over nine orders of magnitude below the dose criterion. For all practical purposes, this is a zero dose.

Results from some of the cases, particularly for the UG geosphere, show mass flows that are orders of magnitude below even this insignificant amount. To allow comparison of cases, mass flow axis limits for these cases are extended to $10^{-15} \text{ g a}^{-1}$ or lower. Concentrations corresponding to these flows are well below the detection limits of the most advanced analytic equipment and should be considered as equivalent to zero.

5.2 Reference Case (NE-RS1-F3 & NE-UG-RS1-F3)

The NE-RS1 model is the steady-state geosphere with the reference horizontal gradient (0.002) in the Guelph/Salina A0 and Salina A2 evaporite formations. It is simulated with the 3DS model only as the 2DR model does not support horizontal gradients. This section presents results for the base case geosphere and updated geosphere (UG).

5.2.1 NE-RS1-F3

5.2.1.1 Flow Results

Flow modelling results are presented in nine figures on the following pages. Figure 5.1 through to Figure 5.5 present the hydraulic head profiles on 2-dimensional vertical and plan sections through the model, with magnified views at a number of key locations, namely the repository, the concrete monolith bulkhead, and the seals near the permeable Silurian units. Figure 5.6 through Figure 5.10 show the advective velocity magnitudes and vectors for the same model regions.

Figure 5.1 through Figure 5.4 reveal the basic attributes of the groundwater system. The reduced pressure and relatively high hydraulic conductivity of the repository and the surrounding EDZ causes it to act as a drainage system, drawing water from the surrounding formations towards the shaft EDZ. This water flows laterally through the repository and EDZ until it reaches the shaft and migrates upward due to the constant Cambrian overpressure. The reduced pressure in the repository is due to its connection to the lower hydraulic heads at the surface through the increased conductivity shaft EDZ. The shaft and EDZ system also acts as a drain, drawing water in from the adjacent units. One interesting feature is that flow coming up through the shaft EDZ surrounding the concrete plug below the repository is directed outwards from the shaft, through the monolith EDZ and into ring tunnel. This feature is illustrated in Figure 5.4 and Figure 5.10 and is a consequence of the steady-state hydraulics of the system, where the access tunnels, ring tunnels and repository serve as preferential flow paths due to their very high conductivity.

The movement of groundwater is very slow throughout the entire system, as shown by Figure 5.6 to Figure 5.10, with the highest advective velocities on the order of 10^{-2} m a^{-1} . The influence of the horizontal gradient in the permeable Silurian units can be clearly seen as the vertical contour lines within the magenta lines on Figure 5.1. The highest advective velocities in the model system occur in these units, with average linear velocities of approximately 0.01 m a^{-1} in the Guelph/Salina A0 and 0.006 m a^{-1} in the Salina A2 evaporite over the model domain. The slanted contour below the Guelph represents the response of the lower permeability underlying units to the horizontal gradient within the Guelph/Salina A0. Outside of the permeable Silurian units, the highest velocities occur largely in the shaft EDZ. The calculated velocities are a function of Darcy fluxes (which are a function of hydraulic conductivity) and porosity of the material. Higher velocities occur where porosity is relatively low, hydraulic conductivity is relatively high, or particularly where low porosity and higher conductivity coincide.

The vertical hydraulic gradient is steepest in the lowest permeability Silurian units, the Cabot Head and Salina A1. Most of the head drop within the system occurs over the Silurian interval. Figure 5.9 shows that the shaft and EDZ “short-circuit” the gradient across the Salina A1, diverting flow from the Guelph/Salina A0 upwards to the Salina A2 evaporite.

This calculated vertical hydraulic gradient varies substantially from the measured heads on site (Figure 2.2), where the Silurian intervals are at near hydrostatic, with overpressures present in the lower Silurian formations only, and serves as further indication that the current reference hydraulic conductivities and/or the steady-state flow system are not representative of present-day site conditions.

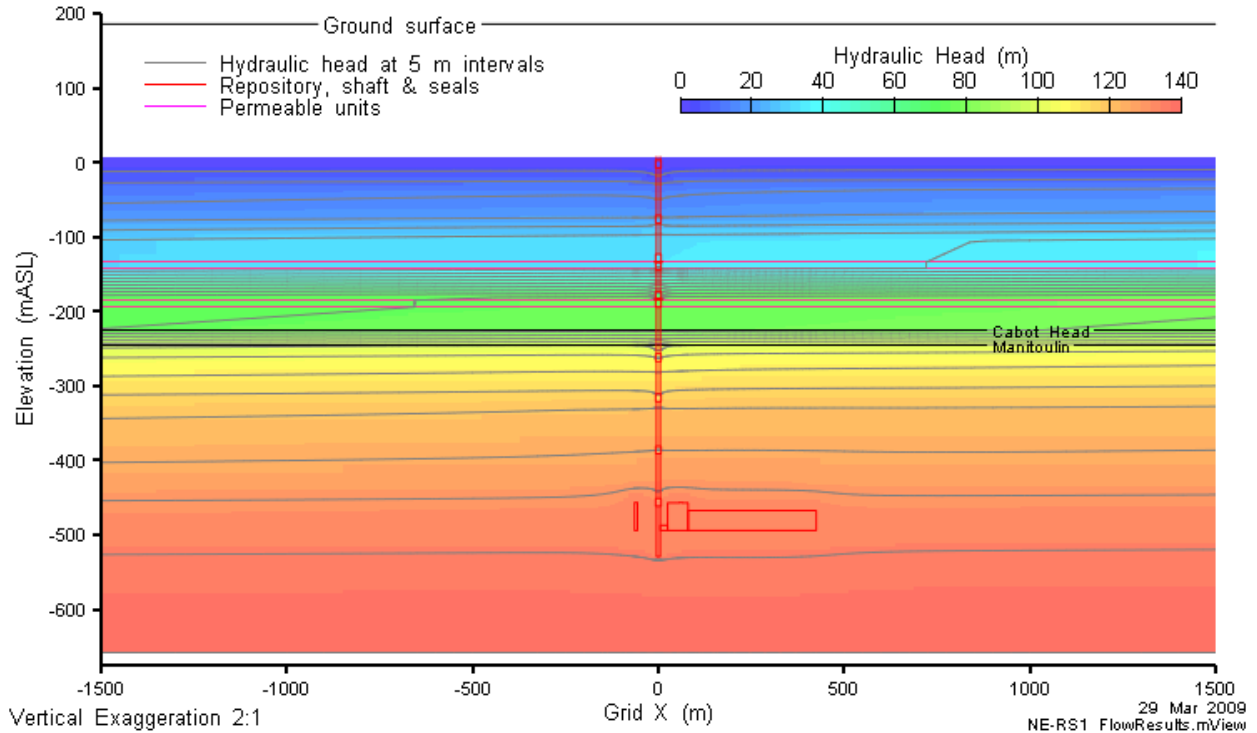


Figure 5.1: NE-RS1-F3 model head contours on a vertical slice through Grid Y=0.

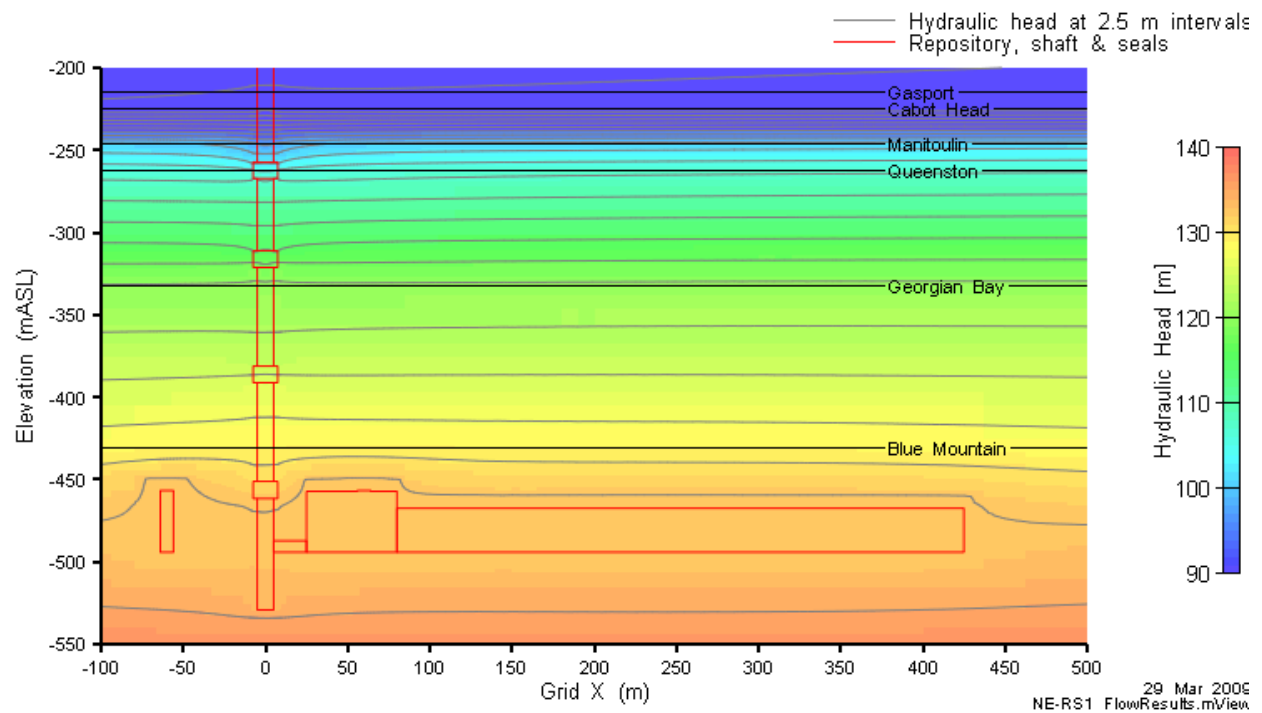


Figure 5.2: NE-RS1-F3 model head contours in the vicinity of the repository on a vertical slice through Grid Y=0.

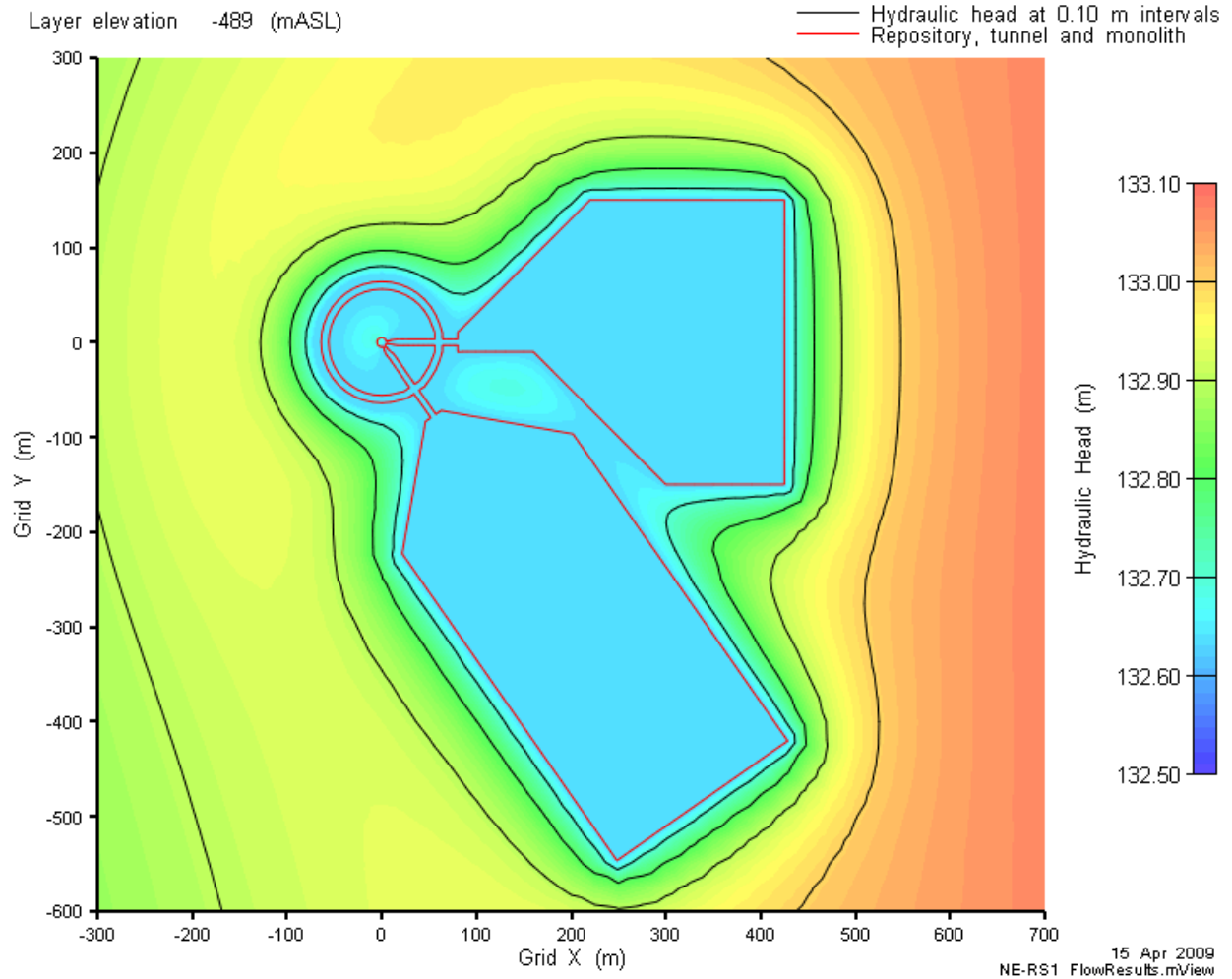


Figure 5.3: NE-RS1-F3 model head contours in the vicinity of the repository on a horizontal slice through elevation -489 mASL.

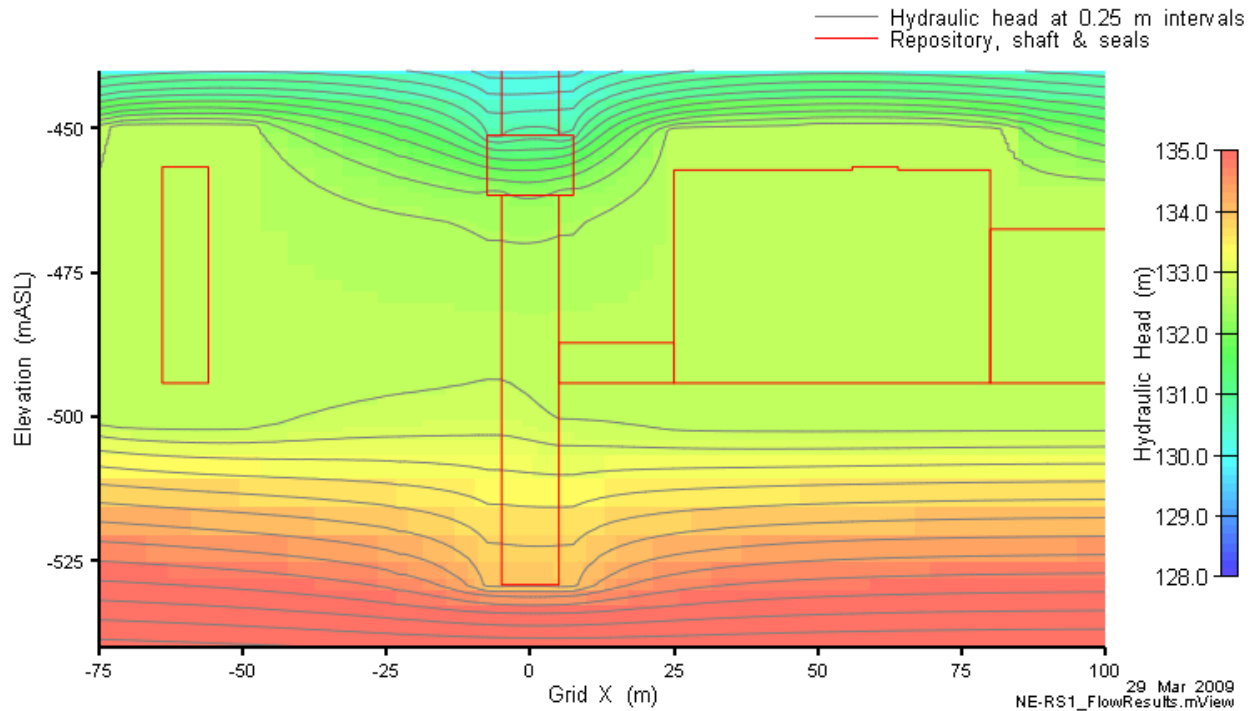


Figure 5.4: NE-RS1-F3 model head contours in the vicinity of the monolith on a vertical slice through Grid Y=0.

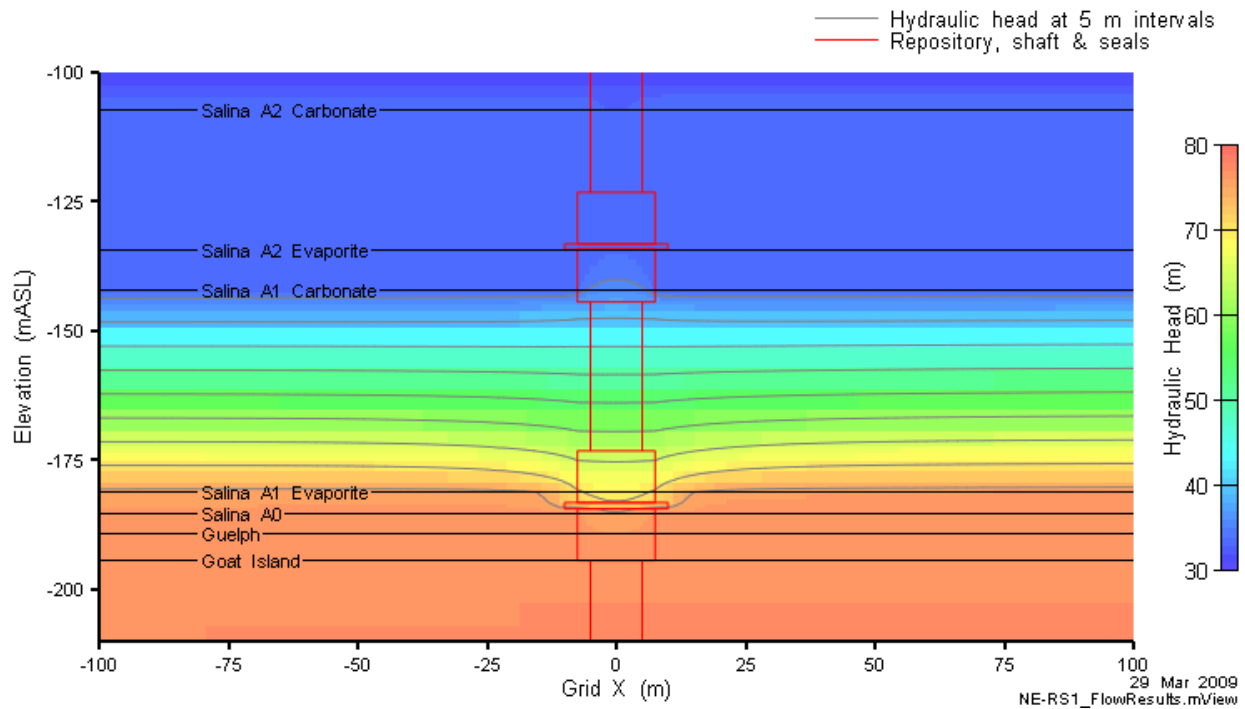


Figure 5.5: NE-RS1-F3 model head contours in the vicinity of the Silurian waterstop seals on a vertical slice through Grid Y=0.

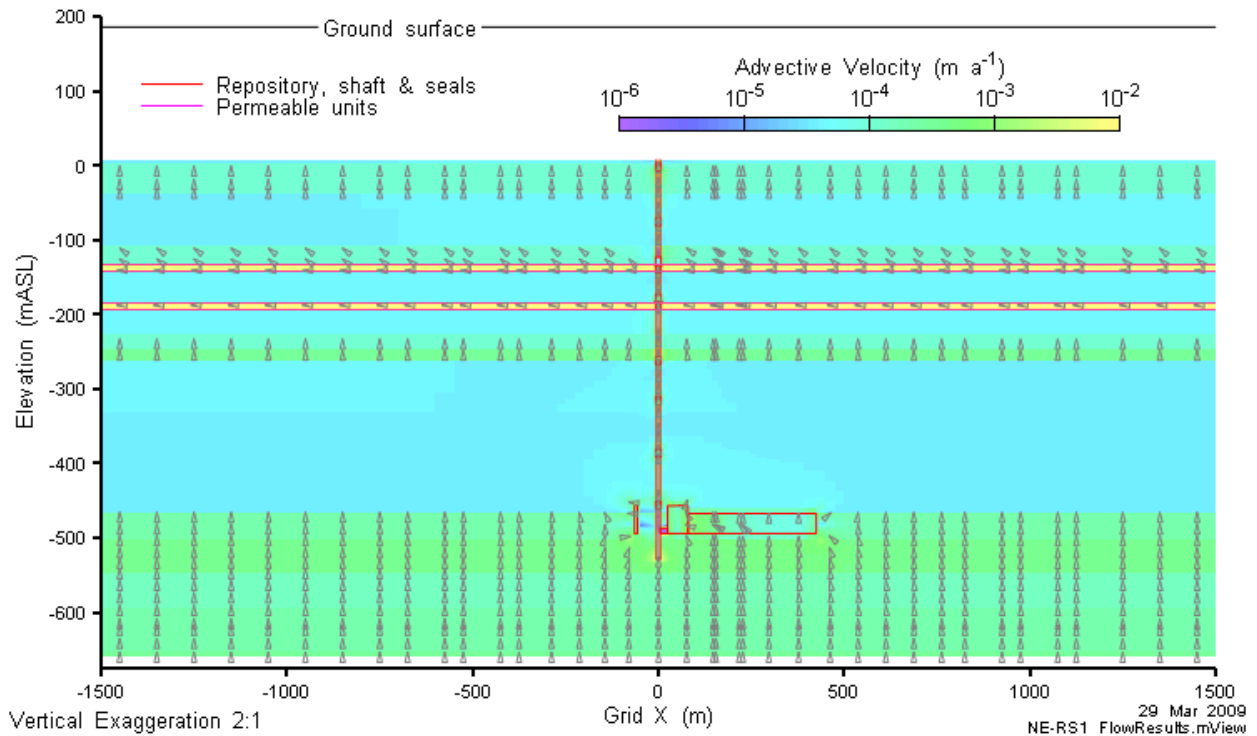


Figure 5.6: NE-RS1-F3 advective velocity magnitude and vectors on a vertical slice through Grid Y=0.

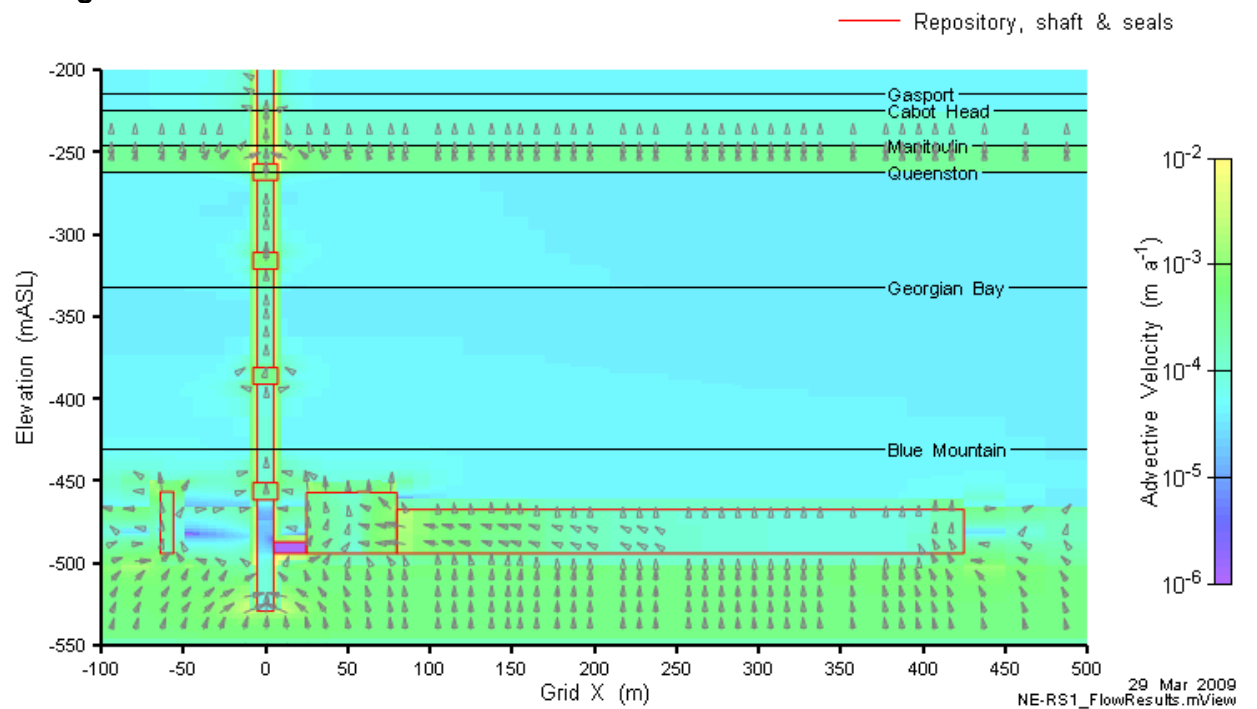


Figure 5.7: NE-RS1-F3 advective velocity magnitude and vectors in the repository and lower shaft on a vertical slice through Grid Y=0.

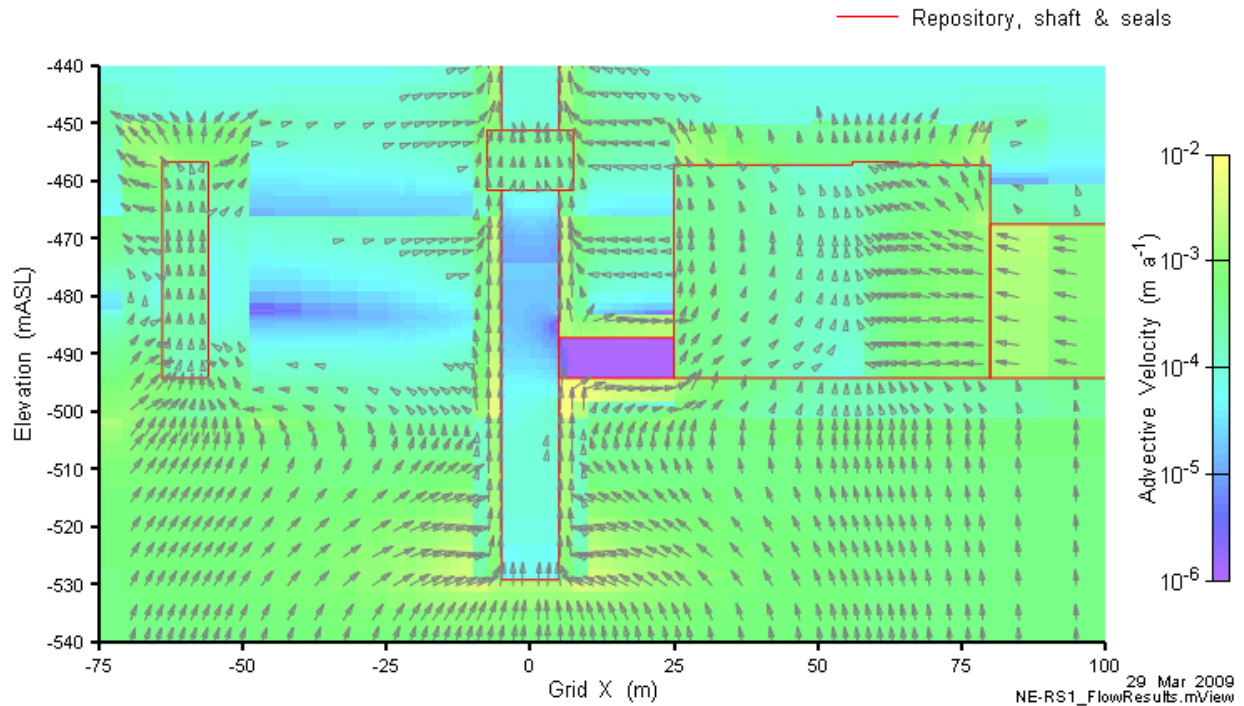


Figure 5.8: NE-RS1-F3 advective velocity magnitude and vectors in the vicinity of the monolith on a vertical slice through Grid Y=0.

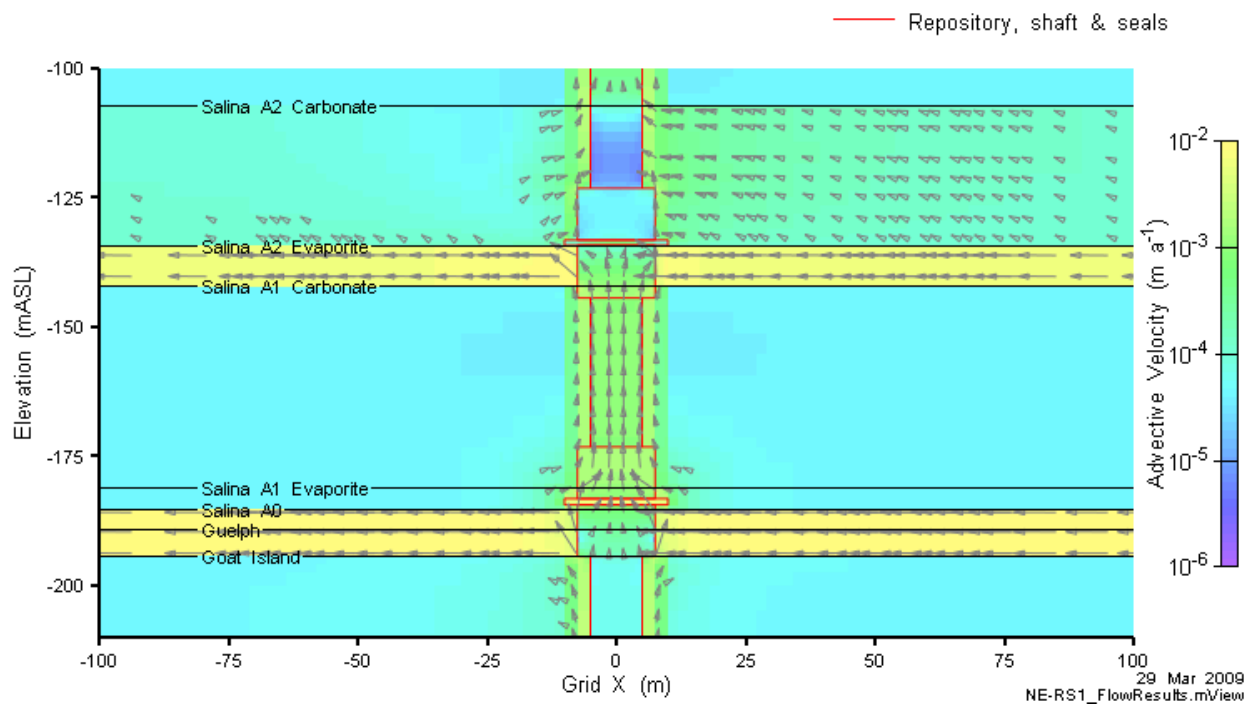


Figure 5.9: NE-RS1-F3 advective velocity magnitude and vectors in the vicinity of the Silurian waterstop seals on a vertical slice through Grid Y=0.

Figure 5.10 clearly shows the flow pattern described earlier, where flow from the shaft EDZ is toward the access and ring tunnels.

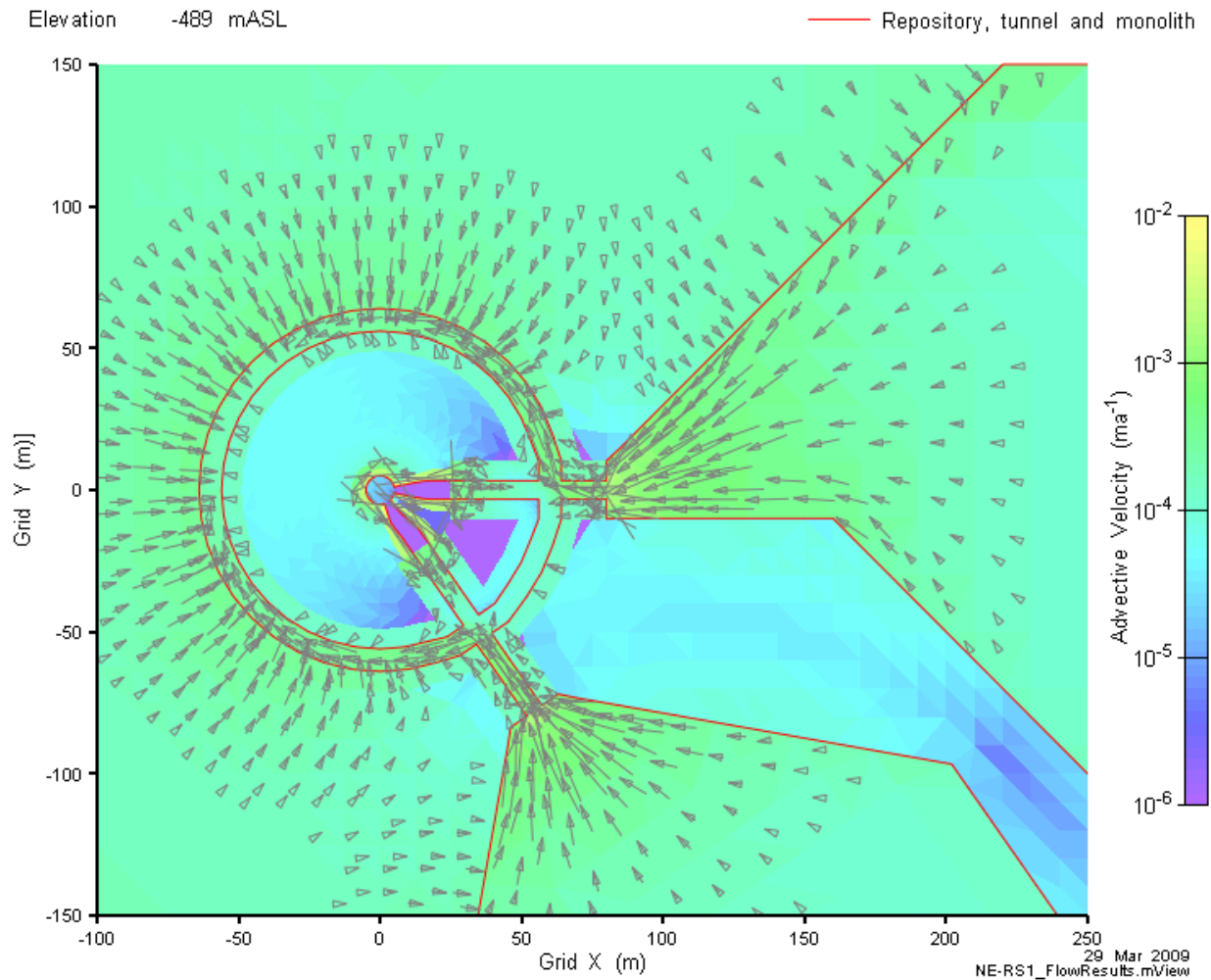


Figure 5.10: NE-RS1-F3 advective velocity magnitude and vectors in the vicinity of the repository on a horizontal slice through elevation -490 mASL.

5.2.1.2 Transport Results

Concentrations of Cl-36 at various times on a vertical slice through $Y = 0$ are presented in Figure 5.11 below. The effect of the shaft is clearly seen in the preferential solute transport in the shaft and the shaft EDZ. The extreme sluggishness of transport is seen in the time of arrival in the Guelph/Salina A0, at approximately 500 000 years after closure.

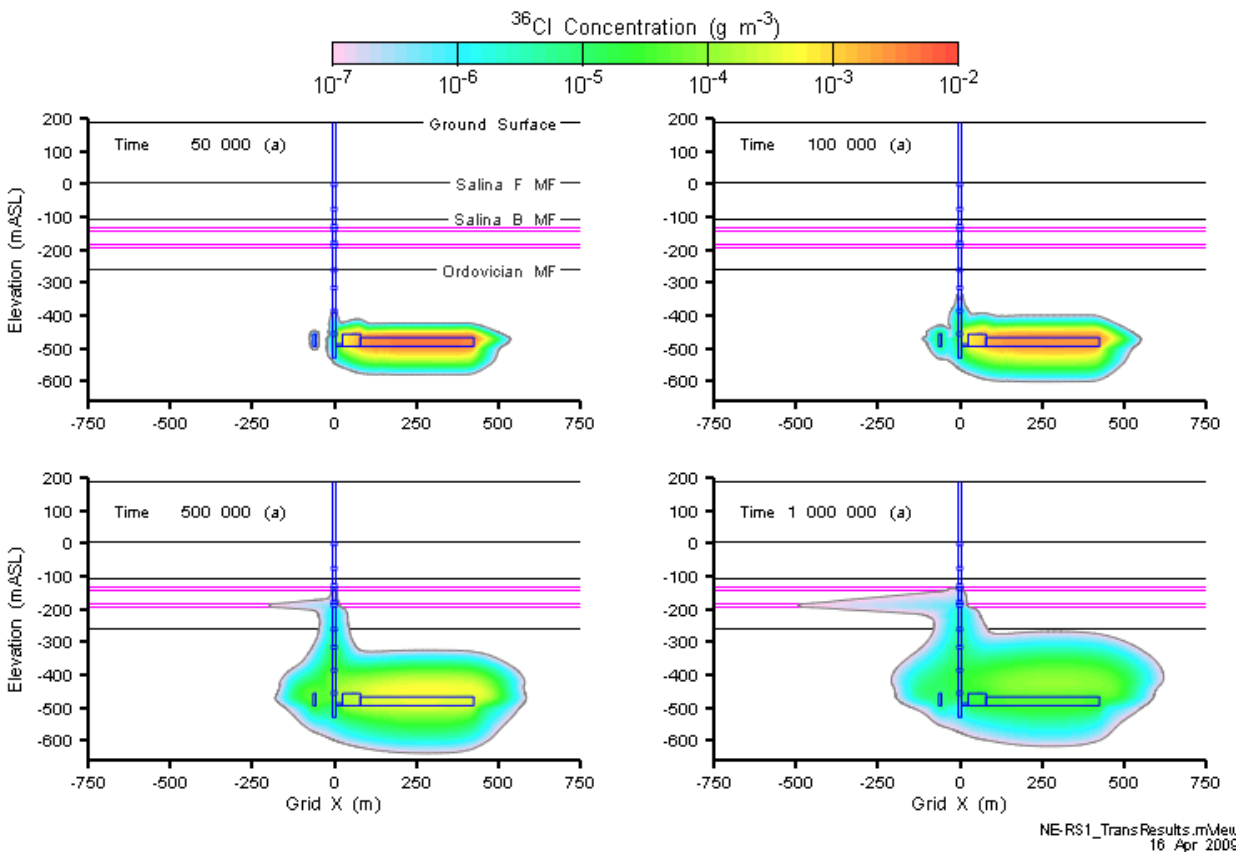


Figure 5.11: NE-RS1 Cl-36 concentration at 50 000, 100 000, 500 000, and 1 000 000 years.

The effect of the horizontal flow field in the Guelph/Salina A0 is evident in the horizontal plume extending to the west of the repository in Figure 5.12 and Figure 5.13. As previously described in Section 5.1.2, the lowest concentration isosurface in Figure 5.12 represents a very low concentration of 10^{-7} g m^{-3} (or 120 Bq m^{-3} , or an equivalent drinking water dose of about $0.1 \mu\text{Sv a}^{-1}$)⁴.

⁴ The groundwater in the deep and intermediate bedrock groundwater zones is highly saline and so is not potable. Therefore, the dose is hypothetical and provided as an indicative value.

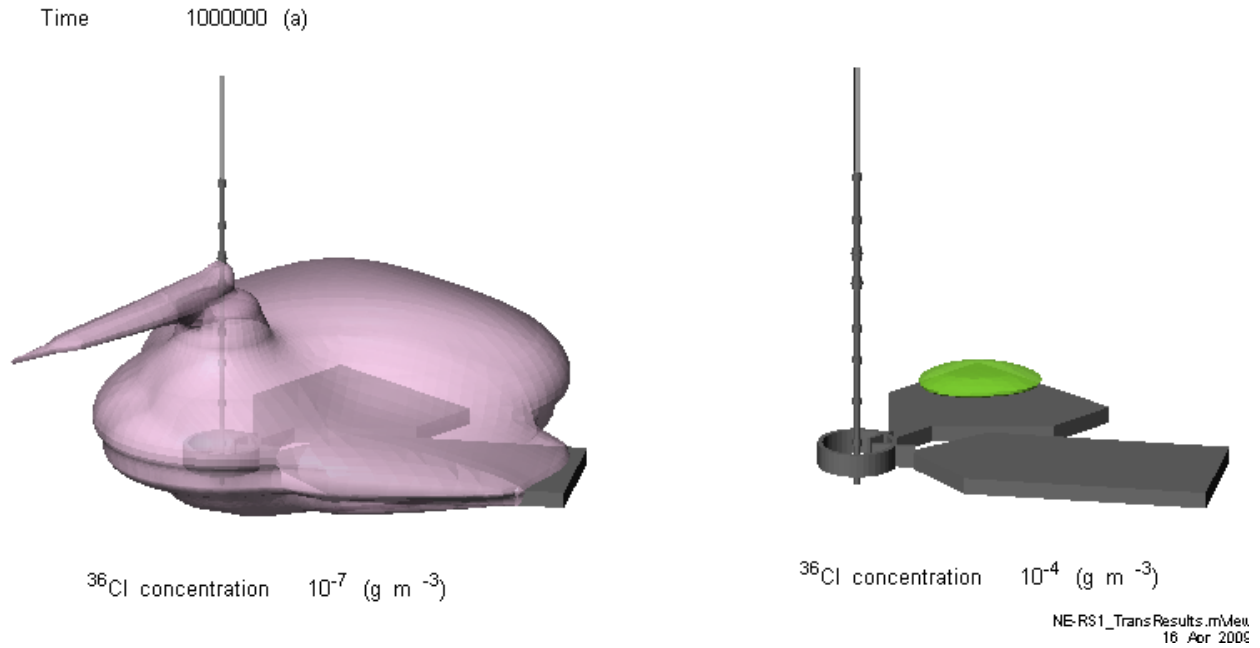


Figure 5.12: NE-RS1 CI-36 concentration isovolumes at 1 000 000 years.

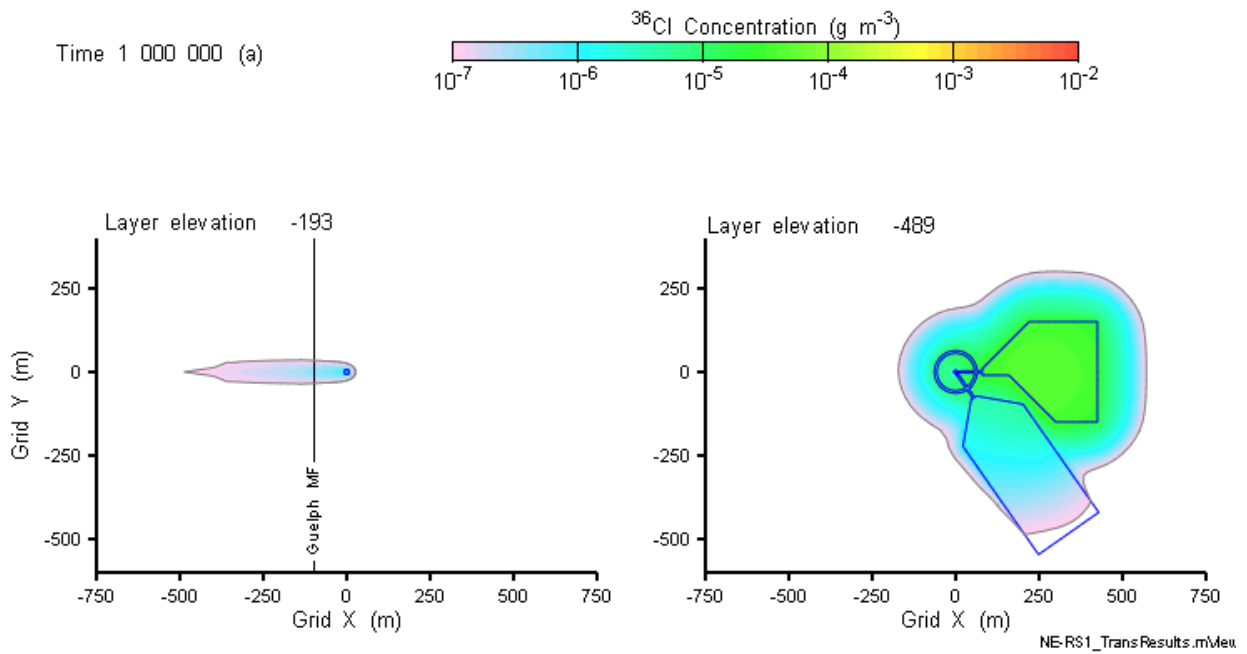


Figure 5.13: NE-RS1 CI-36 concentration in plan section through Guelph and repository at 1 000 000 years.

The horizontal flow field clearly reduces vertical transport of Cl-36 above the Guelph/Salina A0 unit. This is also evident in the mass flow curves shown in Figure 5.14 and Figure 5.15.

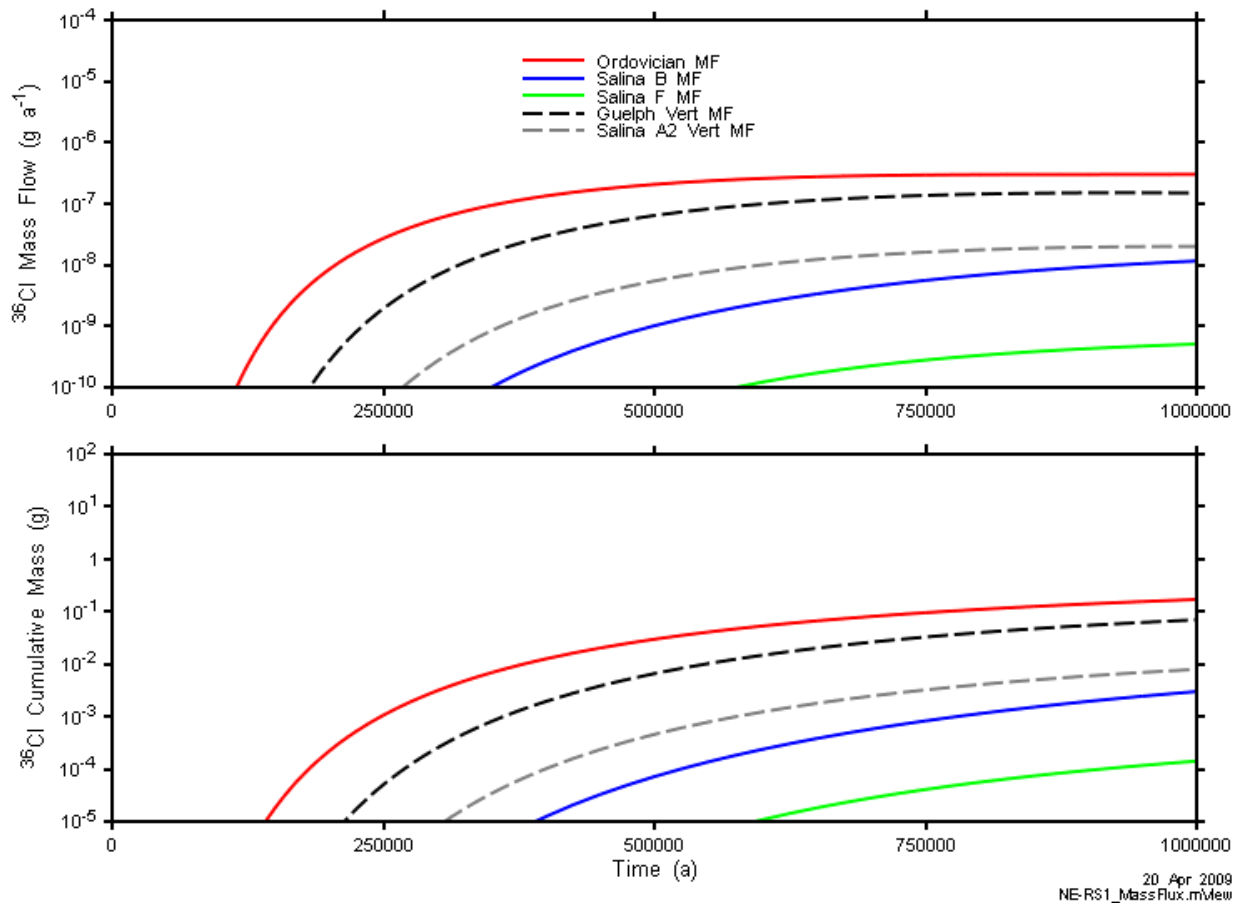


Figure 5.14: NE-RS1-F3 total mass flow and cumulative mass transport.

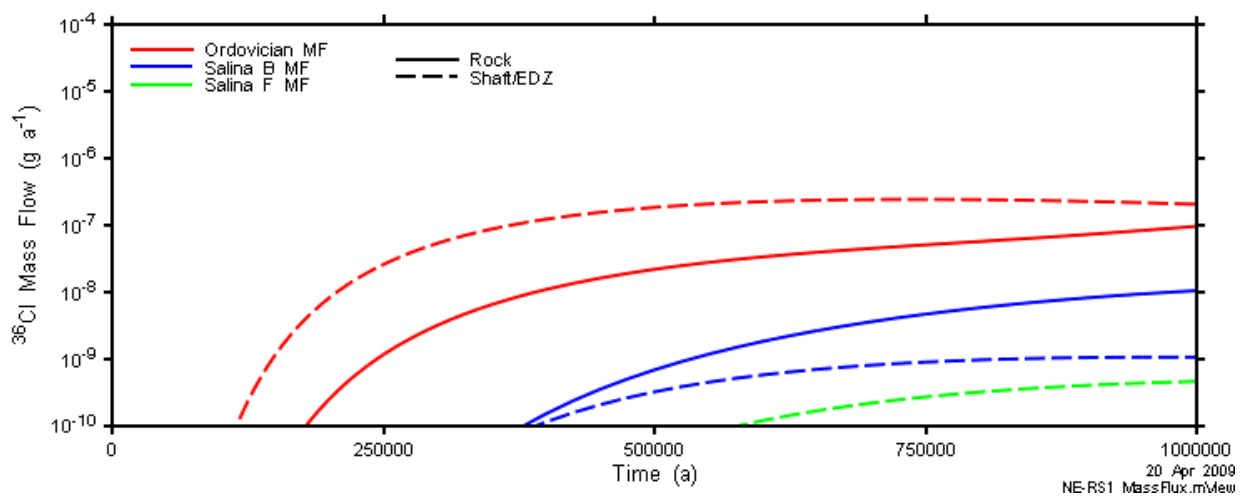


Figure 5.15: NE-RS1-F3 mass flow components.

Some numeric difficulties were encountered in the implementation of the NE-RS1-F3 model. Specifically, in areas of high contrast in advective flow velocities, FRAC3DVS_OPG will

occasionally create mass. This generally leads to instability, which causes premature termination of the simulations. In general, these instabilities were rectified by regriding, usually by the addition of model grid layers in the area of concern. However, some instabilities required further action. A particular point of error was the EDZ surrounding the sump in the Sherman Fall Formation. Advective velocities were reduced by increasing the porosity of the Sherm_I and Sherm_O zones by a factor of 10, from 0.016 to 0.15. This does not affect the head distribution or overall flow system, and reduces advective velocities in an area where little or no advective transport is expected. This approach was applied to all 3DS model cases (normal evolution and disruptive), which used the reference geosphere.

5.2.2 NE-UG-RS1-F3

5.2.2.1 Flow Results

Flow modelling results for the updated geosphere case are presented on a corresponding set of figures to those previously presented for the NE-RS1-F3 case. The results are striking in their contrast to the reference geosphere.

The vertical hydraulic gradient is steepest in the Ordovician formations, particularly the Cobourg and Kirkfield with virtually all Cambrian head dissipated by the top of the Queenston shale. Vertical gradients through the Silurian are much reduced in comparison to the reference geosphere, and are much closer to measured pressures in those formations. The vertical head distribution along the shaft is somewhat different than that within the rock mass. Within the shaft, the asphalt seal extending from the bottom of the Queenston through to the middle of the Georgian Bay (Figure 4.13) is the lowest permeability section. Consequently, the bulk of the head dissipation between the repository and top of the Queenston takes place across this segment as shown in Figure 5.17.

Vertical velocities throughout the model domain are significantly reduced. For the UG geosphere the highest vertical velocities are found within the shaft as the sealing materials are generally of higher conductivity than the inner and outer EDZ. Horizontal velocities in the permeable Silurian units (Guelph and Salina A2 evaporite) are slightly higher than the reference case, with average horizontal linear velocities of approximately 0.013 m a^{-1} in the Guelph and 0.06 m a^{-1} in the Salina A2 evaporite. With the exception of the Guelph and Salina A2 evaporite, velocities seen within the rock mass are virtually zero and are indicative of a diffusion dominated transport regime.

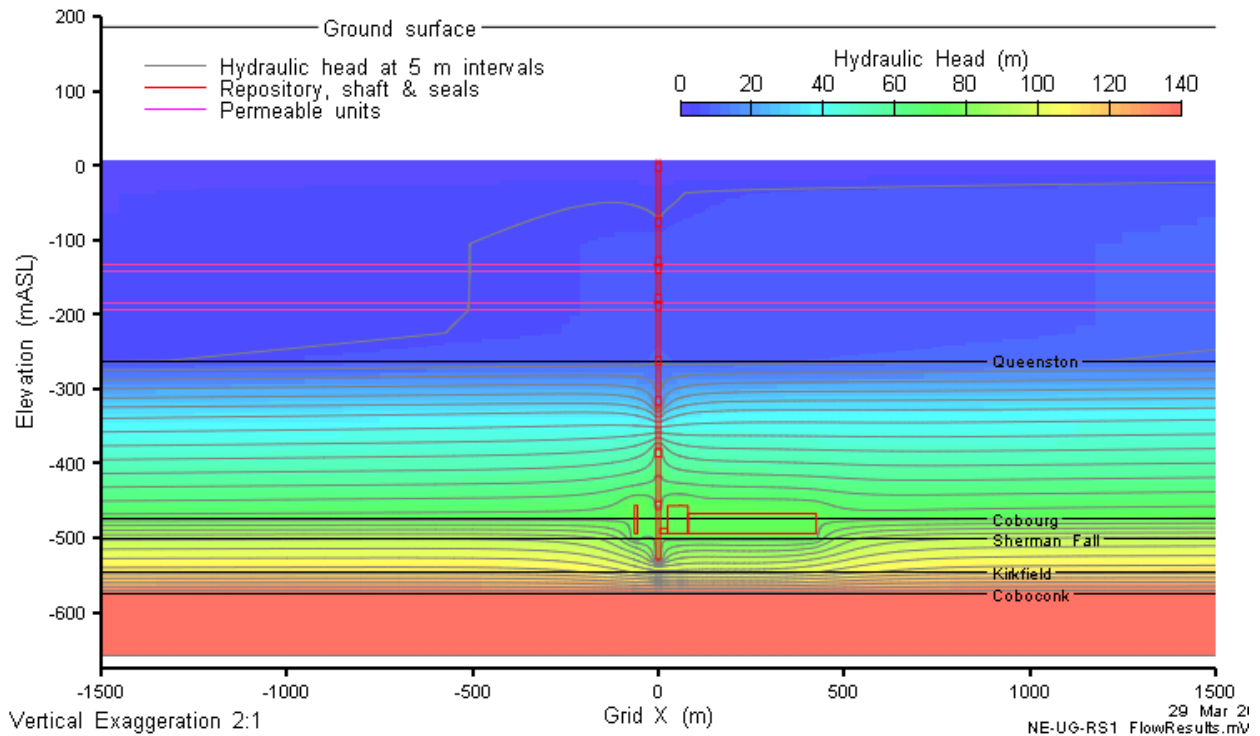


Figure 5.16: NE-UG-RS1-F3 model head contours on a vertical slice through Grid Y=0.

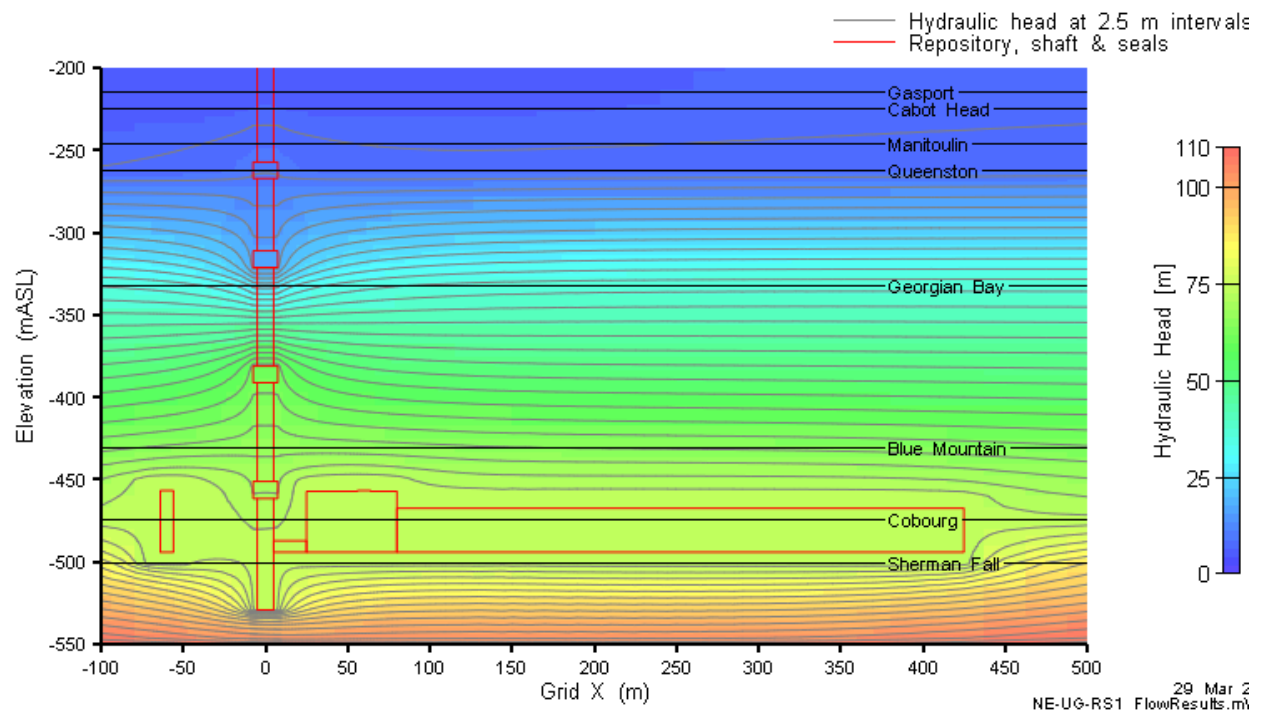


Figure 5.17: NE-UG-RS1-F3 model head contours in the vicinity of the repository on a vertical slice through Grid Y=0.

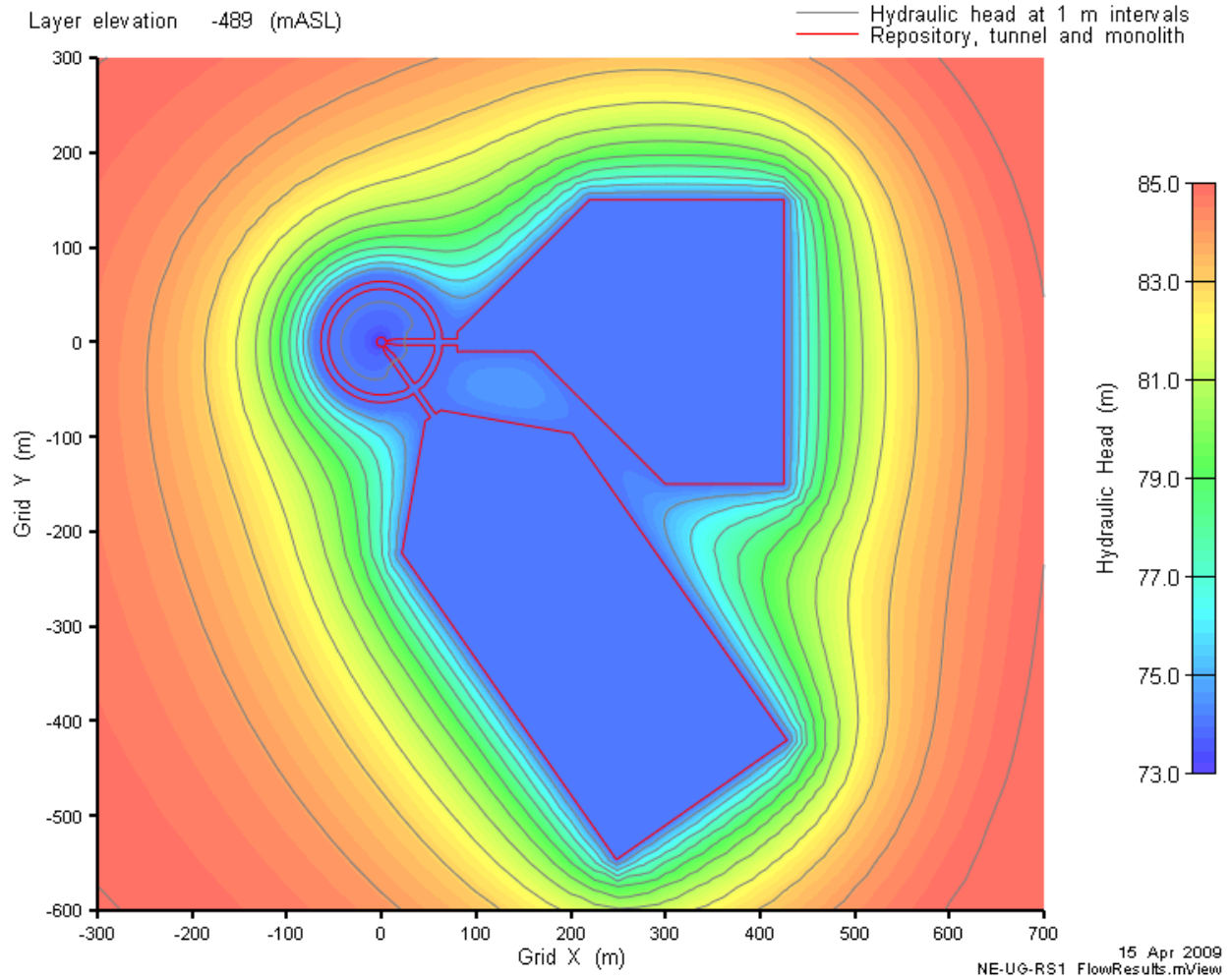


Figure 5.18: NE-UG-RS1-F3 model head contours in the vicinity of the repository on a horizontal slice through elevation -489 mASL.

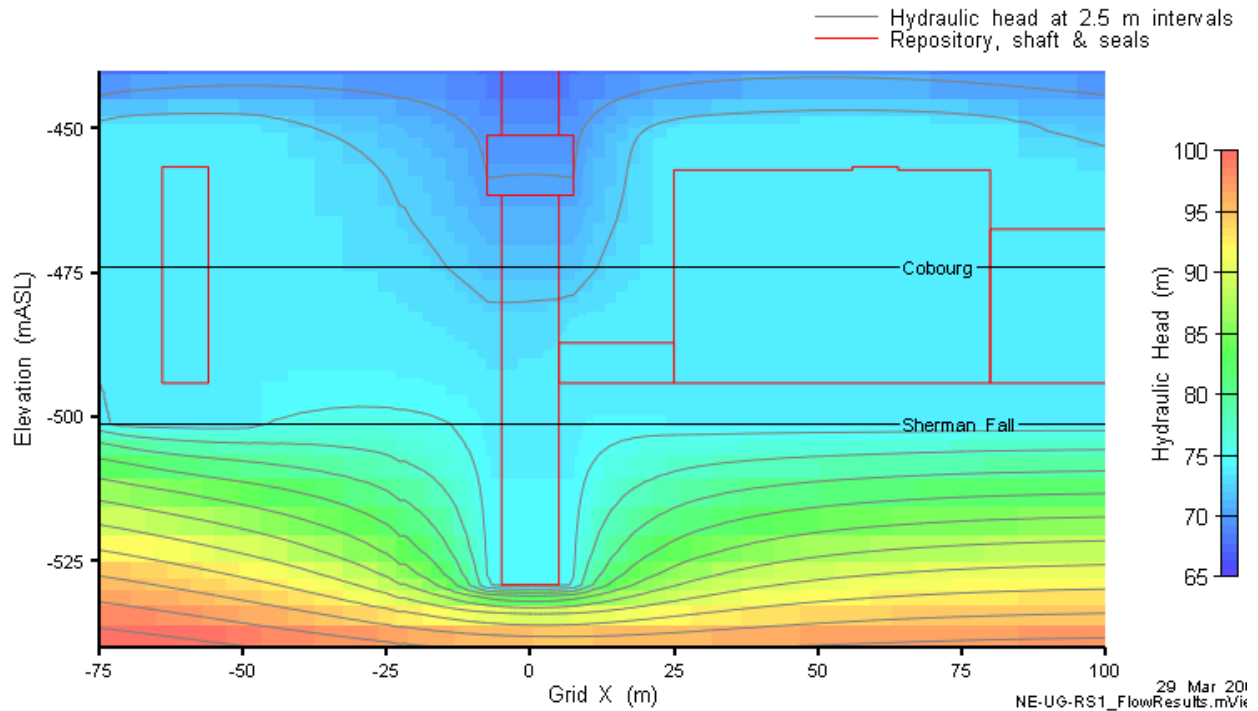


Figure 5.19: NE-UG-RS1-F3 model head contours in the vicinity of the monolith on a vertical slice through Grid Y=0.

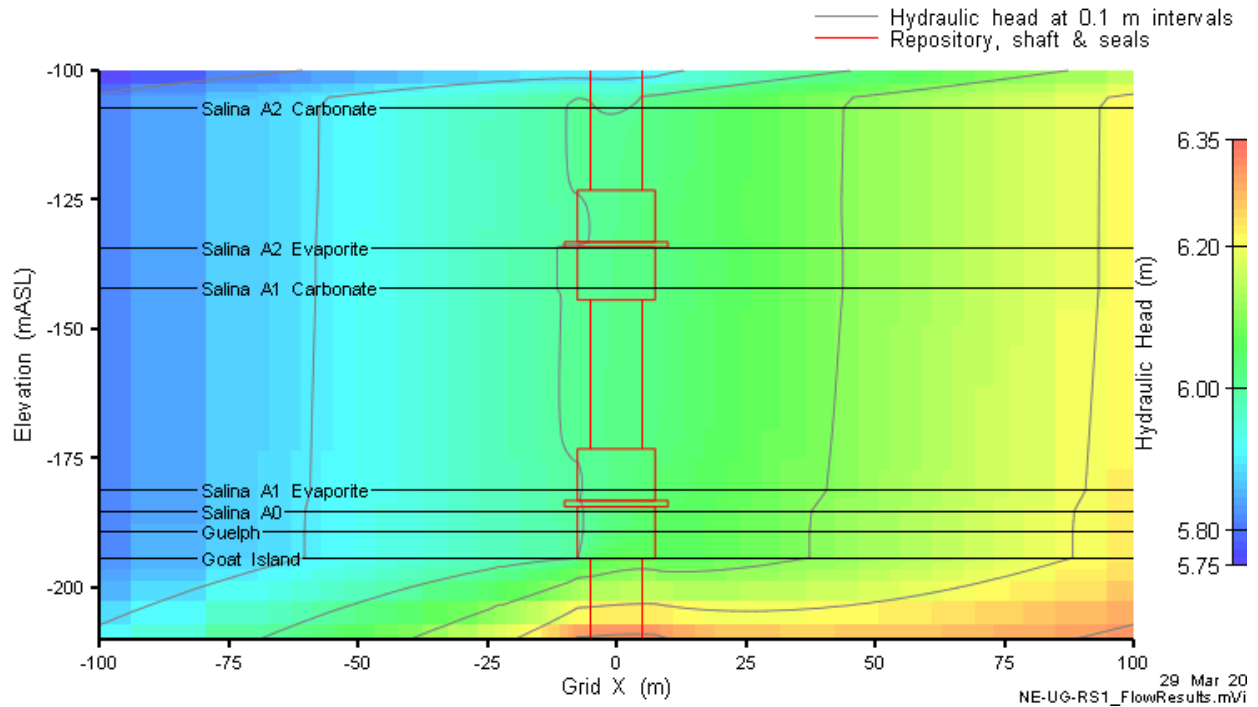


Figure 5.20: NE-UG-RS1-F3 model head contours and advective velocity vectors in the vicinity of the Silurian waterstop seals on a vertical slice through Grid Y=0.

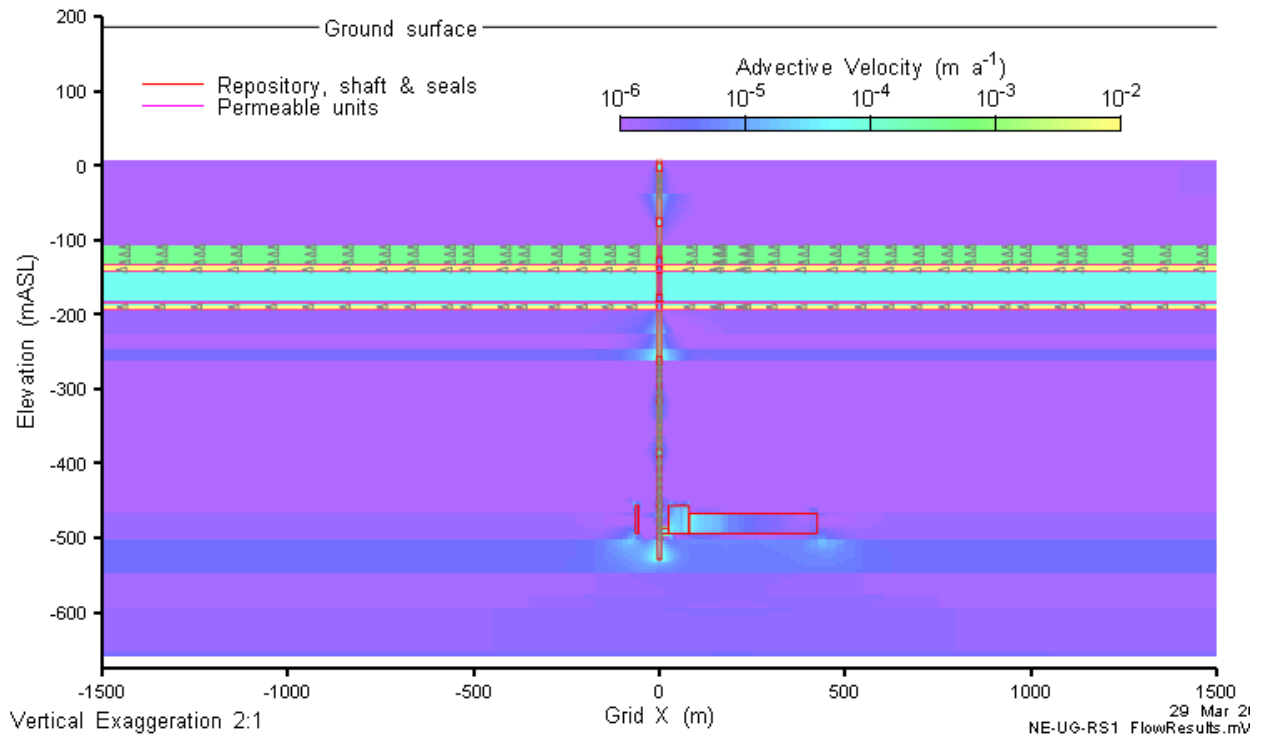


Figure 5.21: NE-UG-RS1-F3 advective velocity magnitude and vectors on a vertical slice through Grid Y=0.

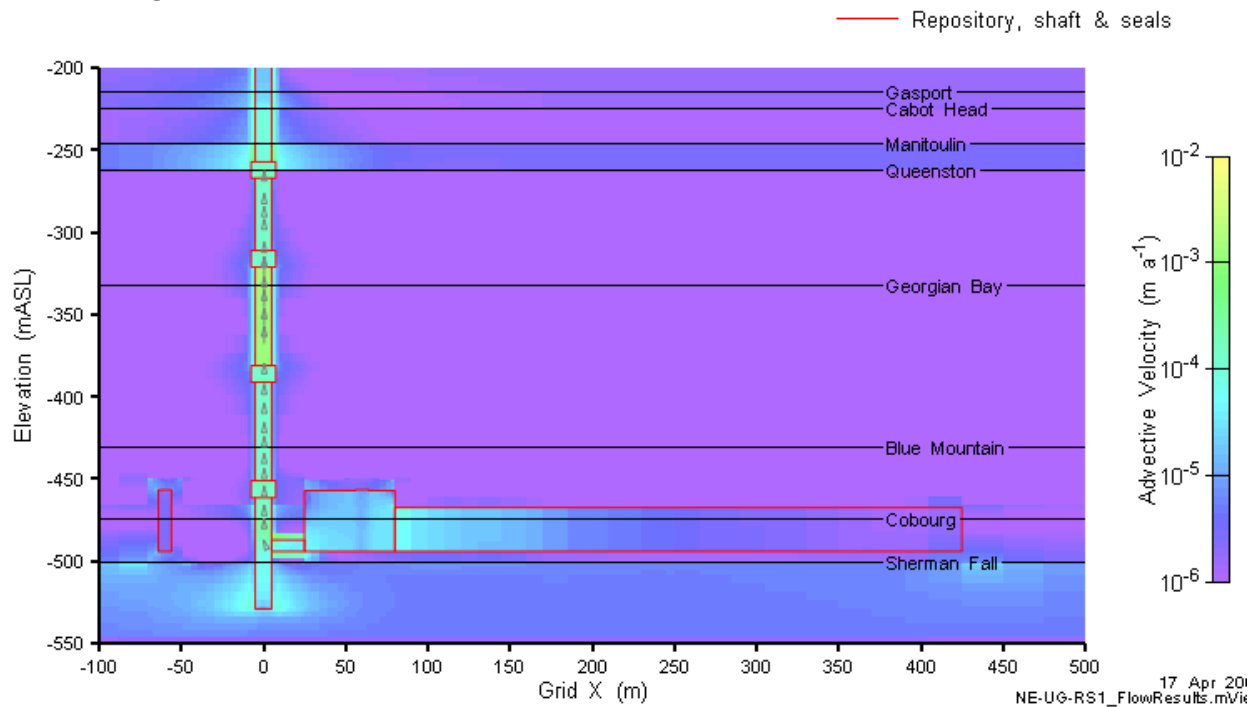


Figure 5.22: NE-UG-RS1-F3 advective velocity magnitude and vectors in the repository and lower shaft on a vertical slice through Grid Y=0.

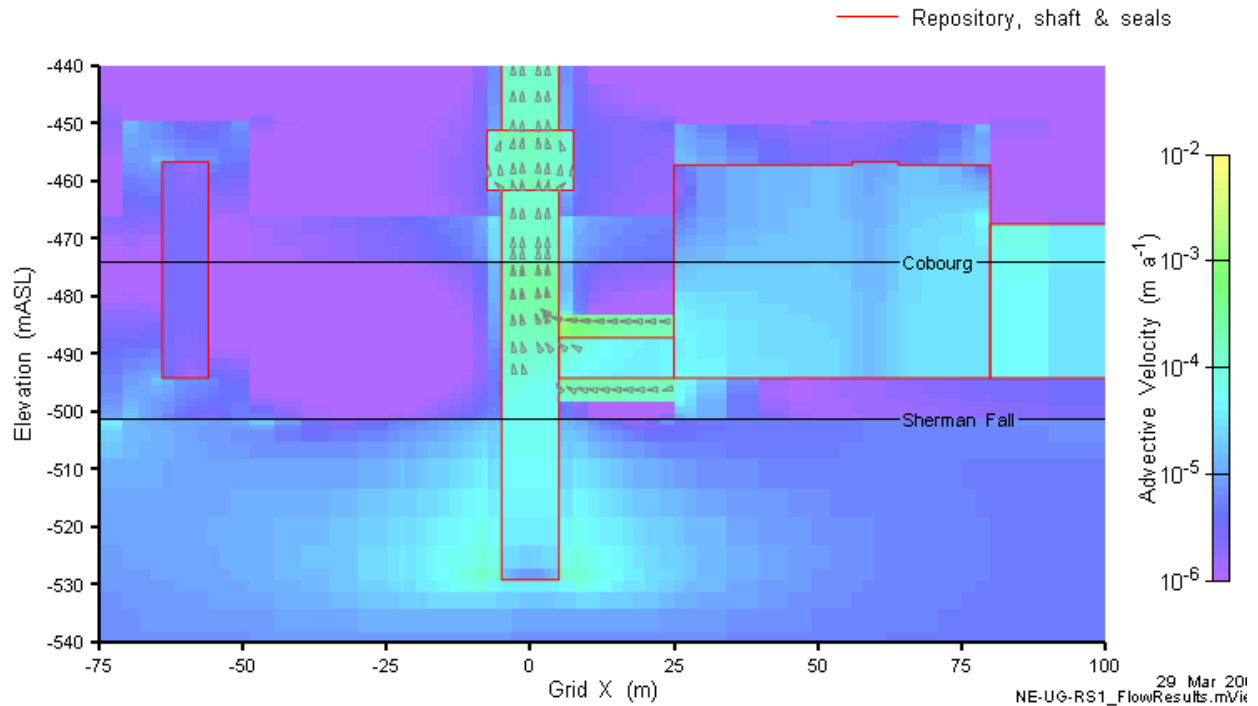


Figure 5.23: NE-UG-RS1-F3 advective velocity magnitude and vectors in the vicinity of the monolith on a vertical slice through Grid Y=0.

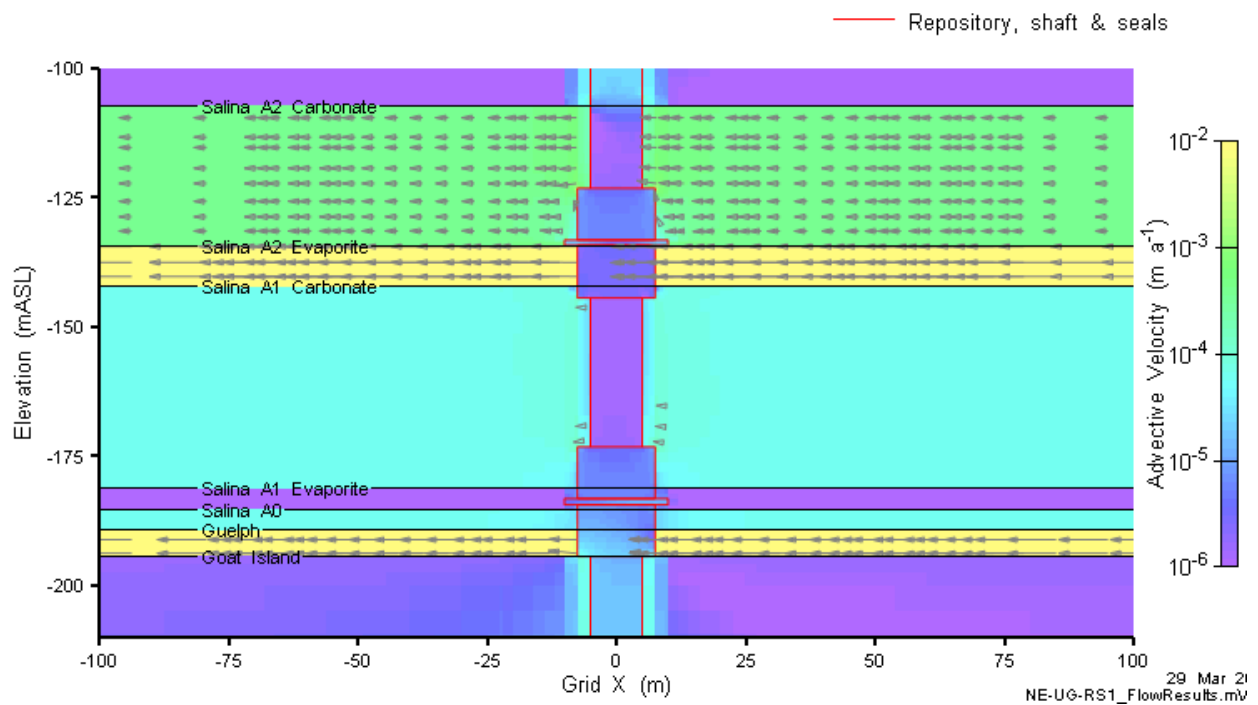


Figure 5.24: NE-UG-RS1-F3 advective velocity magnitude and vectors in the vicinity of the Silurian waterstop seals on a vertical slice through Grid Y=0.

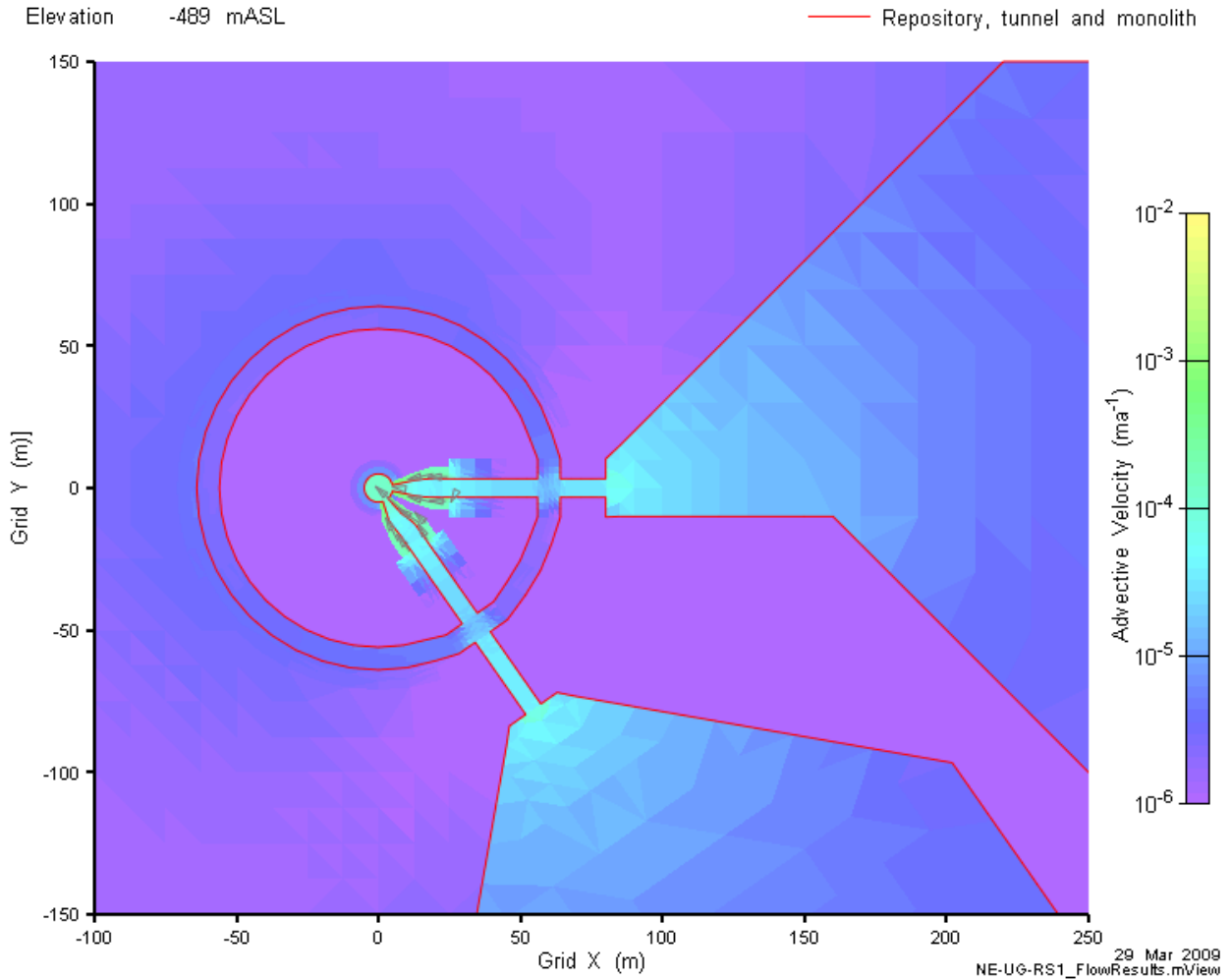


Figure 5.25: NE-UG-RS1-F3 advective velocity magnitude and vectors in the vicinity of the repository on a horizontal slice through elevation -490 mASL.

5.2.2.2 Transport Results

Concentrations of Cl-36 at various times on a vertical slice through Y = 0 are presented in Figure 5.26. The results are consistent with a diffusion dominated flow regime with virtually no advective transport. Some slight preferential flow along the shaft is evident, but is of minor consequence. Similar results are seen in Figure 5.27 and Figure 5.28.

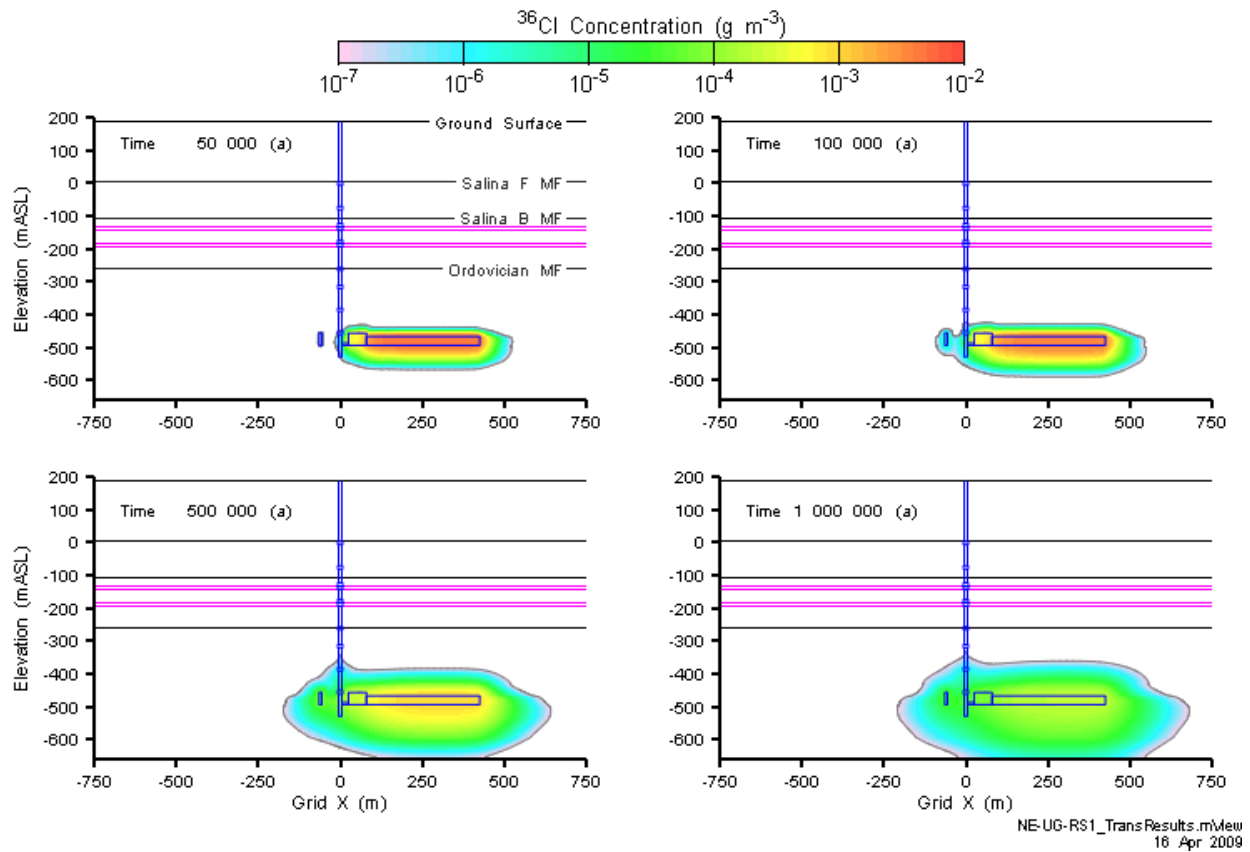


Figure 5.26: NE-UG-RS1 Cl-36 concentration at 50 000, 100 000, 500 000, and 1 000 000 years.

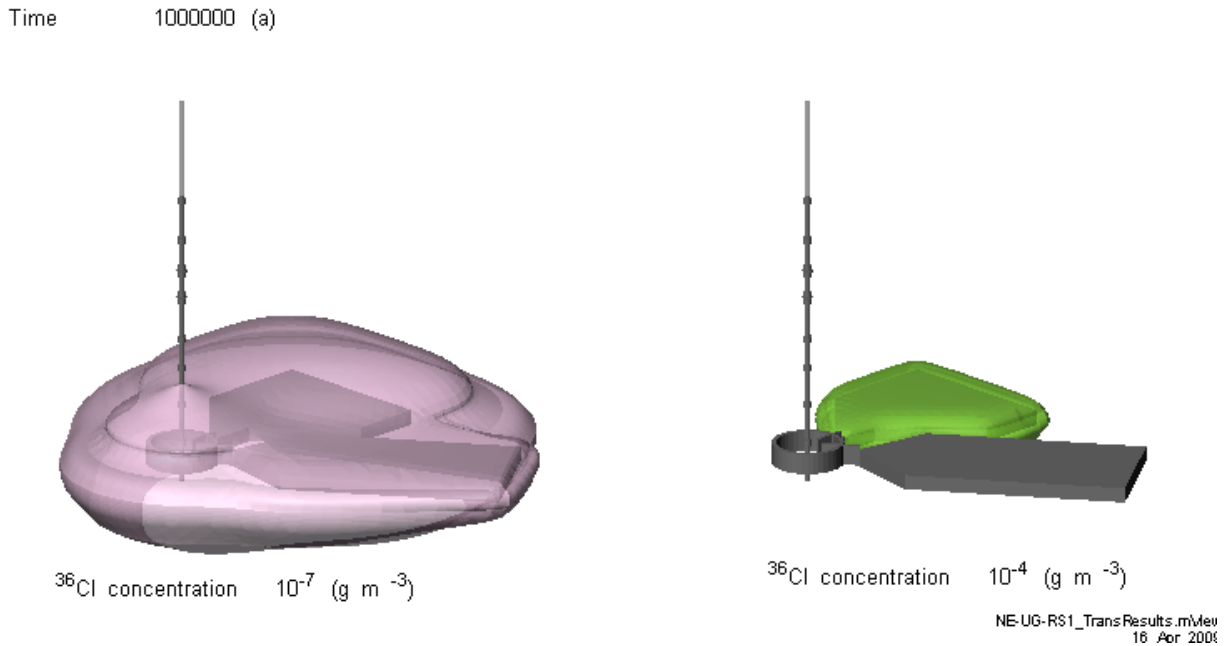


Figure 5.27: NE-UG-RS1 Cl-36 concentration isovolumes at 1 000 000 years.

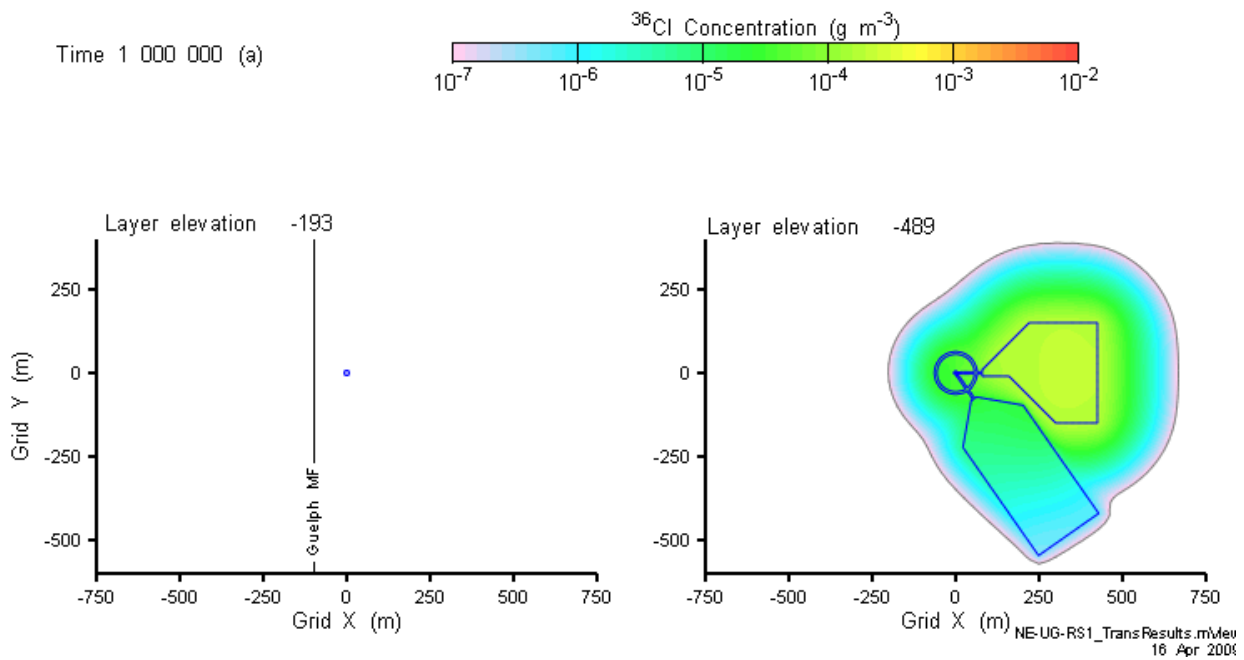


Figure 5.28: NE-UG-RS1 Cl-36 concentration in plan section through Guelph and repository at 1 000 000 years.

Mass flow results shown in Figure 5.29 give further evidence of the extremely low transport rates, with a total flow through the Ordovician system of $1.1 \times 10^{-11} \text{ g a}^{-1}$ at 1 000 000 years. This is lower than the Salina F flow for the NE-RS1 case. The calculated Salina F flow for the NE-UG-RS1 case is $1.7 \times 10^{-20} \text{ g a}^{-1}$. As described in Section 5.1.2, mass flow rates of these orders correspond to concentrations that are well below the detection limit of analytic equipment

and should be considered as effectively zero. They are presented here only for the purposes of comparison.

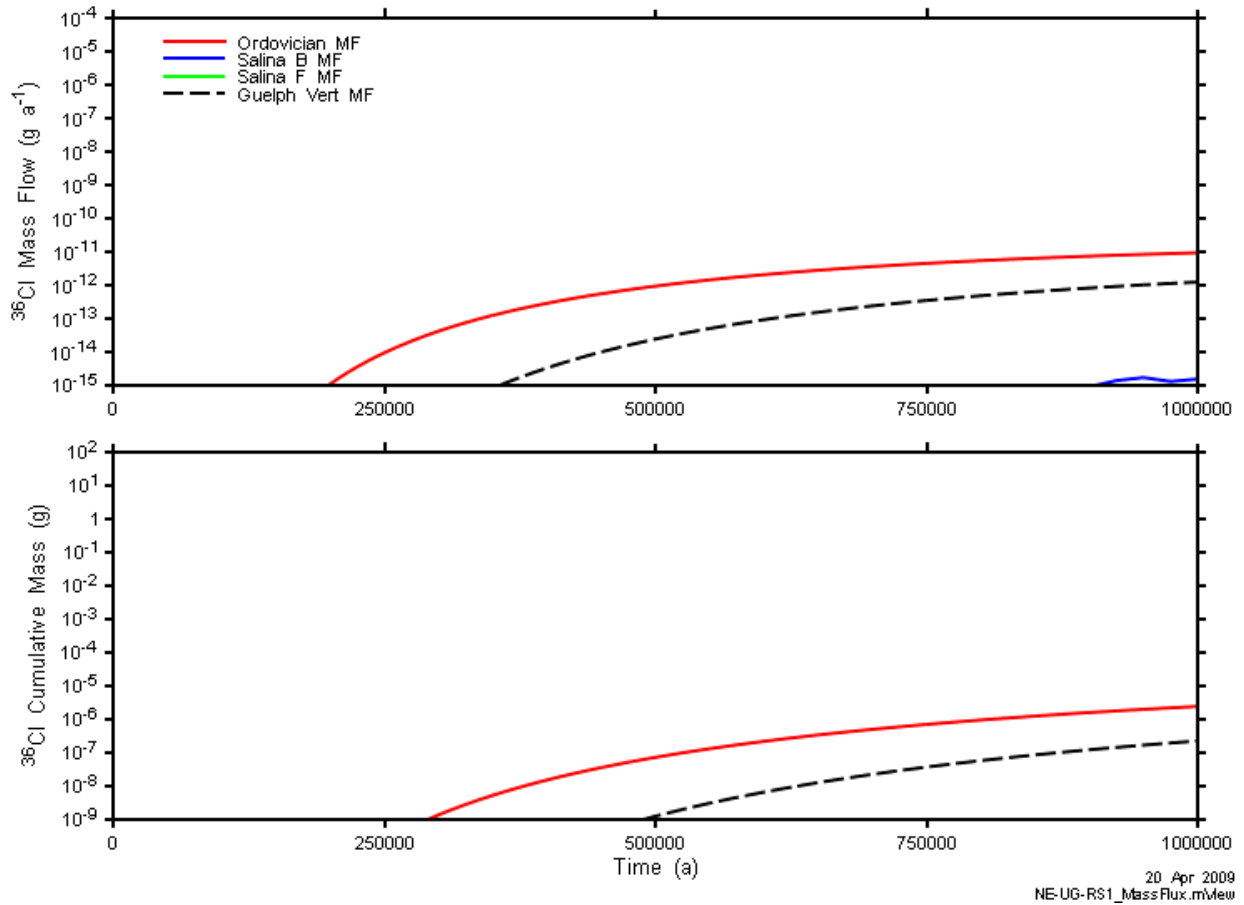


Figure 5.29: NE-UG-RS1-F3 total mass flow and cumulative mass transport. All Salina F mass flows are below Y axis limits

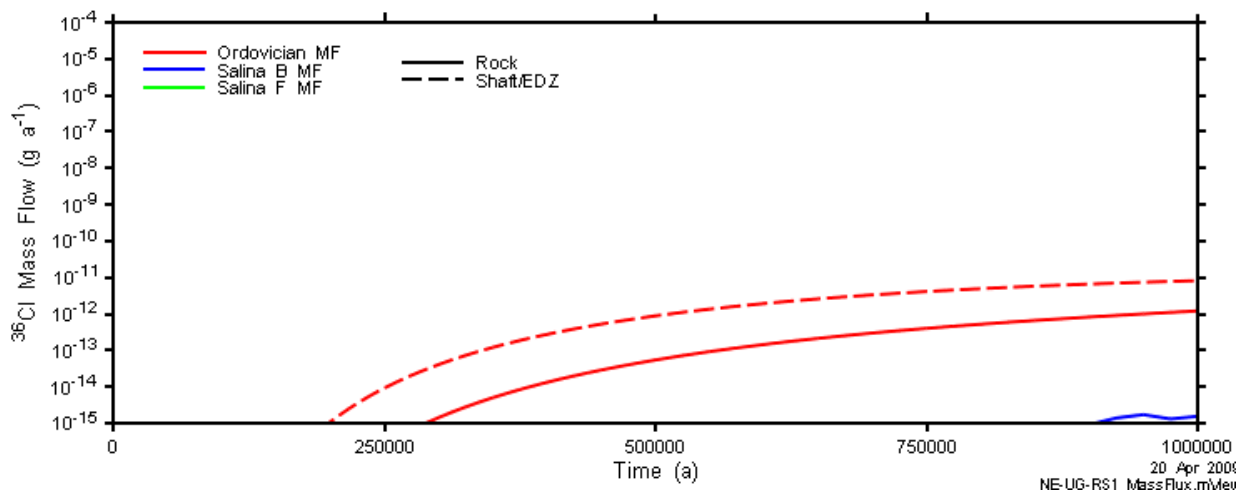


Figure 5.30: NE-UG-RS1-F3 mass flow components. All Salina F mass flows are below Y axis limits.

5.2.3 NE-RS1-3DSU

The NE-RS1-3DSU model was intended to calculate transport through the shallow bedrock groundwater zone using input mass flux into the Salina G as calculated by the 3DS model. However, mass flux into the Salina G for the NE-RS1-F3 case is below the level at which meaningful calculations can be performed. Use of the 3DSU model was deferred to the NE-NHG case. A full description of 3DSU model flow and transport results can be found in Section 5.3.4.

5.3 NE-NHG No Horizontal Flow in Silurian Case (NE-NHG-F3 & NE-NHG-F2)

Unlike the NE-RS1 case, the NE-NHG case does not include a horizontal gradient in the permeable Silurian units and can therefore be simulated with both the 3DS and 2DR models, allowing a direct comparison of results from the two different approaches. Apart from the gradient, the NE-NHG and NE-RS1 cases are identical.

5.3.1 NE-NHG-F3 Results

5.3.1.1 Flow Results

Flow results for the NE-NHG-F3 case are very similar to the NE-RS1-F3 case except for the permeable Silurian units. Results presented in this section will focus on areas of difference only. Hydraulic head contours for the entire system are shown in Figure 5.31.

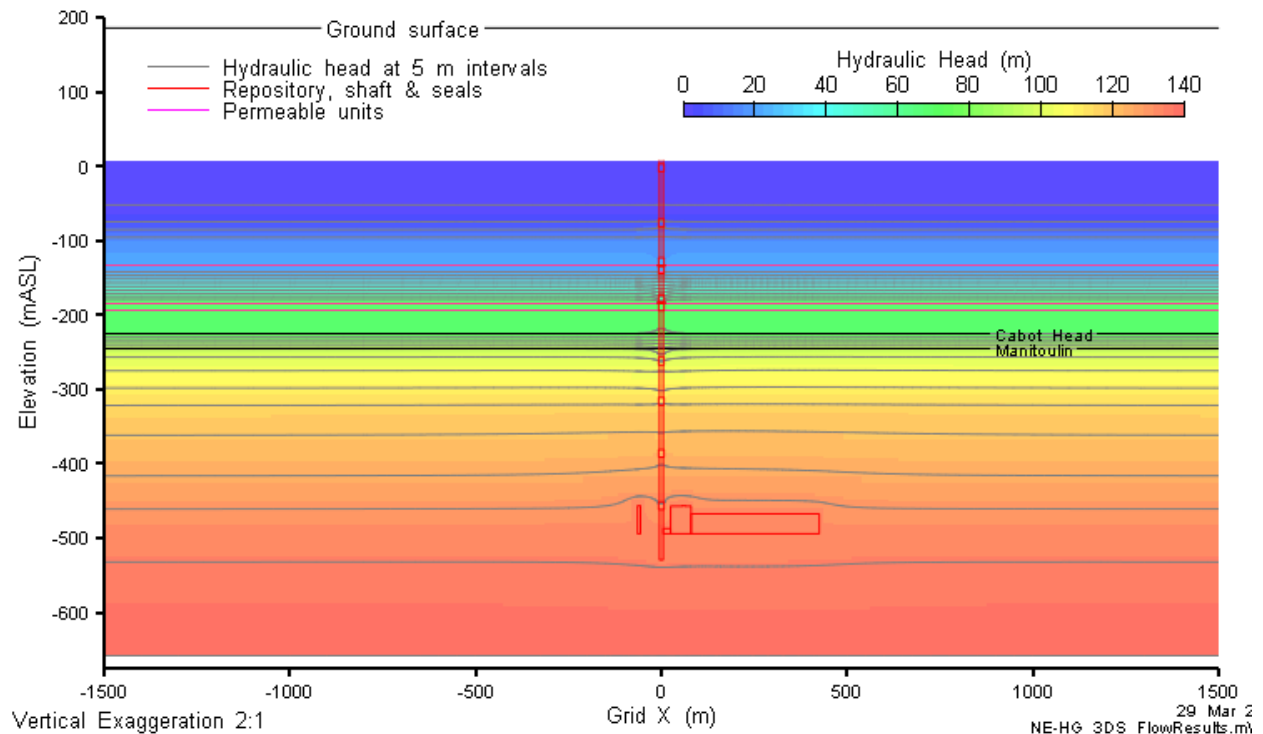


Figure 5.31: NE-NHG-F3 head contours on a vertical slice through Grid Y=0.

Figure 5.32 displays advective velocities and heads in the vicinity of the waterstop seals above the Guelph/Salina A0 and Salina A2 evaporite. Note that the threshold for velocity vector display is a factor of ten lower than that used in other figures in this report to better illustrate flow directions around the seal. Advective velocities actually increase in the concrete relative to the backfilled shaft. Both materials are the same conductivity ($10^{-11} \text{ m s}^{-1}$), but the concrete has a porosity half that of the bentonite/sand. The seals are only marginally effective in preventing vertical flow at this point. The waterstop is an order of magnitude lower conductivity than the concrete, but is relatively thin and does not have a significant effect on flow, as flow is diverted around the seal and then back into the EDZ immediately above the seal. In general, the impacts of the seals on flows in the shaft EDZ are minimal for the base case EDZ parameterization, where the inner EDZ conductivities for the less permeable units are generally a factor of ten higher than the seals themselves. If the conductivity of the inner EDZ were much higher, the concrete seals would be more effective in providing a relative reduction in flow rates in the inner EDZ.

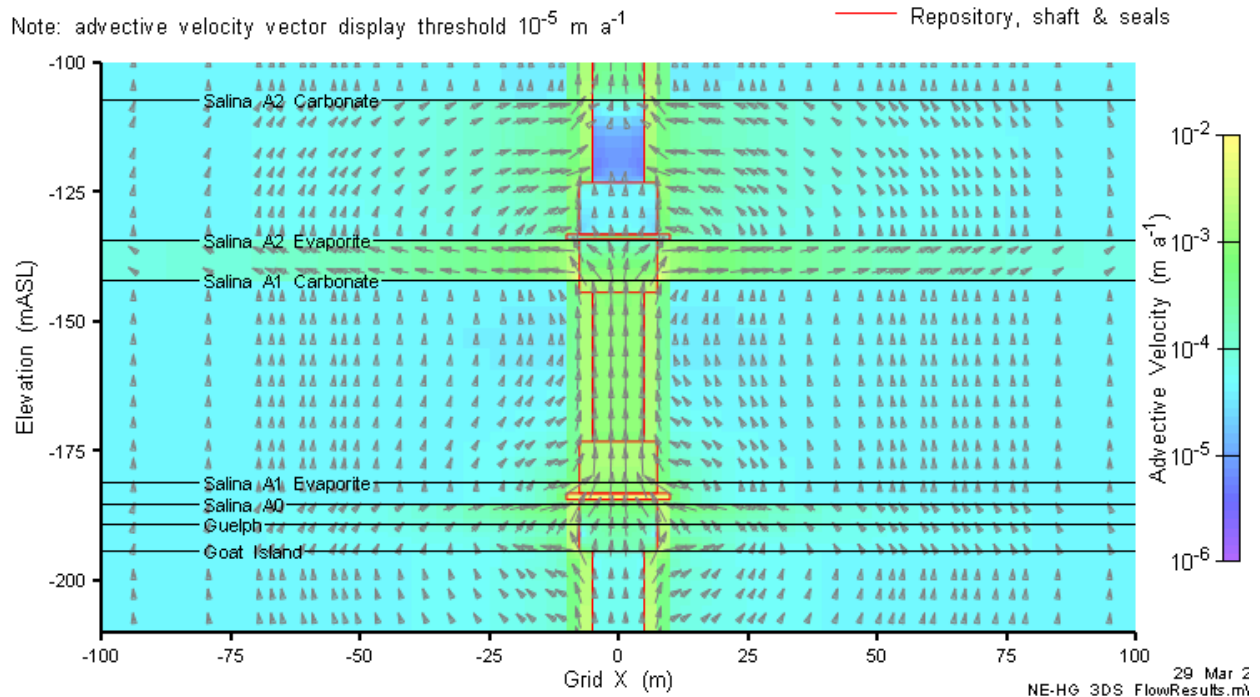


Figure 5.32: NE-NHG-F3 advective velocity magnitude and vectors in the shaft and seals in the vicinity of the S8 waterstop above the Guelph on a vertical slice through Grid Y=0.

5.3.1.2 Transport Results

Transport results are shown in Figure 5.33 through Figure 5.36. In contrast to the NE-RS1-F3 model, Figure 5.33 shows the Cl-36 plume passing the permeable Silurian units and continuing up the shaft and shaft EDZ. However, after 1 000 000 years only a very small fraction of the initial mass of Cl-36 has reached the shallow aquifer system above Salina F.

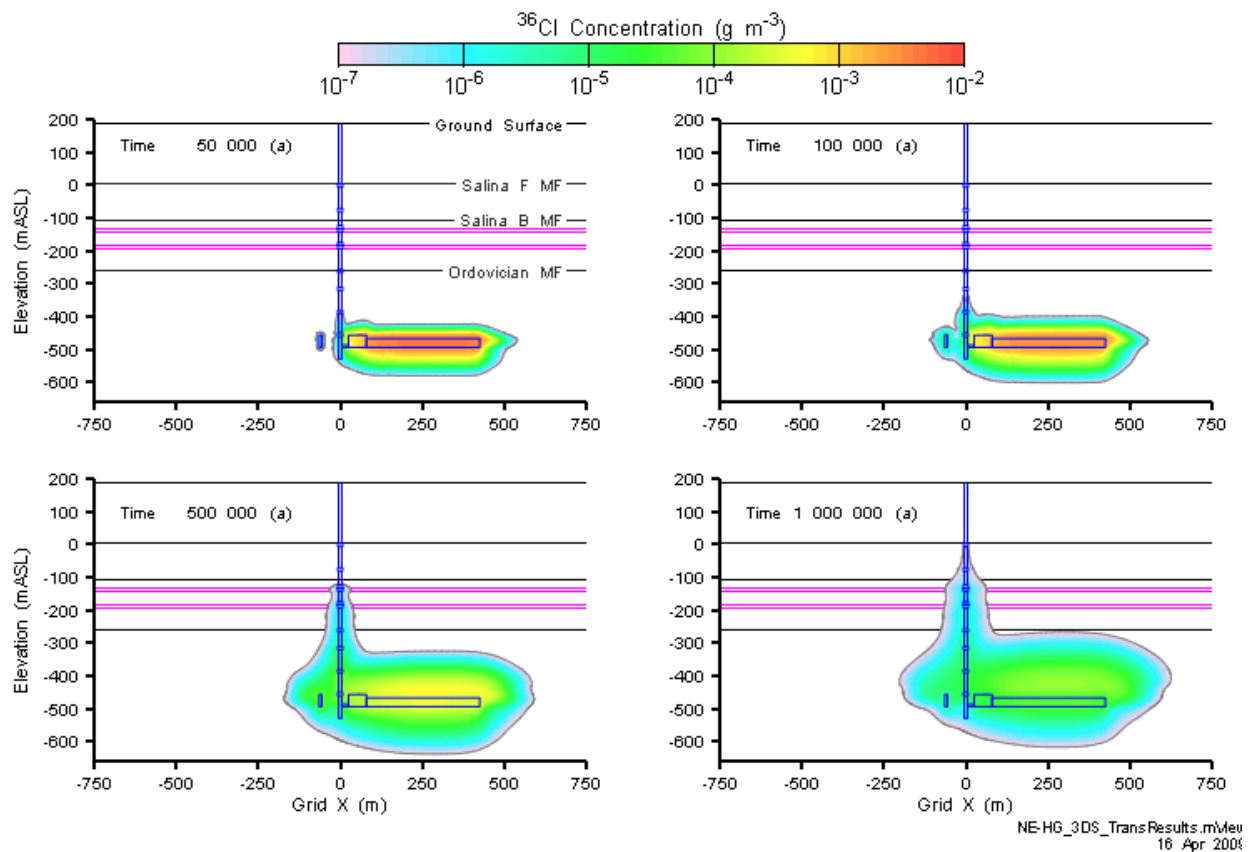


Figure 5.33: NE-NHG-F3 Cl-36 concentration at 50 000, 100 000, 500 000, and 1 000 000 years.

Figure 5.34 illustrates that the extent of transport is very limited horizontally, with the 10⁻⁷ g m⁻³ isovolume extending at most several hundred metres from the shaft and East panel. However, transport does extend above the Guelph/Salina A0 in both the shaft/EDZ system and the rock mass. This is in contrast to the NE-RS1 model where the Guelph/Salina A0 captures nearly all vertical mass flow, dilutes it, and transports it horizontally.

Time 1000000 (a)

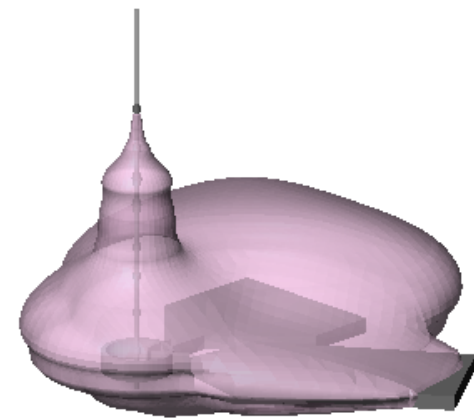
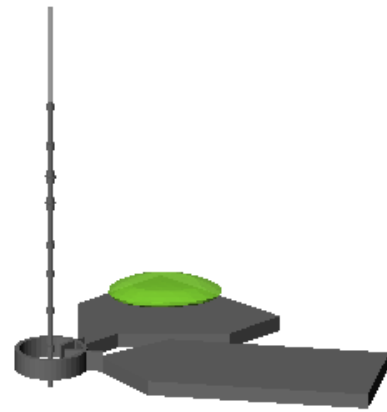
³⁶Cl concentration 10⁻⁷ (g m⁻³)³⁶Cl concentration 10⁻⁴ (g m⁻³)NE-HG_3DS_TransResults.mView
16 Apr 200

Figure 5.34: NE-NHG-F3 Cl-36 concentration isovolumes at 1 000 000 years.

Figure 5.35 and Figure 5.36 supports similar conclusions. Shaft and EDZ mass flow through the Salina B and Salina F planes is approximately a factor of five higher than the NE-RS1 results. The impact on mass flow through the rock mass is less pronounced (less than a factor of two for the Salina B mass flow plane). Nonetheless, total mass flow is extremely low. After 1 000 000 years only approximately 0.002% of the initial Cl-36 mass has reached the Salina F unit. The rate of mass transport across this plane never exceeds 10⁻⁸ g/a.

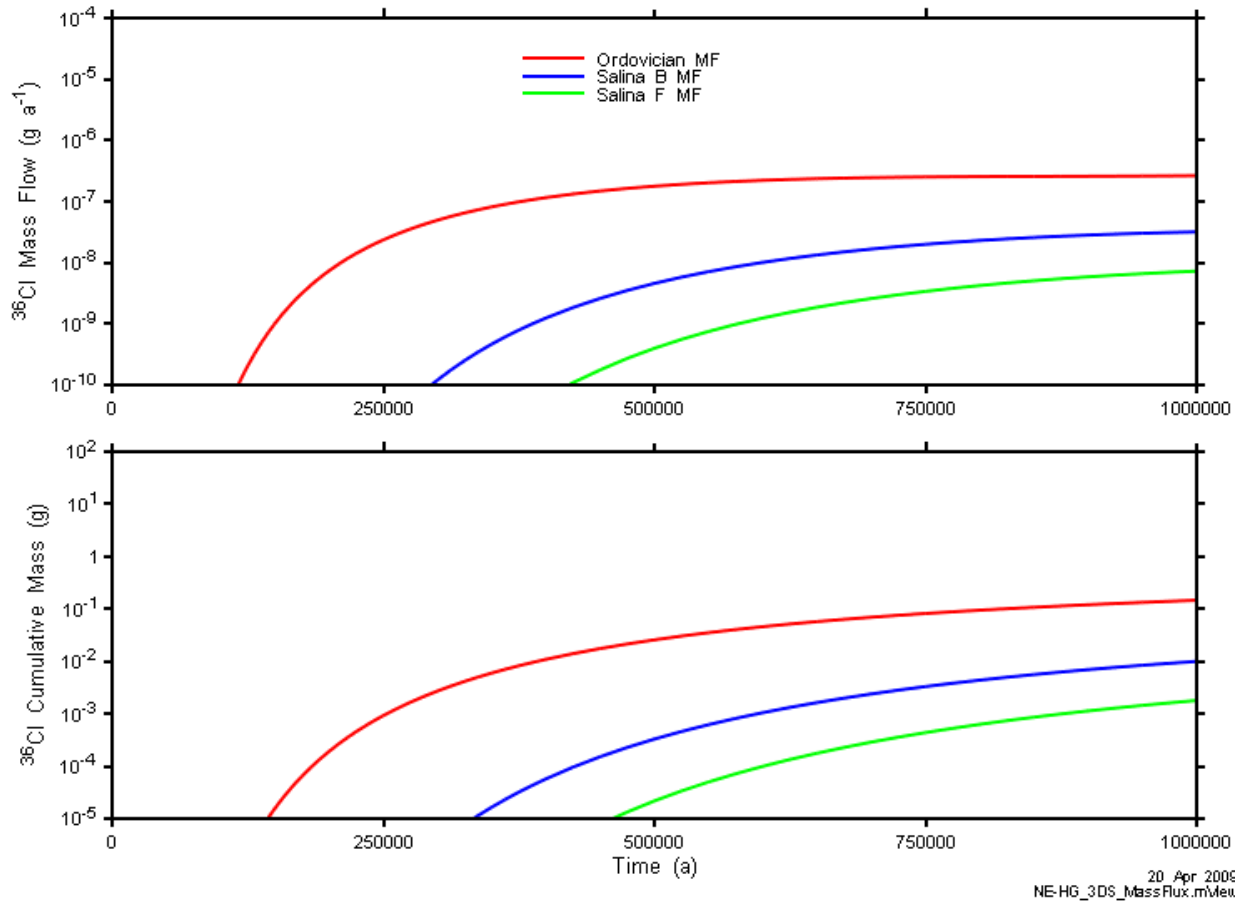


Figure 5.35: NE-NHG-F3 total mass flow and cumulative mass transport.

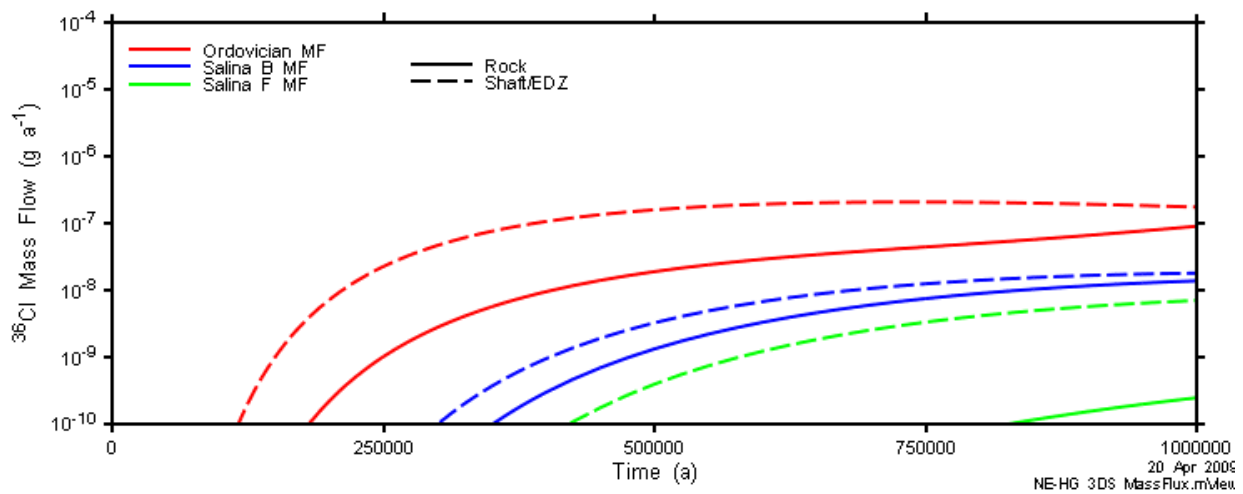


Figure 5.36: NE-NHG-F3 mass flow components.

5.3.2 NE-NHG-F2 Results

These are the 2D radial model results.

5.3.2.1 Flow Results

Hydraulic head contours and advective velocity magnitudes are shown in Figure 5.37 through Figure 5.40. The head and velocity distribution throughout the rock mass in the 2DR model is virtually identical to that determined by the 3DS model. The calculated hydraulic behaviour of the repository and shaft system is also very similar to the 3DS model. Some differences exist in the immediate vicinity of the access tunnel, monolith and shaft bottom (compare Figure 5.8 and Figure 5.39), which reflect the simplifications made to the 2DR model in these areas.

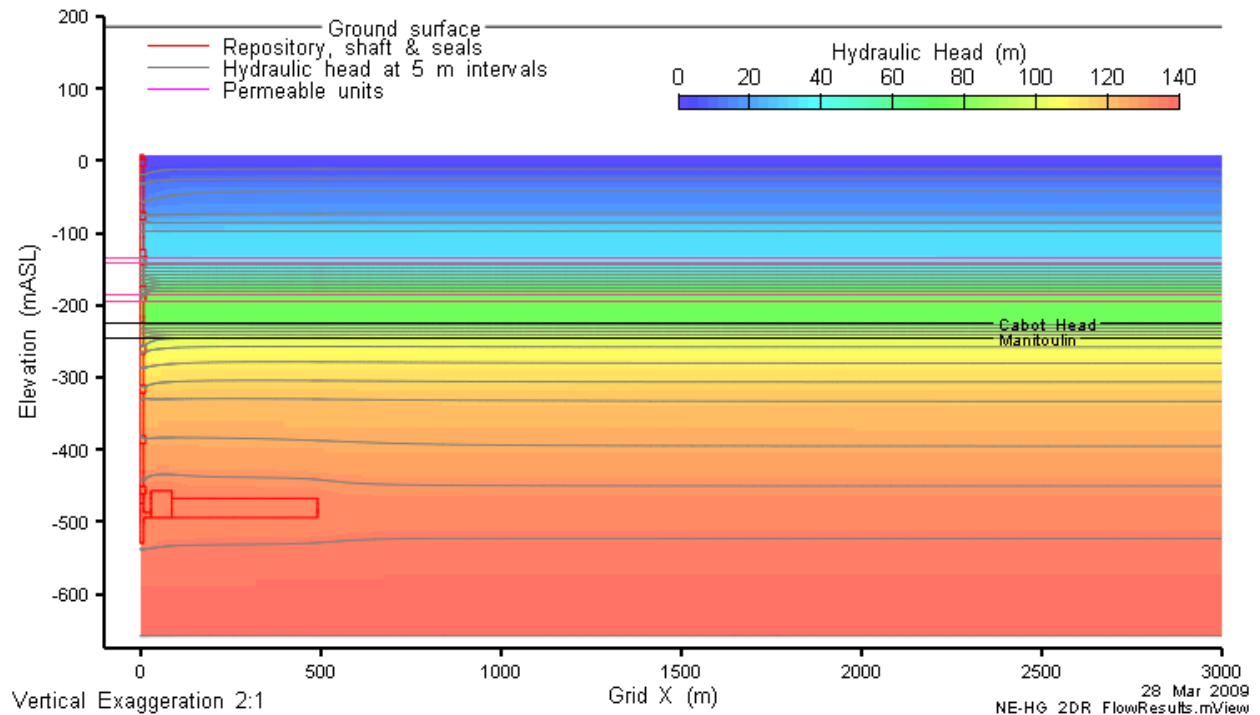


Figure 5.37: NE-NHG-F2 head contours for the entire model domain.

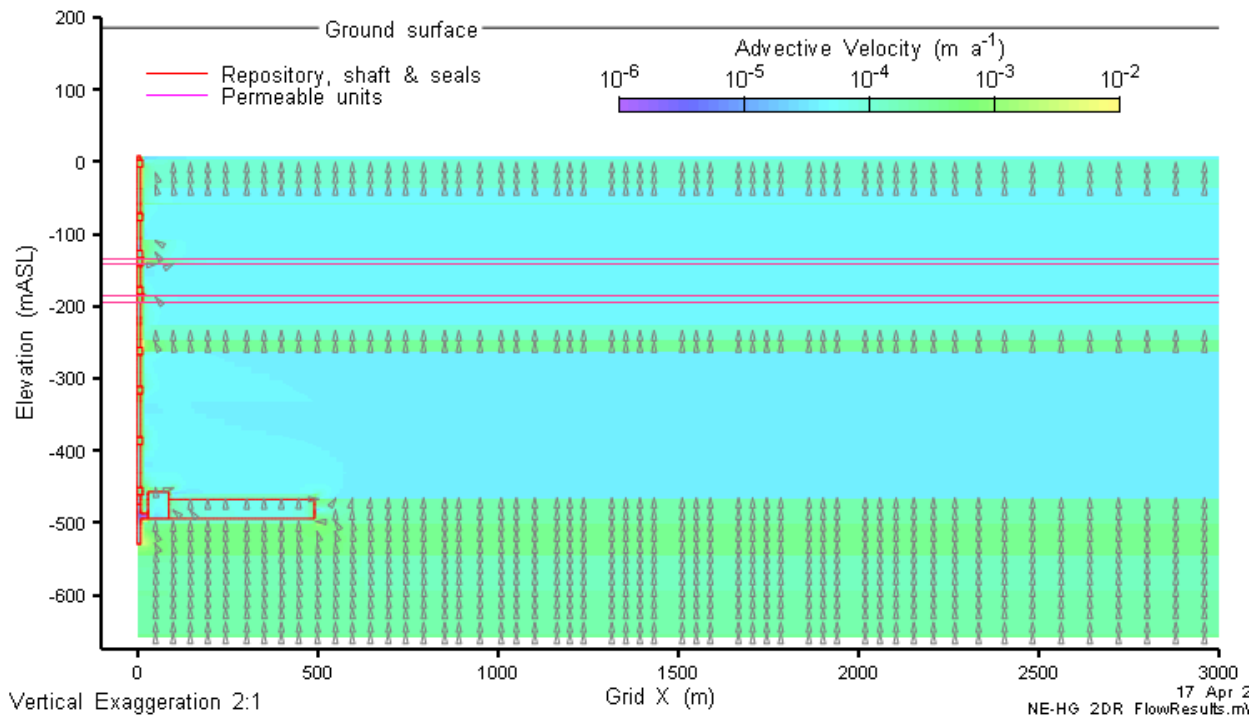


Figure 5.38: NE-NHG-F2 advective velocity magnitude and vectors for the entire model domain.

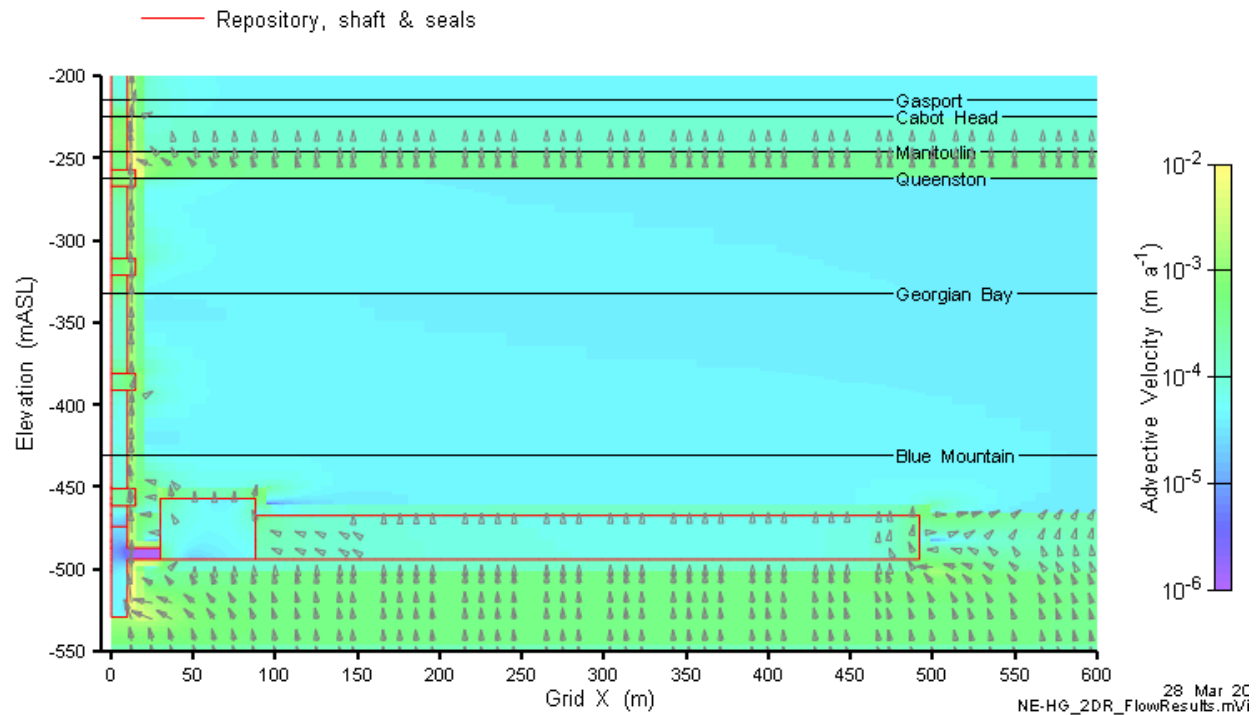


Figure 5.39: NE-NHG-F2 advective velocity magnitude and vectors in repository and lower shaft.

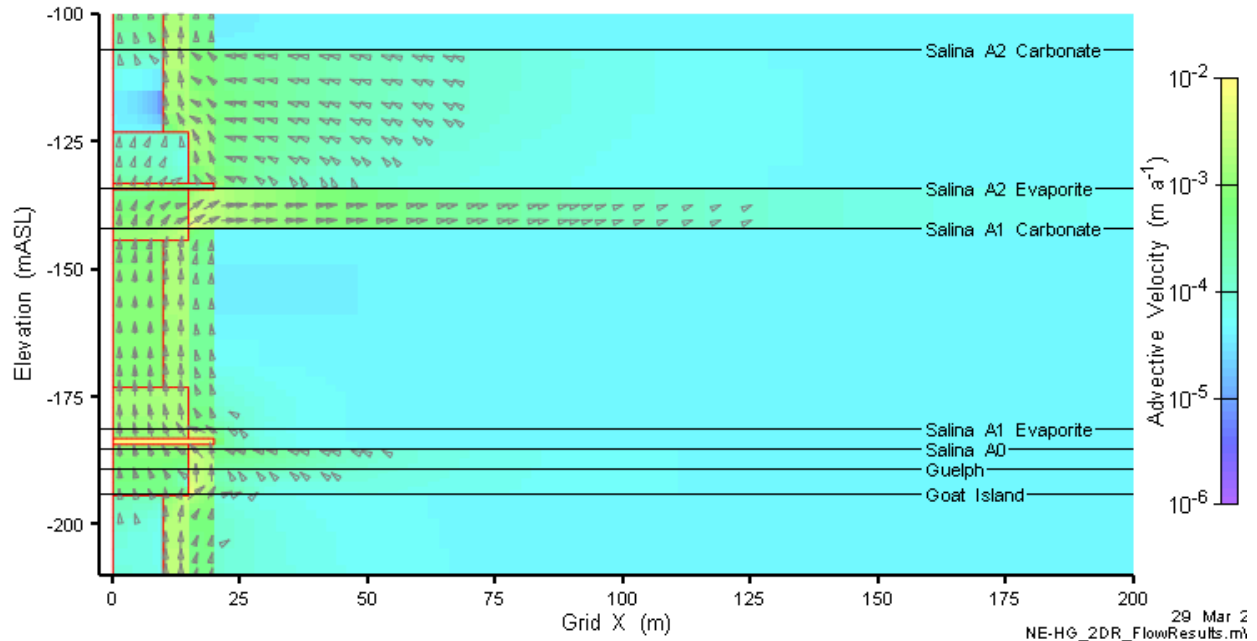


Figure 5.40: NE-NHG-F2 advective velocity magnitude and vectors in vicinity of Silurian seals.

5.3.2.2 Transport Results

Transport results are shown in Figure 5.41 through Figure 5.43. The calculated distribution of Cl-36 in the system in the rock mass is very similar in shape to that calculated by the 3DS model. Differences in specific contours (e.g. the presence of the 10^{-3} contour at 100 000 years in Figure 5.41) are due to the higher initial concentration in the East panel of the 3DS model. Within the shaft/EDZ system, the 2DR Cl-36 plume has migrated further upwards (cf. Figure 5.33 and Figure 5.41). Consequently, calculated rates of Cl-36 mass transport in the 2DR system are higher than those for the 3DS NE-NHG model particularly via the shaft/EDZ. The total cumulative Cl-36 flow across the Salina F MF plane is a factor of 70 higher in the 2DR NE-NHG model.

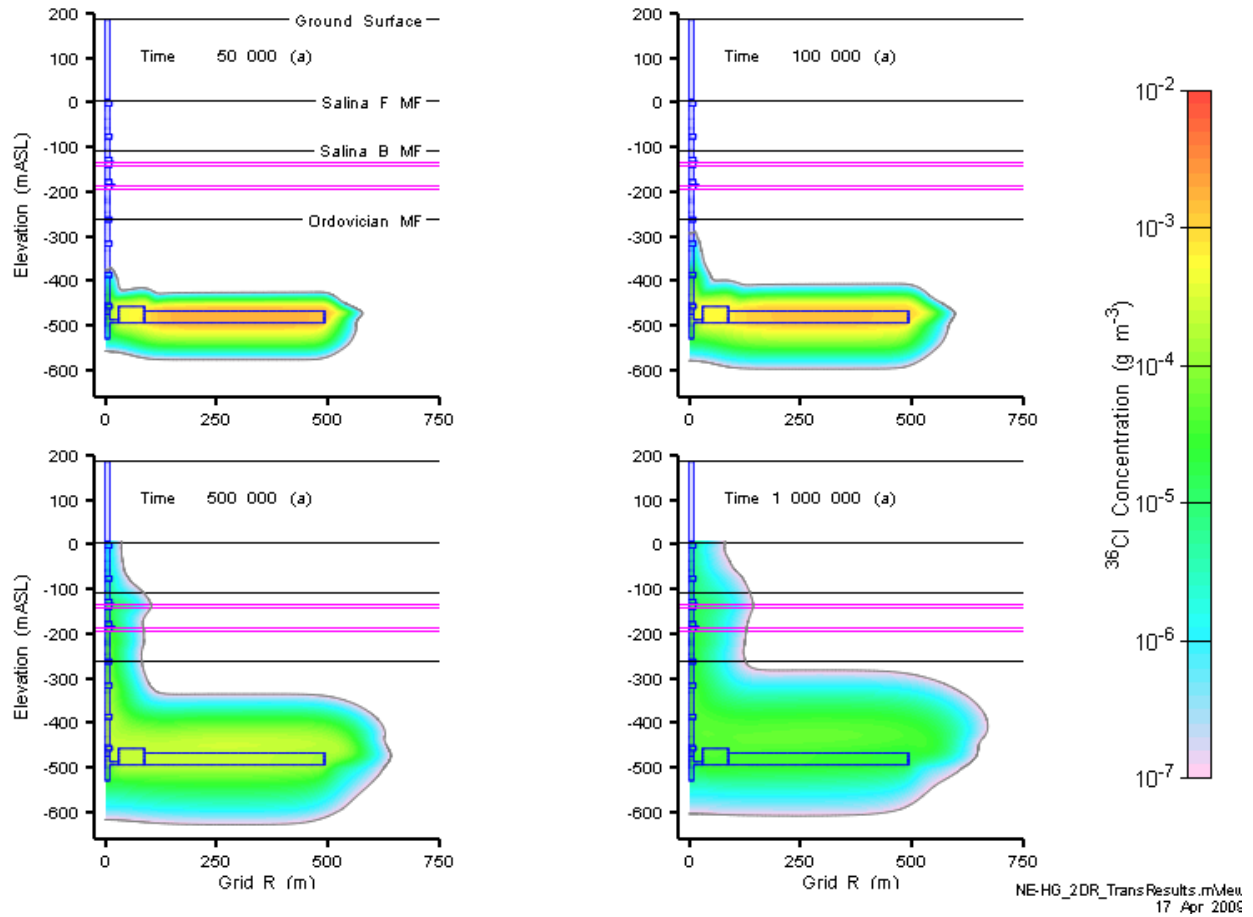


Figure 5.41: NE-NHG-F2 Cl-36 concentration at 50 000, 100 000, 500 000, and 1 000 000 years.

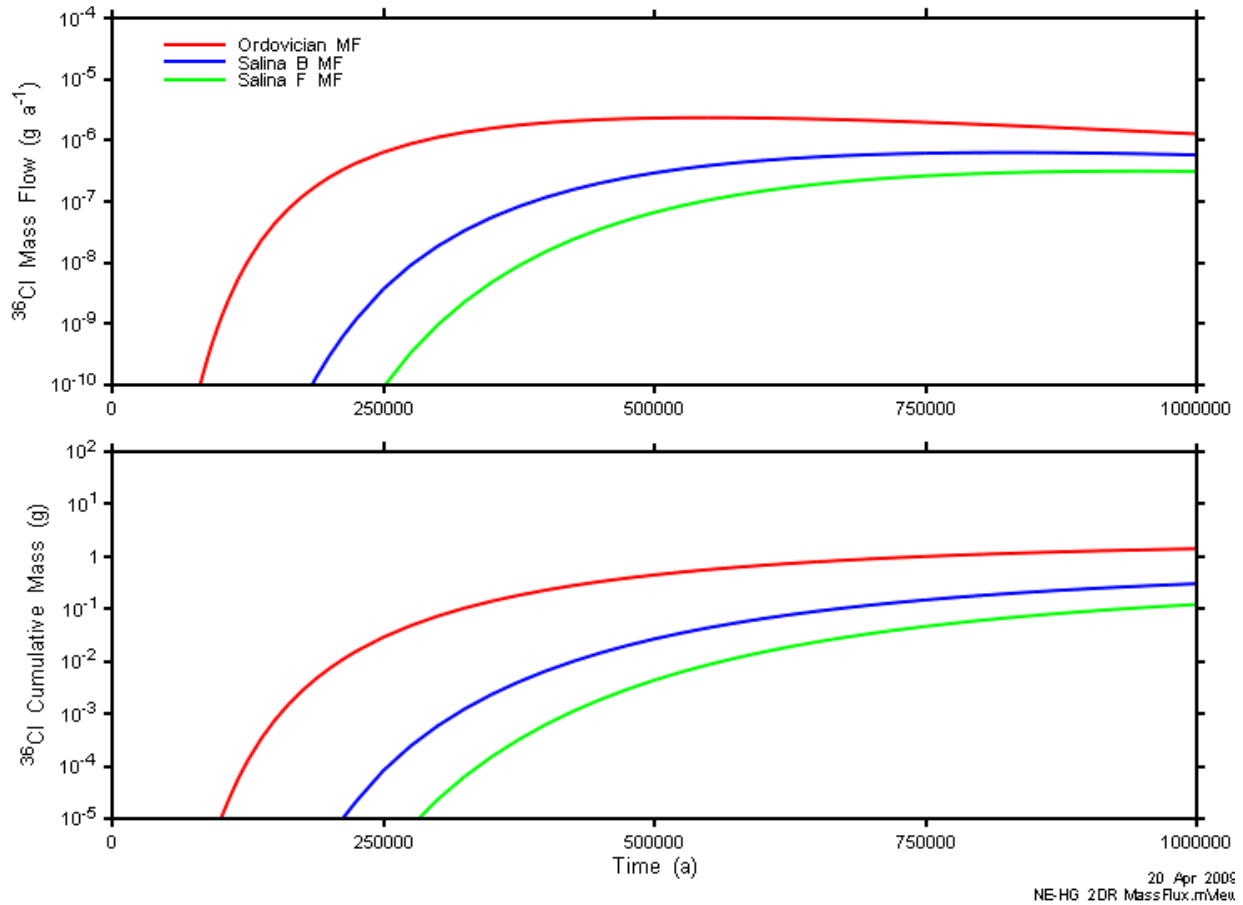


Figure 5.42: NE-NHG-F2 total mass flow and cumulative mass transport.

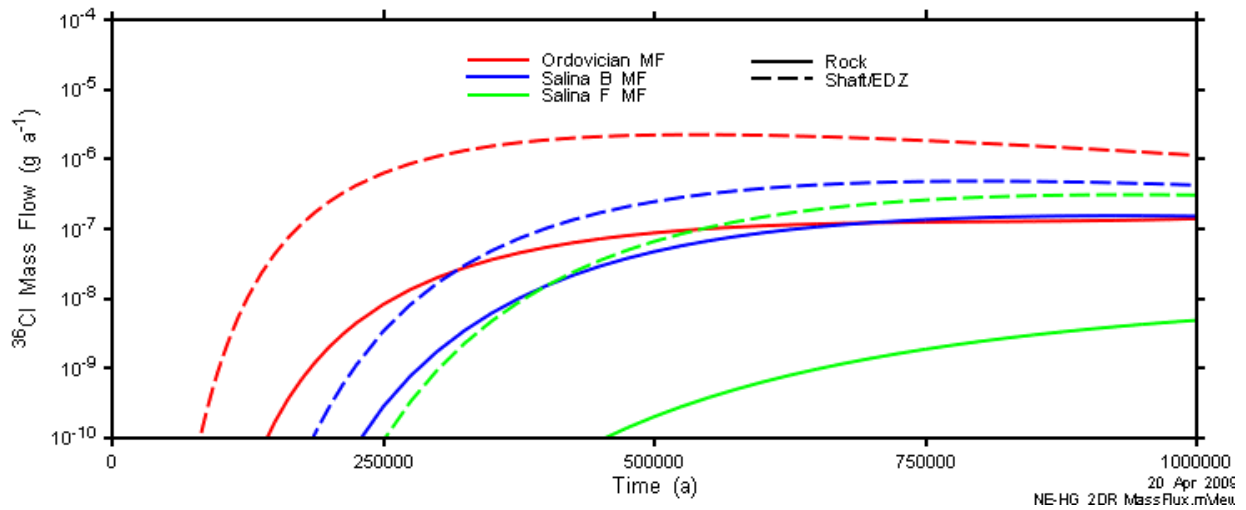


Figure 5.43: NE-NHG-F2 mass flow components.

5.3.3 2DR and 3DS Results Comparison

The general consistency of flow model results between the 2DR and 3DS models is demonstrated by comparing vertical fluid flux through the shaft and EDZ at each layer in the model. The resulting profiles show where the shaft/EDZ is gaining water from the formation (increasing flux with increasing elevation) or losing water to the formation (decreasing flux with increasing elevation). Results are presented in Figure 5.44.

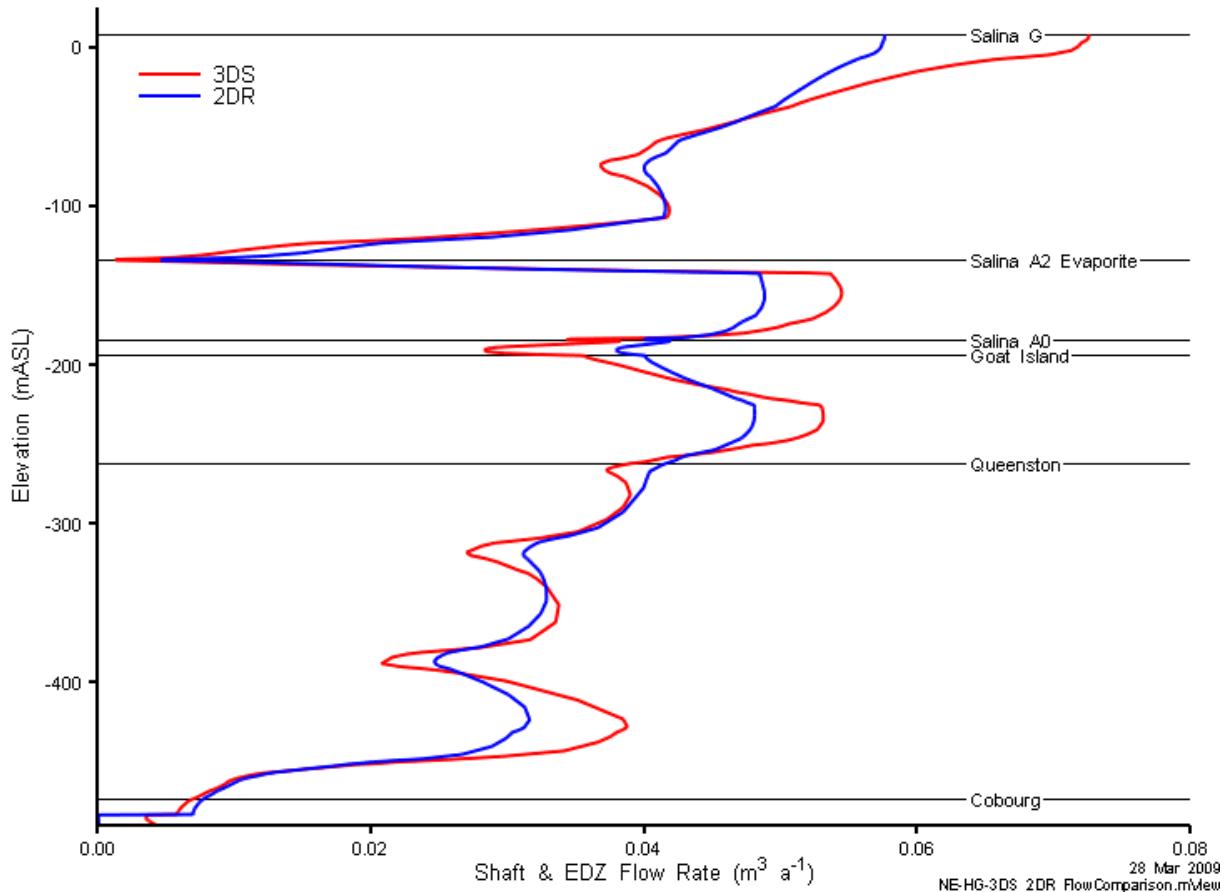


Figure 5.44: Comparison of NE-NHG-F3 and NE-NHG-F2 vertical fluid flux through shaft and EDZ.

For the most part the fluxes are very similar. In general, the 2DR model diminishes the impact of different units on the overall vertical flow, with the 3DS model showing greater extremes of fluctuation. This is likely due to the reduced area of contact between the Shaft/EDZ system and the rock mass for the 2DR model, caused by the selection of the 90 degree 2DR conceptual model. Although shaft/EDZ cross sectional areas are identical for 3DS and 2DR (see Table 4-5), the shaft/EDZ circumference of the 2DR model is half that of the 3DS model. Flow into and out of the shaft is a function of circumferential area and gradient, so the greater area of the 3DS model results in larger flow fluctuations.

The effect of the asphalt waterstop seals at the Salina A0 and Salina A2 is clear, with approximately 40% of the shaft flux being forced into the formation at the first seal and nearly

all flux at the upper seal. It is equally clear that the flow soon recovers above the plug, as water diverted into the rock mass returns to the shaft and EDZ. As discussed previously in Section 5.3.1.1, the seals do not have a significant impact on total EDZ flow for the base case EDZ parameterization.

Figure 5.45 compares mass flow in the Shaft/EDZ system (top) and mass flow in the rock mass (bottom) from the 2DR and 3DS NE-NHG model results. The model results compare well, with the 2DR model being approximately a factor of ten higher in the shaft/EDZ and broadly similar at 1 000 000 years for the rock mass. The primary reason for the higher flux appears to be the reduced area of contact between the EDZ and rock mass in the 2DR model as compared to the 3DS model as described above. In addition to greater dilution in the 3DS models, the reduced area will also reduce diffusional flux outward. This limits the amount of diffusion into the rock mass, thus increasing the mass of Cl-36 retained in the vertically flowing shaft/EDZ system.

Section 7.1 provides more discussion of the relative merits of each modelling approach.

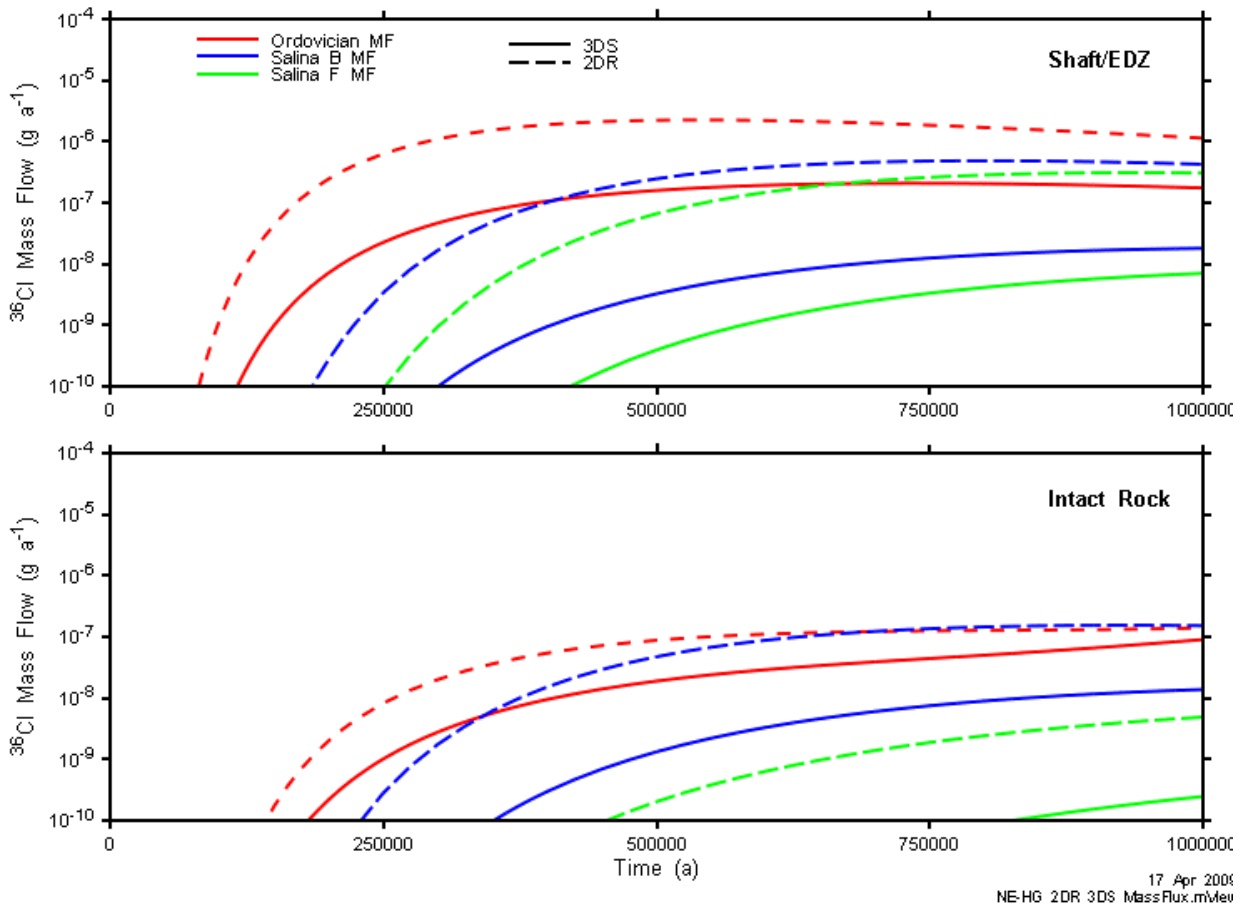


Figure 5.45: Comparison of Cl-36 mass flow results for the 3DS and 2DR NE-NHG models in the Shaft/EDZ system and in the rock mass

17 Apr 2008
NE-HG 2DR 3DS MassFlux.m/Meu

5.3.4 3DSU Results

5.3.4.1 Flow Results

Hydraulic head and advective velocity plots for the 3DSU model are shown below in Figure 5.46 and Figure 5.47. The influence of the pumping well can be clearly seen. Advective velocities are highest in the permeable Bass Island Formation and in the immediate vicinity of the pumping well.

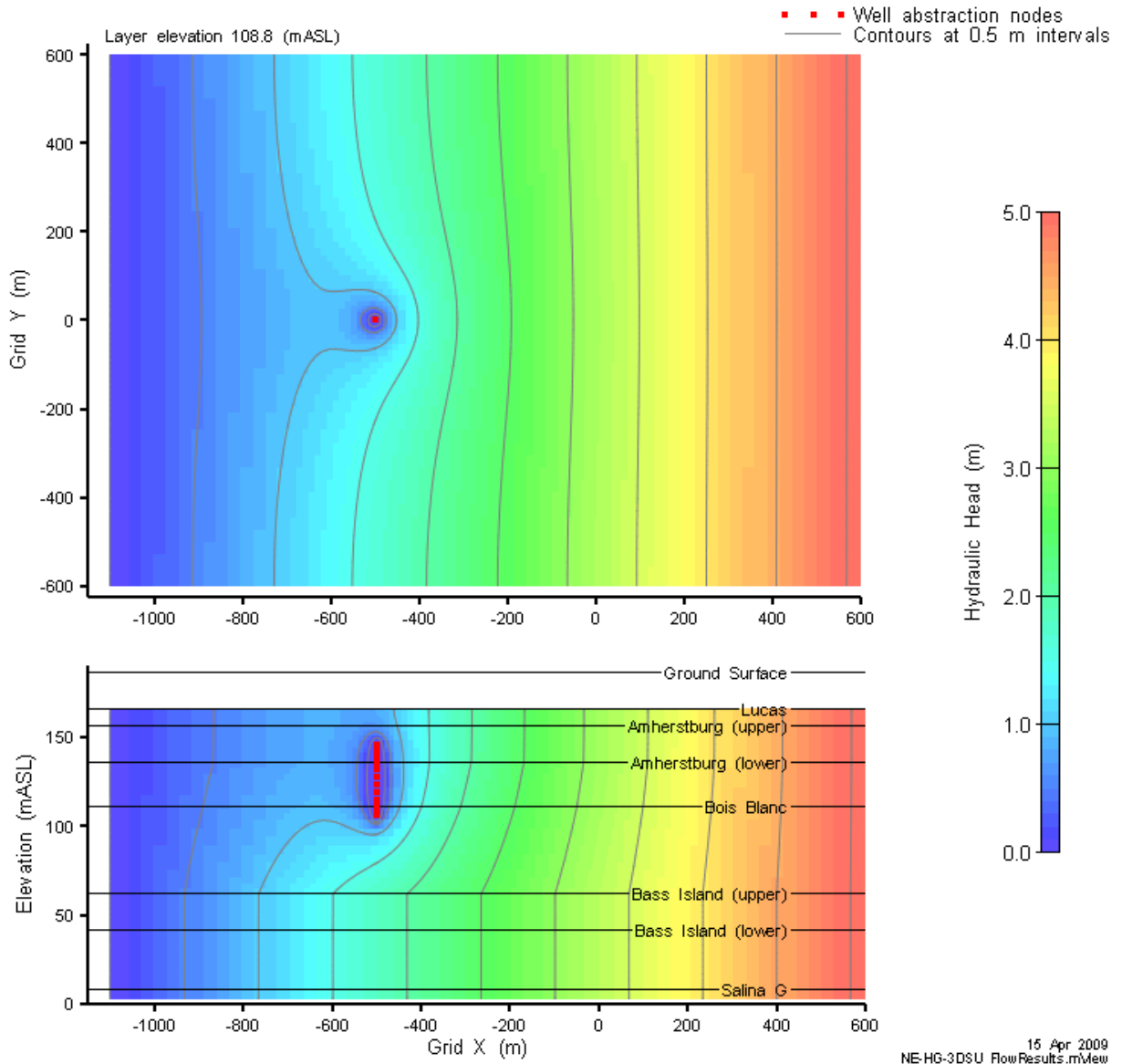


Figure 5.46: NE-NHG-3DSU head contours for the entire model domain.

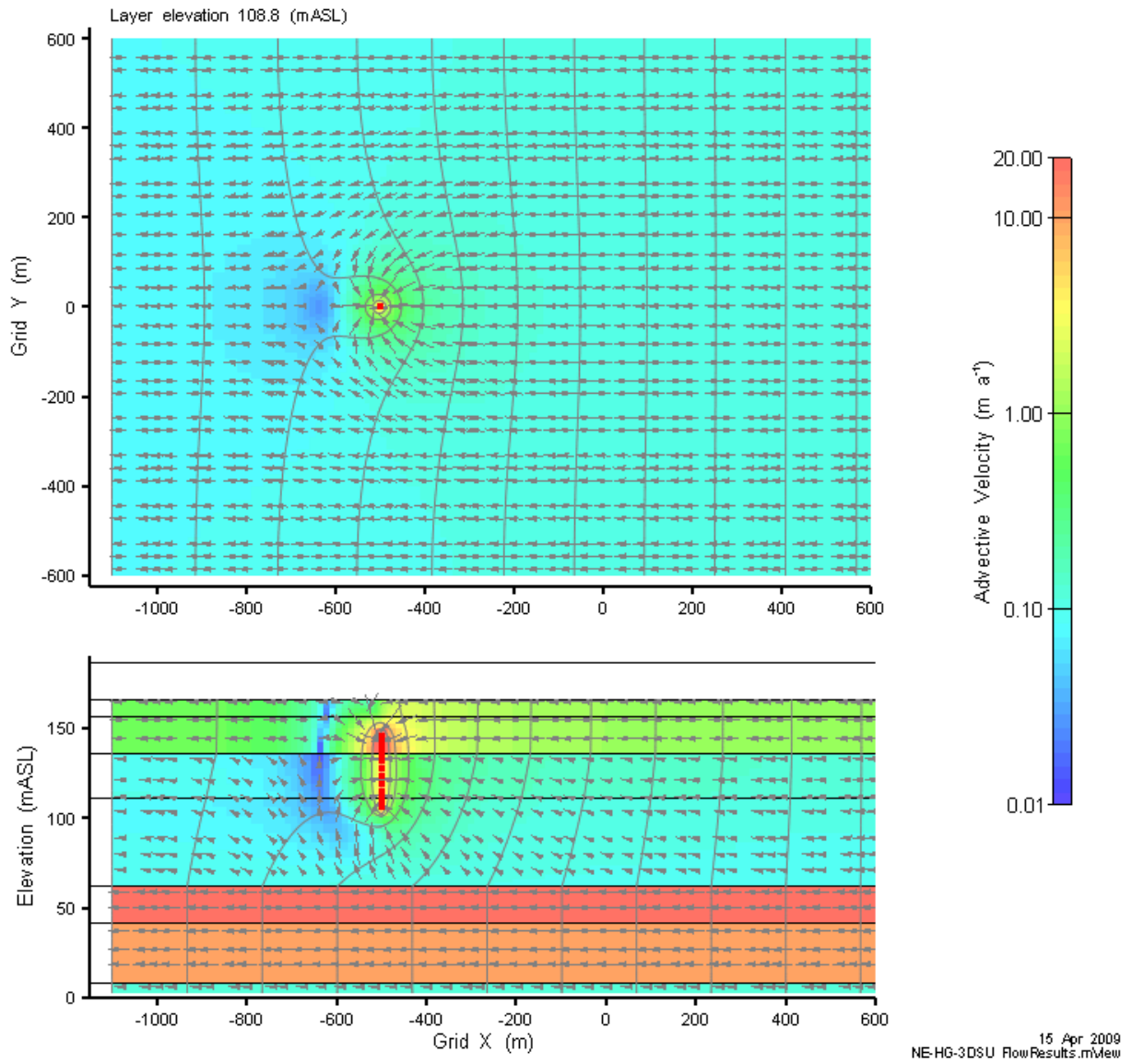


Figure 5.47: NE-NHG-3DSU advective velocity magnitude and vectors for the entire model domain.

5.3.4.2 Transport Results

Contaminant input for the 3DSU model was taken from the NE-NHG-F2 model. These flows are higher than the NE-NHG-F3 model and are thus conservative. Mass flow across entire the Salina F MF plane was summed and applied as a mass flux source term at the shaft location, representing the mass flow exiting the Salina F unit. Transport was modelled for the same 1 000 000 year period as the 3DS and 2DR models. The concentration plume at 1 000 000 years is shown in Figure 5.48 through Figure 5.50 on two horizontal planes and one vertical plane. Note that concentration limits for the plots are six orders of magnitude lower than discussed in Section 5.1.2 for other spatial concentration plots. All results (including the source concentration) are below the 10^{-7} g m^{-3} lower limit used in other plots. The concentration in the upper aquifer is extremely low, and the majority of the Cl-36 bypasses the well. The maximum concentration in any well node throughout the simulation is $1.1 \times 10^{-12} \text{ g m}^{-3}$, which corresponds to a dose approximately eight orders of magnitude below the dose criterion.

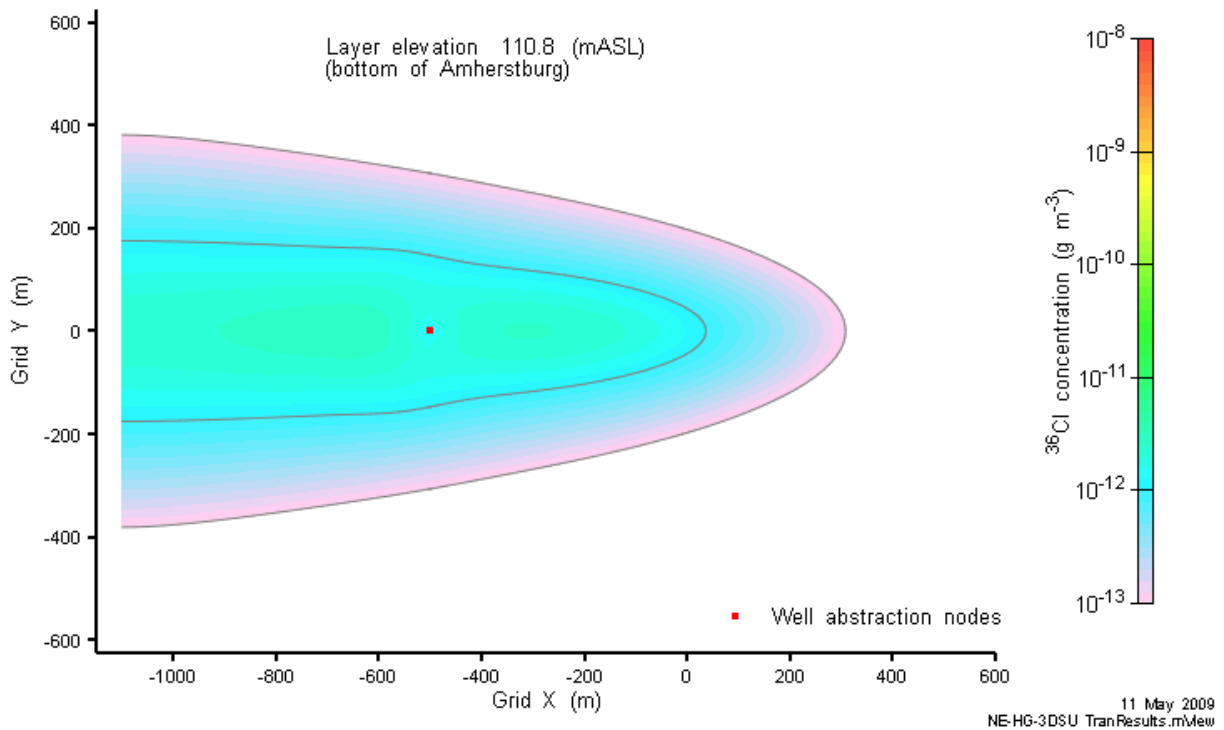


Figure 5.48: NE-NHG-3DSU Cl-36 concentration in horizontal plane through water-supply well at 1 000 000 years.

11 May 2009
NE-NHG-3DSU TranResults.mView

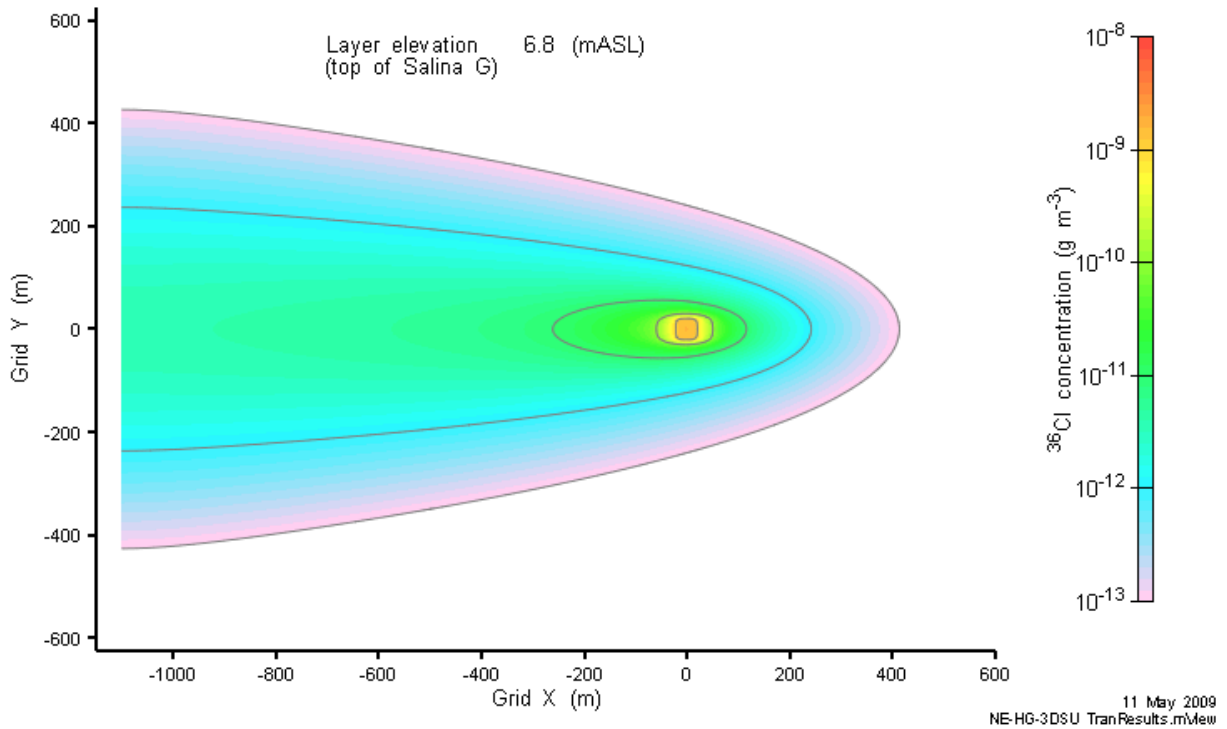


Figure 5.49: NE-NHG-3DSU CI-36 concentration in horizontal plane through top of Salina G Formation at 1 000 000 years.

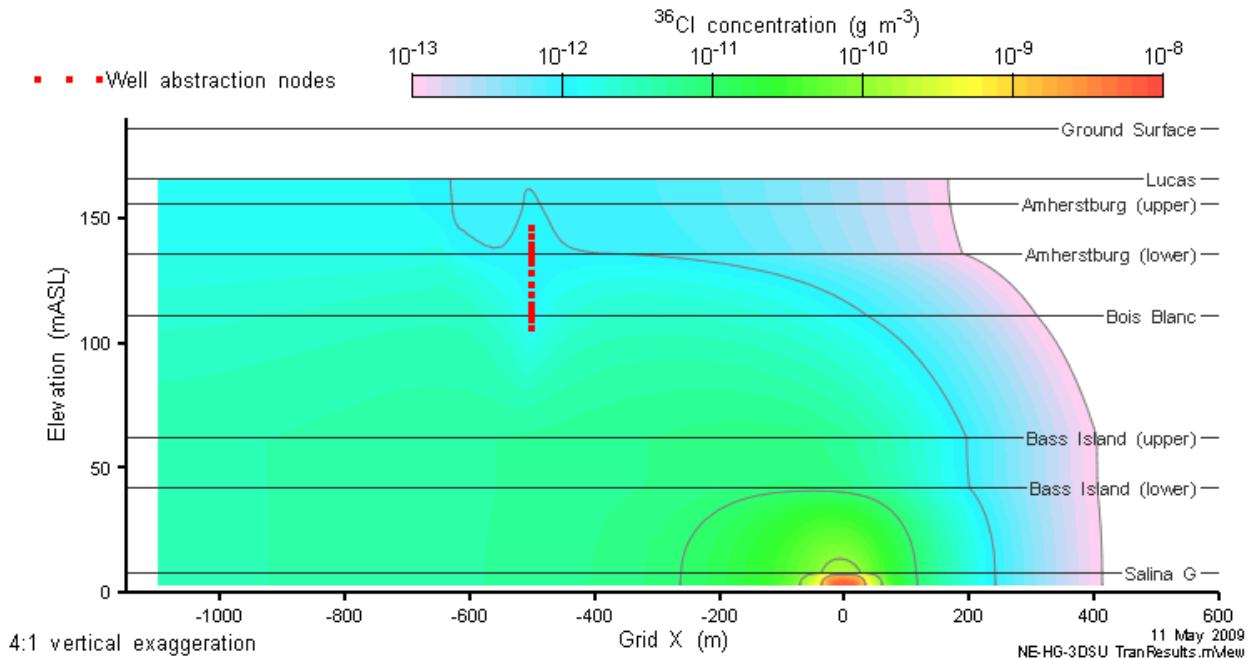


Figure 5.50: NE-NHG-3DSU CI-36 concentration on vertical plane through water-supply well and source at 1 000 000 years.

The same is seen in the mass transport curves in Figure 5.51, where approximately 1% of the total input mass is captured by the well (80 m depth). The remainder leaves the boundaries of the model and is assumed here to reach the lake.

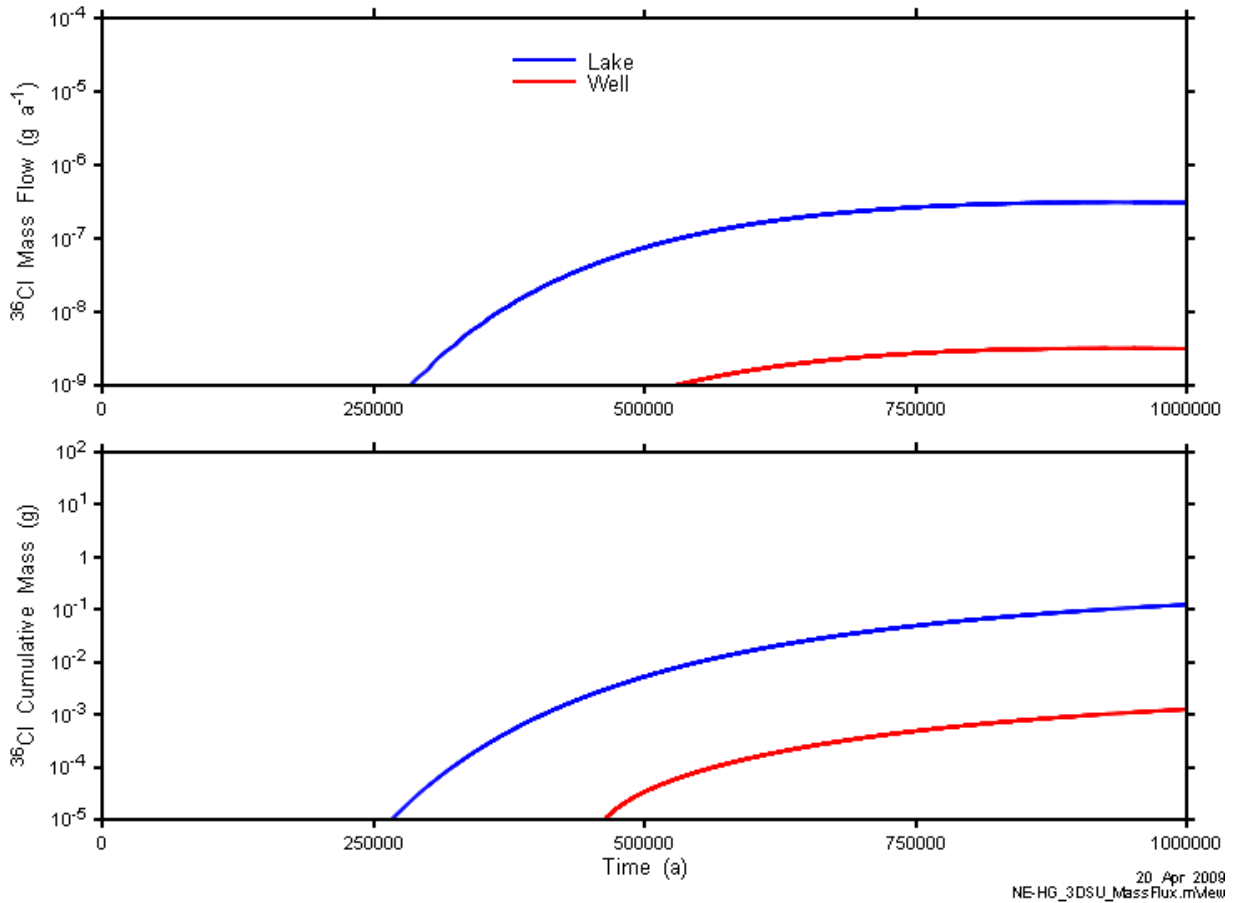


Figure 5.51: Mass transport to Lake Huron and the pumping well for the 3DSU NE-NHG model.

5.4 NE-UG-NHG-F2 Updated Geosphere, No horizontal flow in Silurian, Transient Flow from environmental heads

The NE-UG-NHG transient flow case is intended to address the impact of observed underpressures in the Ordovician sequence. The initial conditions are based on the pressure profile observed at site and previously shown in Figure 2.2.

5.4.1 Flow Results

Figure 5.52 shows the transient hydraulic head profiles at Grid R = 1000 m beyond the hydraulic influence of the repository. Using the updated geosphere material parameters, the Ordovician shale underpressure are not substantially dissipated within the 1 000 000 year simulation period.

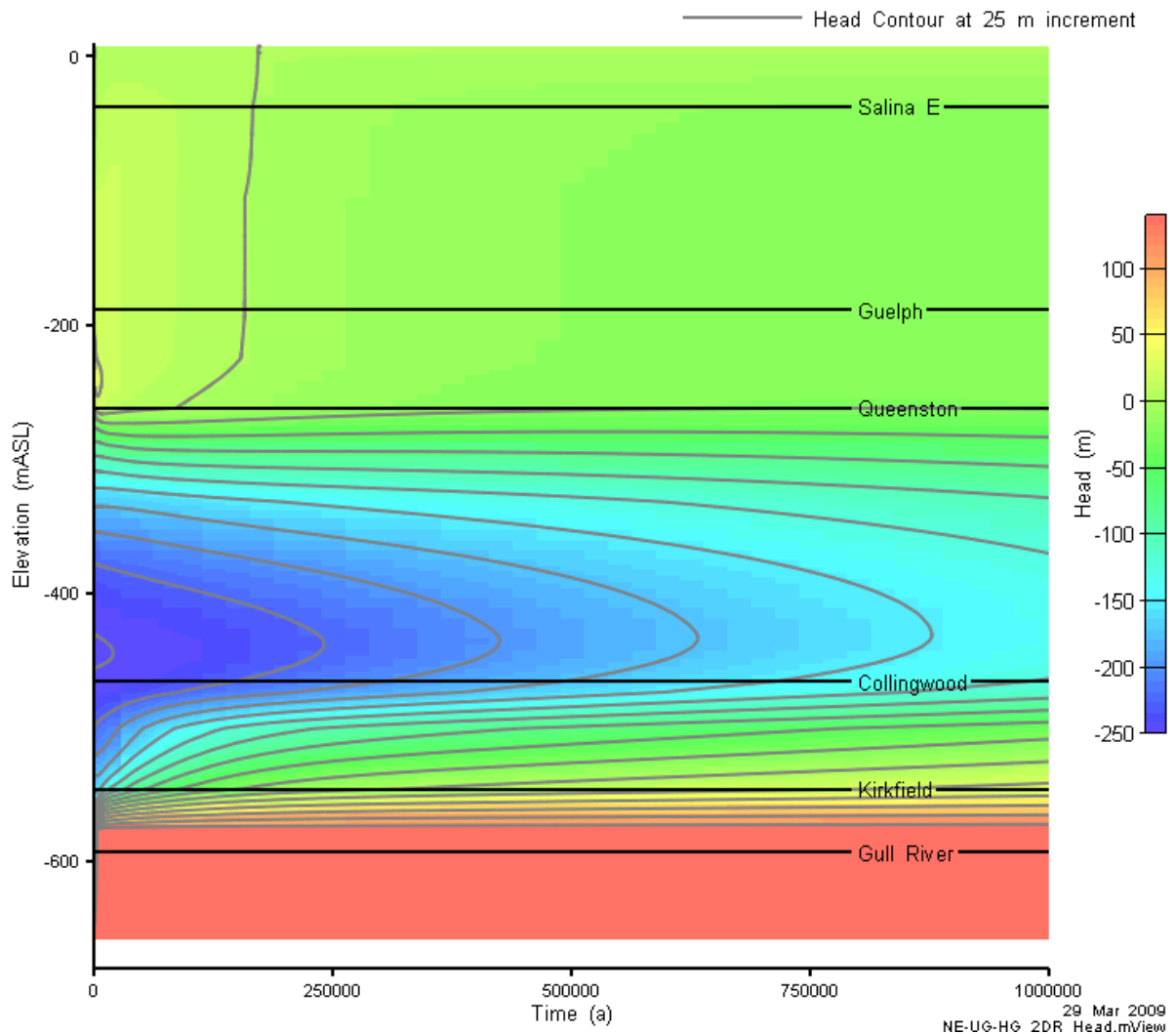


Figure 5.52: NE-UG-NHG-F2 transient hydraulic head versus time at R = 1000 m.

Figure 5.53 is an alternate representation of the same results, showing the simulated hydraulic profile at selected times. The flow simulation time was extended to 7.5Ma and the results of a steady-state run are also shown on the figure. The initial profile is shown at $t = 0.5$ a. Within 10 000 years the overpressure in the lower Silurian has substantially dissipated and the overall Silurian profile shows very little vertical gradient, except over the low permeability Salina F. The gradient in the lower Ordovician (Coboconk and Gull River) has also dissipated.

At 1 000 000 years, the underpressure in the Ordovician has reduced from a peak of -250 m to approximately -140 m. Even after 7 500 000 years complete dissipation (i.e. return to steady-state profile) has not occurred.

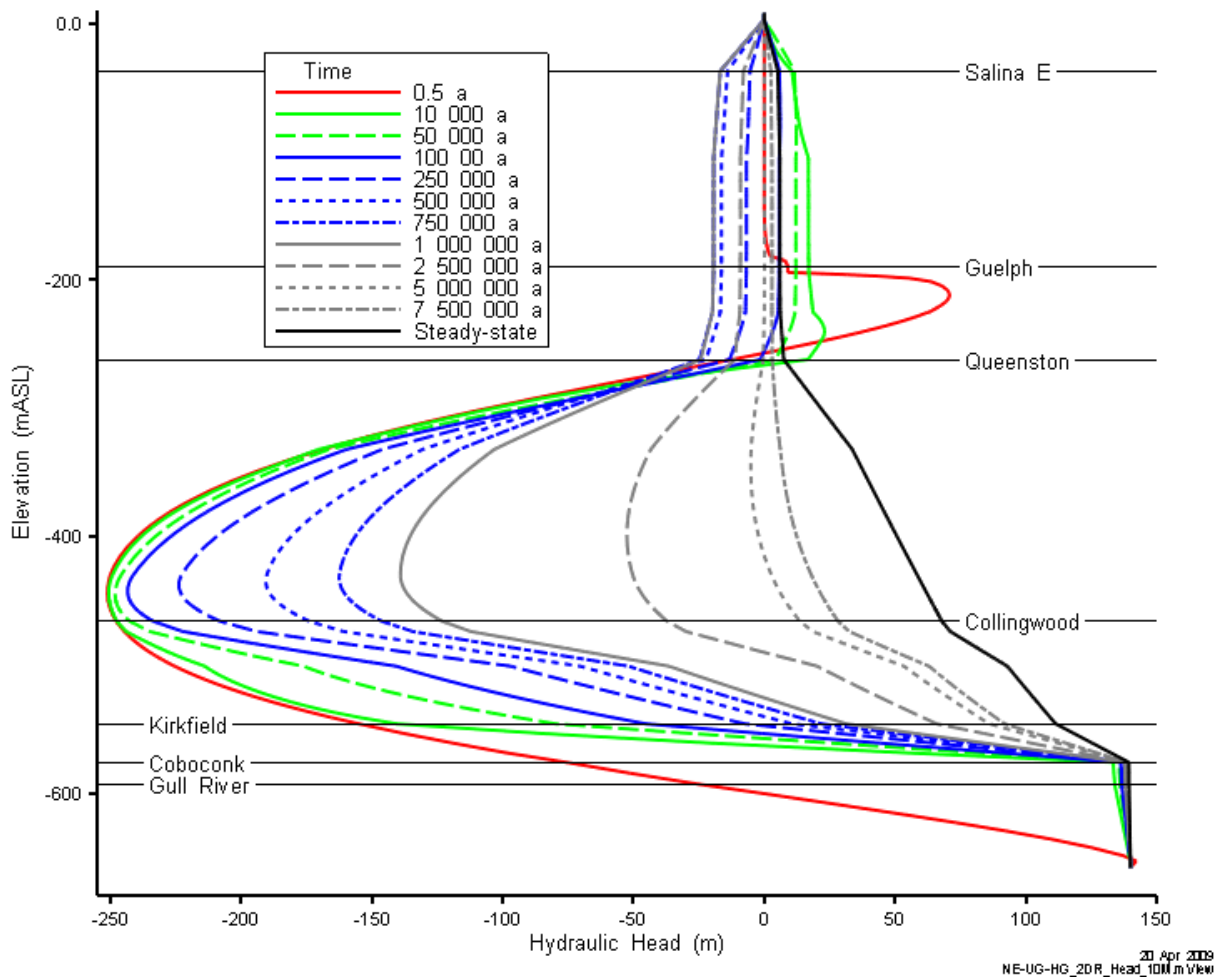


Figure 5.53: NE-UG-NHG-F2 hydraulic head profiles at R = 1000 m.

Figure 5.54 illustrates the head profile surrounding the repository at 1 000 000 years. The repository remains significantly more underpressured than the surrounding rock.

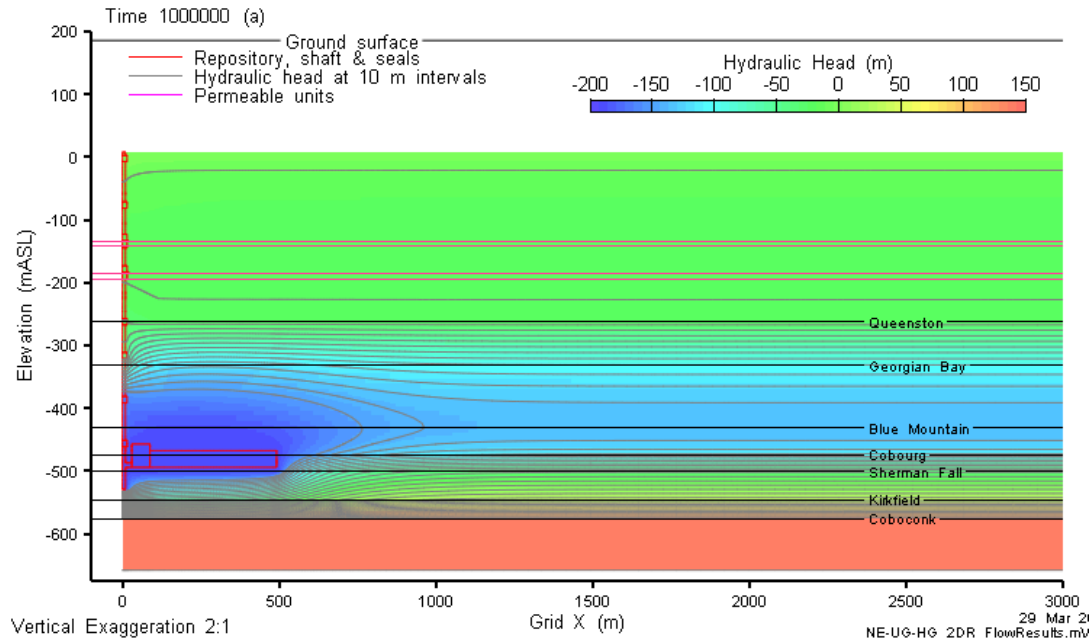


Figure 5.54: NE-UG-NHG-F2 head contours on a vertical slice at 1 000 000 years.

Advective velocities are directed toward the repository at all times as shown in Figure 5.55 with flow directed down the shaft EDZ. Note that the figure has an expanded velocity range and reduced threshold for vector display.

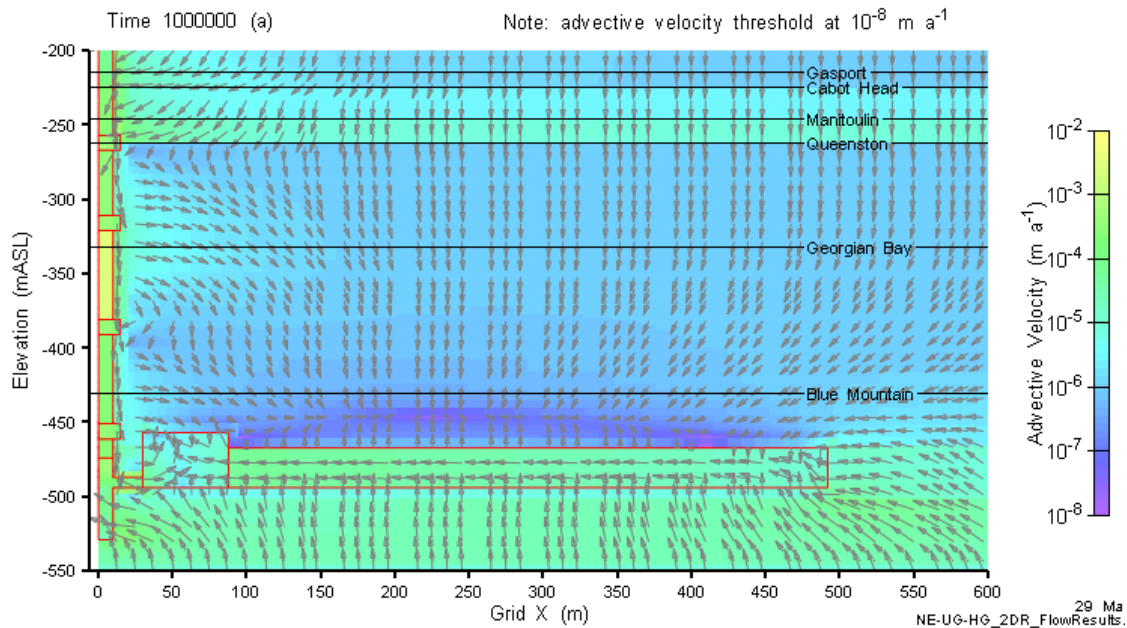


Figure 5.55: NE-UG-NHG-F2 advective velocity magnitude and vectors in the vicinity of the repository at 1 000 000 years.

5.4.2 Transport Results

Concentration and mass transport results are shown in Figure 5.56 and Figure 5.57. The transient flow domain further reduces the negligible transport previously seen for the NE-UG-RS1 case.

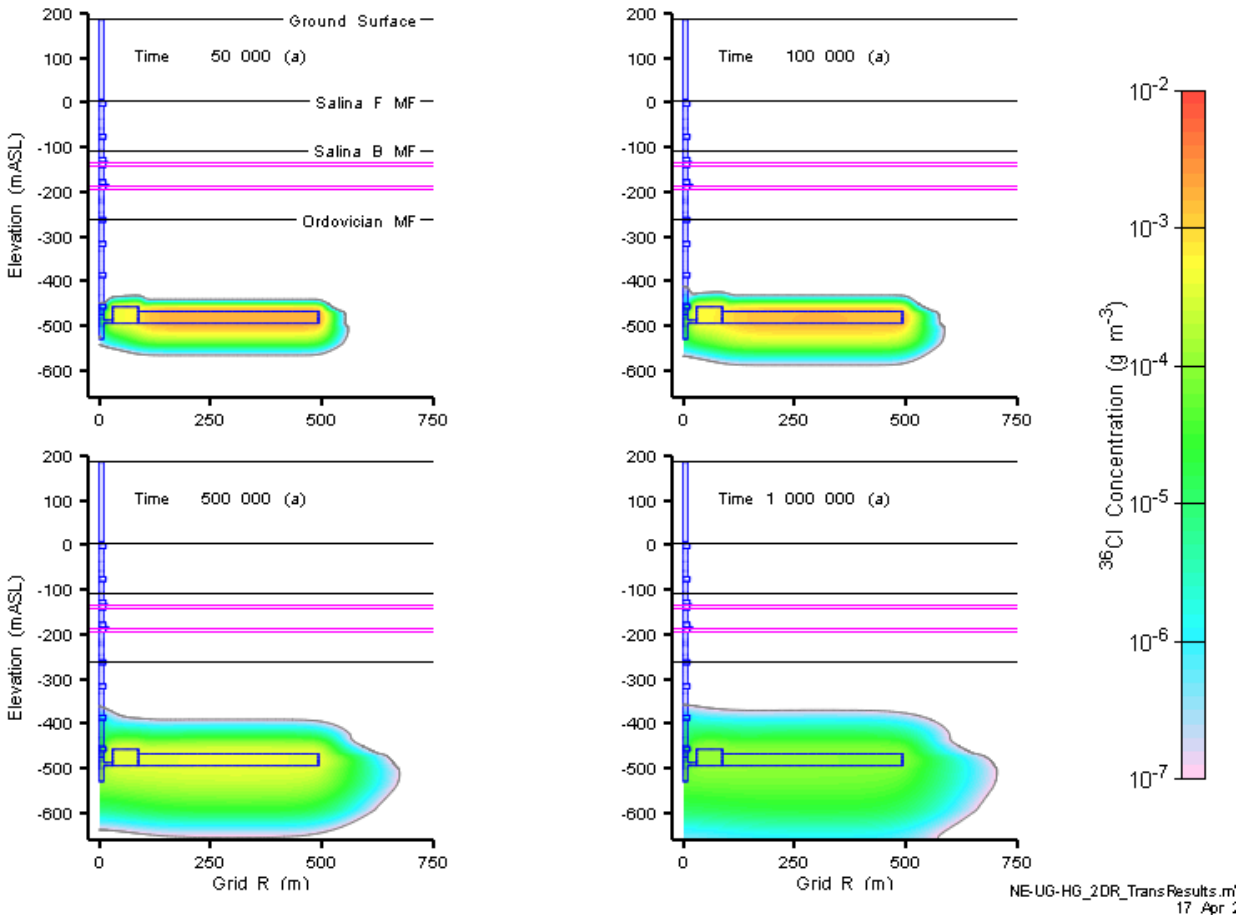


Figure 5.56: NE-UG-NHG-F2 Cl-36 concentration at 50 000, 100 000, 500 000, and 1 000 000 years.

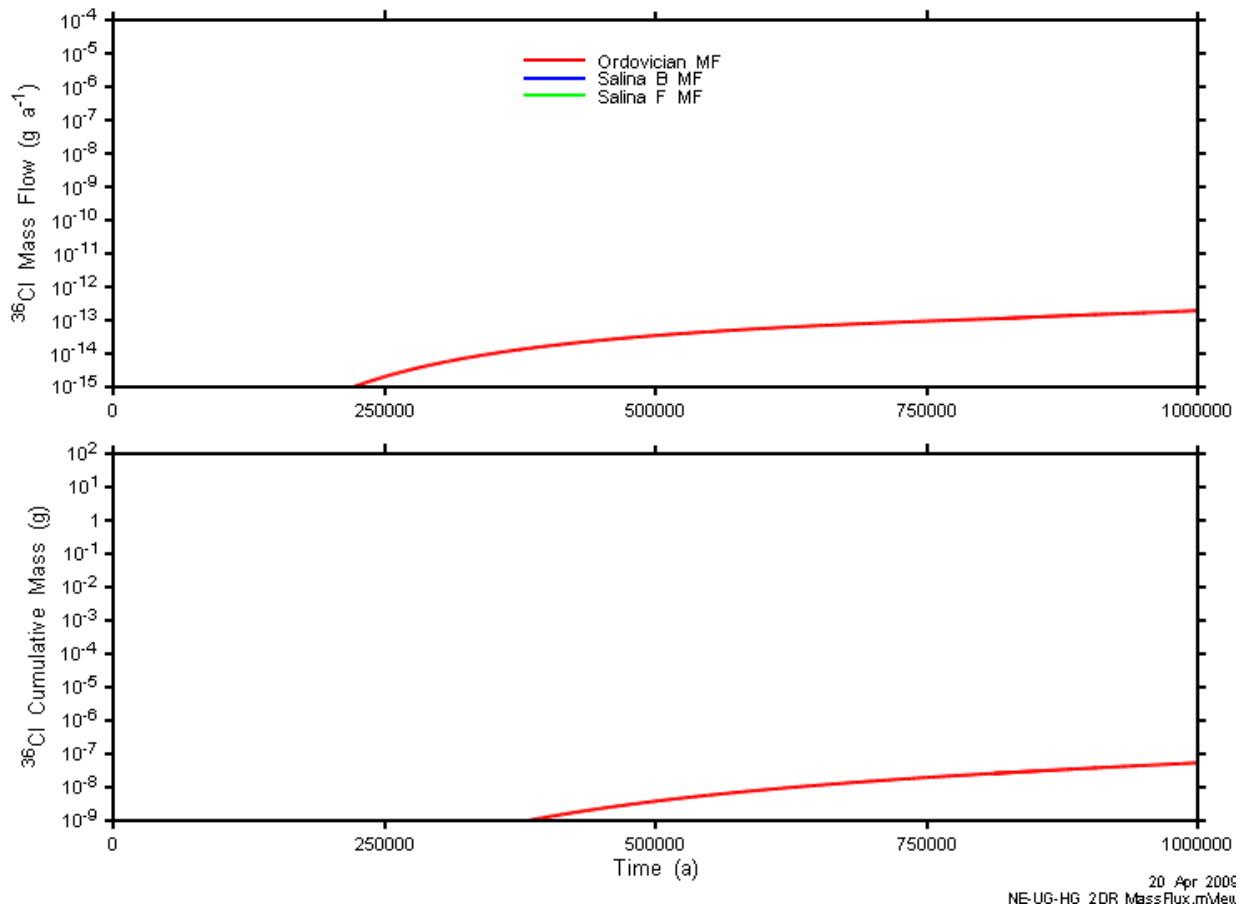


Figure 5.57: Mass transport results for the NE-UG-NHG-F2 model. Salina B and Salina F results are below Y axis limits.

5.5 NE-EDZ: Higher Conductivity in Shaft EDZ (NE-EDZ-F2 and NE-UG-EDZ-F2)

In this modelling case, the rock properties are identical to those in the reference and in the updated geosphere (UG) model, but the shaft EDZ permeability is much higher. Additionally, the concrete bulkheads and asphalt water stops in the EDZ are assumed to be ineffective.

5.5.1 NE-EDZ-F2 Results

5.5.1.1 Flow Results

Within the rock mass, flow results for the NE-EDZ-F2 model are similar to the NE-NHG-F2 modelling case. However, velocities in the shaft EDZ are much higher (see Figure 5.58) than in the NE-NHG-F2 case as is flow in the Silurian units. The colour legend in the figures has been expanded to accommodate the increased velocities. The maximum velocity in the shaft inner EDZ is on the order of 1.5 m a^{-1} .

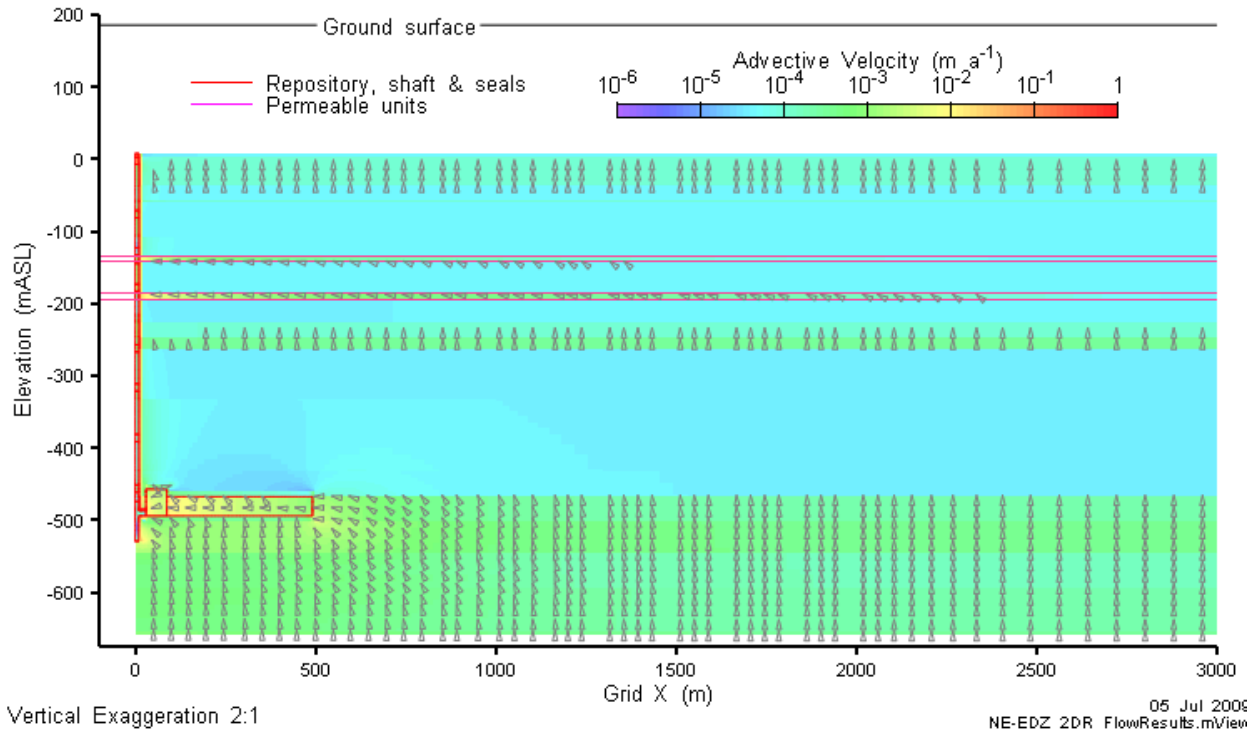


Figure 5.58: NE-EDZ-F2 advective velocity magnitude and vectors in repository and lower shaft.

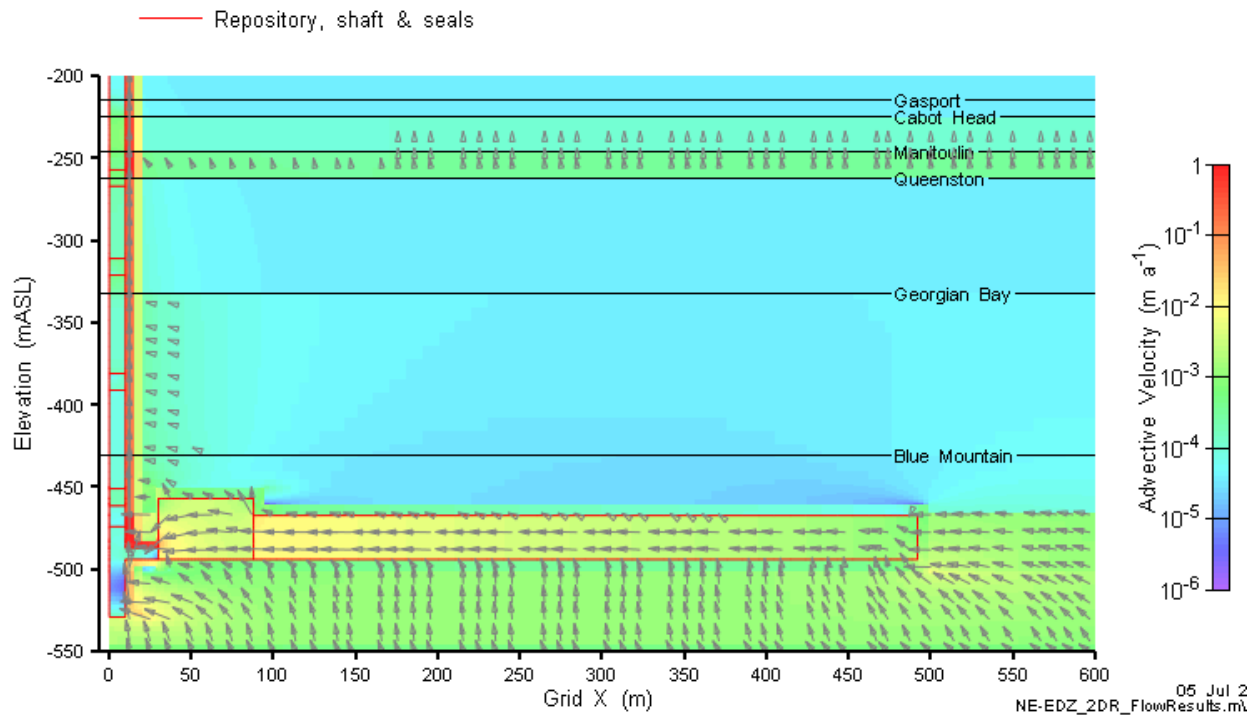


Figure 5.59: NE-EDZ-F2 advective velocity magnitude and vectors in vicinity of repository.

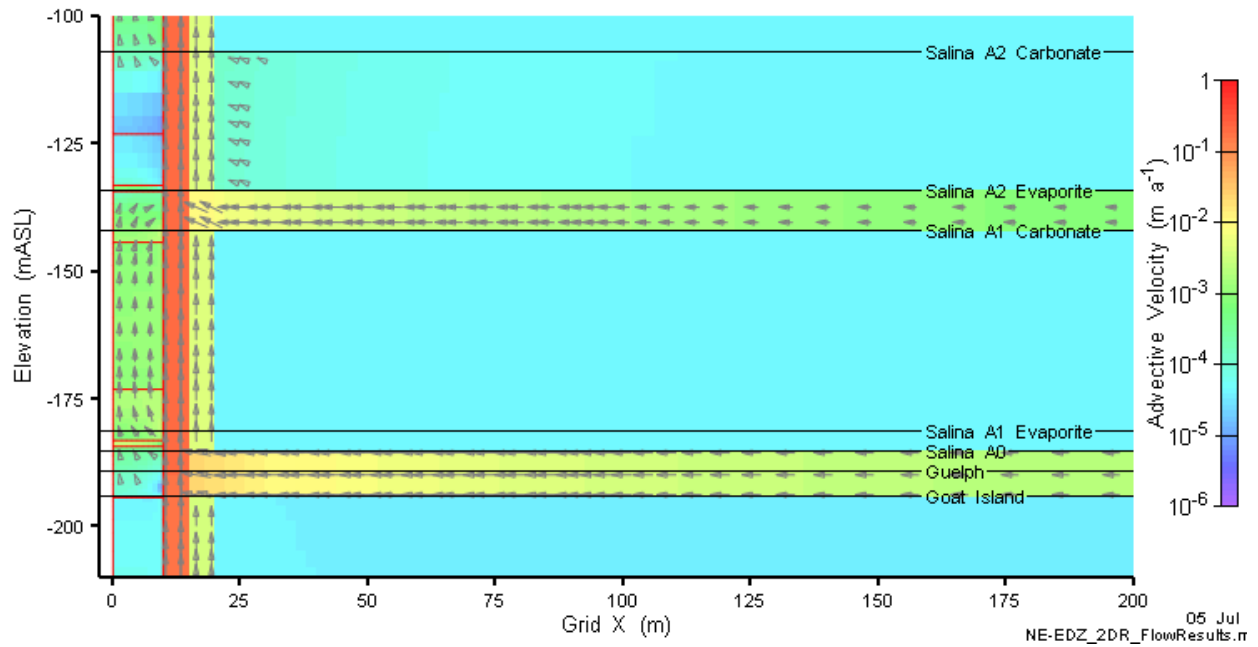


Figure 5.60: NE-EDZ-F2 advective velocity magnitude and vectors in vicinity of Silurian seals.

5.5.1.2 Transport Results

The high velocities in the shaft EDZ lead to much more rapid transport of Cl-36, as shown in Figure 5.61 through Figure 5.63.

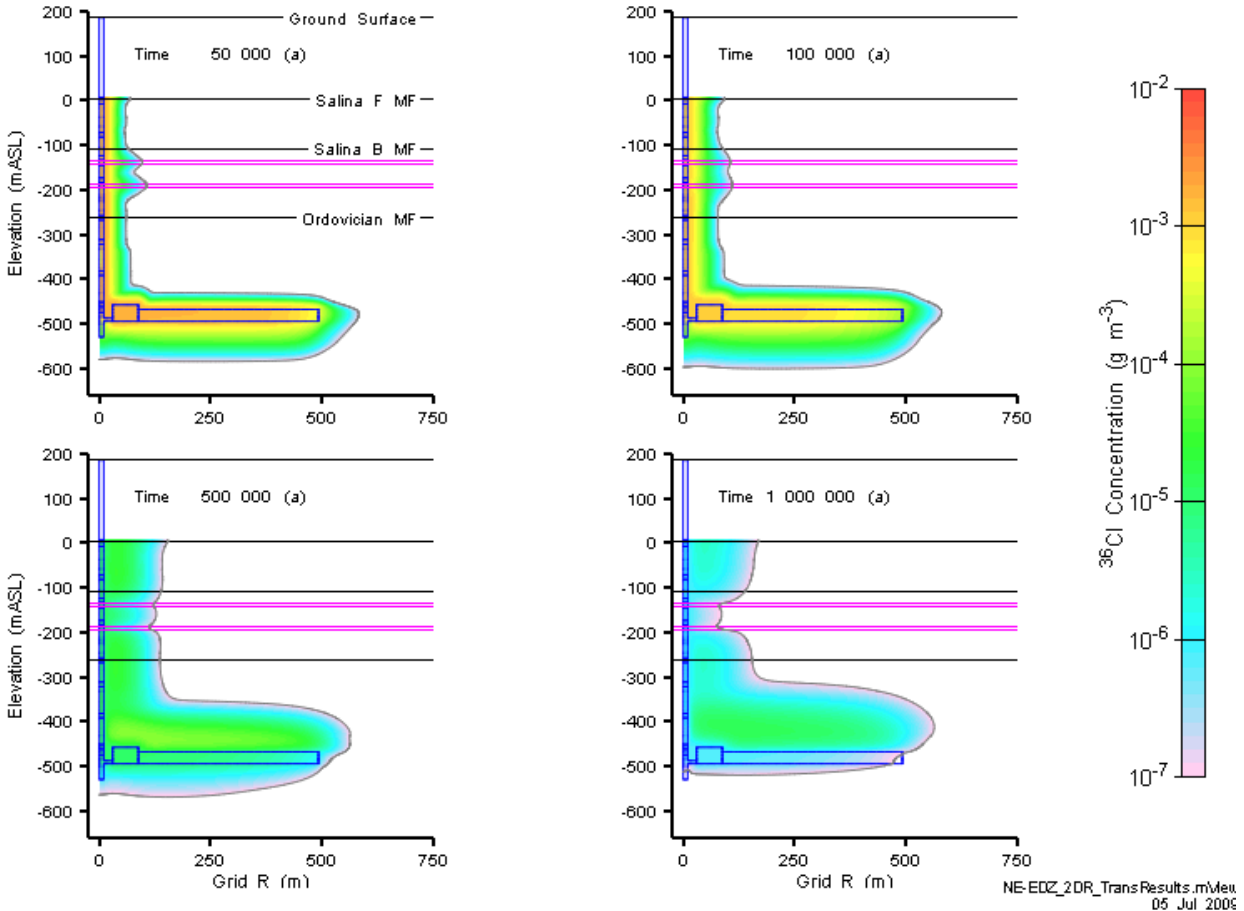


Figure 5.61: NE-EDZ-F2 Cl-36 concentration at 50 000, 100 000, 500 000, and 1 000 000 years.

Note that the upper limit of the mass flow Y-axis has been increased by two orders of magnitude and the cumulative mass Y-axis has been increased one order of magnitude as compared to previous mass transport figures. The peak mass flux occurs at approximately 40 000 years. The mass flow curves for the shaft EDZ at the Salina B and Salina F control planes look almost identical to that at the Ordovician control plane. The total mass reaching the shallow aquifer system after 1 000 000 years represents roughly 60% of the dissolved Cl-36 mass. The maximum mass transport rate is approximately 0.005 grams of Cl-36 per year.

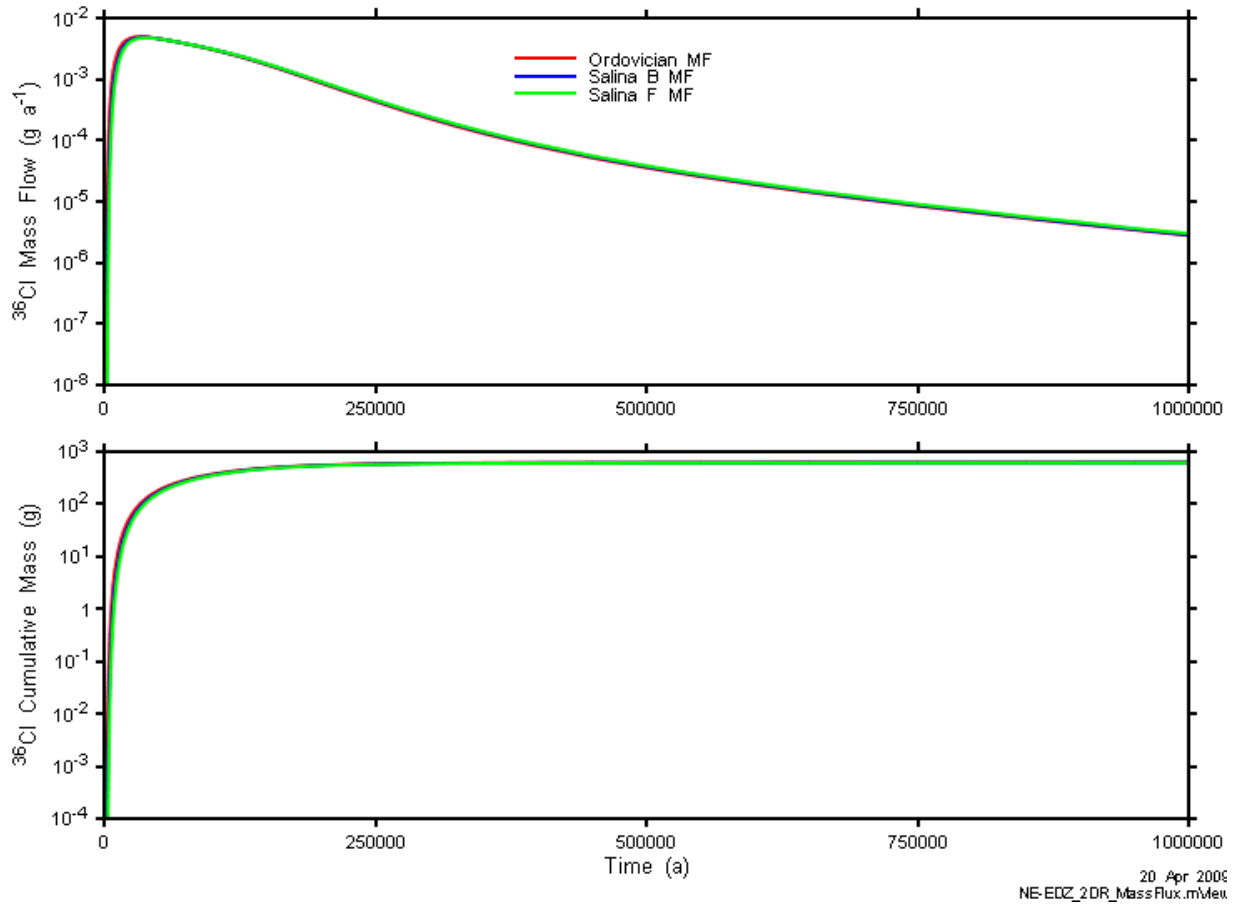


Figure 5.62: NE-EDZ-F2 mass transport results. Note that the vertical axis limits differ from other mass flow figures.

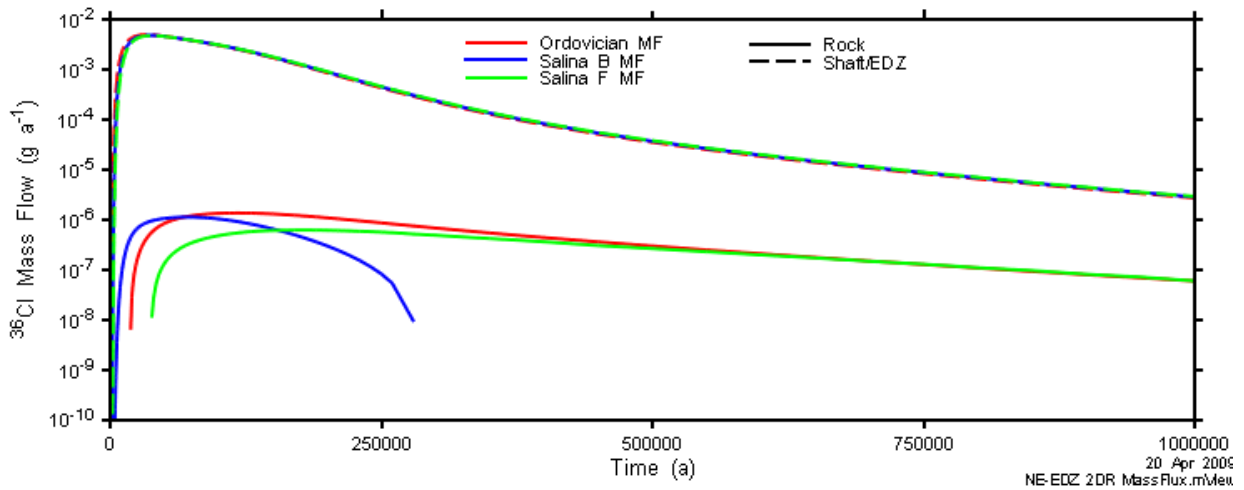


Figure 5.63: NE-EDZ-F2 mass flow components.

5.5.2 NE-UG-EDZ-F2 Results

The following results are for the same permeable shaft/EDZ model as the previous section, but with the lower-permeability (UG) geosphere.

5.5.2.1 Flow Results

Within the rock mass, flow results for the NE-UG-EDZ-F2 model are much slower than the NE-EDZ-F2 case and are similar to the NE-UG-RS1-F3 modelling case for the rock mass. Velocities in the shaft EDZ are much higher than the NE-UG-RS1-F3 case (see Figure 5.58)

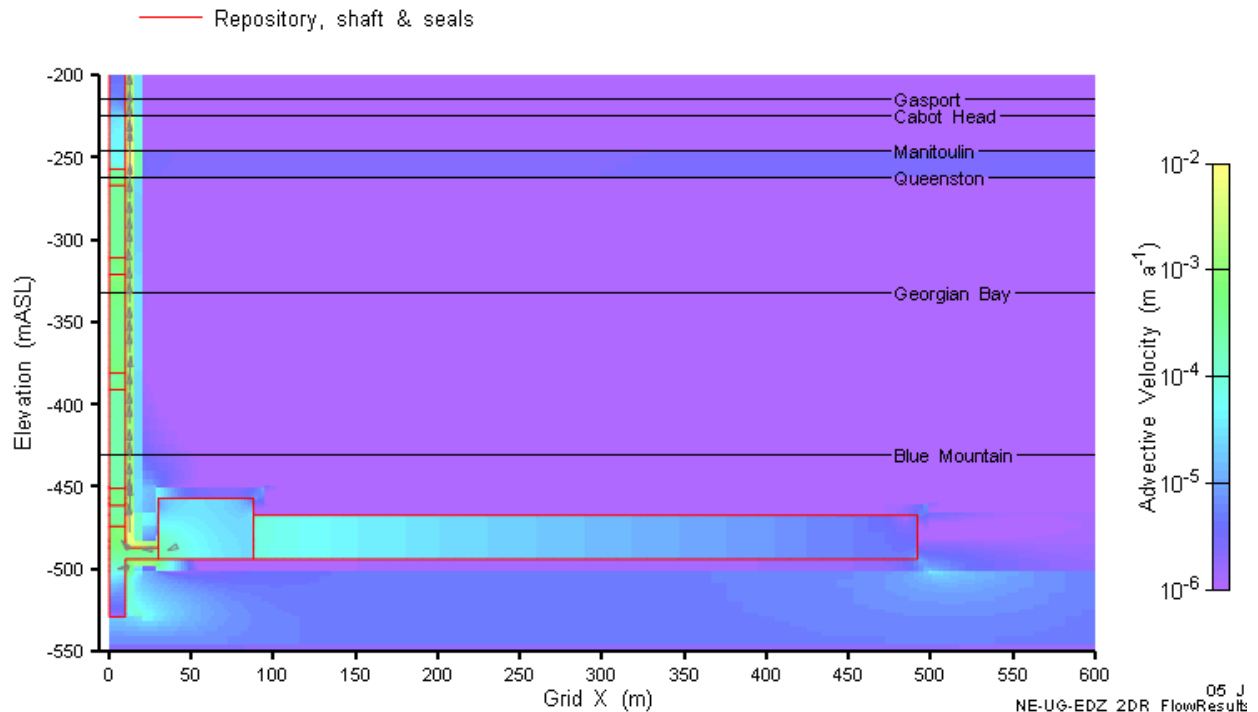


Figure 5.64: NE-UG-EDZ-F2 advective velocity magnitude and vectors in repository and lower shaft.

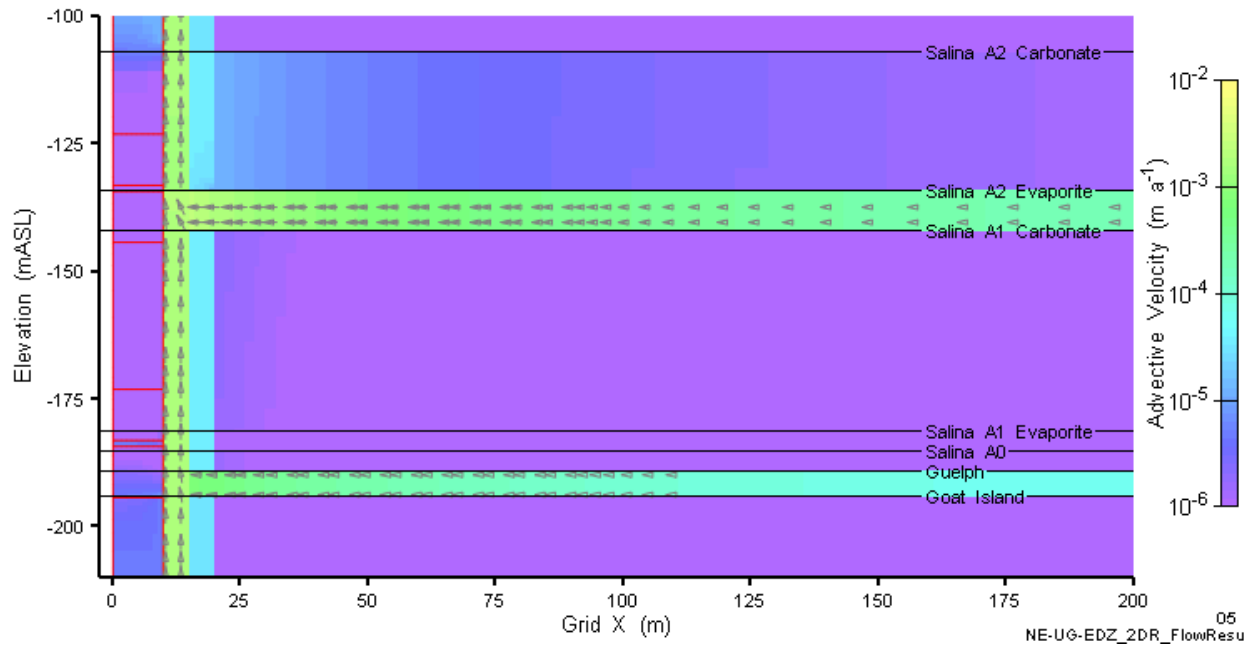


Figure 5.65: NE-UG-EDZ-F2 advective velocity magnitude and vectors in vicinity of Silurian seals.

5.5.2.2 Transport Results

The high velocities in the shaft EDZ lead to much more rapid transport of CI-36 than the NE-UG-RS1 case, but still much lower than the NE-EDZ case, as shown in Figure 5.66 through Figure 5.68.

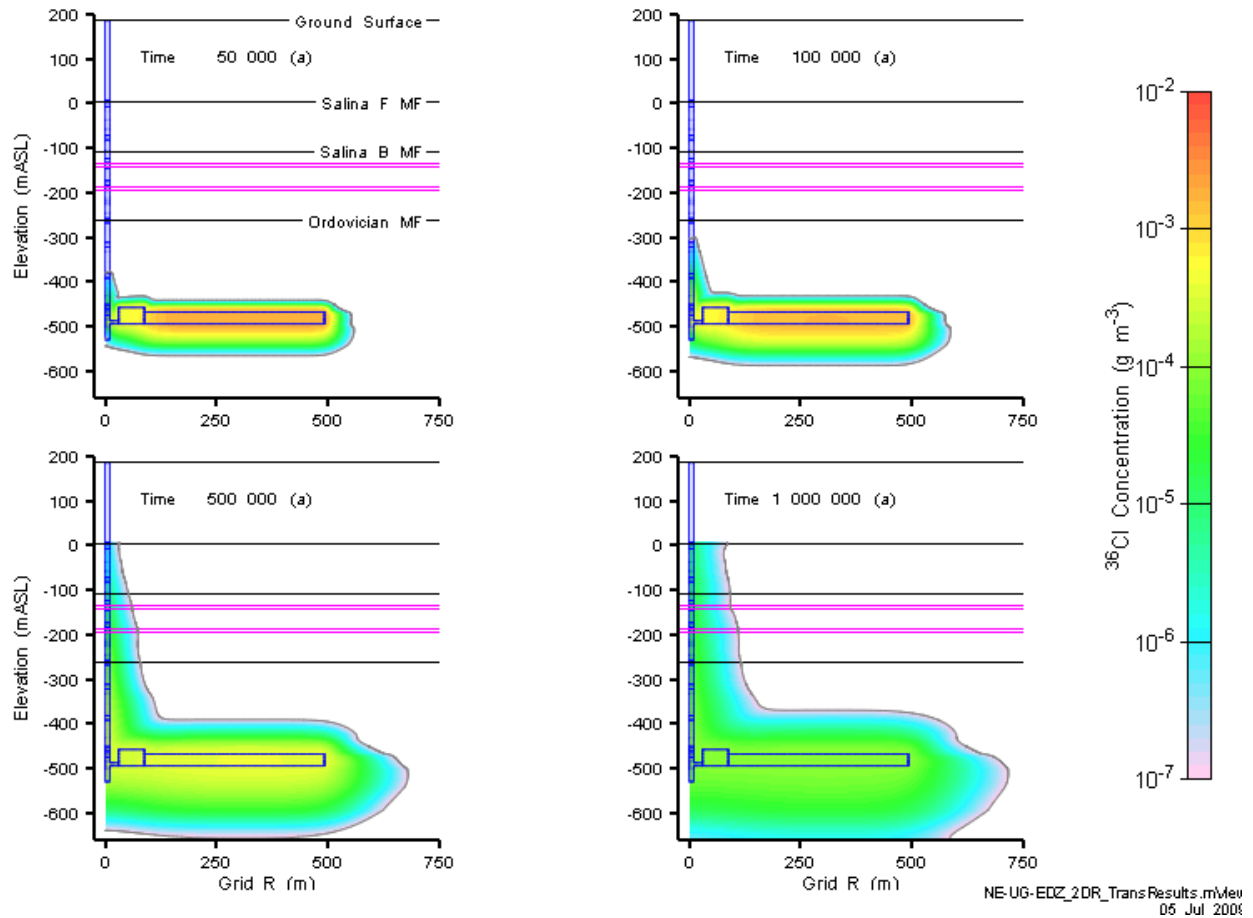


Figure 5.66: NE-UG-EDZ-F2 CI-36 concentration at 50 000, 100 000, 500 000, and 1 000 000 years

Note that the upper limit of the mass flow Y-axis is the same as for the NE-EDZ-F2 case for comparison purposes.

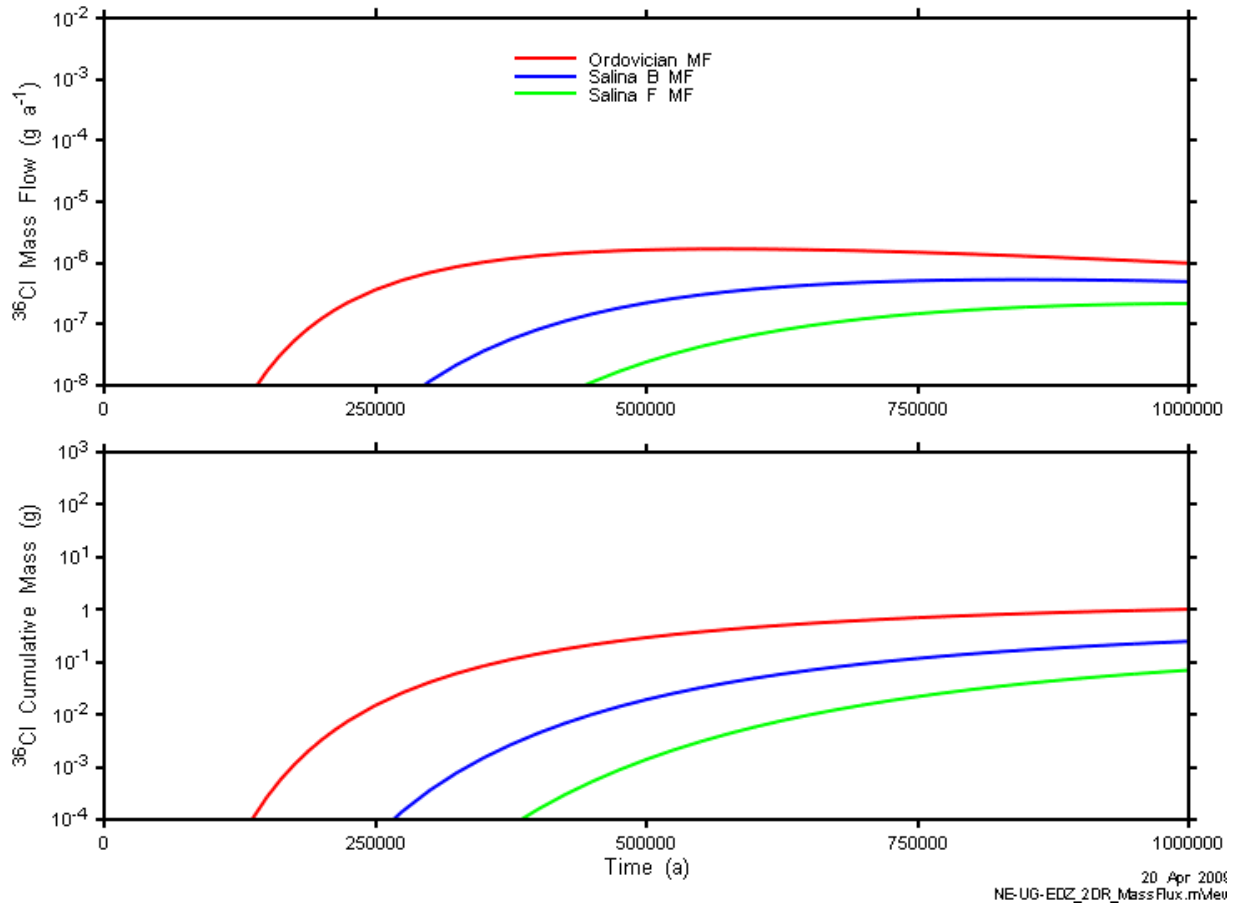


Figure 5.67: NE-UG-EDZ-F2 mass transport results. Note that the vertical axis limits differ from other mass flow figures.

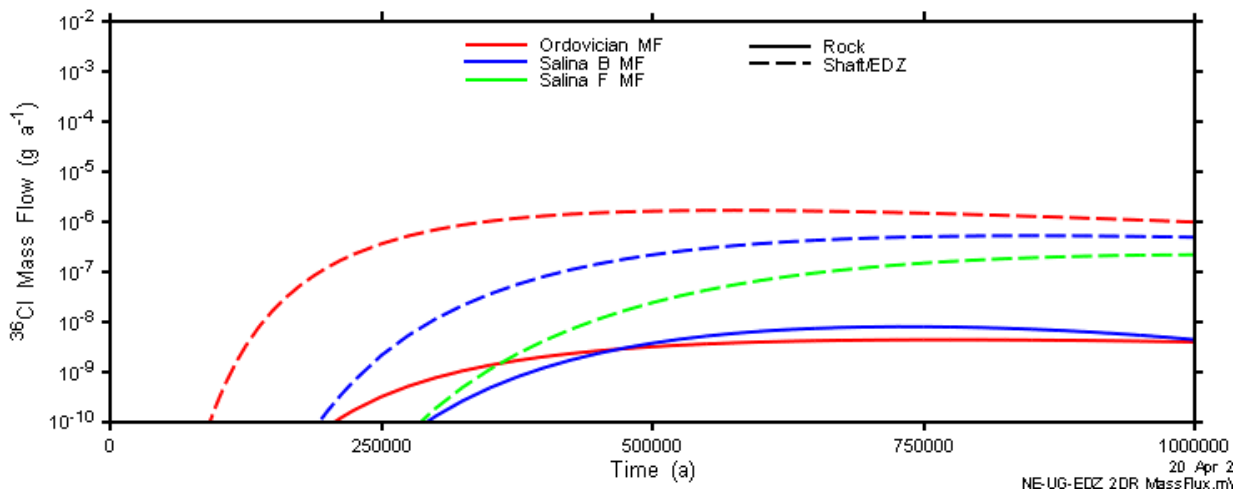


Figure 5.68: NE-UG-EDZ-F2 mass flow components.

5.6 NE-UG-RD1: Concrete seals through access and ring tunnel

The NE-UG-RD1 case is based on the NE-UG-RS1 case, except the access tunnels and ring tunnels have been filled with concrete at closure. Emplacement rooms are not backfilled. This has eliminated rockfall in the tunnels and has decreased the extent of the EDZ surrounding the tunnels.

5.6.1 Flow Results

As compared to the NE-UG-RS1 modelling case, the effect of the property changes in NE-UG-RD1 is to slightly reduce the amount of water flow through the repository and into the shaft (see Figure 5.69).

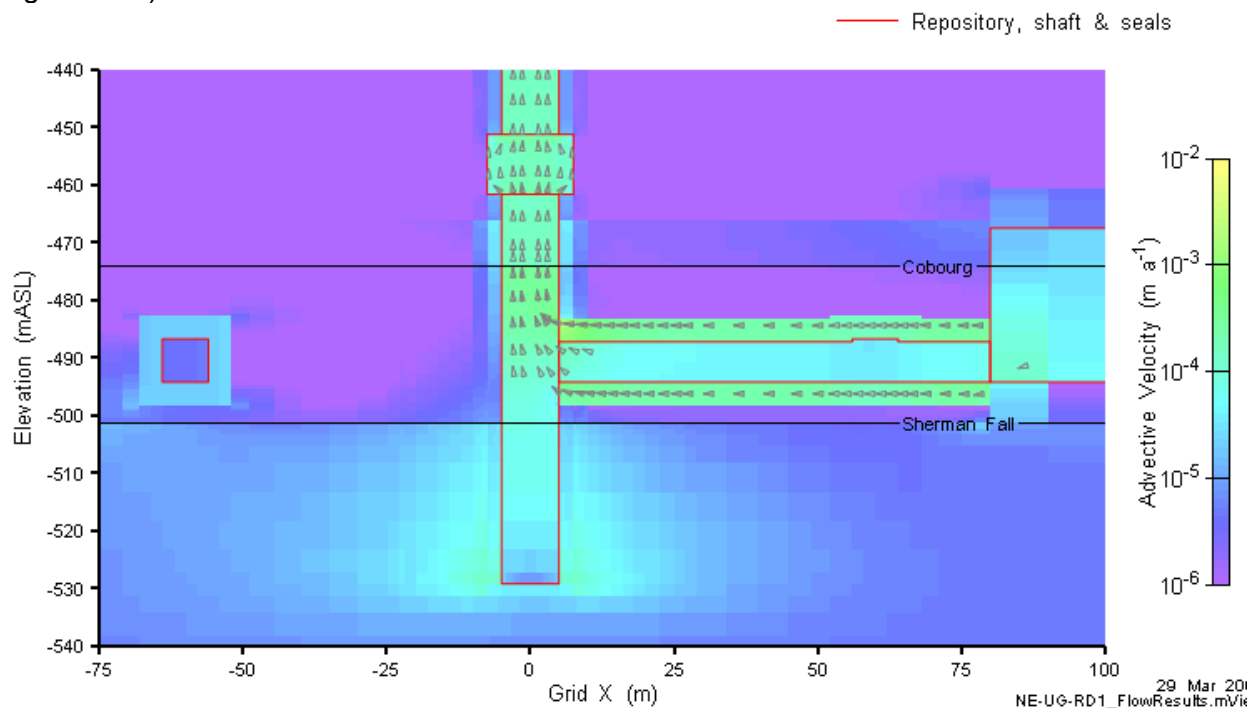


Figure 5.69: NE-UG-RD1-F3 advective velocity magnitude and vectors in the repository and lower shaft on a vertical slice through Grid Y=0.

5.6.2 Transport Results

The reduced flow rate leads to a delay and slight reduction in the Cl-36 mass flow in both the shaft and in the rock mass. Figure 5.70 shows Cl-36 concentration contours. Figure 5.71 shows the mass transport rates at the control planes. Concentration distributions and mass transport rates are very similar to those calculated for the NE-UG-RS1 model.

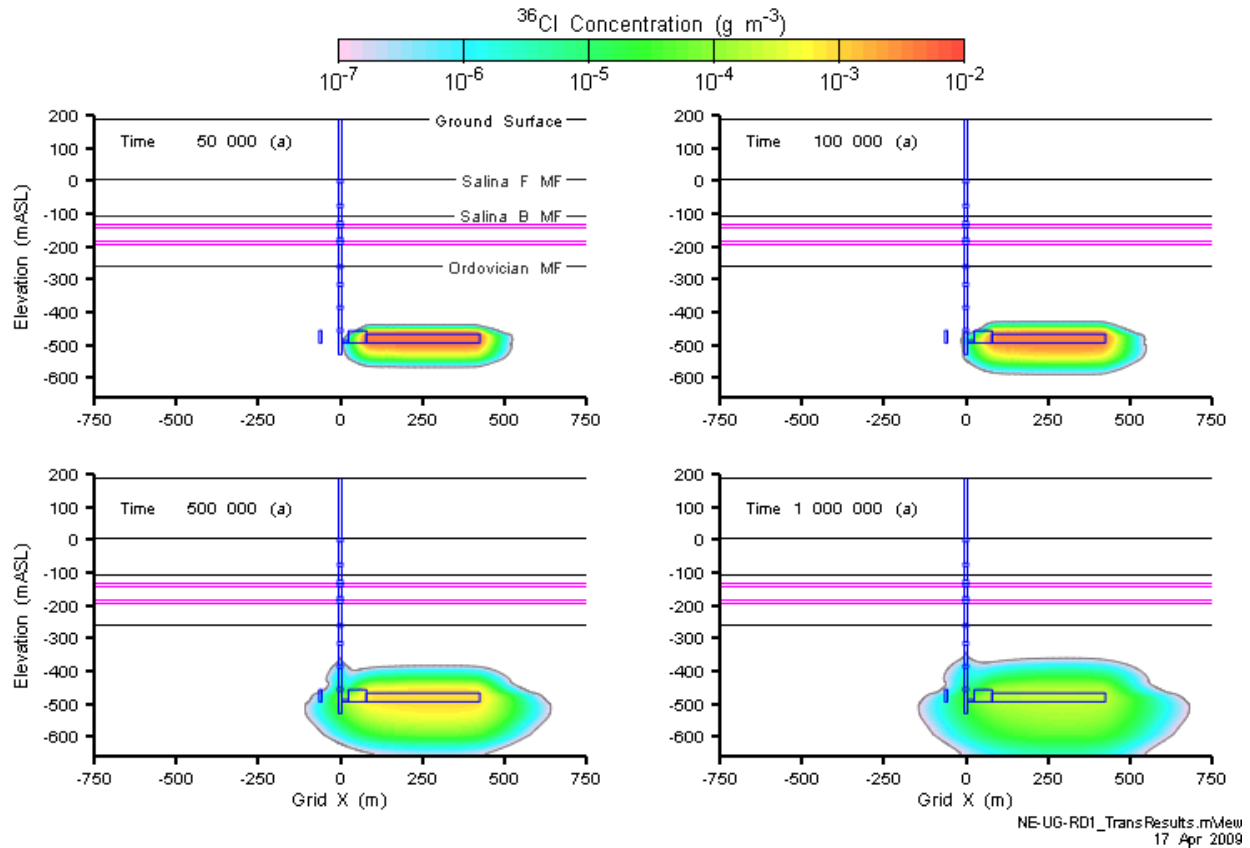


Figure 5.70: NE-UG-RD1-F3 Cl-36 concentration at 50 000, 100 000, 500 000, and 1 000 000 years.

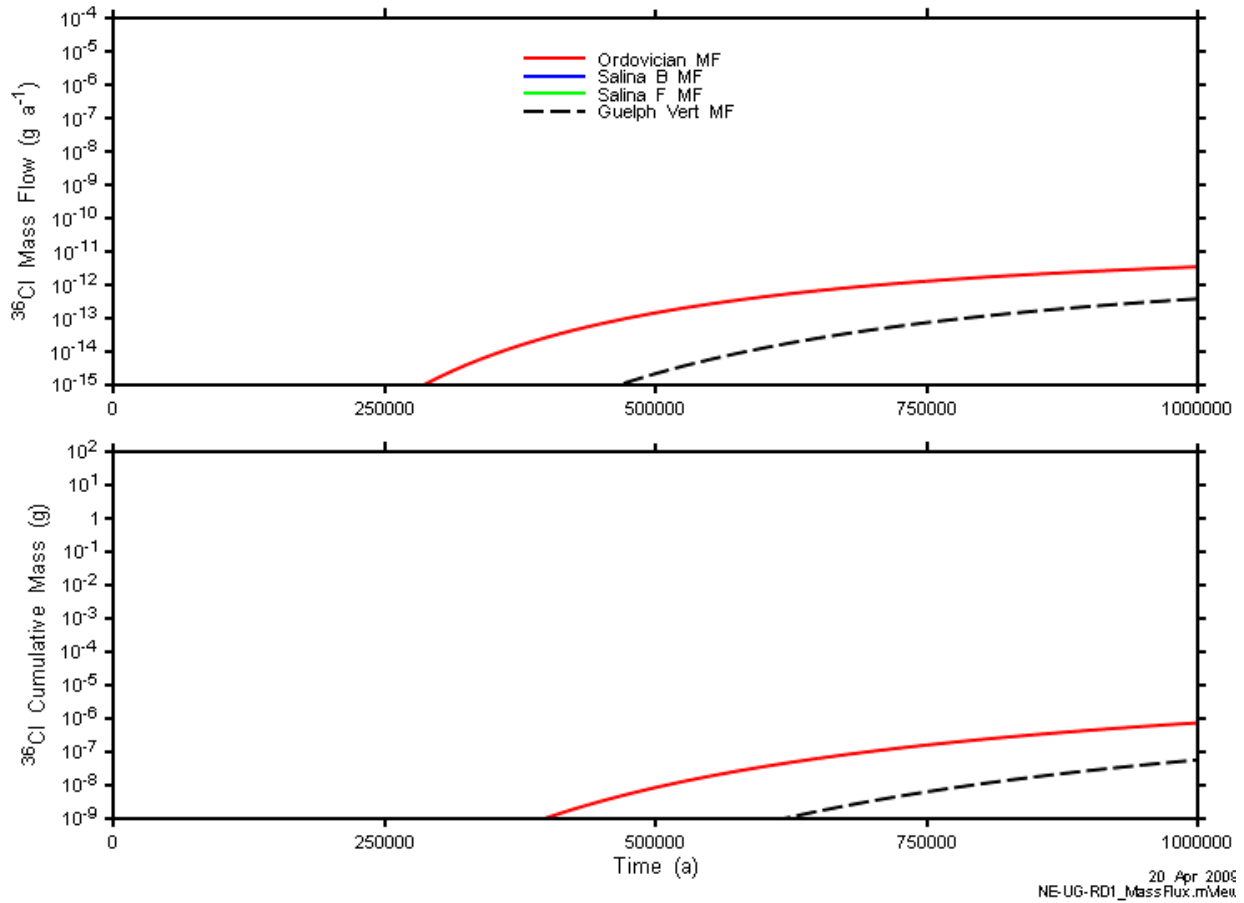


Figure 5.71: NE-UG-RD1-F3 total mass flow and cumulative mass transport.

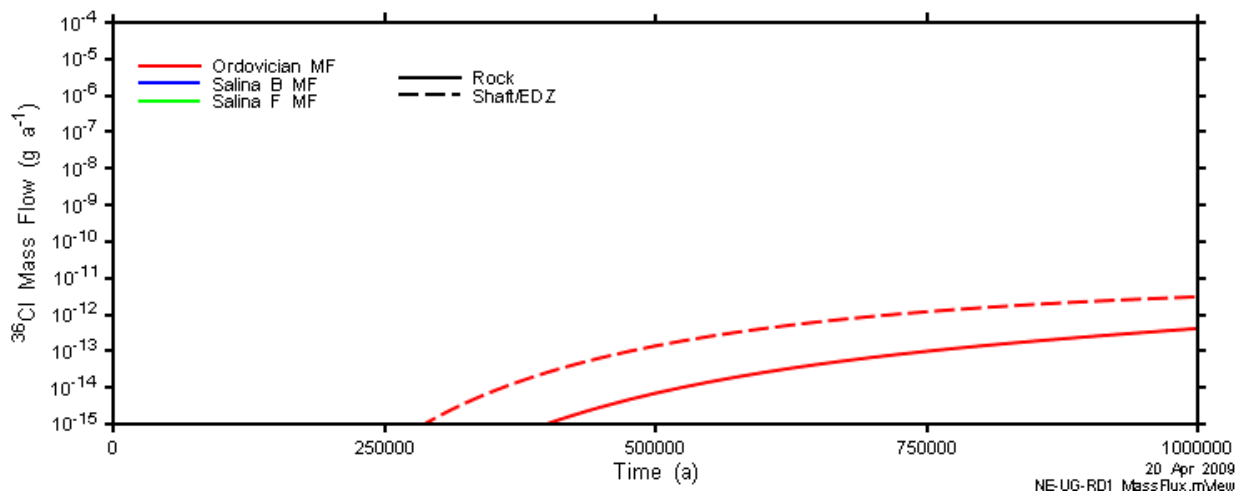


Figure 5.72: NE-UG-RD1-F3 mass flow components.

6. RESULTS FOR THE DISRUPTIVE SCENARIOS

This section presents results for the four scenarios described in Table 3-2. Results for each case are presented in terms of flow and transport.

6.1 HI-GR-F3: Exploration borehole intersecting the repository

An exploration borehole penetrates the East panel. Drilling is terminated, and the borehole is conservatively assumed to be filled with a high-conductivity material.

6.1.1 Flow Results

Hydraulic head and advective velocities are shown in Figure 6.1 through Figure 6.4. The hydraulic response to the borehole dominates the flow domain. Hydraulic head within the repository is lowered, with all flow gradients directed from the rock mass toward the repository, except for the flux up the borehole. Advective velocities up the borehole are not presented in the figure as the borehole is represented as a 1D line element within the model and is not included in the 3D element velocity output.

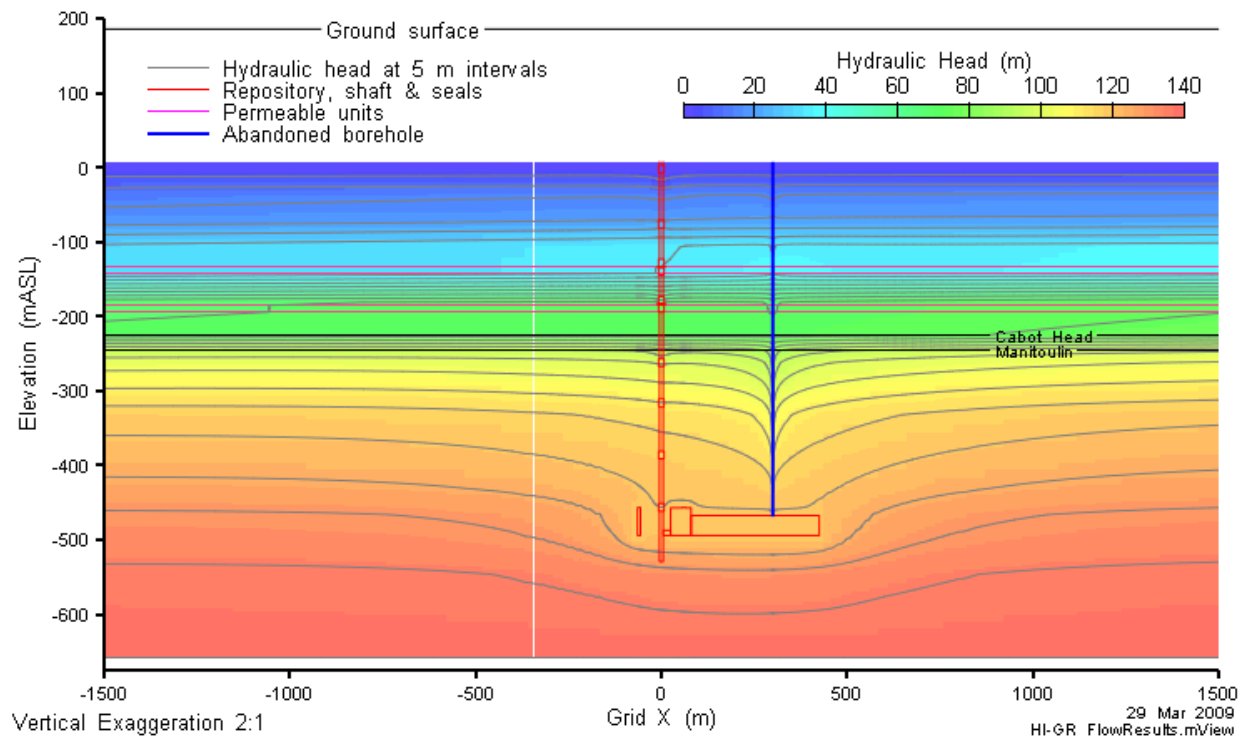


Figure 6.1: HI-GR-F3 head contours on a vertical slice through Grid Y= 10.

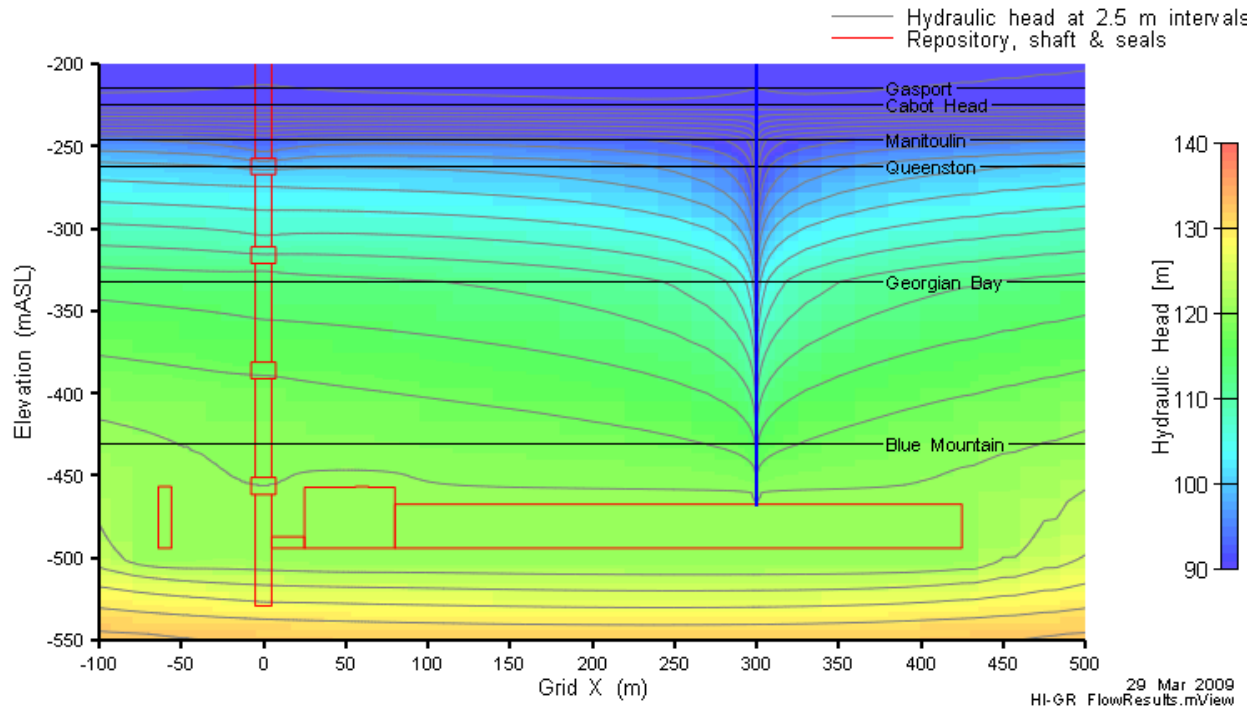


Figure 6.2: HI-GR-F3 head contours in the vicinity of the repository on a vertical slice through Grid Y=10.

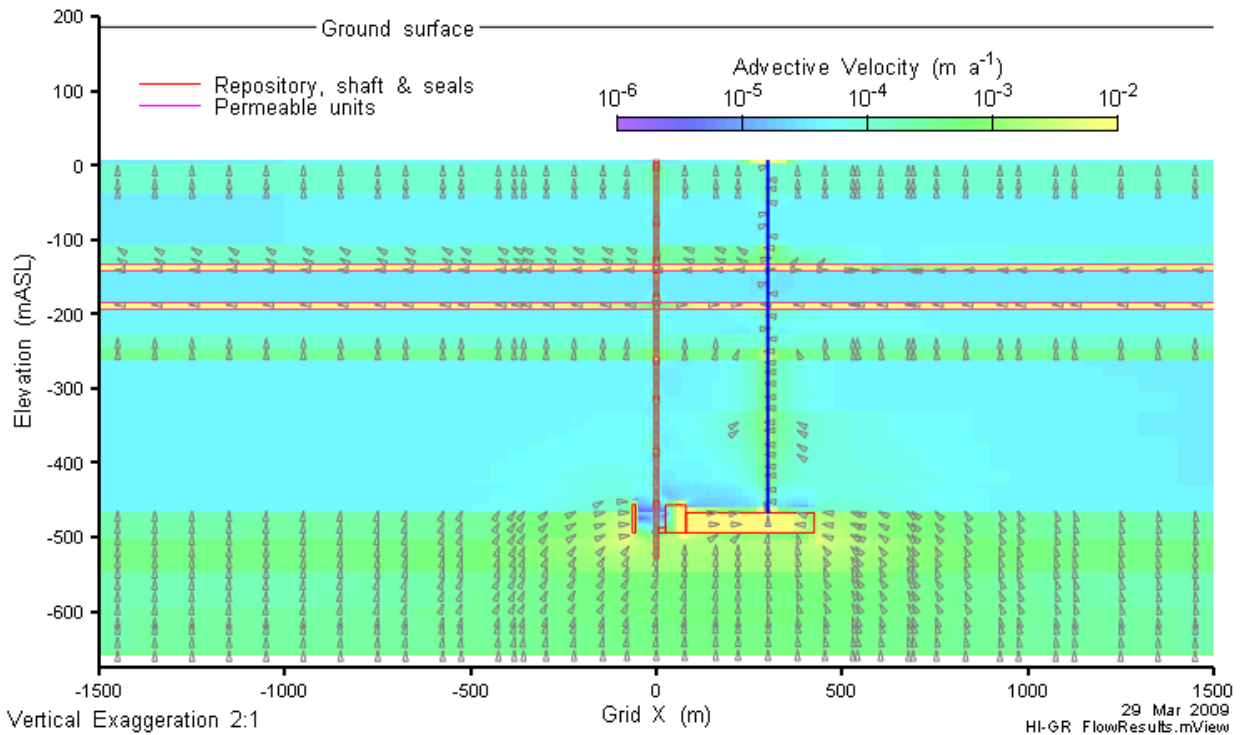


Figure 6.3: HI-GR-F3 advective velocity magnitude and vectors on a vertical slice through Grid Y=10.

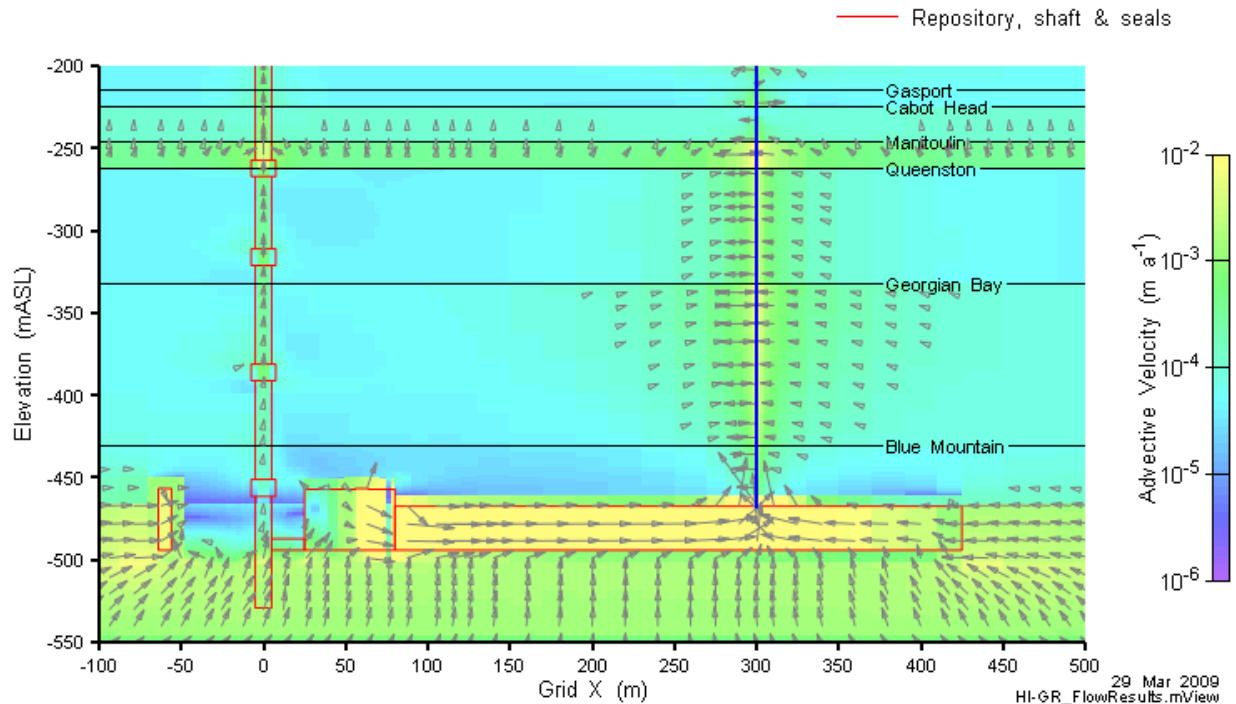


Figure 6.4: HI-GR-F3 advective velocity magnitude and vectors in the vicinity of the repository on a vertical slice through Grid Y=10.

Any casing present in the borehole is assumed to be ineffective in the long term and so fluid can be transferred into the borehole from the surrounding (and vice versa) over its entire length. This can serve to dilute contaminants being transported up the borehole. Figure 6.5 is representation showing fluid flux in the borehole. Initial flow rate at the top of the repository EDZ is approximately $7 \text{ m}^3 \text{ a}^{-1}$. Significant flow enters the borehole at the permeable Guelph/Salina A0 unit where the fluid flow rate increases by a factor of nearly three; from approximately $8 \text{ m}^3 \text{ a}^{-1}$ to $20 \text{ m}^3 \text{ a}^{-1}$. However, a substantial amount of the fluid leaves the borehole at the Salina A2 evaporite, where flow up the borehole reduces to approximately $11 \text{ m}^3 \text{ a}^{-1}$. This behaviour is a consequence of the base case geosphere, which results in significant hydraulic gradient across the Salina A1 unit. The abandoned borehole serves to short-circuit the gradient and thus attracts substantial flow from and to the permeable units.

Flows in the low-permeability UG geosphere would be much reduced due to both lower permeabilities in the formations supplying the initial flow to the repository and to reduced gradients in the Silurian formations.

The use of constant fluid density in these simulations adds some conservatism to these results. If the effects of salinity were incorporated, a portion of the very saline water being produced from all formations below the Salina A1 would tend to sink and spread along the bottom of the much less saline Salina A2 evaporite. Nonetheless, a substantial amount of the produced fluid will still be transported up the borehole.

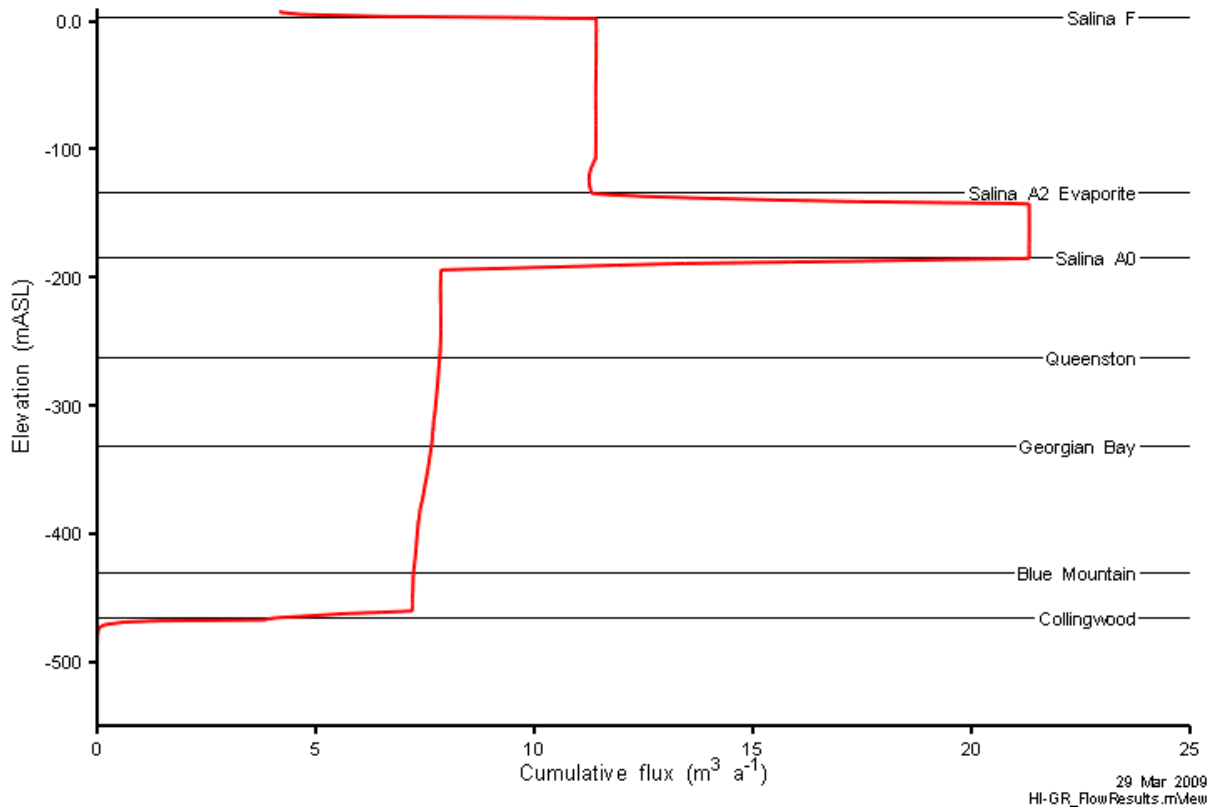


Figure 6.5: HI-GR-F3 cumulative fluid flow gain and loss in the abandoned exploration borehole.

6.1.2 Transport Results

Figure 6.6 shows the CI-36 concentration contours at four different times, starting at 1 000 years. Early time concentrations in the borehole and vicinity are very high. Unlike the NE-RS1 case, there is little transport into the Guelph/Salina A0/Salina A2 evaporite, due to the fluid flow into borehole described above. Although the horizontal gradient is created by the specified head boundary conditions on these permeable Silurian units, it is overwhelmed by the vertical gradient up the borehole. A significant portion of the plume exits the borehole at the Salina A2 evaporite, as shown in Figure 6.7. The fluid flow gained from the other formations into the borehole also serves to dilute the mass flow up the well, thus reducing concentrations in the upper units. (Numerical error resulted in some small negative calculated concentrations at the right edge of the repository. For presentation purposes, the absolute value of concentration is shown in the figure.)

Figure 6.8 shows borehole mass flux and borehole concentrations at three elevations. The effect of dilution by groundwater flow coming into the borehole at the permeable Guelph/Salina A0 unit is apparent in the difference between the Ordovician and Salina concentrations.

Approximately 40% of the CI-36 mass initially in the system exits the model at the top of the borehole within 100 000 years.

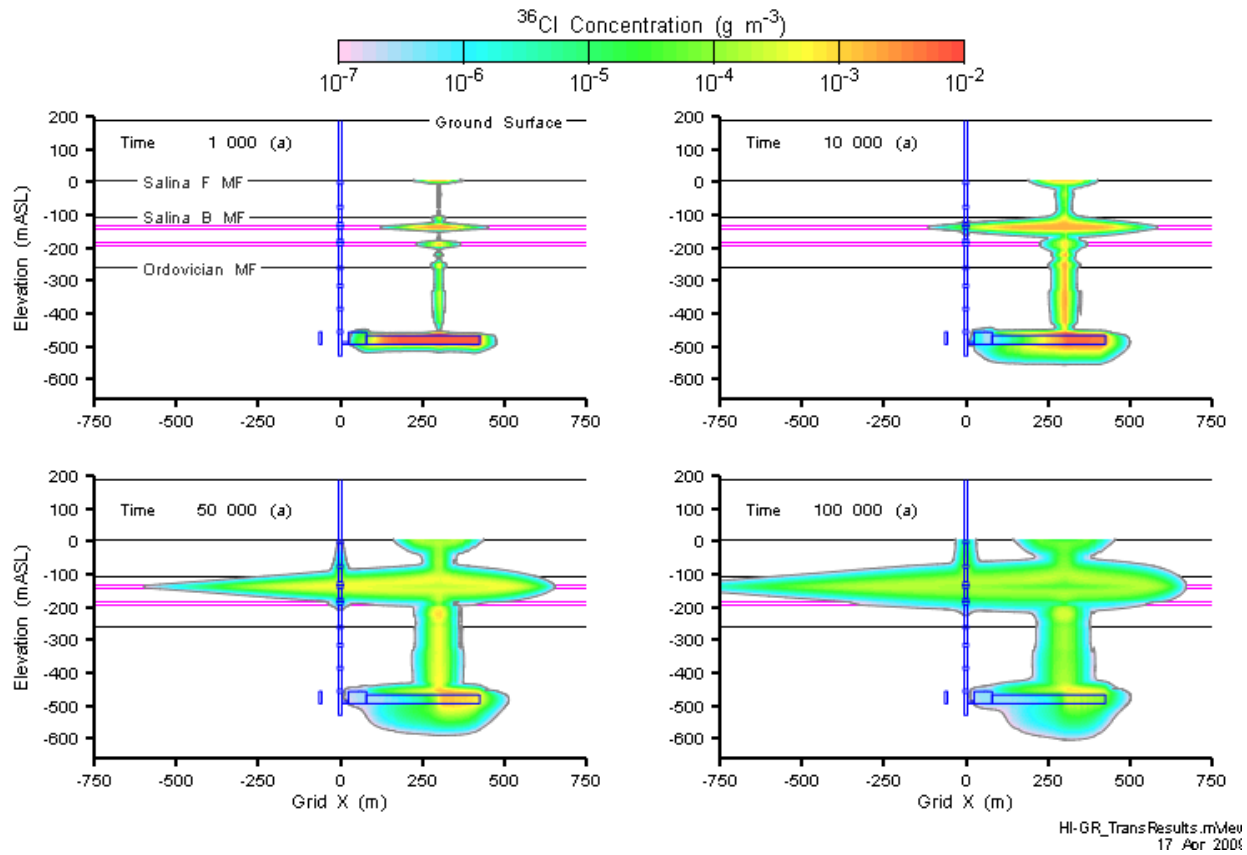


Figure 6.6: HI-GR-F3 CI-36 concentration at 1 000, 10 000, 50 000, and 100 000 years.

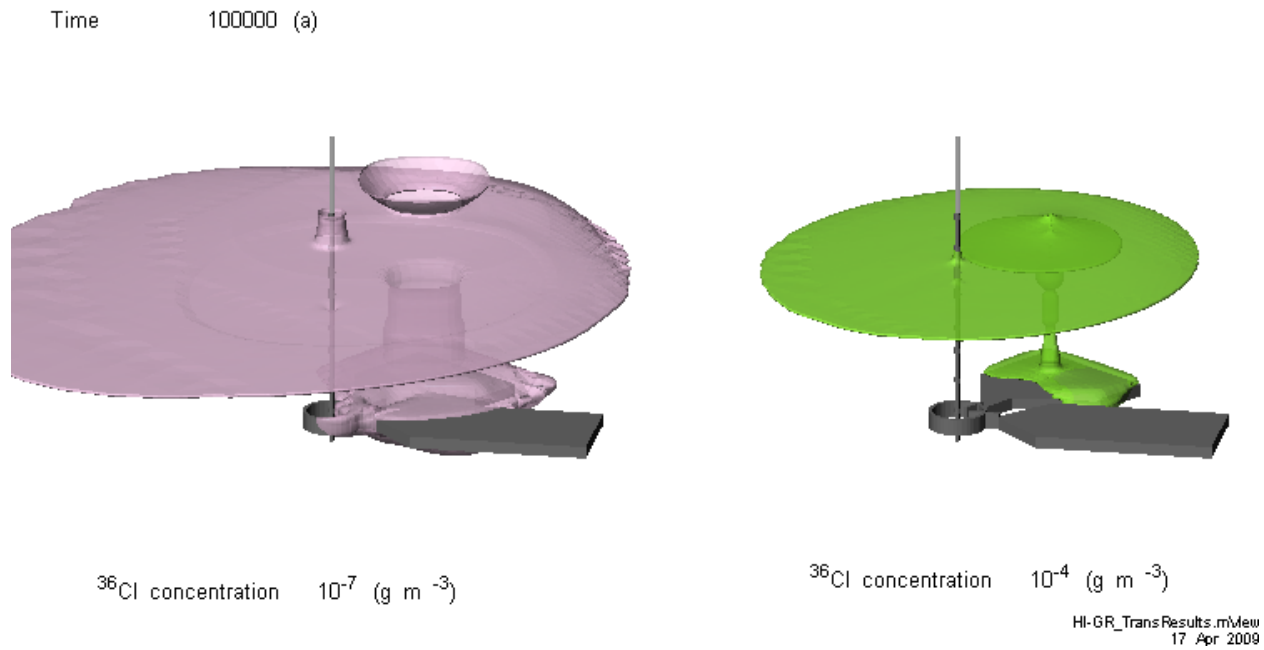


Figure 6.7: HI-GR-F3 CI-36 concentration isovolumes at 100 000 years.

Note that FRAC3DVS_OPG does not output the mass fluxes from the one-dimensional borehole elements. Instead, the advective mass flows in the borehole at the top of the Queenston, Salina B and Salina F units were calculated by multiplying the concentrations at the node locations by the steady-state fluid flux at that location. Consequently, they do not include the contribution of dispersive flow up the well. Cumulative mass is calculated by integrating the advective mass flow.

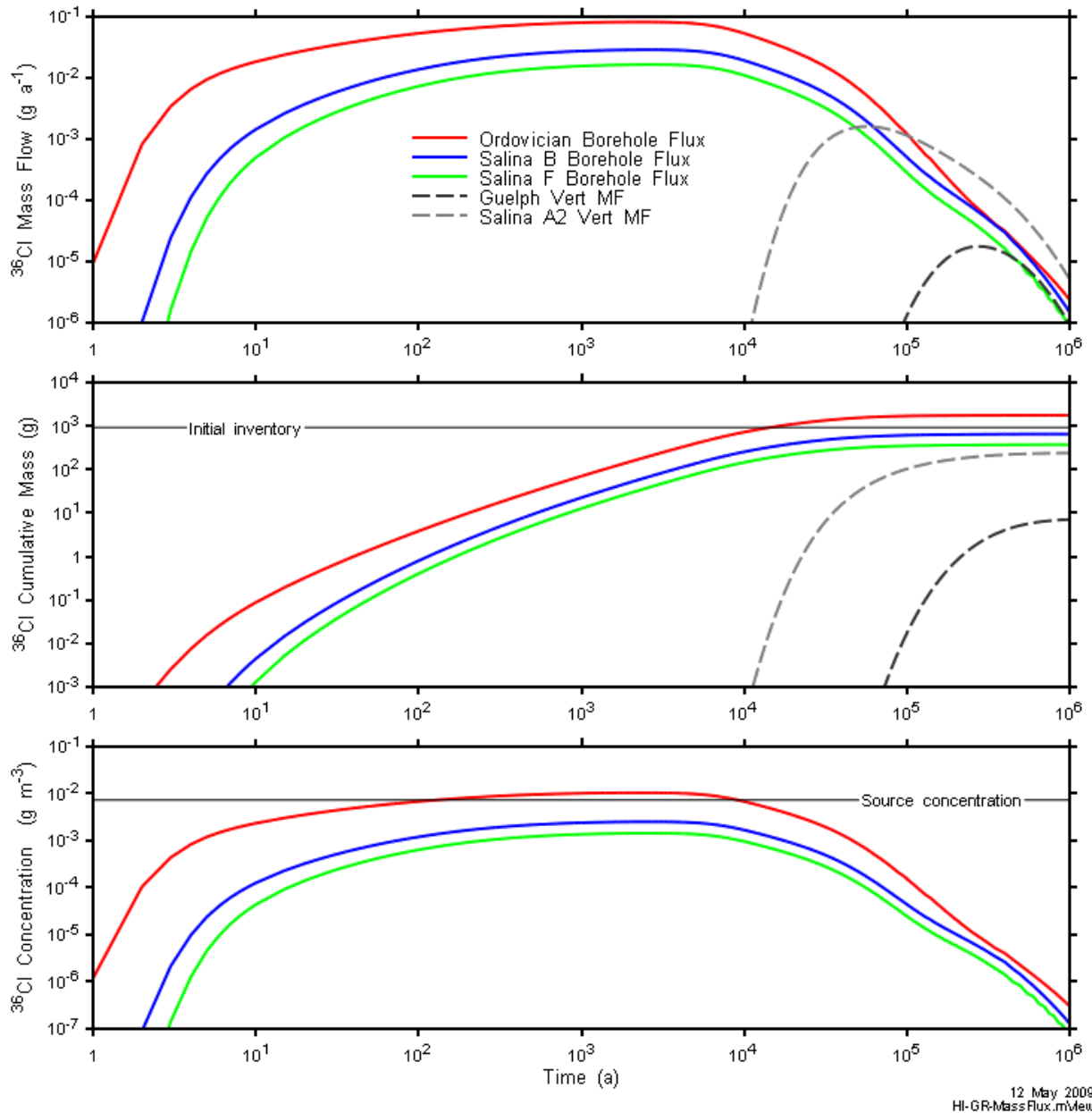


Figure 6.8: HI-GR-F3 CI-36 mass transport in the exploration borehole.

12 May 2009
HI-GR-MassFlux.mvMew

The HI-GR case was numerically difficult to run and the results show several numeric issues.

- At early times, the concentration of Cl-36 at the bottom of the borehole exceeds the initial source concentrations by almost a factor of two. Consequently the mass flux and cumulative mass flows through the borehole are approximately double the initial mass in the system (Figure 6.8). This is an appreciable error; however, the net effect here is conservative, i.e., it overstates the potential releases.
- Cl-36 mass creation was found at the bottom of the shaft sump and in layers below the facility. The numerical error was artificially eliminated by setting the EDZ and rock mass nodes in the vicinity of the sump and below to a fixed concentration of 0.0. This approach had no discernable impact on other calculated concentrations.
- Negative Cl-36 concentrations were also calculated at some nodes at the periphery of the panels at the repository elevations. However, the errors did not accumulate in these areas (i.e., there was no consequent mass creation).

Overall, the results of this case should be considered preliminary, but are considered indicative of the behaviour and likely to overestimate the potential impacts.

6.2 SF-ES1: Failure of entire seal system (SE-ES1-F2 & SF-UG-ES1-F2)

The SF-ES1 modelling case is similar to case NE-EDZ, but represents a more extreme case in which both the shaft EDZ and the shaft sealing materials have extremely high hydraulic conductivities.

6.2.1 SF-ES1-F2 Results

6.2.1.1 Flow Results

The very high hydraulic conductivity in the shaft causes a severe perturbation of the flow system. As shown in Figure 6.9, large quantities of flow are being diverted through the repository towards the shaft. Figure 6.10 through Figure 6.12 indicate that groundwater velocities are much greater in this case as compared to the NE-NHG-F2 case (compared to Figure 5.38 and Figure 5.39 respectively). Note that the colour map and velocity range on Figure 6.10 and Figure 6.11 has been expanded. The highest velocities, which occur in the shaft, are on the order of 1 m a^{-1} . As in the NE-EDZ modelling case, significant flow is drawn from the Guelph/Salina A0 unit towards the more conductive shaft (see Figure 6.11). Head profiles at the external boundary are somewhat different than the NE-NHG-F2 case, indicating that the zero flow boundaries are impacting the flow system. The most significant difference is that flow in the permeable Salina A2 evaporite is away from the shaft in this case, and toward the shaft in the NE-NHG case. Test simulations, not presented here, were performed using fixed head boundaries extracted from NE-NHG-F2 results. No significant difference in contaminant mass flows were found between the zero-flow and fixed-head boundary cases, although fluid velocities in the Salina A2 were reversed for the fixed-head boundaries, flowing into the shaft. This additional flow resulted in some dilution, reducing concentrations in the shaft by approximately 40%, however mass flows are reduced by only 10%. Similar conclusions apply to the SF-UG-ES1 and SF-US cases presented in Section 6.2.2 and Section 6.3.

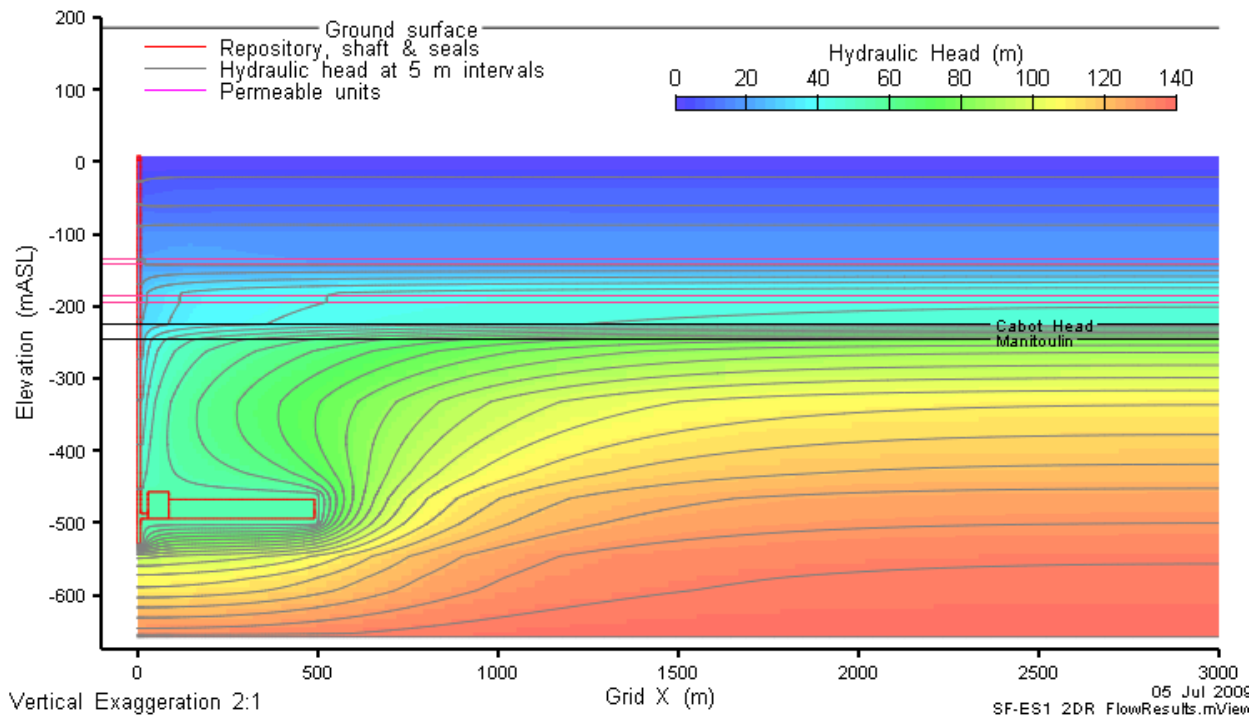


Figure 6.9: SF-ES1-F2 head contours for the entire model domain.

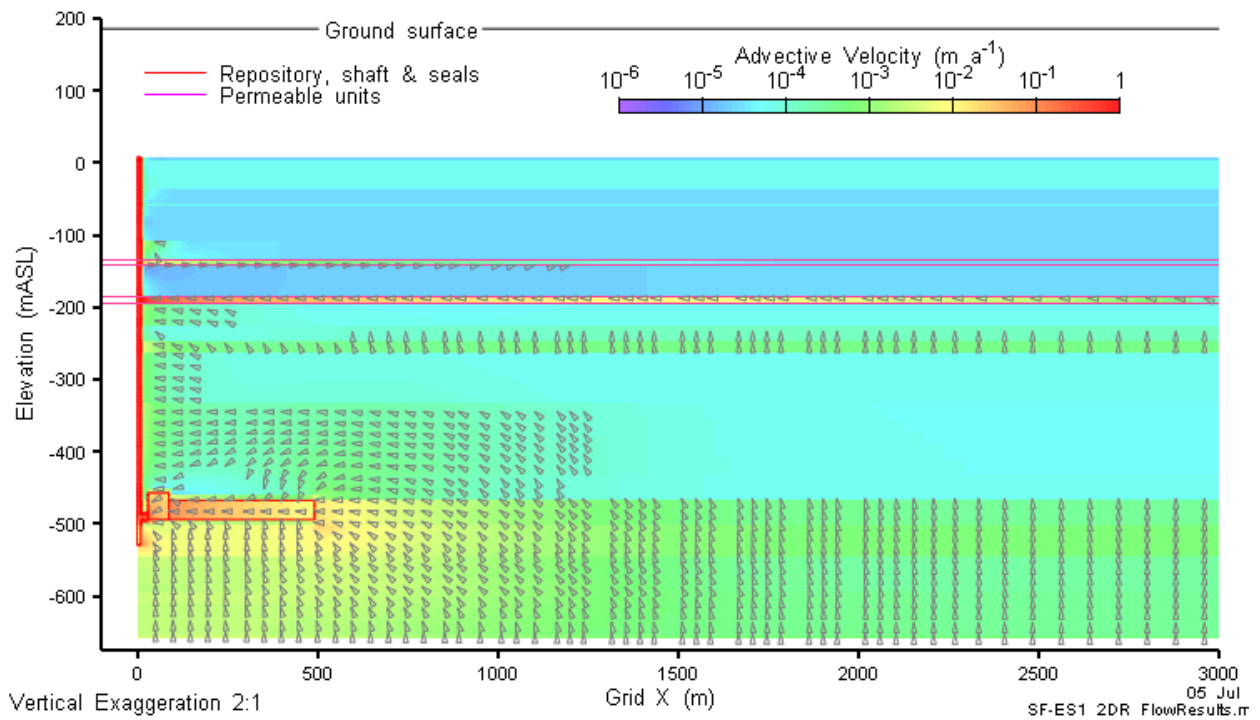


Figure 6.10: SF-ES1-F2 advective velocity magnitude and vectors for the entire model domain.

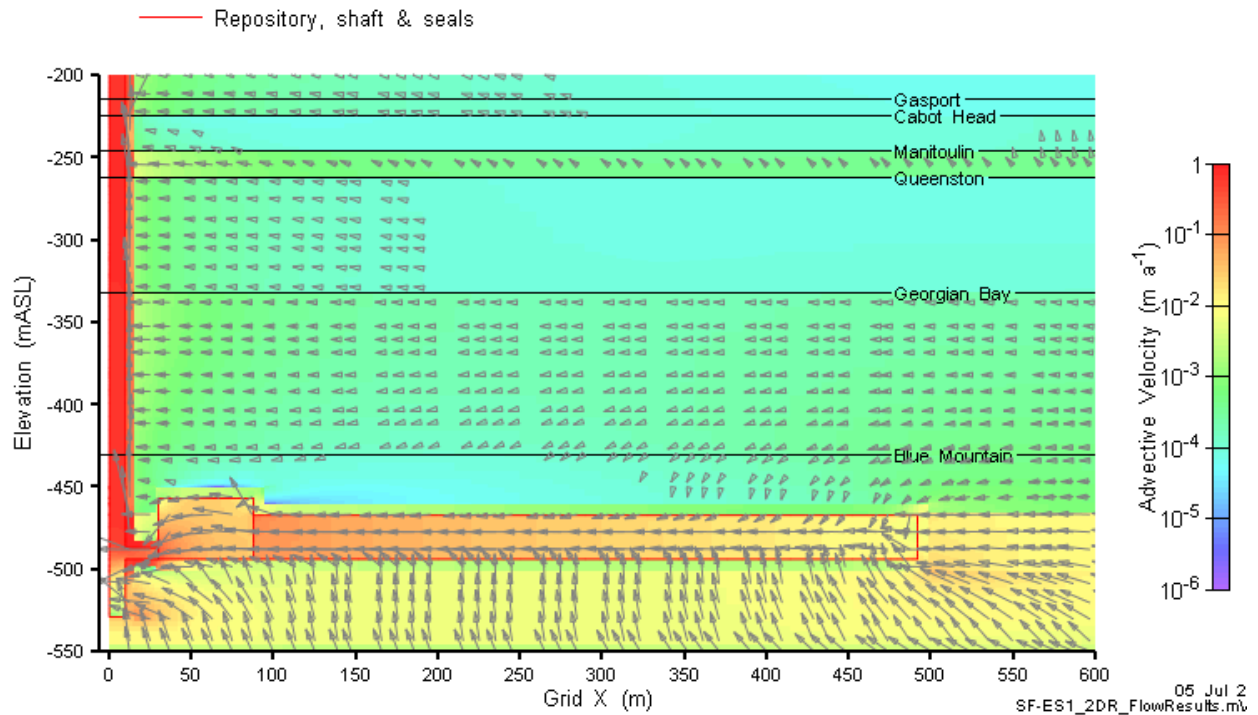


Figure 6.11: SF-ES1-F2 advective velocity magnitude and vectors in repository and lower shaft.

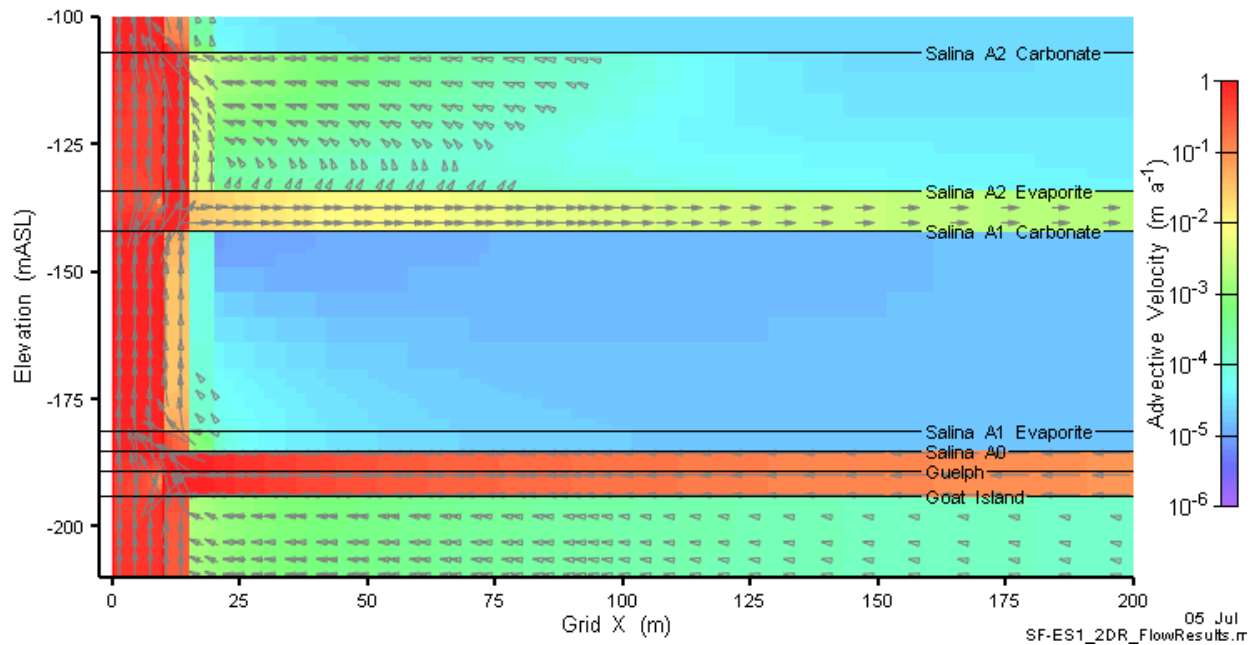


Figure 6.12: SF-ES1-F2 advective velocity magnitude and vectors in the vicinity of the Silurian seals.

6.2.1.2 Transport Results

The transport results from the SF-ES1-F2 modelling case are rapid in comparison the NE-NHG-F2 case. As shown in Figure 6.13, the Cl-36 is transported rapidly out of the repository and up the shaft. The rapid transport up the shaft is also clearly evident in Figure 6.14 and Figure 6.15, where mass flow rates peak at approximately 5100 years. Note that figures use a log time scale and expanded vertical axis to capture the response. The cumulative mass curves for the shaft/EDZ show that most of the Cl-36 originally in the repository has reached the surface within roughly 30 000 years.

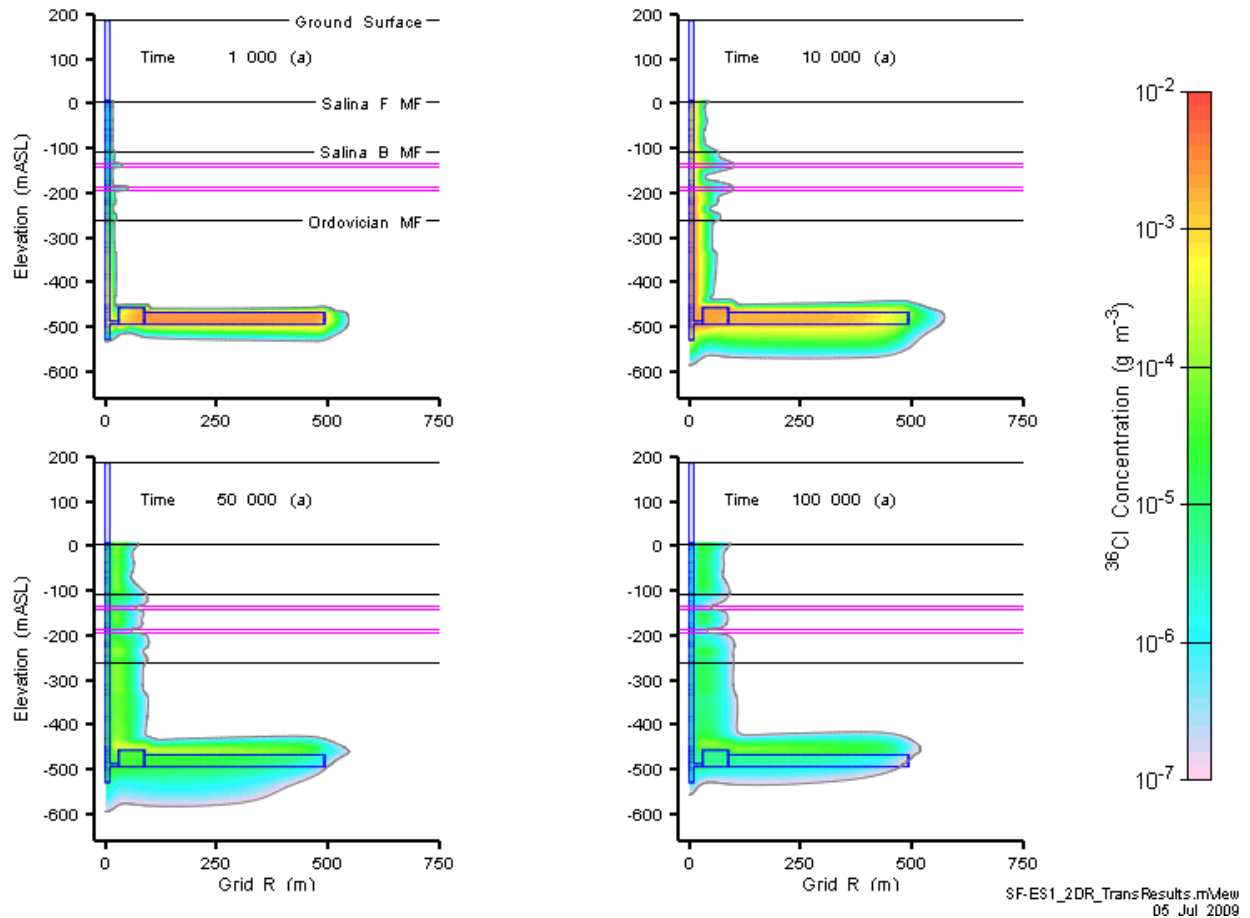


Figure 6.13: SF-ES1 Cl-36 concentration at 1 000, 10 000, 50 000, and 100 000 years.

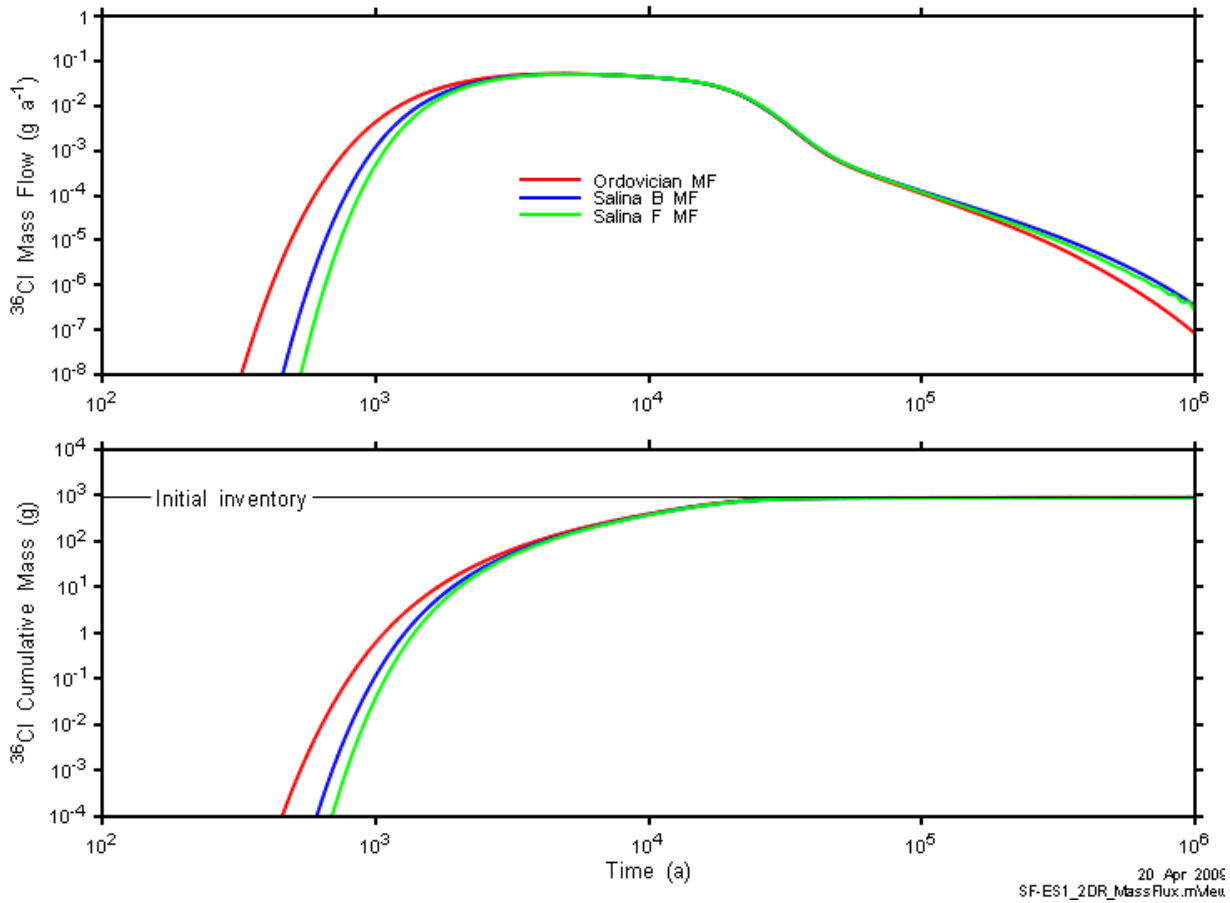


Figure 6.14: SF-ES1 CI-36 total mass flow and cumulative mass transport.

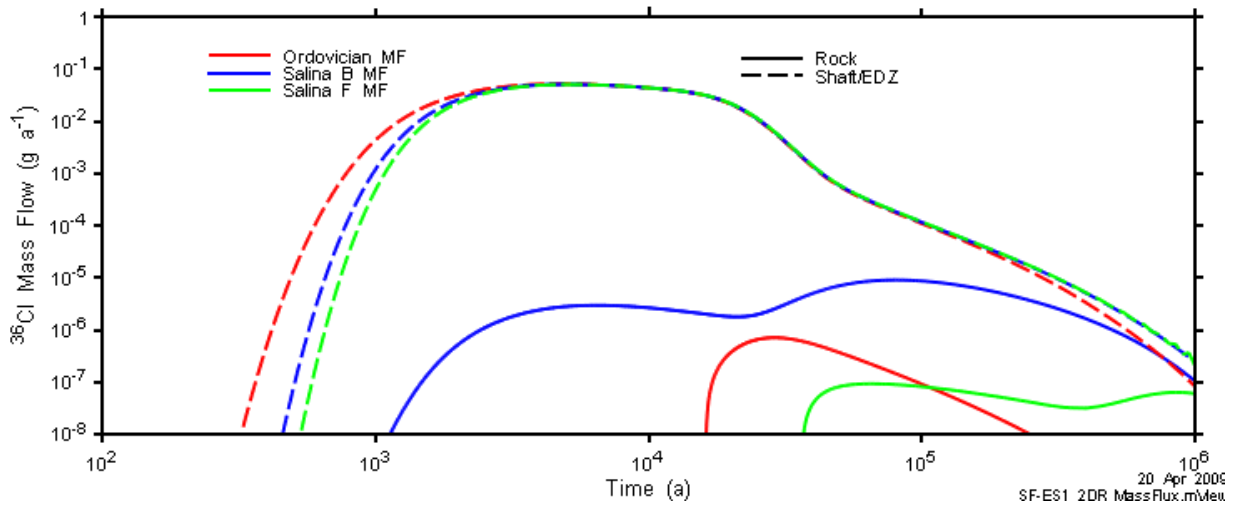


Figure 6.15: SF-ES1-F2 mass flow components.

6.2.2 SF-UG-ES1-F2 Results

6.2.2.1 Flow Results

The updated geosphere (UG) case results offer a more extreme head profile, but significantly moderated advective velocity regime as compared to the SF-ES1-F2 results. Flow is still being diverted through the repository towards the shaft; however the lower permeability rocks surrounding the repository limit the available volume. Figure 6.17 through Figure 6.19 indicate that groundwater velocities are much lower than the SF-ES1-F2 case.

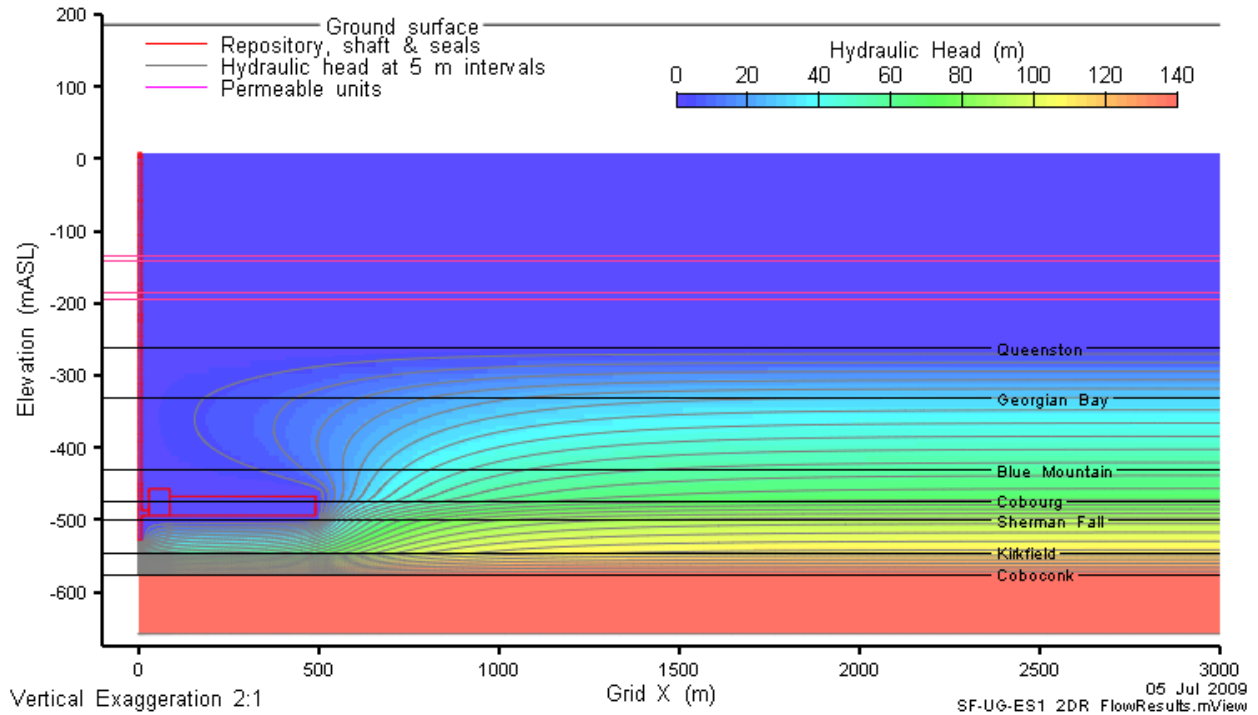


Figure 6.16: SF-UG-ES1-F2 head contours for the entire model domain.

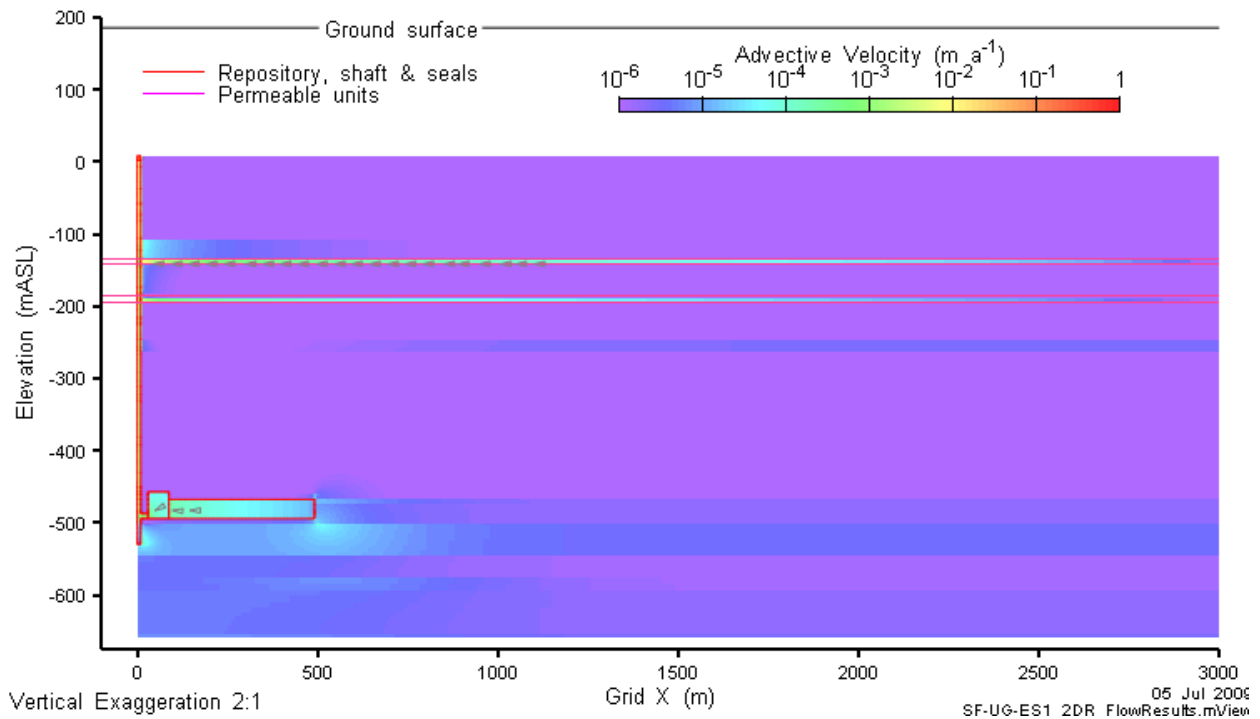


Figure 6.17: SF-UG-ES1-F2 advective velocity magnitude and vectors for the entire model domain.

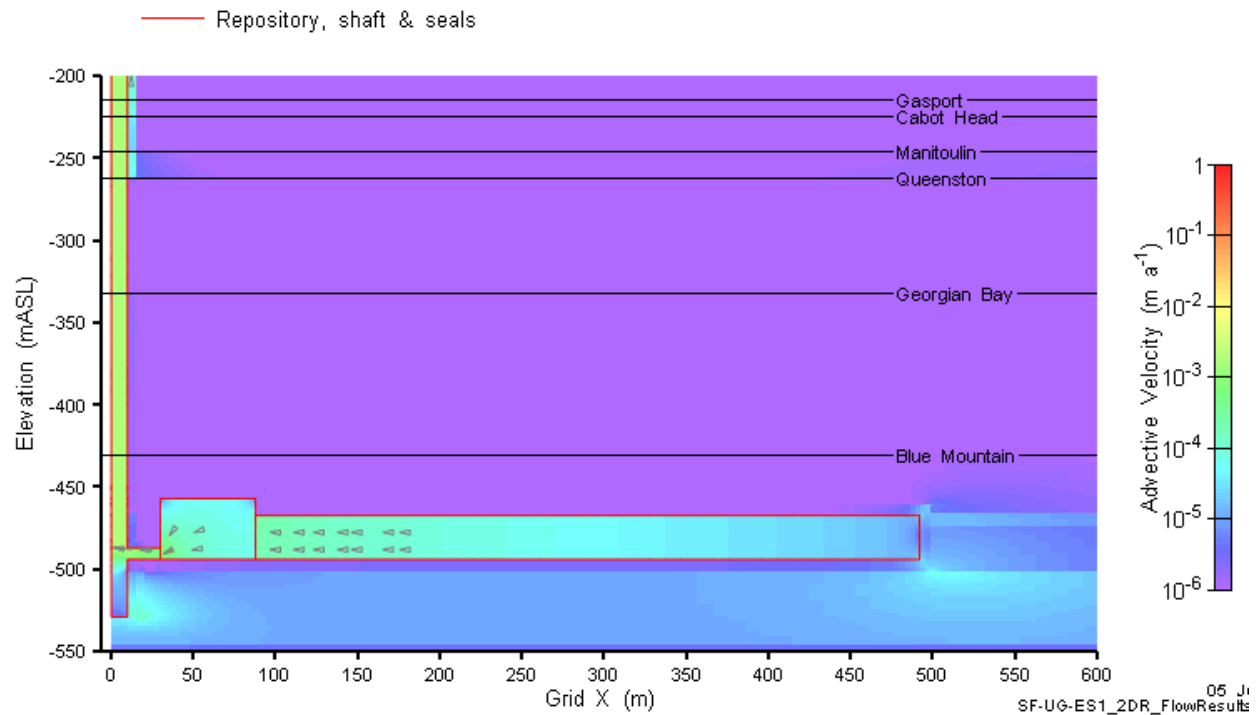


Figure 6.18: SF-UG-ES1-F2 advective velocity magnitude and vectors in repository and lower shaft.

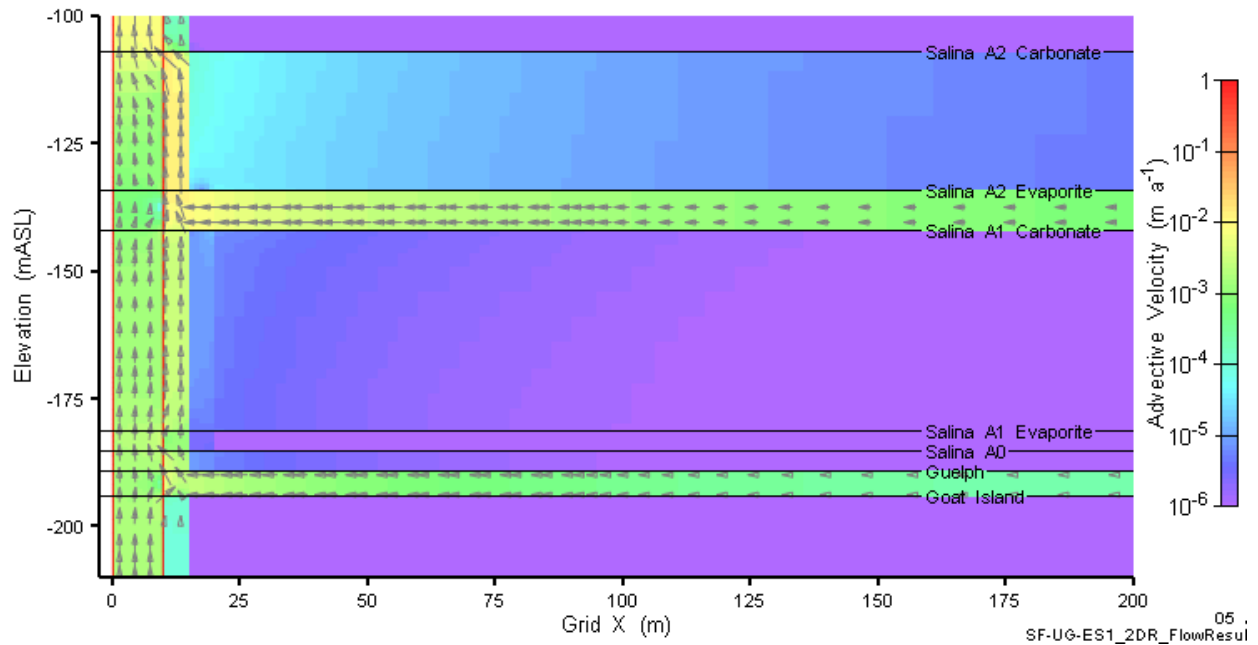


Figure 6.19: SF-UG-ES1-F2 advective velocity magnitude and vectors in the vicinity of the Silurian seals.

6.2.2.2 Transport Results

The SF-UG-ES1-F2 case results (Figure 6.20) show much lower rates of transport than the SF-ES1-F2 case. However, transport is still greater than the NE-UG-EDZ case, showing that adequate shaft closure remains important, even in extremely low flow conditions.

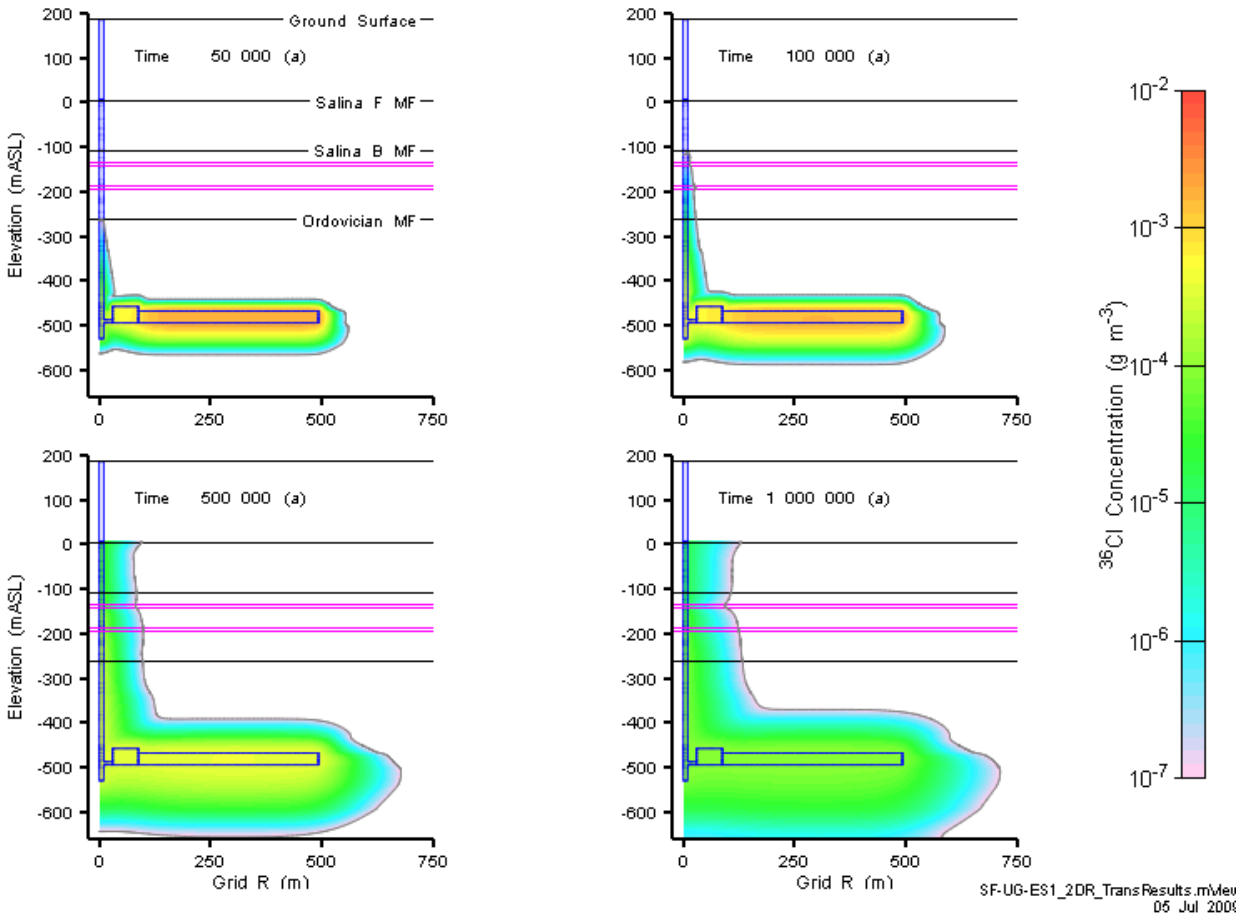


Figure 6.20: SF-UG-ES1 Cl-36 concentration at 50 000, 100 000, 500 000, and 1 000 000 years.

The significantly reduced rates are clearly evident in Figure 6.21 and Figure 6.22. Figures are plotted using the same Y axis scales as the SF-ES1 case figures to facilitate comparison.

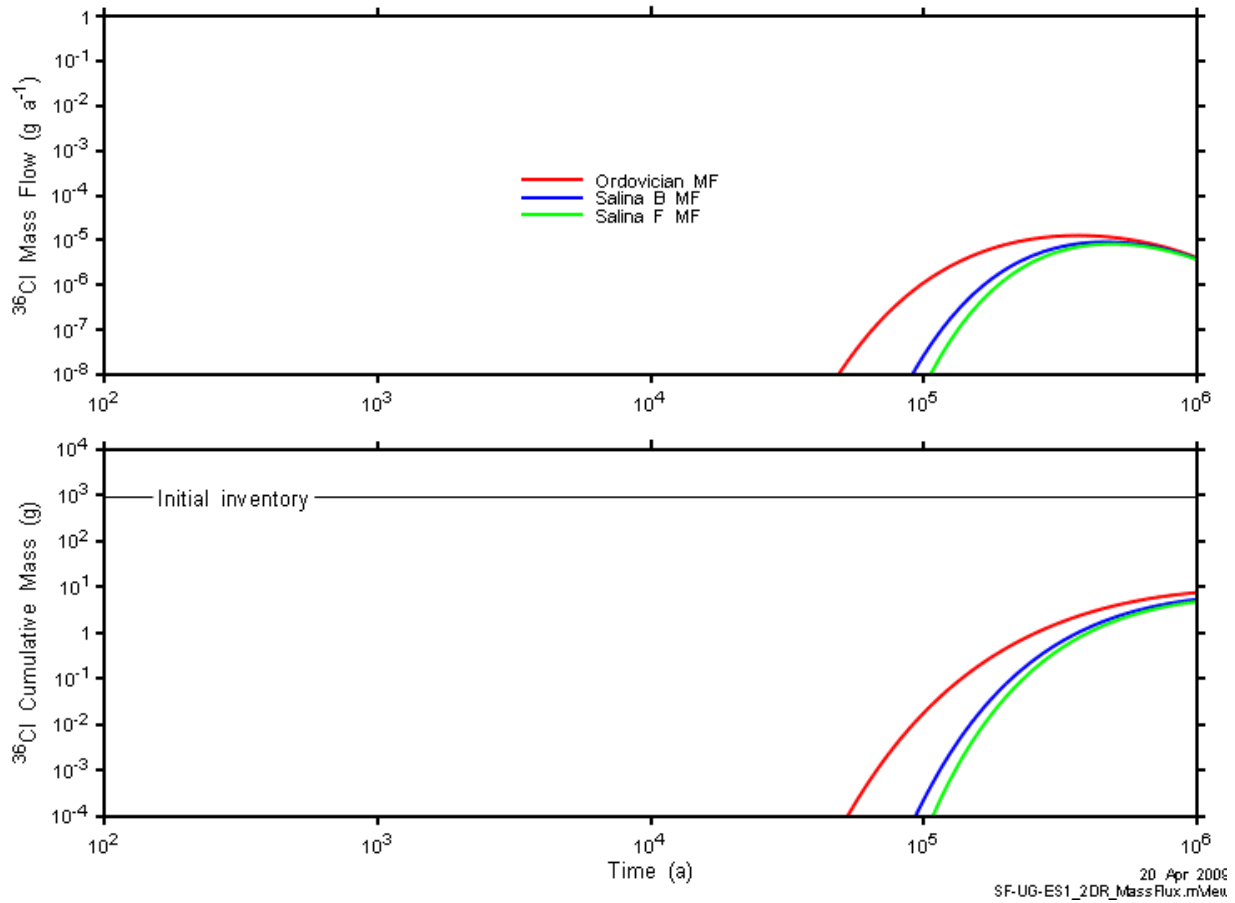


Figure 6.21: SF-UG-ES1 CI-36 total mass flow and cumulative mass transport.

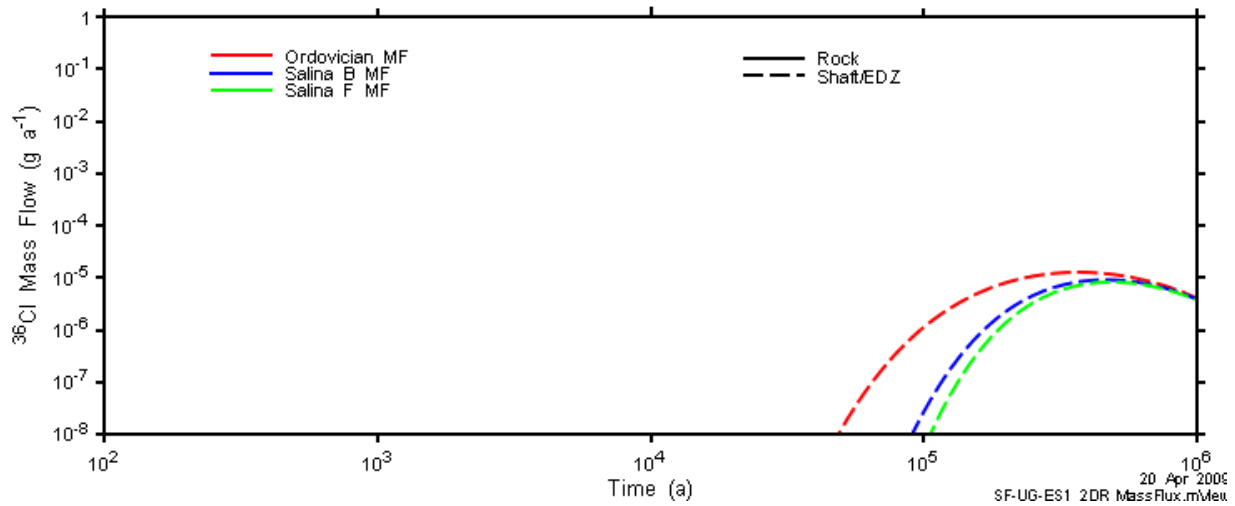


Figure 6.22: SF-UG-ES1-F2 mass flow components.

6.3 SF-US-F2: Failure of upper seal system

In the SF-US-F2 modelling case only those seal components above the Ordovician formations are compromised.

6.3.1 Flow Results

The compromised seal system substantially affects the Silurian formations only, as shown in Figure 6.23 through Figure 6.26. The highest velocities, which occur in the shaft, are on the order of 0.8 m a^{-1} . As in the SE-ES1-F2 modelling case, significant flow is drawn from the Guelph/Salina A0 unit towards the more conductive shaft.

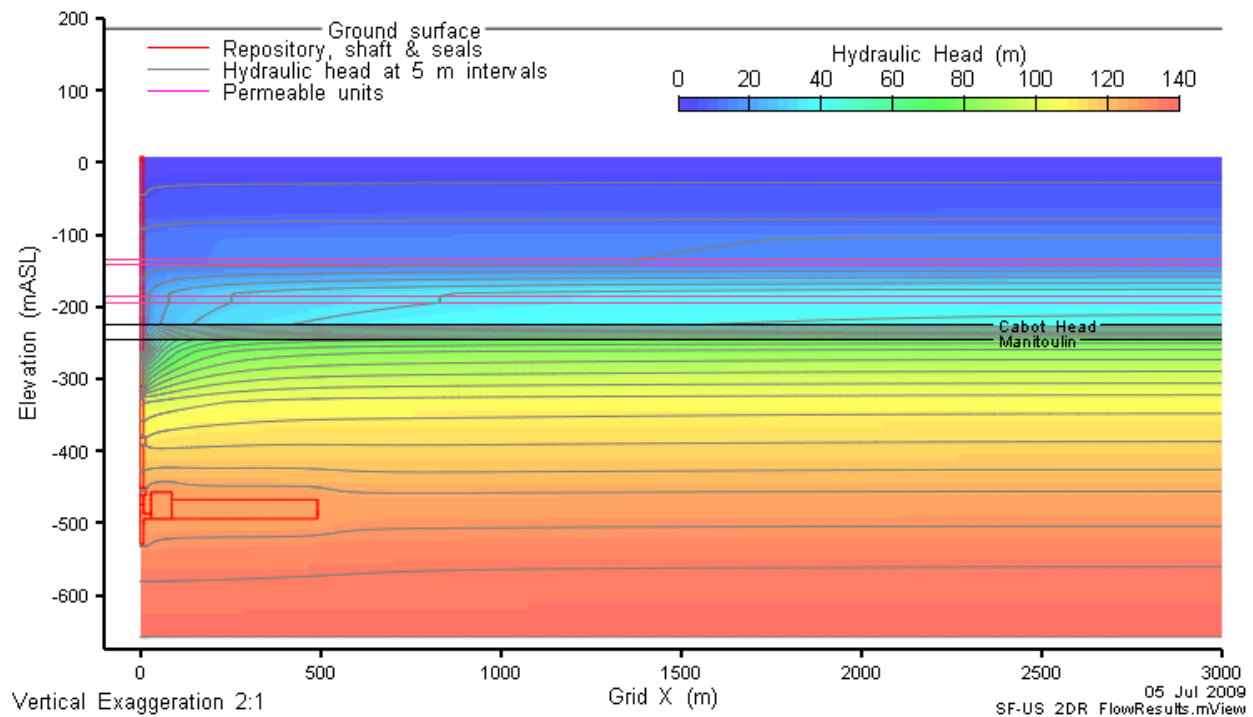


Figure 6.23: SF-US-F2 head contours for the entire model domain.

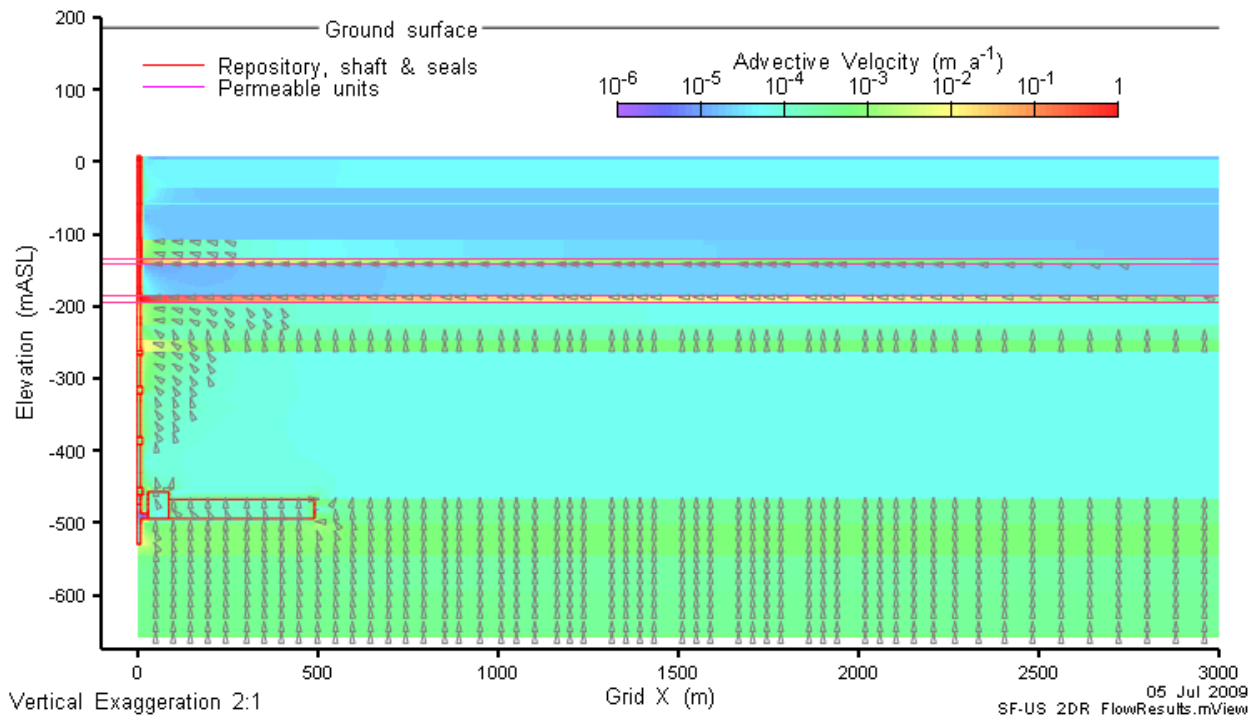


Figure 6.24: SF-US-F2 advective velocity magnitude and vectors for the entire model domain.

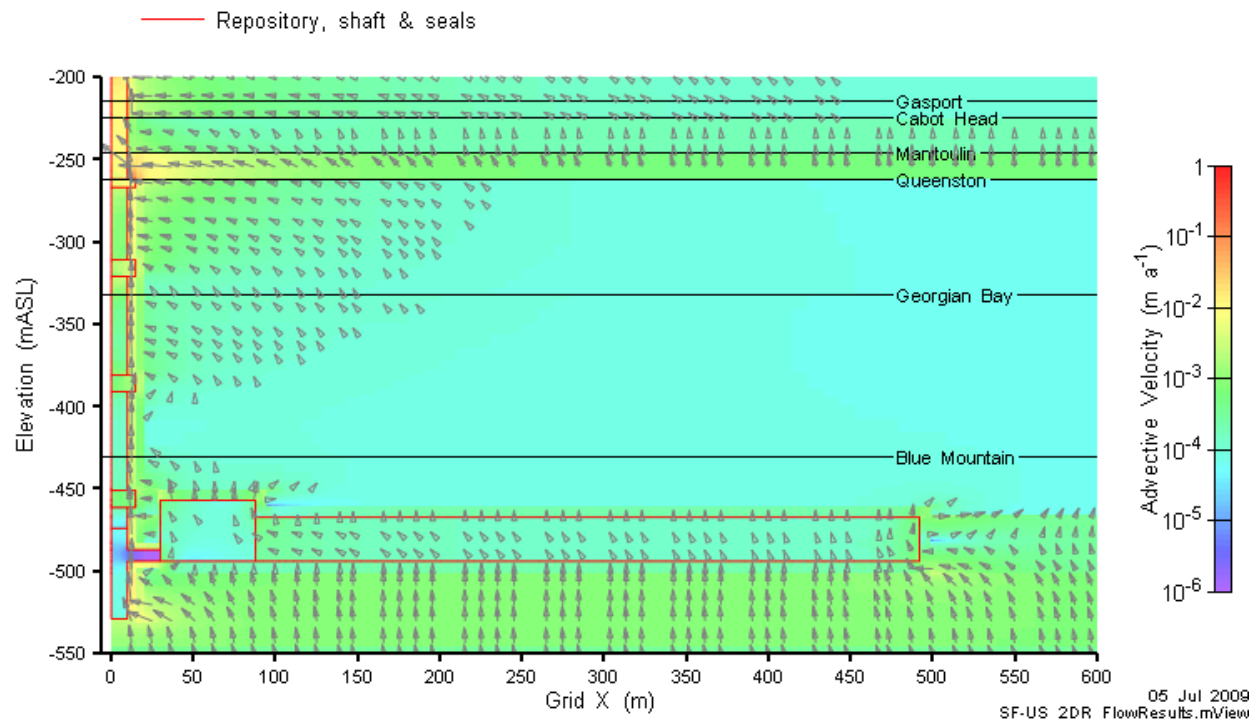


Figure 6.25: SF-US-F2 advective velocity magnitude and vectors in repository and lower shaft.

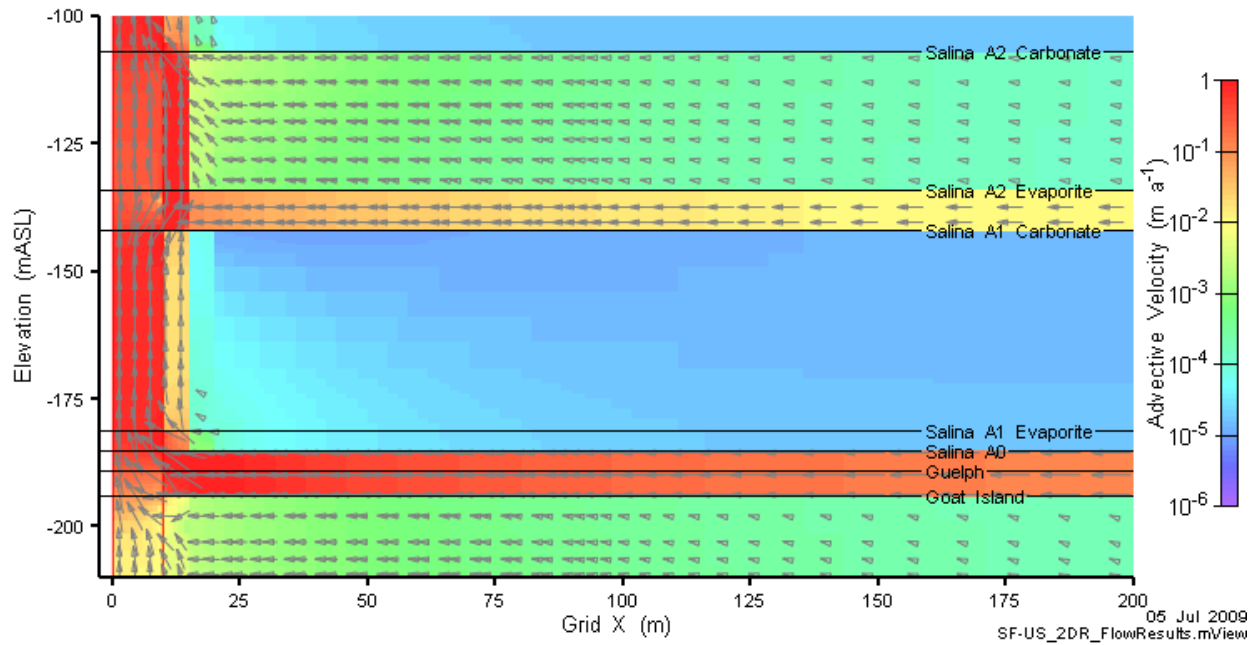


Figure 6.26: SF-US-F2 advective velocity magnitude and vectors in the vicinity of the Silurian seals.

6.3.2 Transport Results

Transport results (Figure 6.27 through Figure 6.29) are consistent with the flow results. Once contaminants reach the upper shaft, they move quickly out of the model. However, the lower seal components perform adequately in retaining CI-36 in the repository and Ordovician system. The rapid transport up the shaft in the Silurian is clearly evident in Figure 6.28 and Figure 6.29, where mass flow rates are essentially identical at all planes.

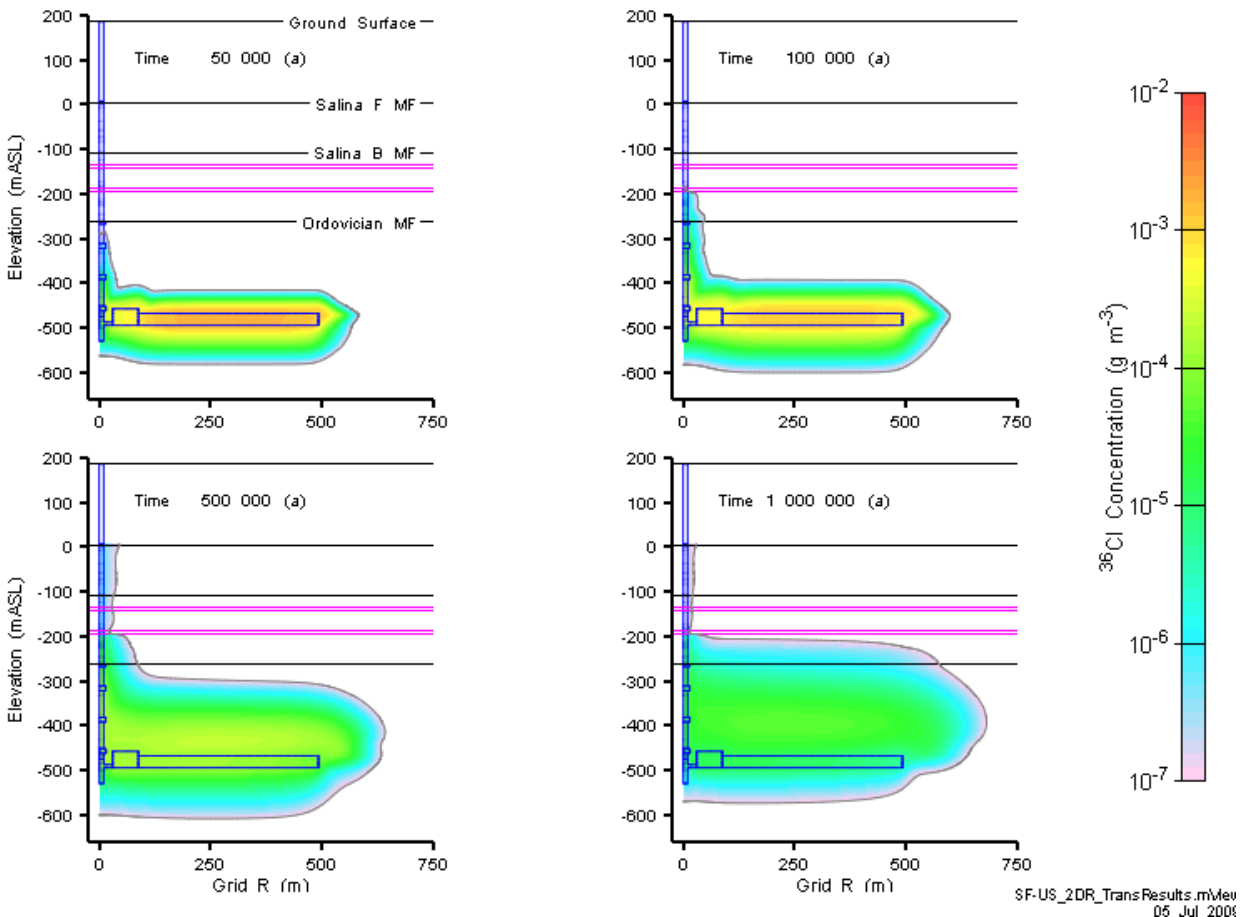


Figure 6.27: SF-US-F2 CI-36 concentration at 50 000, 100 000, 500 000, and 1 000 000 years.

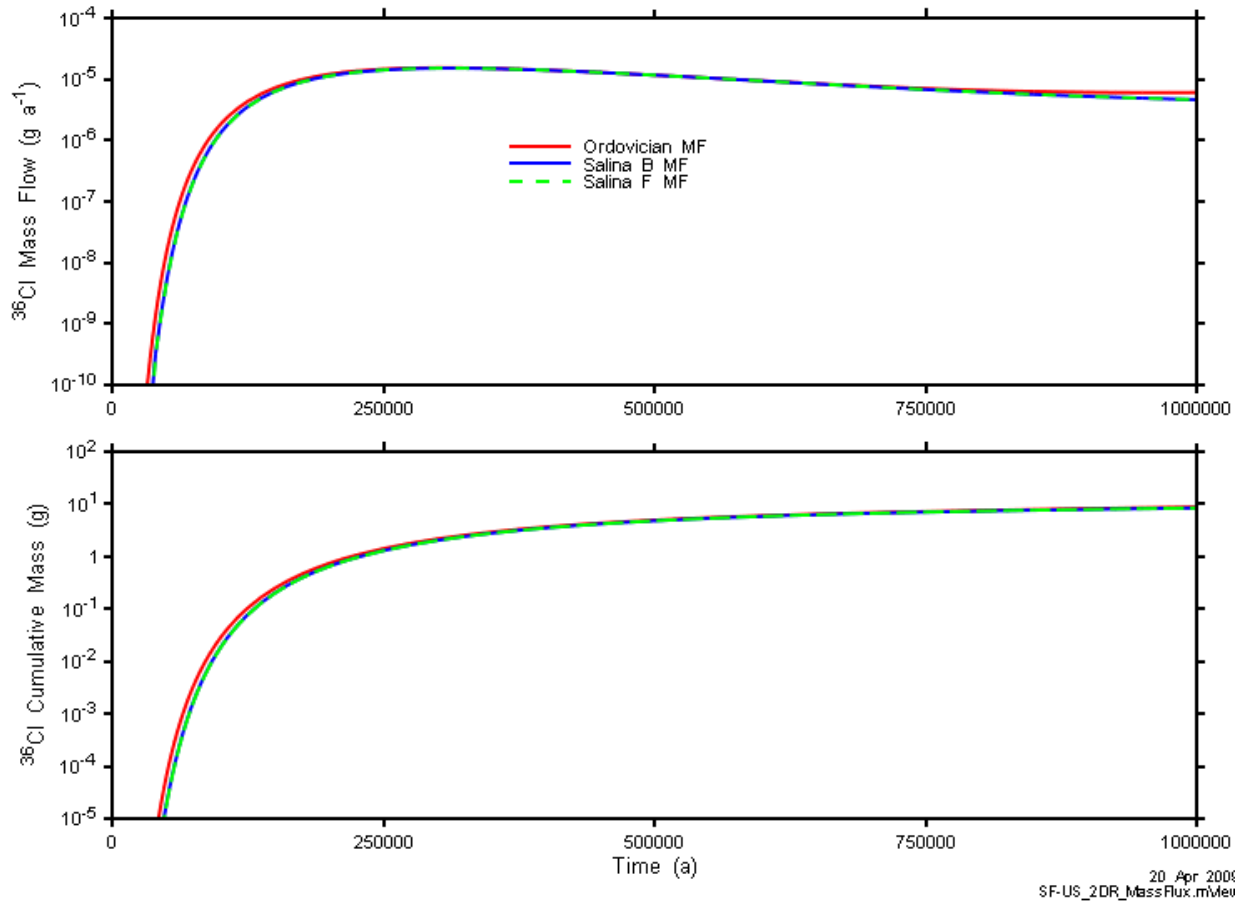


Figure 6.28: SF-US-F2 Cl-36 total mass flow and cumulative mass transport.

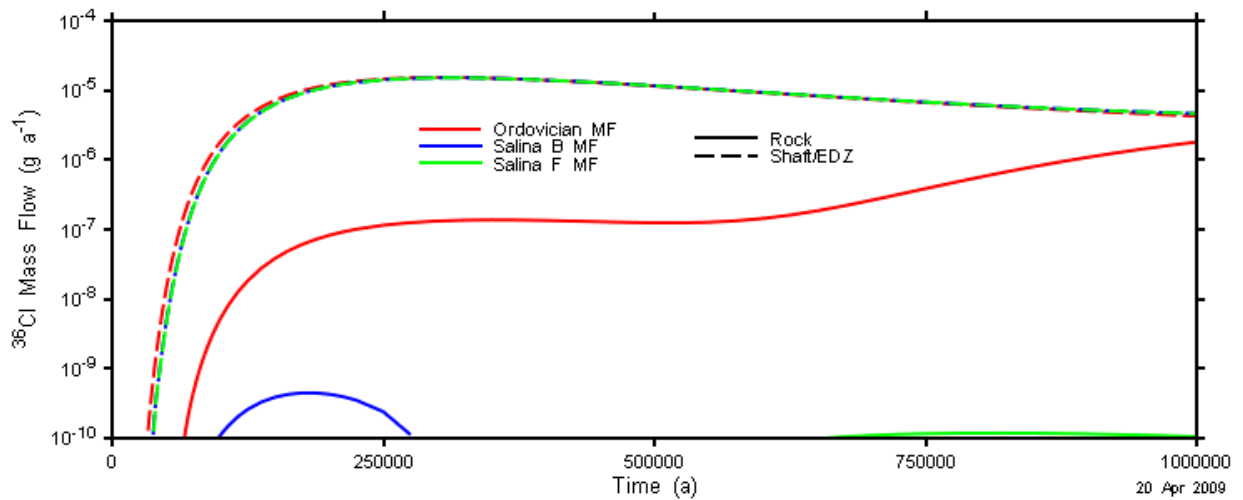


Figure 6.29: SF-US-F2 mass flow components.

6.4 EE-BC-F3: Extreme Earthquake

The EB-BC-F3 case adds a higher permeability vertical fault located outside the site characterization zone surrounding the facility. The fault is assumed to have been re-activated by an extremely large earthquake.

6.4.1 Flow Results

Hydraulic head contours are shown in Figure 6.30 and advective velocities in Figure 6.31. The fault has virtually no impact on the head or overall advective velocity distribution. The head gradient is predominantly vertical and the fault is located sufficiently distant from the repository as to be outside the zone of hydraulic influence. The vertical head distribution in the fault is identical to the adjacent rock mass as the vertical conductivity profile is essentially identical in shape, although shifted by three orders of magnitude. Advective velocities within the fault itself are consequently three orders of magnitude higher than in the rock mass.

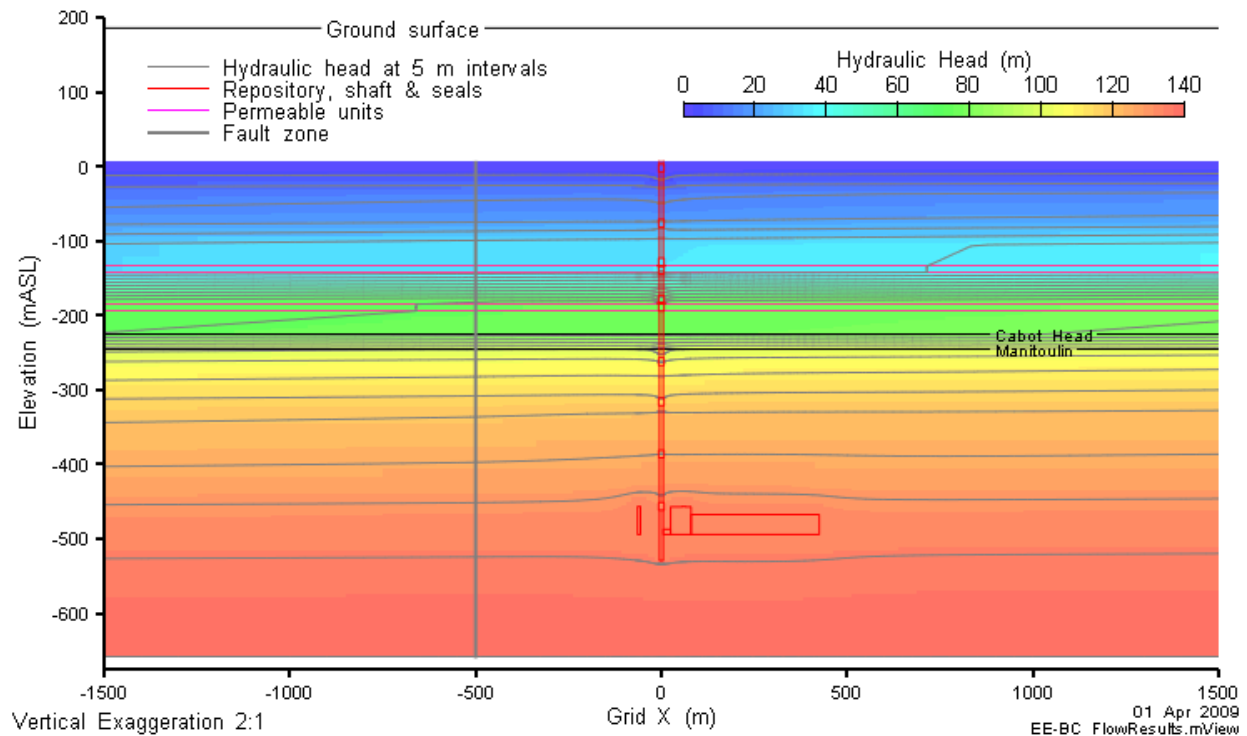


Figure 6.30: EE-BC-F3 head contours on a vertical slice through Grid Y=0.

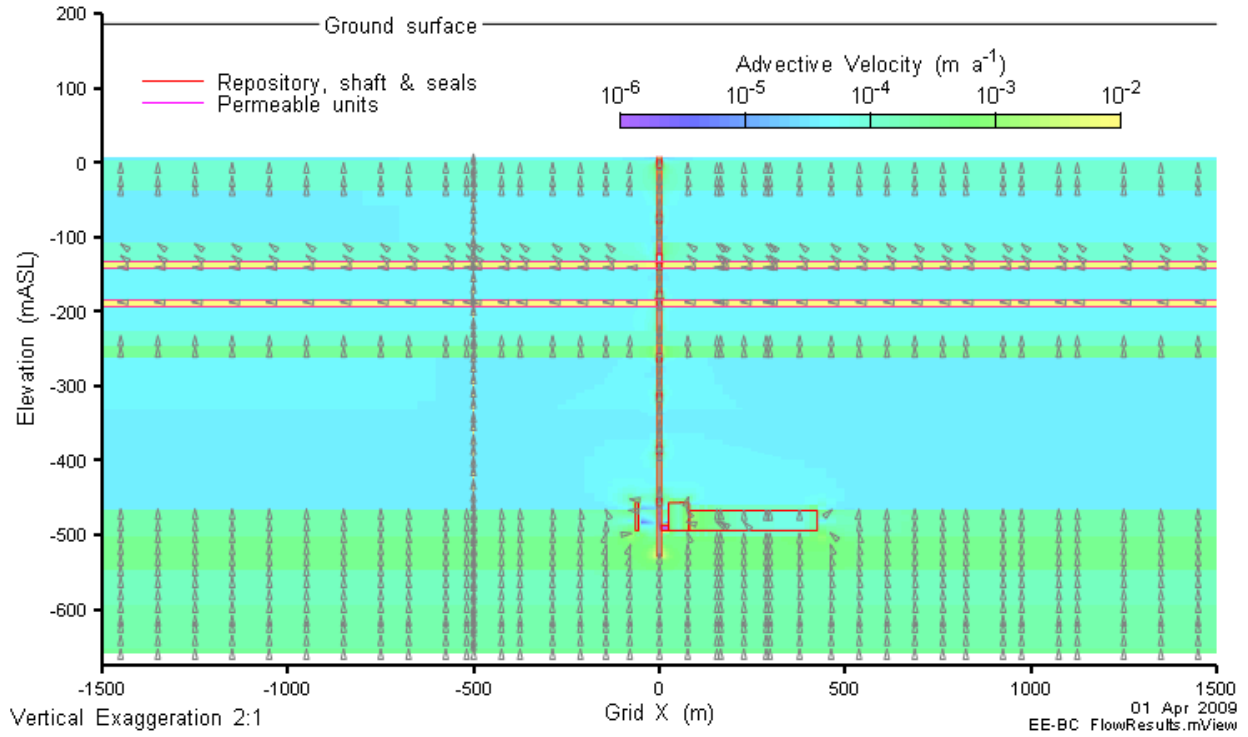


Figure 6.31: EE-BC-F3 advective velocity magnitude and vectors on a vertical slice through Grid Y=0.

6.4.2 Transport Results

Figure 6.32 shows the ^{36}Cl concentration contours at four different times. An additional contour line has been added to the figures at 10^{-8} g m^{-3} to show the influence of the fracture. Results are virtually identical to the NE-RS1-F3 results (Figure 5.11), except at 1 000 000 years where a minor degree of transport up the fracture is apparent.

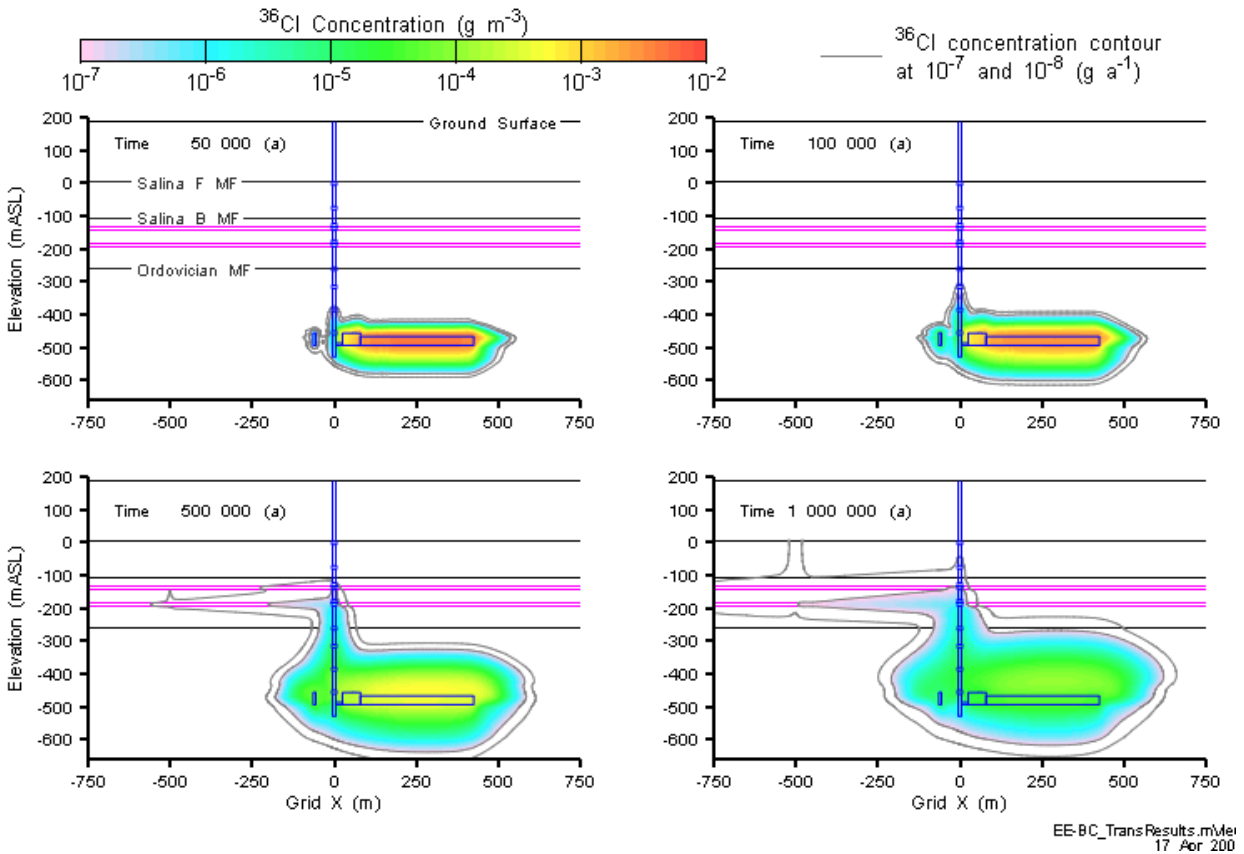


Figure 6.32: EE-BC-F3 ^{36}Cl concentration at 50 000, 100 000, 500 000, and 1 000 000 years.

The structure of the transport plume is shown in Figure 6.33.

Time 1000000 (a)

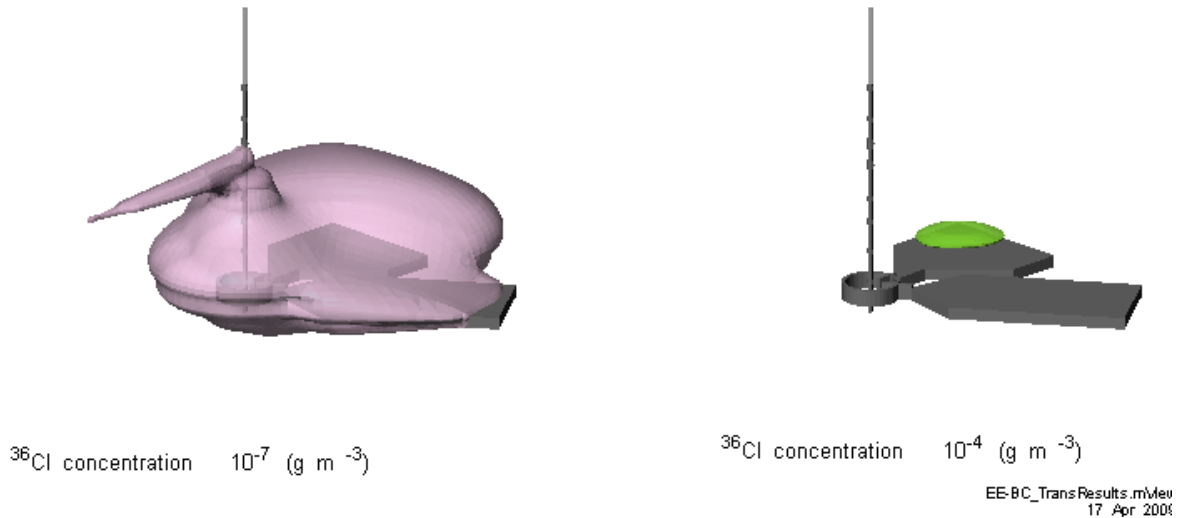


Figure 6.33: EE-BC-F3 Cl-36 concentration isovolumes at 1 000 000 years.

The Cl-36 mass flow and cumulative Cl-36 mass flow results are presented in Figure 6.34 and Figure 6.35. A third mass flow category, Fault, has been added to Figure 6.35 to show transport through the fault at the mass flow planes. At long times, transport through the fault is apparent in the Salina B plane.

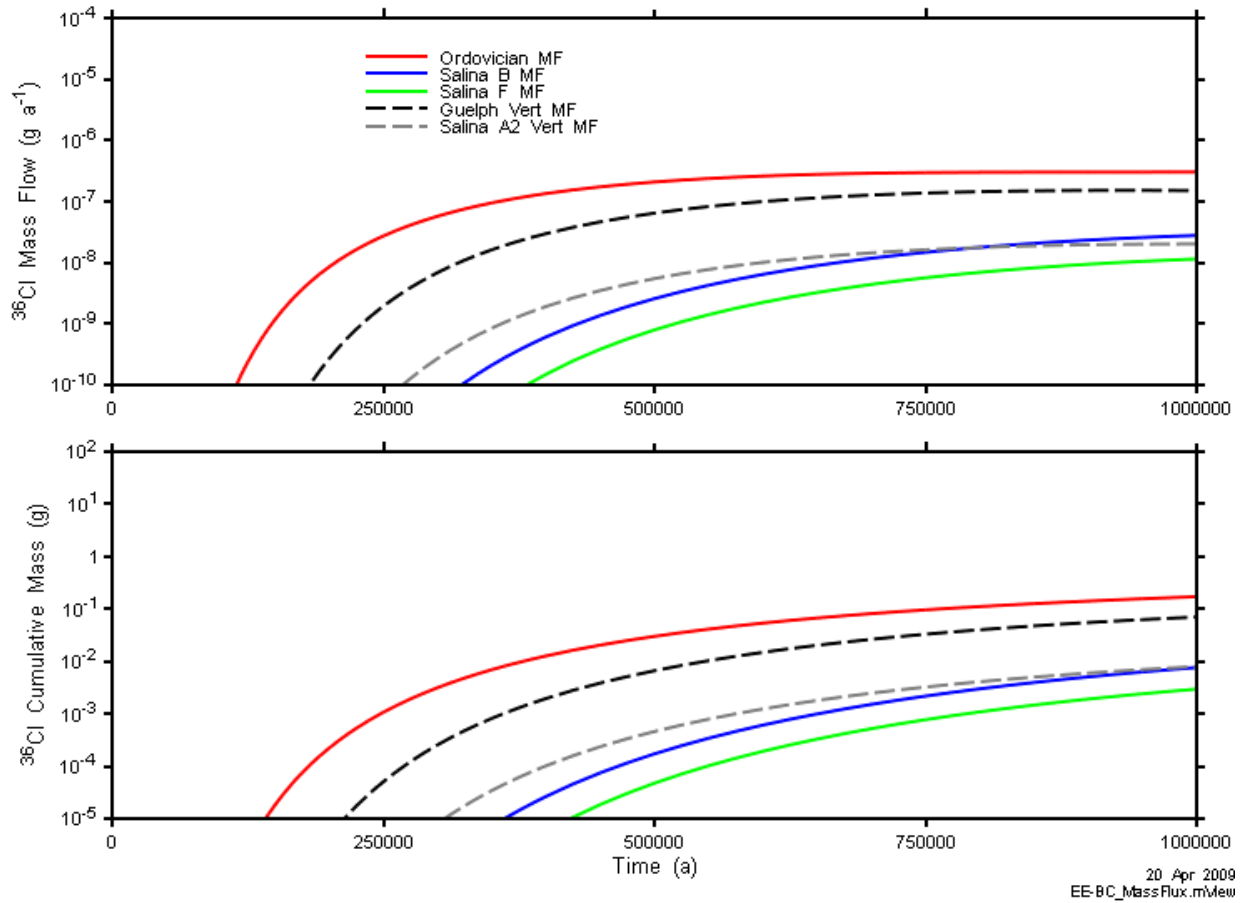


Figure 6.34: EE-BC-F3 Cl-36 mass transport results.

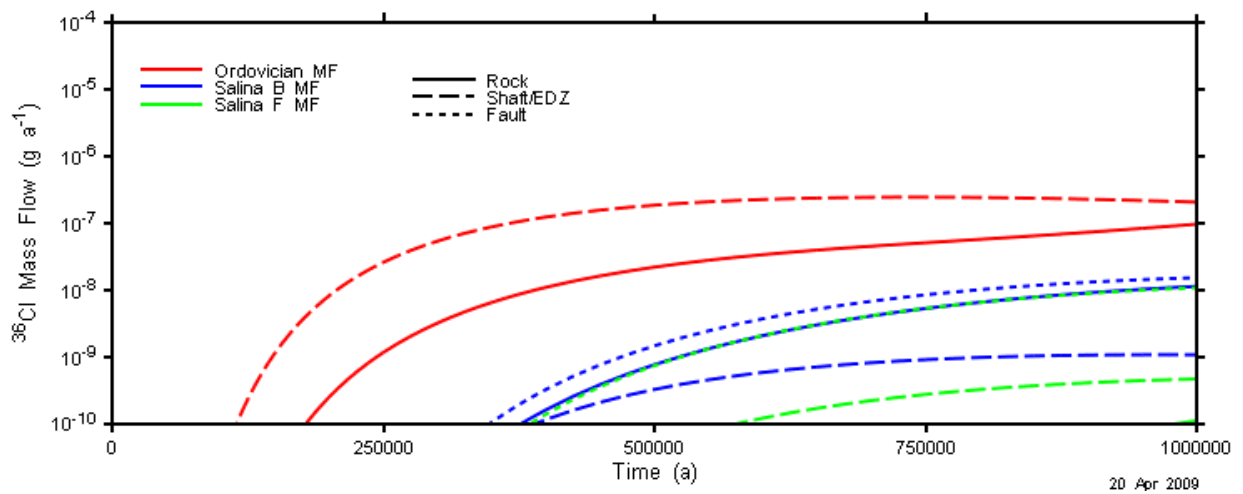


Figure 6.35: EE-BC-F3 mass flow components.

6.5 OB-BC-F3: Open Borehole

The DGR site will have several deep boreholes around the repository, used for site characterisation initially and for monitoring during and after operation. These boreholes will not intersect the repository itself, but will be some distance away. In all cases, the boreholes will be licensed through the Ontario Ministry of Natural Resources and they will respect the exclusion zone around the repository footprint. Furthermore, they will be appropriately sealed at the end of their useful lifetime. Consequently they will have no effect on the performance of the system.

However, if a deep borehole were not properly sealed, then it could provide a small but permeable pathway for the migration of contaminants from the repository. The OB-BC-F3 case therefore adds a poorly sealed exploration borehole in proximity to the site. The borehole location is approximately that of the DGR-3 site investigation borehole.

6.5.1 Flow Results

The borehole has a large effect on the local flow system in the vicinity of the repository. Hydraulic head contours are shown in Figure 6.36 and Figure 6.37. Advective velocities are shown in Figure 6.38. The borehole serves as a sink at the repository horizon, drawing flow in. Within the permeable Silurian units the borehole is a short-circuit between the Guelph/Salina A0 and Salina A2 evaporite, taking flow in from the Guelph/Salina A0 and expelling flow at the Salina A2 evaporite. This behaviour is a consequence of the base case geosphere, which results in significant hydraulic gradient across the Salina A1 unit, and would likely not occur to the same extent with the UG geosphere.

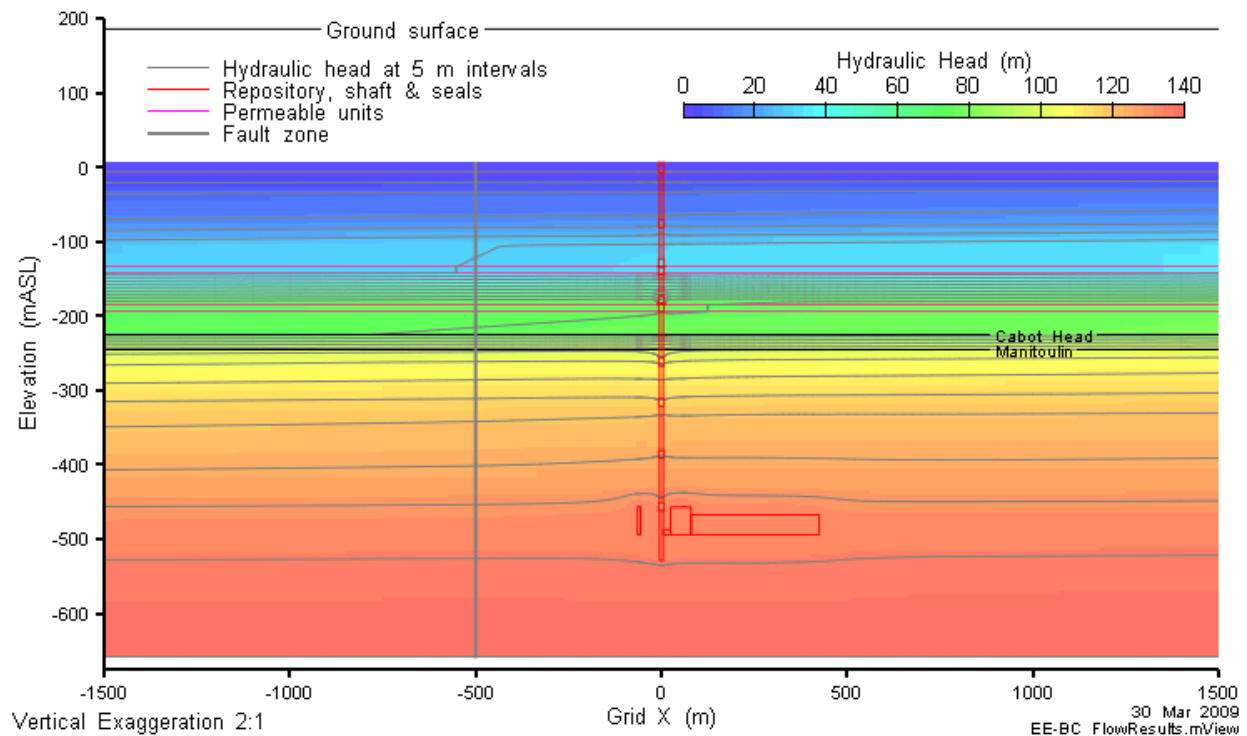


Figure 6.36: OB-BC-F3 head contours on a vertical slice through Grid Y=0.

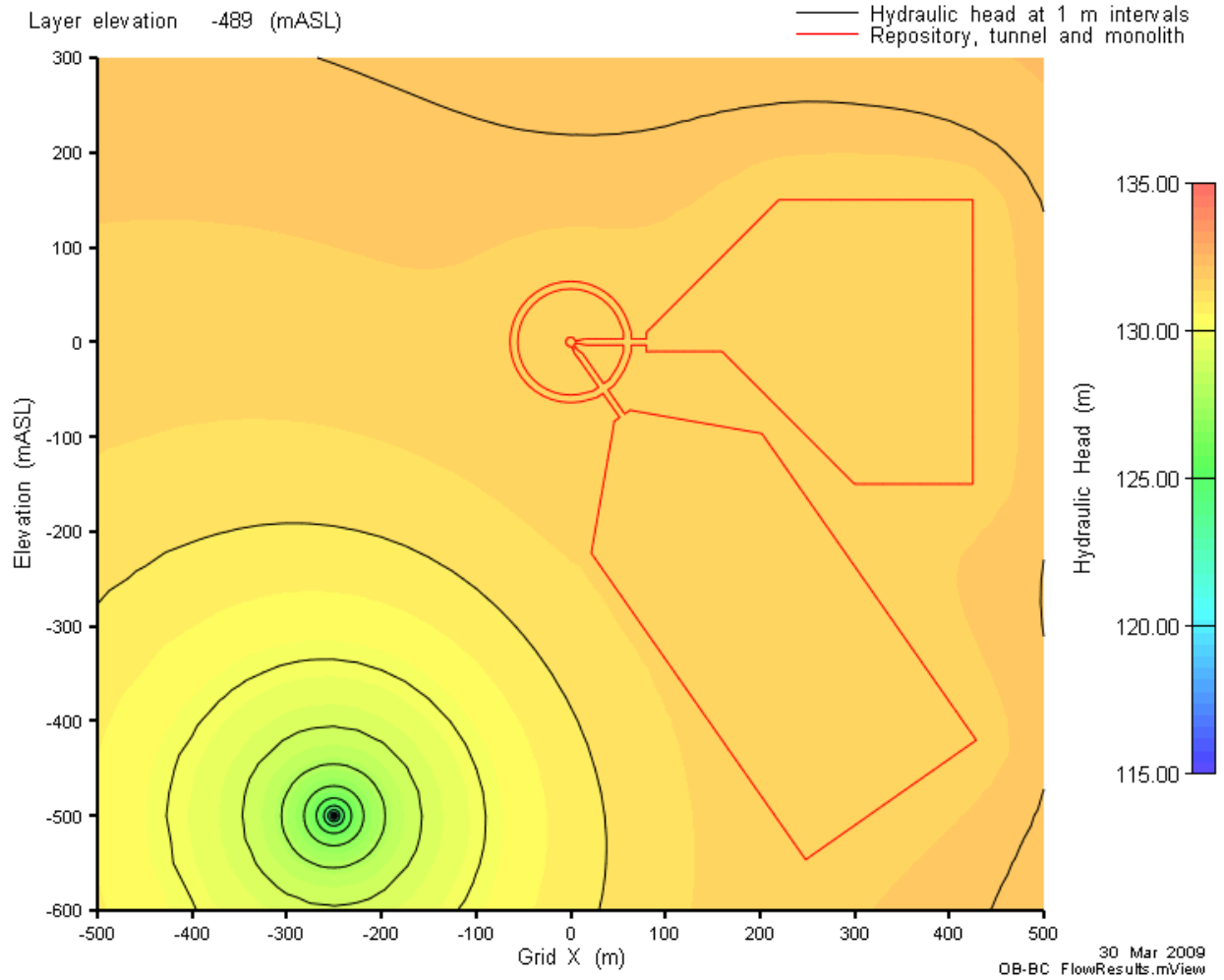


Figure 6.37: OB-BC-F3 head contours on a plan section through the repository.

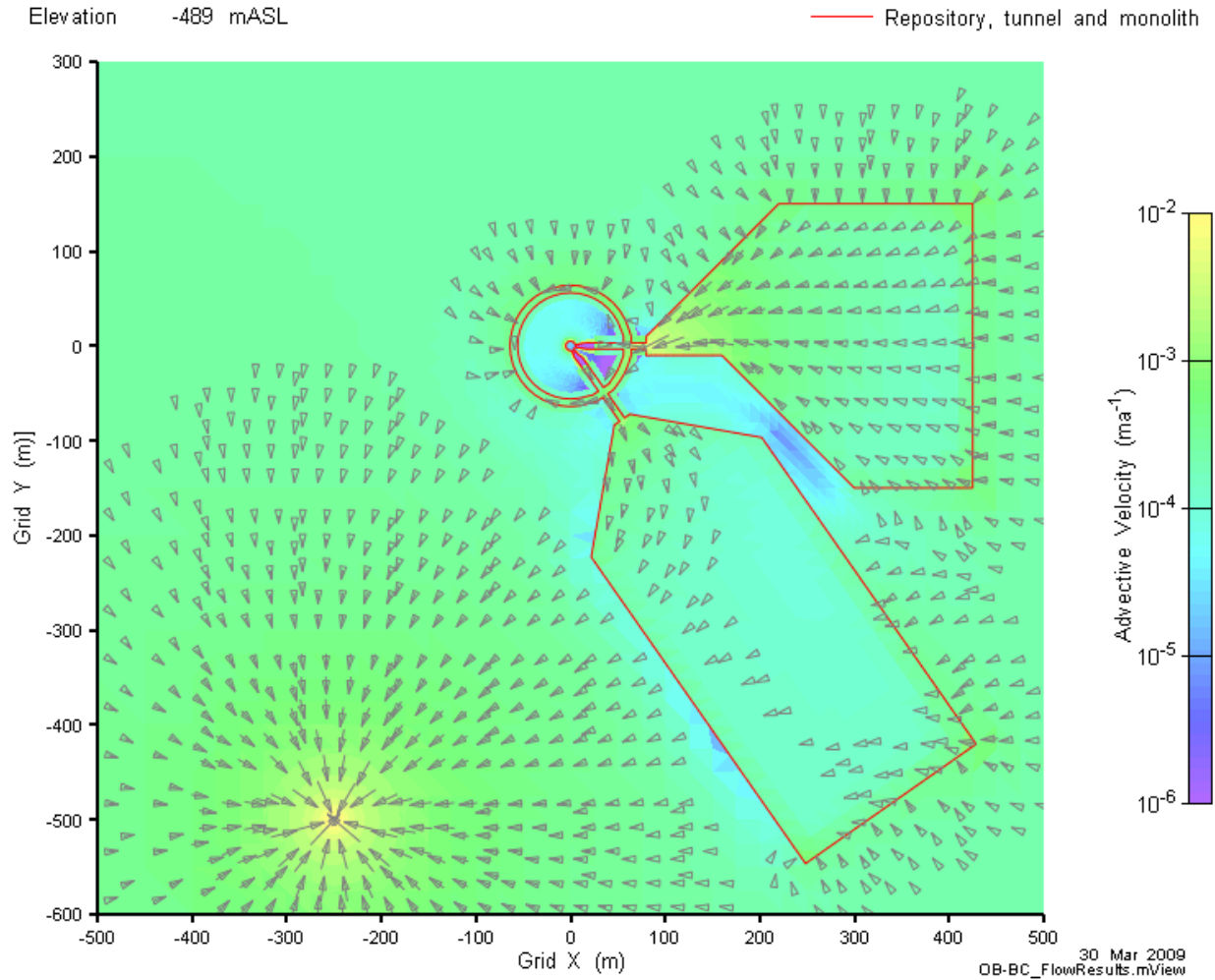


Figure 6.38: OB-BC-F3 advective velocity magnitude and vectors on a plan section through the repository

6.5.2 Transport Results

Figure 6.39 shows the CI-36 concentration contours at four different times. Results are similar to the NE-RS1-F3 results, except that transport within the Guelph/Salina A0 is attenuated. The reason for this is shown in Figure 6.40, where transport in the Guelph/Salina A0 is diverted towards the borehole.

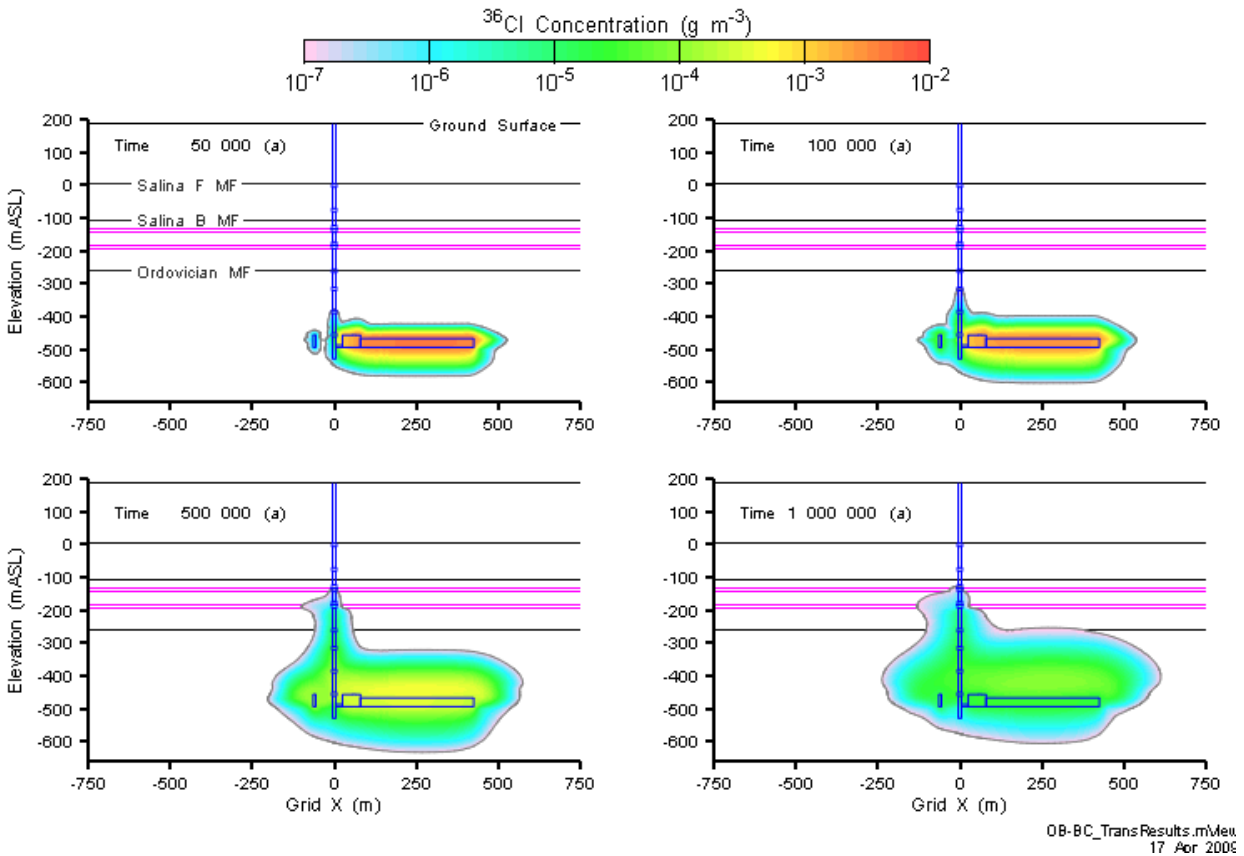


Figure 6.39: OB-BC-F3 CI-36 concentration at 50 000, 100 000, 500 000, and 1 000 000 years.

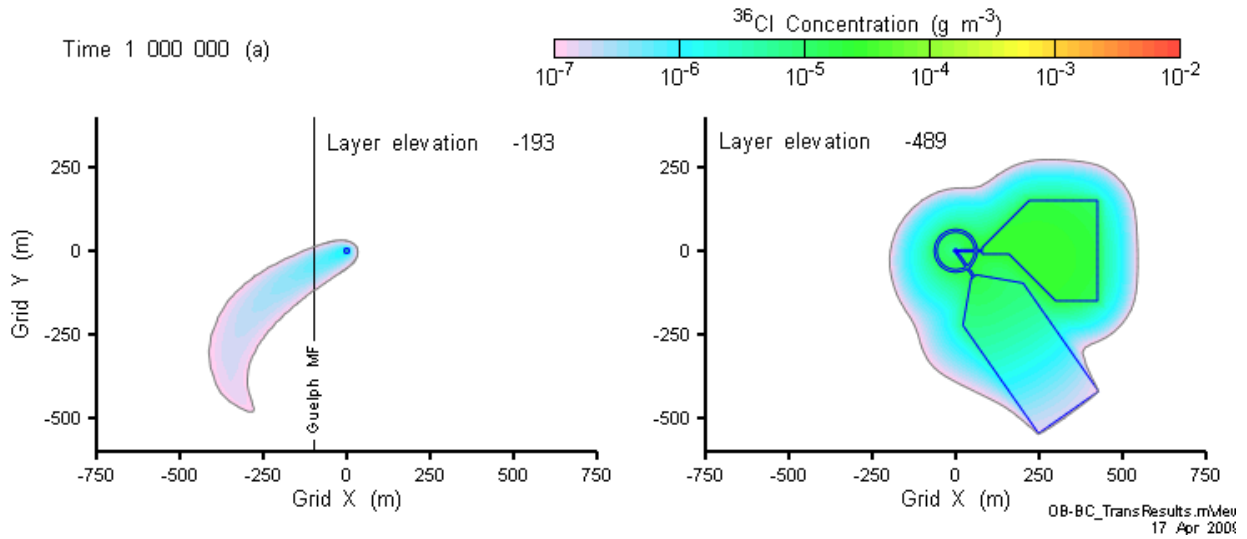


Figure 6.40: OB-BC-F3 Cl-36 concentration at Guelph and repository elevations at 1 000 000 years.

The structure of the transport plume is also apparent in Figure 6.41. Note that the influence of the borehole has caused dilution within the repository panels, reducing the maximum concentration below 10⁻⁴ g m⁻³ so that the higher concentration isovolume is not present.

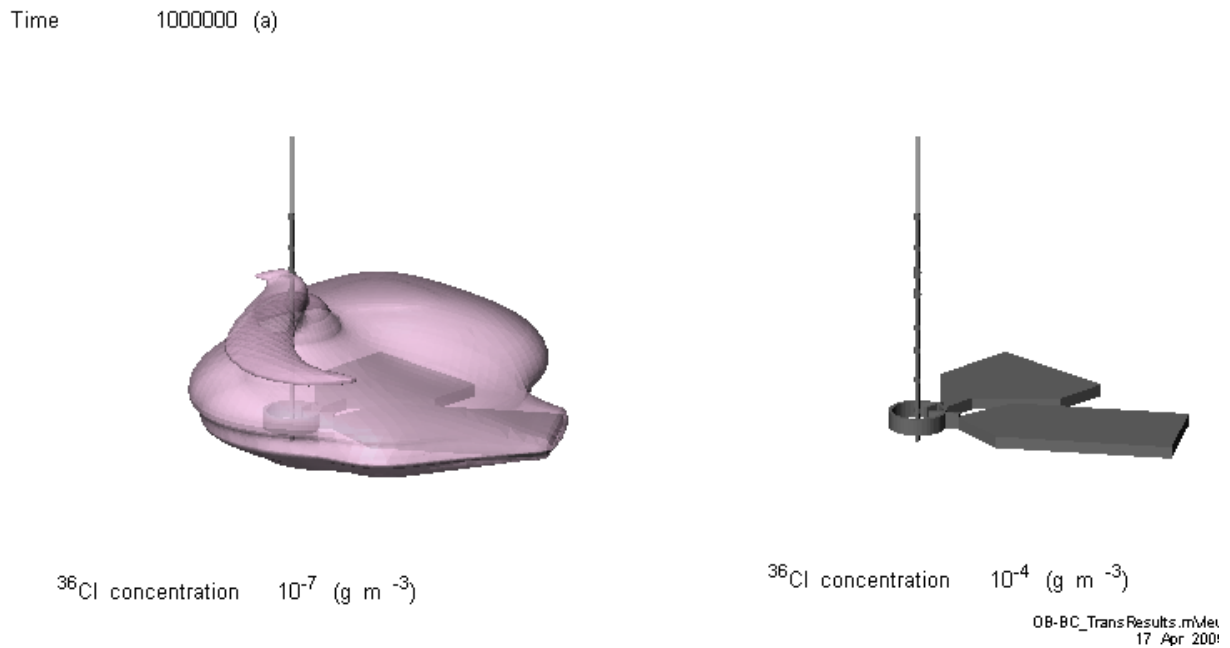


Figure 6.41: OB-BC-F3 Cl-36 concentration isovolumes at 1 000 000 years.

The CI-36 mass flow and cumulative CI-36 mass flow results are presented in Figure 6.42 and Figure 6.43. They are very similar to the NE-RS1 results, indicating little impact from the borehole.

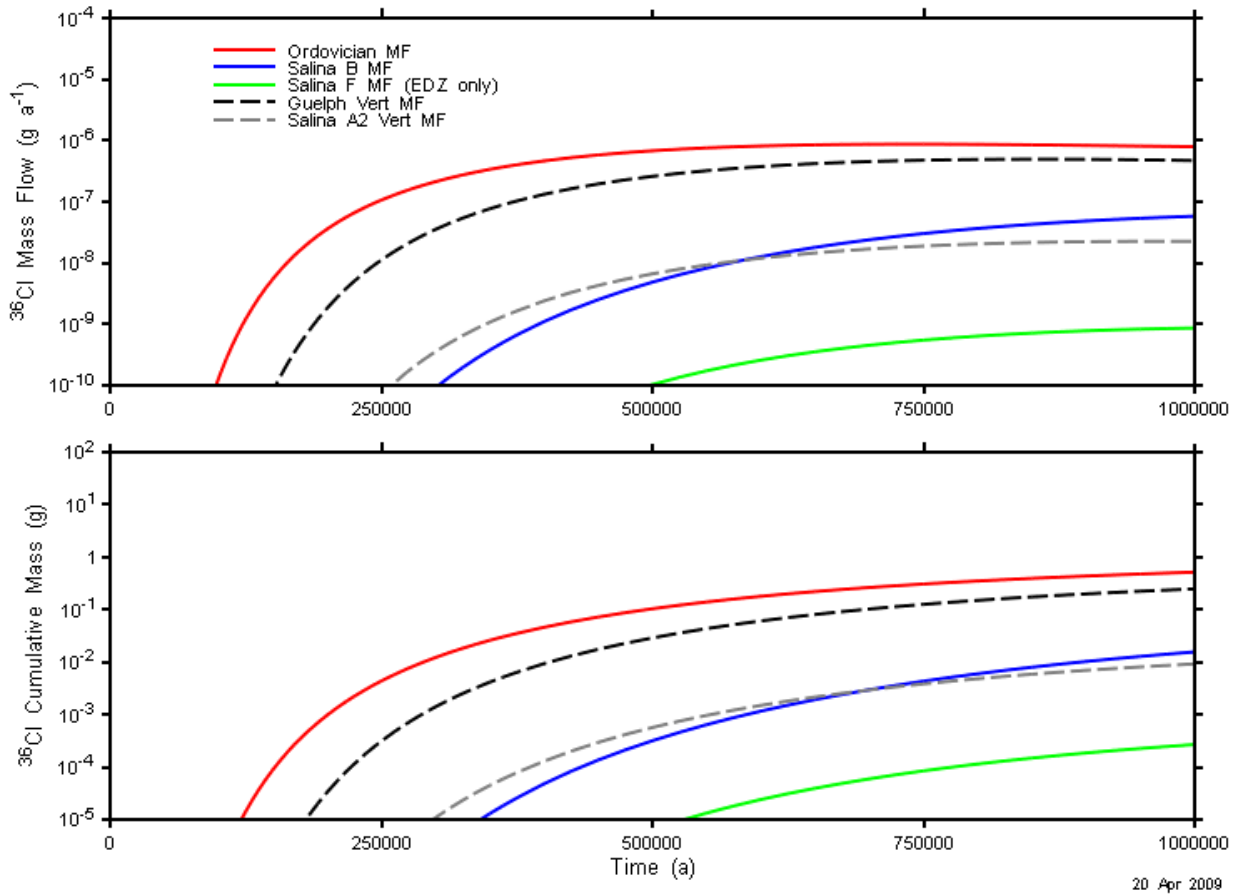


Figure 6.42: OB-BC-F3 CI-36 mass transport results.

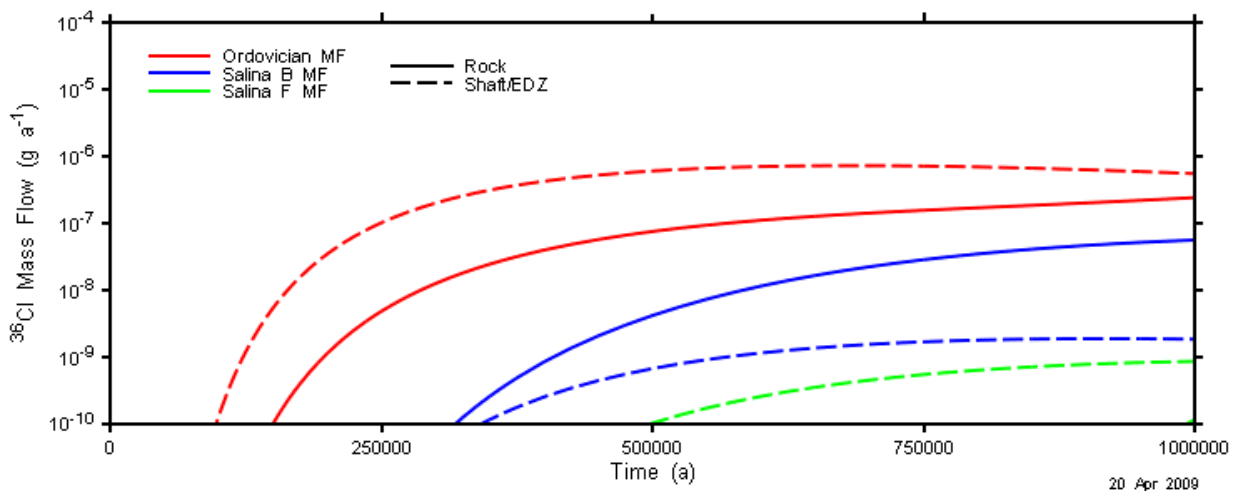


Figure 6.43: OB-BC-F3 mass flow components.

The OB-BC-F3 results were subject to some minor numeric errors where negative concentrations occurred at various points in the Silurian rock mass. These caused consequent negative mass fluxes and total mass at absolute values several orders of magnitude below the EDZ mass fluxes. Only EDZ mass flux and cumulative mass results are presented above for the Salina F mass flux plane in Figure 6.42.

7. RESULTS ASSESSMENT AND COMPARISON

This section presents a summary assessment of the modelling work presented in this document and a comparison of the results from all cases.

7.1 MODELLING APPROACH COMPARISON

The system was simulated using two modelling approaches; the simplified 2DR model and the more computationally intensive 3DS model. Application of the 3DS model to all cases would ensure more accurate treatment of the geometry. However, the 3DS model is more numerically difficult, and in some cases the 3DS model suffered from mass creation errors (the nature of which resulted in higher apparent releases).

The results from the 2DR model are useful for two reasons.

1. Cross-comparison of the two models provides verification of numerical model correctness.
2. Gas transport modelling described in Calder et al. (2009) uses the 2DR modelling approach exclusively, as 3DS type modelling is not presently practical for the numerically demanding two-phase gas model. Verification of the general suitability of the 2DR groundwater modelling approach builds confidence in the usefulness of the 2DR gas transport results.

A comparison of 3DS and 2DR mass transport results was previously presented in Section 5.3.3. The 2DR model produces results that are similar to the 3DS model, but which are generally more conservative in terms of estimating Cl-36 releases to the environment and, hence, the risks to potential exposure groups.

The 2DR model overestimates mass flow up the shaft and EDZ system. This causes significant differences in early-time results comparisons. However, at the end of the 1 Ma simulation period, flows are largely similar. As discussed in Section 5.3.3, this overestimate is at least partially due to the reduced interface area between the shaft EDZ and rock mass of the 2DR model in comparison to the 3DS model.

7.2 CALCULATION CASE COMPARISONS

Figure 7.1 through Figure 7.3 shows total (sum of shaft/EDZ and rock mass) vertical mass flow and cumulative mass through the top of the Salina F unit and horizontal mass transport through the permeable Silurian units for: Normal Evolution Scenario base case geosphere cases; Normal Evolution Scenario updated geosphere cases; and Disruptive Scenario cases, respectively. Unlike most mass flux figures presented in Section 5 and Section 6, the X axis is logarithmic time to better show the relative timing of the cases. Furthermore, the Y axis range on the figures has been expanded far below physically meaningful values to allow case comparison.

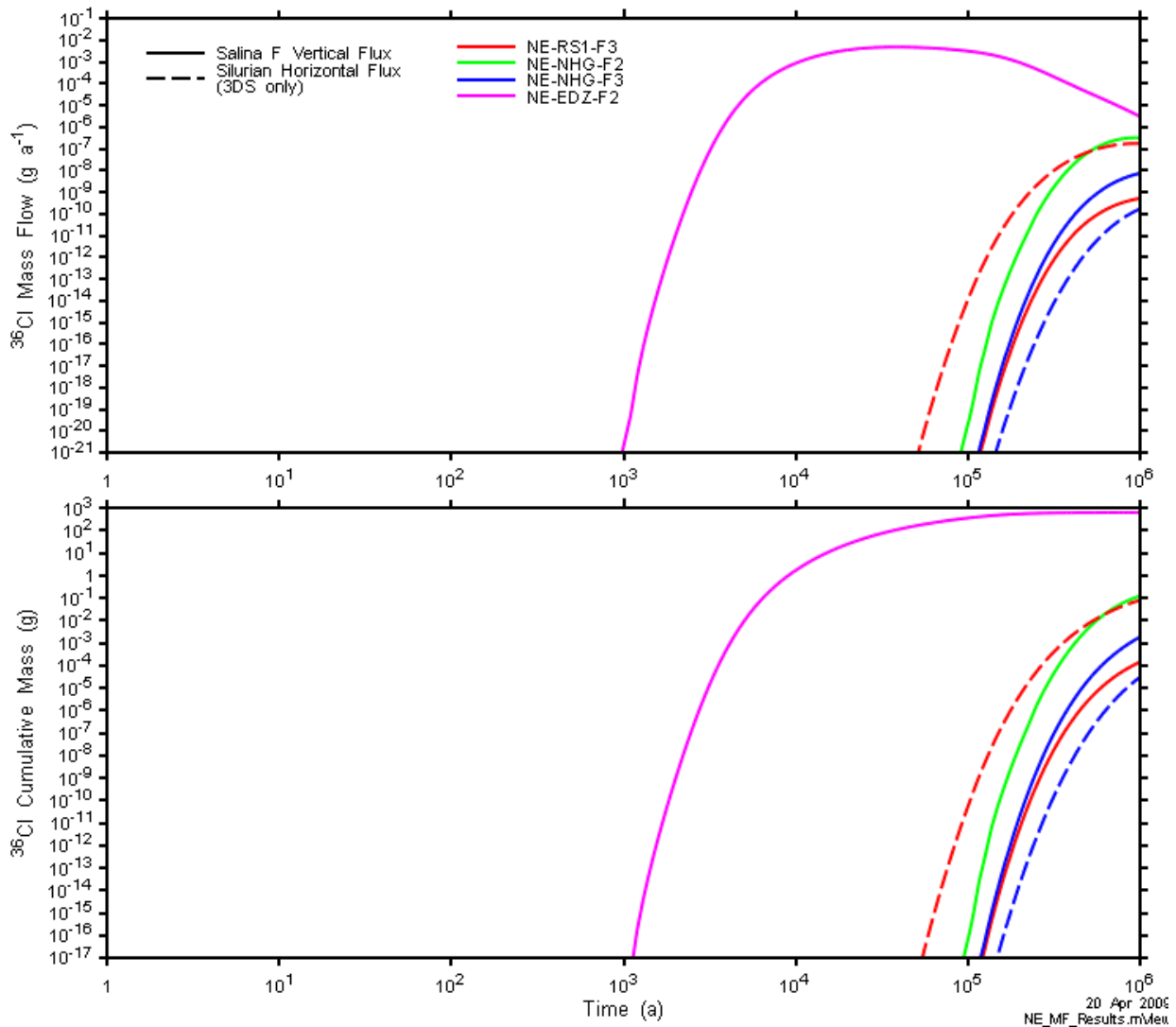


Figure 7.1: Cl-36 vertical mass transport across the Salina F MF plane and horizontal mass transport through permeable Silurian units (3DS only) for all Normal Evolution Scenario base case geosphere cases.

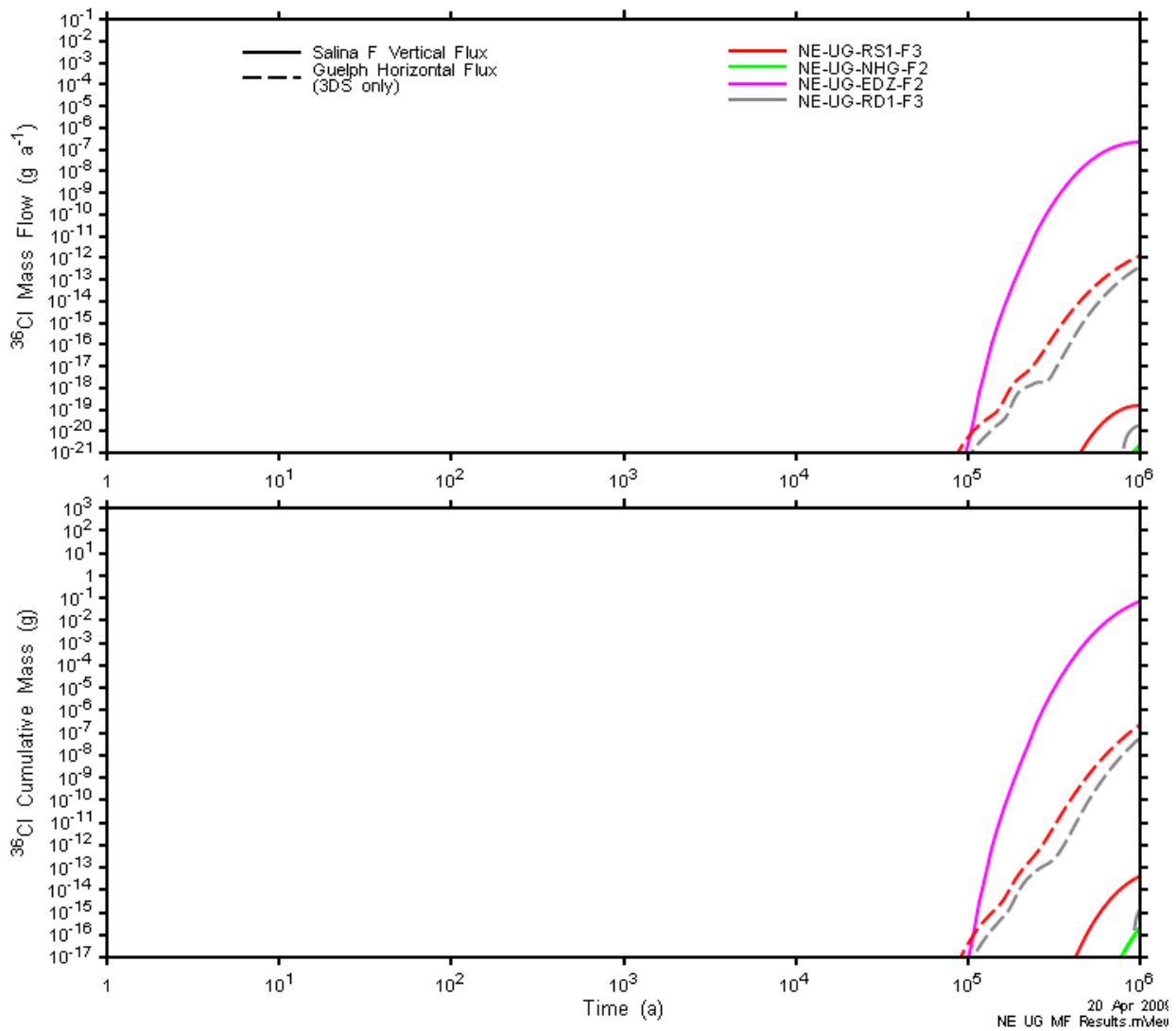


Figure 7.2: Cl-36 vertical mass transport across the Salina F MF plane and horizontal mass transport through permeable Silurian units (3DS only) for all Normal Evolution Scenario Updated Geosphere (NE-UG-) cases.

20 Apr 2008
NE UG MF Results.mView

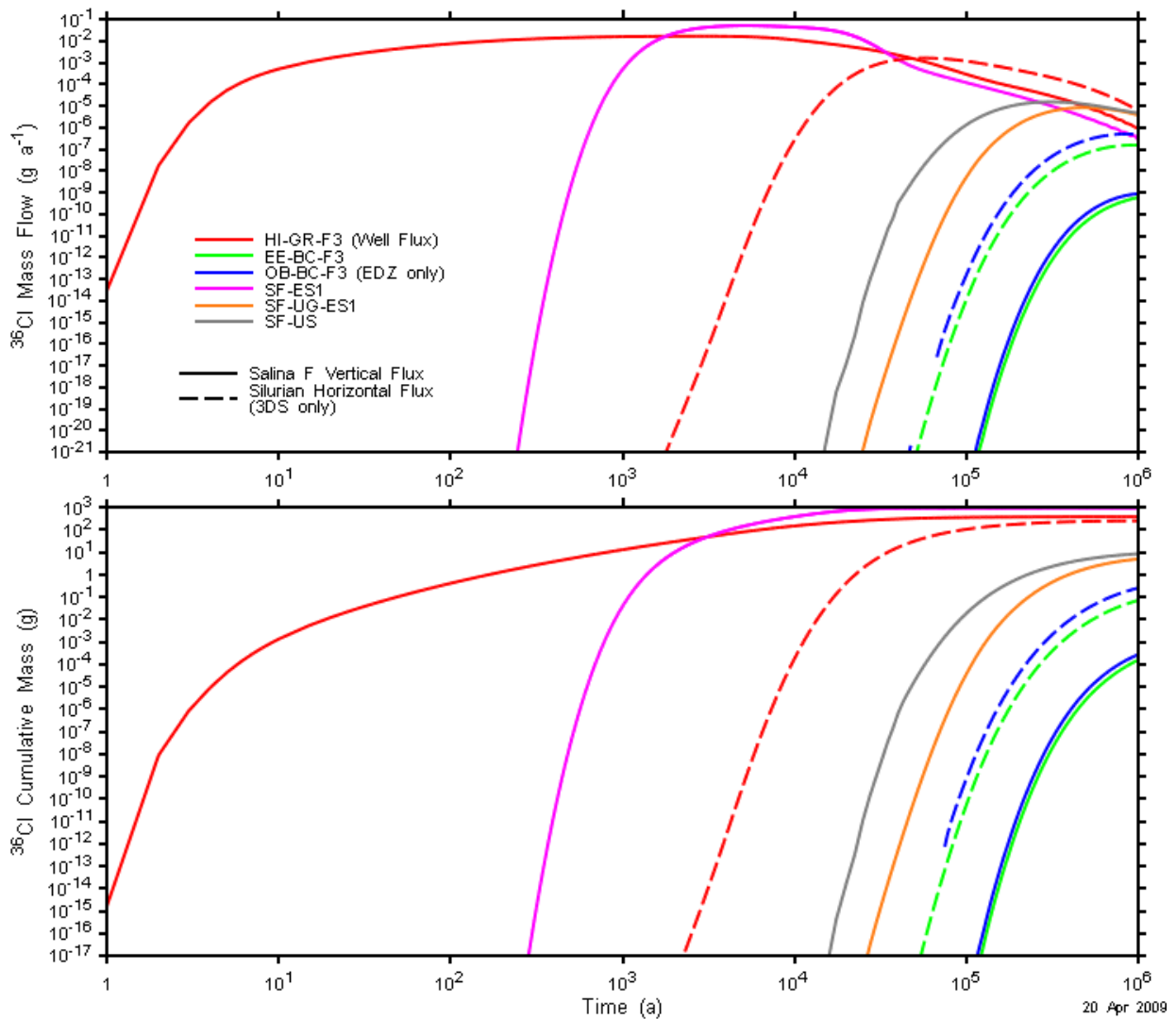


Figure 7.3: Cl-36 vertical mass transport across the Salina F MF plane and horizontal mass transport through permeable Silurian units (3DS only) for all Disruptive Scenario cases.

Note that potential impacts from releases are not evaluated in this document; they are addressed in the Normal Evolution Scenario Analysis report (Walke et al. 2009a) and the Human Intrusion and Other Disruptive Scenarios Analysis report (Penfold and Little 2009). The detailed groundwater modelling assesses only the magnitude and timing of releases.

The figures above reveal the following summary characteristics.

1. There is excellent containment of radionuclides for all NE cases with the exception of the NE-EDZ case.
2. The UG geosphere significantly improves system performance. There is virtually no release from the repository horizon except for the NE-UG-EDZ case, which is similar in magnitude to the NE-RS1 case.

3. For the 3DS cases, horizontal mass transport through the permeable Silurian units is a significant factor in reducing the mass exiting the system at the top of the Salina F.
4. The Disruptive Scenarios describe releases with much greater magnitude and earlier impact than the Normal Evolution Scenario but a significantly lower likelihood.

These figures, and the supporting detailed figures presented in Section 5 and Section 6, also lead to the conclusion that the shaft/EDZ system is the most significant route for contaminant transport from the facility. Transport through the rock mass was not significant for any scenario.

A quantitative comparison of cases and scenario characteristics follows.

- The results for the NE-EDZ, NE-UG-EDZ, SF-ESI, and SF-UG-ES1 cases indicate that an important parameter controlling long-term performance of the repository is the shaft sealing system. The NE-EDZ and NE-UG-EDZ cases represent the possibility that excavation induced damage around the shafts leads to increases in permeability adjacent to the shaft. The case also assumes that attempts to impede flow with concrete bulkheads in the inner EDZ and asphalt waterstops in the outer EDZ are not effective. In the NE-EDZ case, roughly 60 percent of the initial mass of CI-36 reaches the shallow bedrock groundwater zone during the 1 000 000 year simulation time. The SF-ES1 case represents a total failure of the shaft seal system. The parameters used are equivalent to backfilling the shaft with sand or sandy gravel, making a failure on this scale extremely unlikely. In this case nearly all of the initial mass of CI-36 has reached the shallow aquifer system within 30 000 years. The effectiveness of the Ordovician sealing system is reflected in the difference between the SF-ES1 and SF-US cases, where the SF-US case cumulative mass is a factor of approximately 100 lower than the SF-ES1 case. However, the SF-US-F2 case results are a factor of 70 higher than the NE-NHG-F2, which indicates the importance of the Silurian sealing system.
- The UG cases show vastly better performance than corresponding reference geosphere cases. The largest contrast, between the NE-NHG and the NE-UG-NHG, is over 14 orders of magnitude. This is not an entirely fair comparison as the NE-UG-NHG case also includes the effects of transient flow due to repressurization. However, a steady-state version of NE-UG-NHG, not presented in this report, resulted in an 11 order of magnitude reduction. Impact of the geosphere on the shaft failure case was less significant, with a reduction factor of approximately 200 for SF-UG-ES1 compared to SF-ES1. This reduction reflects the reduced fluid flow into the repository for the UG cases. The EDZ case reduction factor was greater at approximately 9000, and represents the combined effect of reduced fluid flow into the repository and reduced permeability in the EDZ.
- The NE-RS1-F3 case includes a horizontal gradient in the permeable Silurian units. As compared to the NE-NHG-F3 comparison case, this horizontal flow zone significantly reduces transport into the shallow bedrock groundwater zone by diverting flow that would otherwise discharge to the zone. For the NE-RS1-F3 case 0.08 g is diverted through the permeable units at 1 000 000 years with 1.4×10^{-4} g exiting the system vertically through the Salina F. By contrast, with the NE-NHG-F3 case 1.8×10^{-3} g crosses the Salina F plane.

- For the HI-GR case, cumulative flow in the Silurian units is nearly 40% of the initial inventory. However, this flow is based upon an inflated mass flow rate caused by the well mass creation errors noted in Section 6.1.2 and may be considered conservative (i.e. an overstatement of actual transport) in that respect.
- The impact of the ring and access tunnel sealing in the NE-UG-RD1 case is perceptible, but largely inconsequential, given the already low mass flows for the UG cases. However, the ring and access tunnel sealing may have greater impact on cases with more extreme EDZ assumptions and could also reduce releases for cases with various degrees of shaft seal failure.

Table 7-1 presents a summary of cumulative mass and peak mass flow for each calculation case simulated as a general metric of system performance. The table also includes the time of peak mass flow for the Salina F metric. Figure 7.4 and Figure 7.5 provide a visual representation of the same data for the Salina F metric only. Figure 7.6 and Figure 7.7 show horizontal transport through the Silurian formation for 3DS modelling cases only. Note that with the exception of the NE-UG-EDZ-F2 case, results from UG geosphere cases are too low to appear on the plots.

The results confirm the discussion above, that the main determinant on mass transfer to the biosphere is the performance of the shaft seals and shaft EDZ system. The rock mass provides an extremely effective barrier system to groundwater transport of radionuclides.

Table 7-1: Summary of cumulative CI-36 mass and peak CI-36 mass flow for all calculation cases

Plane	Cumulative CI-36 Mass Crossing (g)			Max. CI-36 Mass Flow Rate (g a ⁻¹)			Peak Flow Time (a)
	Ordovician Vertical	Salina F Vertical	Silurian Horizontal	Ordovician Vertical	Salina F Vertical	Silurian Horizontal	Salina F Vertical
2DR							
NE-NHG	1.4E+00	1.2E-01		2.3E-06	3.1E-07		950000
NE-UG-NHG	5.4E-08	2.2E-16		1.9E-13	2.3E-21		1000000
NE-EDZ	6.2E+02	6.1E+02		4.9E-03	4.7E-03		38500
NE-UG-EDZ	1.0E+00	7.0E-02		1.7E-06	2.2E-07		1000000
SF-ES1	9.0E+02	8.9E+02		5.1E-02	5.0E-02		5175
SF-UG-ES1	7.7E+00	4.9E+00		1.3E-05	8.2E-06		500000
SF-US	8.8E+00	8.4E+00		1.5E-05	1.5E-05		300000
3DS							
NE-RS1	1.7E-01	1.4E-04	7.8E-02	3.0E-07	5.1E-10	1.7E-07	1000000
NE-UG-RS1	2.4E-06	4.1E-14	2.2E-07	9.4E-12	1.5E-19	1.2E-12	1000000
NE-NHG	1.5E-01	1.8E-03	3.0E-05	2.6E-07	7.3E-09	1.7E-10	1000000
NE-UG-RD1	7.4E-07	1.4E-15	6.2E-08	3.5E-12	1.7E-20	3.8E-13	1000000
HI-GR	1.8E+03	3.7E+02	2.4E+02	8.2E-02 [*]	1.6E-02 [*]	1.6E-03	2700
EE-BC	1.7E-01	3.0E-03	7.8E-02	3.0E-07	1.1E-08	1.7E-07	1000000
OB-BC	5.2E-01	2.2E-04	2.6E-01	8.7E-07	9.8E-10	4.9E-07	1000000

* HI-GR vertical results are borehole flow only (see Section 6.1.2)

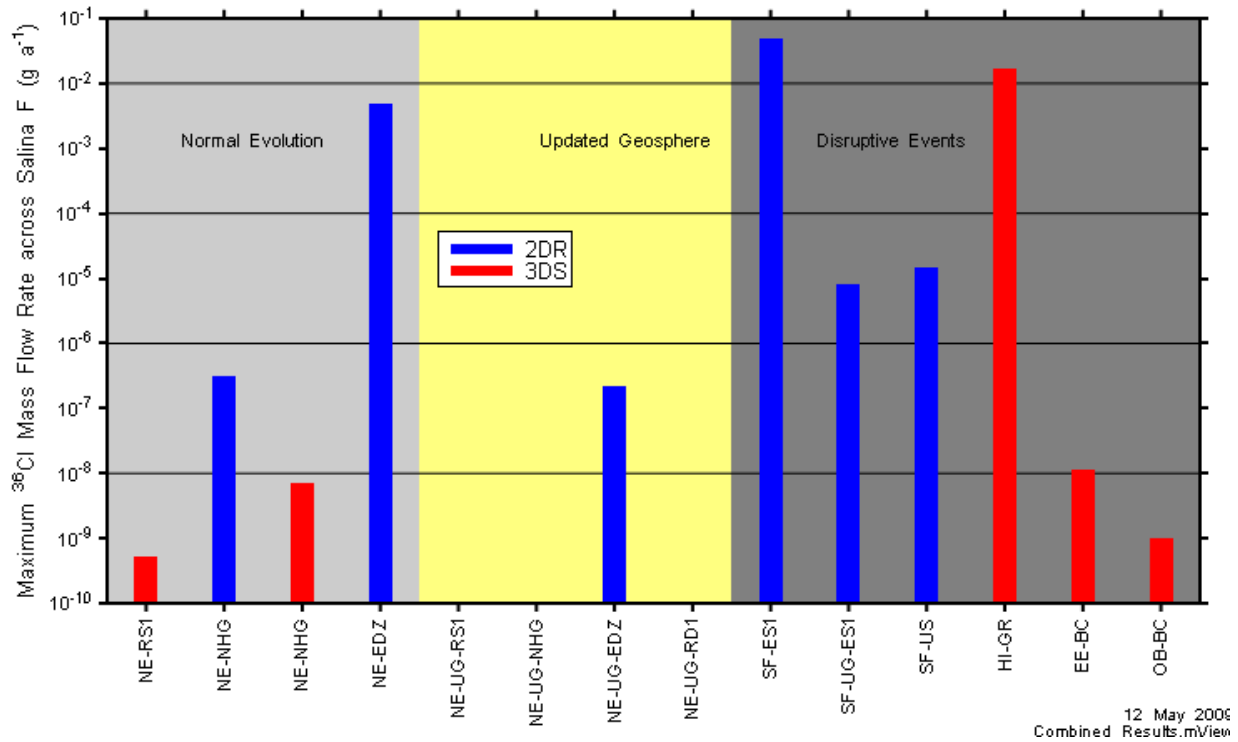


Figure 7.4: Peak Cl-36 mass flow across the Salina F MF plane for all modelling cases. All UG case results except NE-UG-EDZ are below Y axis limit.

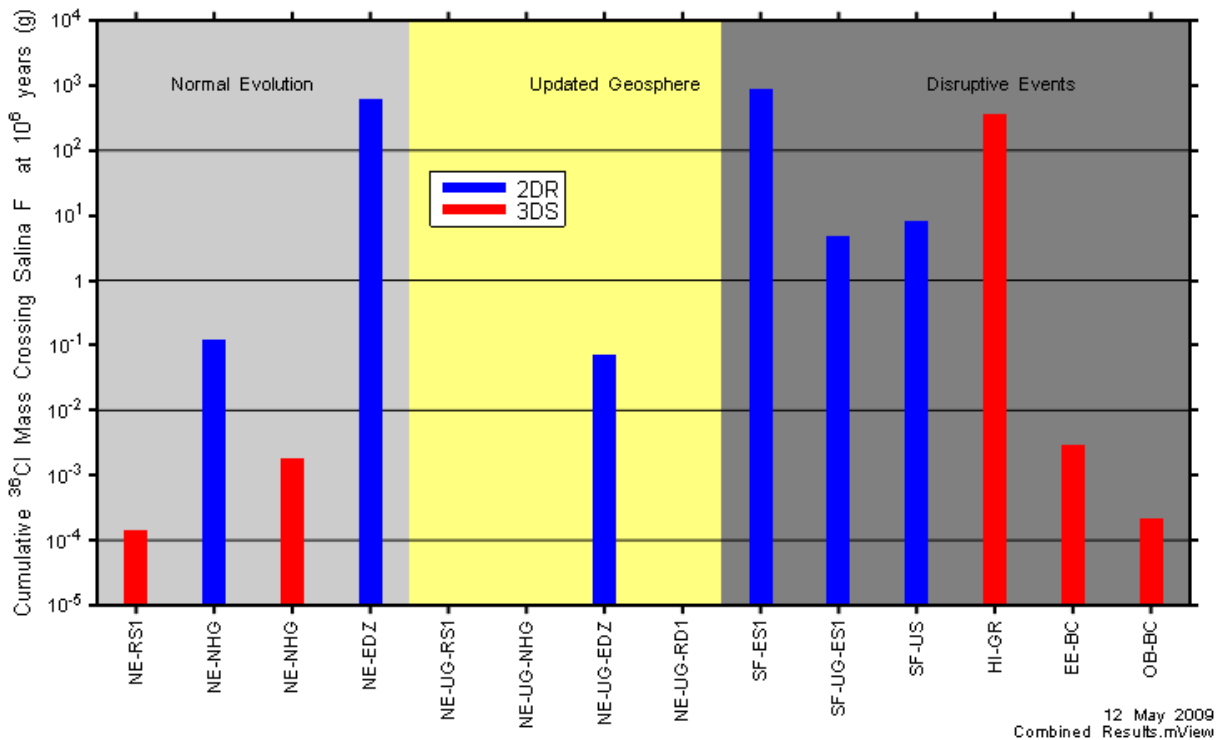


Figure 7.5: Cumulative Cl-36 mass flow across the Salina F MF plane for all modelling cases. All UG case results except NE-UG-EDZ are below Y axis limit.

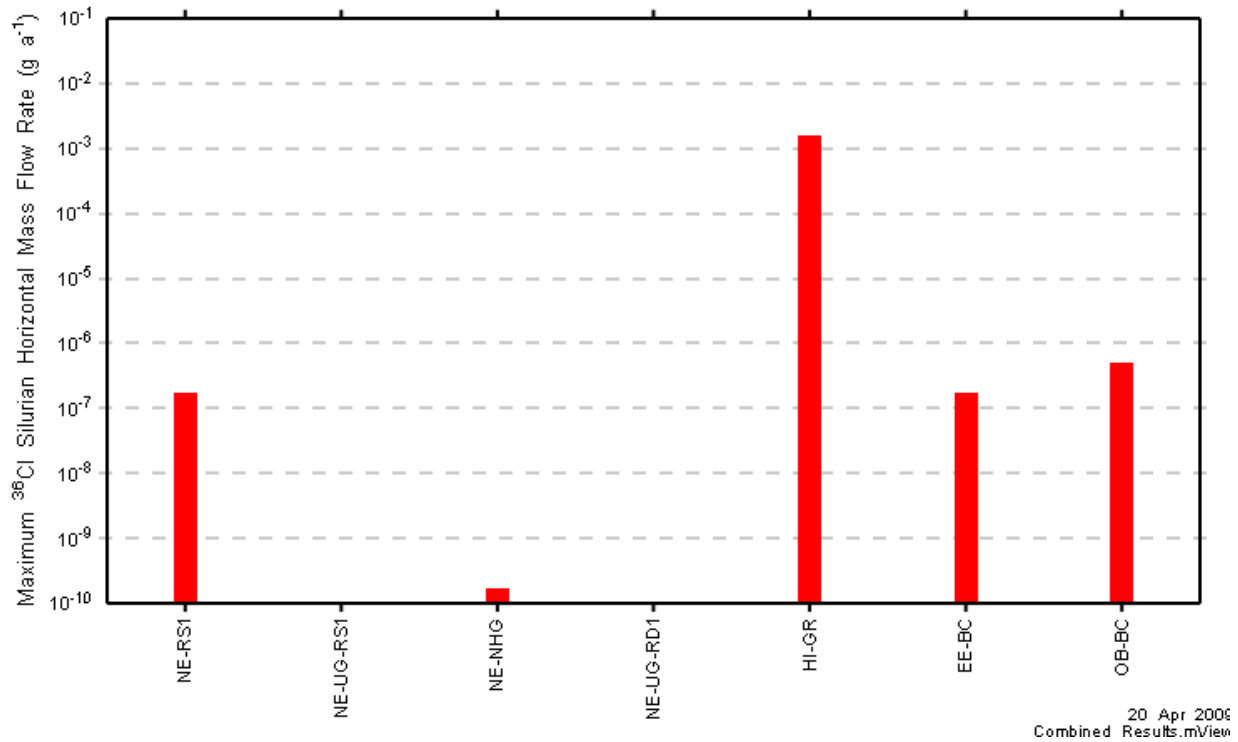


Figure 7.6: Peak horizontal Cl-36 mass flow across the Silurian formations for all 3DS modelling cases. All UG case results are below Y axis limit.

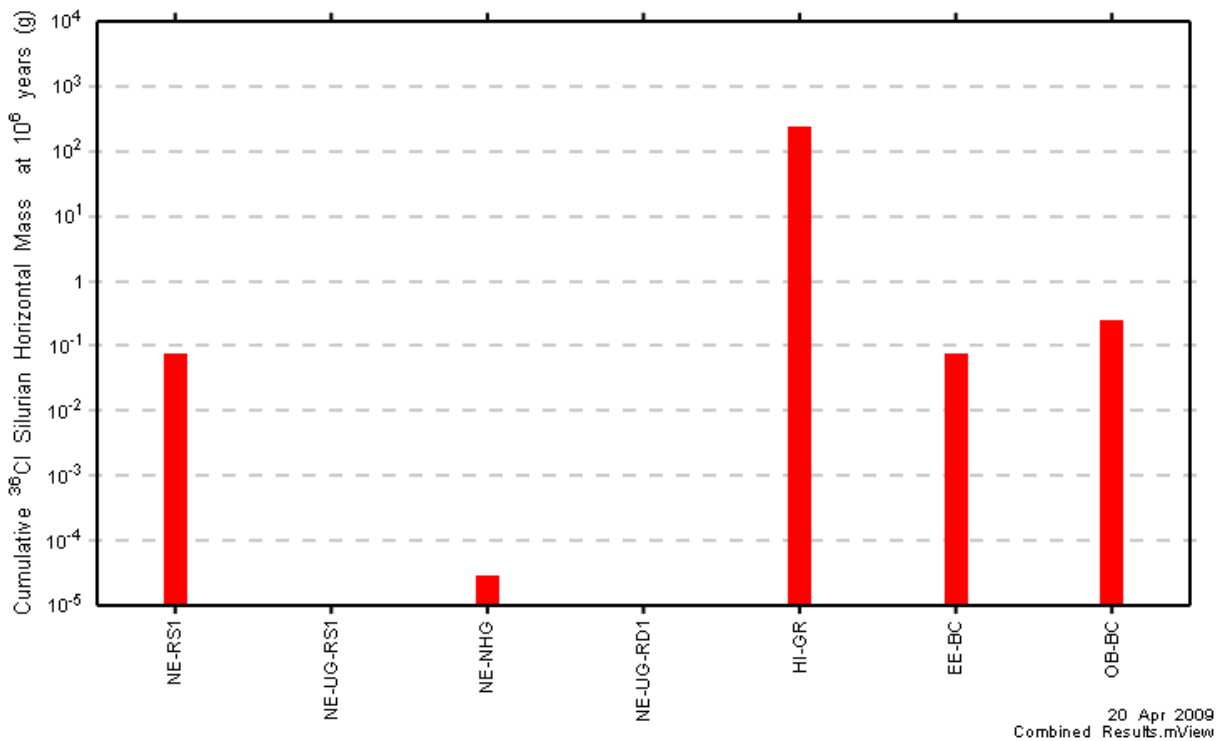


Figure 7.7: Cumulative horizontal Cl-36 mass flow across the Silurian formations plane for all 3DS modelling cases. All UG case results except NE-UG-EDZ are below Y axis limit.

8. UNCERTAINTIES AND ISSUES FOR FURTHER WORK

Uncertainties in results presented in this report arise from a variety of sources, including: the conceptual geosphere model, the numerical modelling approach, and the parameterization. Sources of uncertainty and possible future approaches to reducing uncertainty and optimizing system behaviour are discussed in the following subsections.

8.1 GEOSPHERE CONCEPTUAL MODEL UNCERTAINTY

Our understanding of the geosphere history and future evolution is described in the Geosynthesis report (Gartner Lee 2008a), and the repository system evolution is summarized in the System and its Evolution report (Little et al. 2009). Specific areas of uncertainty that have significant impact on groundwater transport results are listed below, along with how they are currently addressed in this study.

1. **Mechanism of Ordovician underpressures:** Mass flow from the repository will be significantly reduced as long as underpressures persist in the Ordovician units as prevailing liquid gradients will be downward at all points above the repository horizon, including the shaft and EDZ system. Pressure partitioning due to two-phase flow effects, and erosional and glacial unloading, have been identified as possible sources of the measured underpressure in other low-permeability systems. As the mechanism for underpressure generation is not known with certainty, the long term behaviour cannot be predicted. Therefore, with one exception (the NE-UG-NHG case), the current study makes the conservative assumption that the underpressures have been dissipated to steady state. In the transient NE-UG-NHG case, where current measured underpressures form the initial conditions, the underpressures persist for well in excess of 1 Ma with the effect of virtually eliminating transport from the repository.
2. **Time dependence of Cambrian overpressure:** In the predominantly steady-state analyses presented in this report, vertical flow in the shaft/EDZ system is driven by high pressure in the Cambrian unit forming the lower boundary of the modelled system. If steady-state flow is assumed, this gradient determines flow of water from the surrounding rocks into the repository and subsequently through the shaft/EDZ system. The impact of the gradient is mitigated substantially by reduced permeability in the UG geosphere cases. Although this pressure is proven present from site characterization results, its origin and therefore evolution is currently unknown. In the current study, the Cambrian pressure has been assumed constant.
3. **Future glaciation events:** The impact of future glaciation events on the rock mass, repository, shaft, seals, and shaft EDZ is not modelled. The primary effects at the repository horizon are expected to be transient overpressurization during glacial advances followed by dissipation during glacial retreats. Hydrological and chemical impacts will also occur, primarily in the shallow bedrock groundwater zone. This is supported by site characterization information and modelling as described in the Geosynthesis report (Gartner Lee 2008a). In the current study, constant climate conditions have been assumed.

8.2 MODELLING ASSUMPTIONS AND APPROACH

The groundwater modelling presented in this report conservatively assumes instant resaturation, generally steady-state constant-density flow with a fixed Cambrian excess pressure, and instant dissolution of the entire Cl-36 inventory.

The repository itself will initially be unsaturated. Due to the low-permeability of the host rock, it will take considerable time to fully resaturate as porewaters seep back into the repository. In addition, gas generated by decomposition of the wastes will also tend to slow down or even stop the resaturation process. These processes are not modelled here. Instead, gas transport modelling results presented in Calder et al. (2009) show a complex resaturation history, with an initial partial resaturation within the first 10 000 years post-closure, followed by expulsion of inflow, followed by a much longer period (hundreds of thousands of years) where the repository remains mostly or entirely dry. For the UG geosphere cases presented in Calder et al. (2009), there is virtually no resaturation over the 1 000 000 year simulation period. If resaturation is accounted for, the groundwater transport of radionuclides will be significantly reduced relative to the full dissolution and instantaneous release presented in this report.

Although some effects of variable-density flow are incorporated by using environmental head to calculate the Cambrian overpressure, other possible impacts are ignored. For example, highly-saline fluid produced from the repository and transported up the shaft would tend to flow out of the shaft when less saline formation waters were encountered such as at the permeable Salina A2 evaporite. Similar effects could impact fluid migrating through the abandoned borehole in case HI-GR.

In general, the groundwater transport results presented in this report are likely conservative. Incorporation of resaturation, gas pressure related effects, variable density flow, and repressurization of transient pressure heads would delay and reduce transport from the repository.

Full resolution of the uncertainties presented by the complexity of two-phase flow and radionuclide transport will require adoption of more complex and less well-proven modelling codes and approaches. Possible approaches should however be investigated for potential application in future work.

A further cause of uncertainty relates to simplifications in spatial representation of the repository system and the geosphere. As noted in Section 2.4, both the 2DR and 3DS models are simplified representations of the actual Hatch (2008) repository and shaft design. Furthermore, the 3DSU model is a simplification of the shallow bedrock groundwater zone. A combined 3DD (3D Detailed) model could incorporate individual vent and main shafts with surface topography and surface water features to provide a model more consistent with reality. Such a model would be numerically demanding and use would likely be limited to confirming applicability of the current modelling approach.

8.3 PARAMETER UNCERTAINTY

Table 7-1 indicate that the base case and sensitivity cases for the Normal Evolution Scenario considered in this report result in a range of outcomes spanning over fifteen orders of magnitude. As all the sensitivity cases were intended to illustrate possible or feasible conceptual models, there is clearly significant uncertainty in understanding and

parameterization of the system. The following list enumerates the major sources of parameter uncertainty.

1. **Geosphere permeabilities:** The UG sensitivity cases result in extremely low mass flows due to the significantly reduced rock mass vertical hydraulic conductivities, which resulted in similarly reduced shaft EDZ conductivities. Additional site characterization data and analyses to confirm the validity of the UG geosphere values should be forthcoming in 2009.
2. **Shaft EDZ characterization:** As a subsurface pathway for contaminant transport, the shaft EDZ is clearly important. The NE-EDZ sensitivity case resulted in the largest mass flow and cumulative mass of the all the Normal Evolution Scenario cases. However, mass flows were significantly reduced for the analogous low permeability geosphere case. As described in Walke et al. (2009b), the current EDZ characterization is largely based on international experience and expert opinion. Additional review and geomechanical modelling is underway in 2009.
3. **Gradient in the permeable Silurian formations:** The Guelph/Salina A0 and Salina A2 evaporite are the permeable units in the intermediate bedrock groundwater zone that could intercept contaminated groundwater transported from below through either the shaft or the rock mass. However, the effect of these units on transport depends on the hydraulic gradient, which will govern the direction and magnitude of horizontal advective flow. There are currently no site data available to confirm current estimates, which are based on regional scale Geosynthesis modelling. Site specific pressure data to allow calculation of for gradients will be available after installation of Westbay casing in DGR3 and DGR-4 in 2009.

The relative importance of individual parameters can be quantified by assessing the contribution of each parameter to overall uncertainty in a modelling metric, such as peak mass flow or cumulative mass flow. The most rigorous approach to doing this is through a probabilistic assessment, followed by stepwise regression analyses.

8.4 REPOSITORY DESIGN OPTIMIZATION

A single sensitivity case, NE-UG-RD1, investigated the effects of backfilling the ring and access tunnels with concrete. Results from that case indicate a slight improvement relative to the corresponding no-backfill base case (NE-UG-RS1). It could be tested whether such backfilling is of more value for the Severe Shaft Seal Failure Scenario for which the shaft seals are significantly degraded.

Given the uncertainties associated with shaft EDZ characterization and shaft seal performance, alternative repository designs may provide other approaches to reducing releases. The 3DS modelling approach presented in this report is a suitable framework for addressing alternative repository designs, which should be developed in consultation with repository engineering. Examples of possible alternatives include: different waste panel sizes and configurations, backfilling of emplacement rooms, and additional shaft sealing options.

9. SUMMARY AND CONCLUSIONS

The long-term performance of the proposed L&ILW repository at the Bruce Nuclear site has been assessed with the use of numeric models of groundwater flow and transport. Base case and sensitivity analyses have been performed for the Normal Evolution Scenario, and four additional scenarios based on disruptive events have been analyzed.

Two primary modelling approaches were used in the assessments: a dimensionally simplified two-dimensional radial model (2DR) which incorporates aggregate properties of the repository and shaft in a computationally efficient model; and a computationally demanding three-dimensional model with a simplified shaft representation and spatially accurate representation of the repository panels and access tunnels. Both models gave comparable results, with 2DR model mass flows higher than that for corresponding 3DS model results, particularly up the shaft/EDZ system. For the normal-evolution comparison case (NE-NHG), the 2DR model estimated roughly a factor of 70 increase in cumulative mass into the shallow bedrock groundwater zone through the shaft/ EDZ system over the 1 Ma assessment period.

A third model, the three-dimensional simplified upper (3DSU) model, was used to simulate the migration of radionuclides in the shallow bedrock groundwater zone, where advective flow towards Lake Huron is the predominant transport mechanism. Mass flow into the shallow zone calculated by the 2DR or 3DS model forms a source term applied at the bottom of the 3DSU model. The model includes a water supply well located down-gradient of the source.

Two geosphere conceptual models were considered – a low-permeable case based on results from DGR-1 and -2 boreholes as described in the Geosynthesis report (Gartner Lee 2008a), and a lower-permeability case based on preliminary results from DGR-3 and -4 boreholes (called UG here).

Results for the Normal Evolution Scenario's base case and sensitivity cases with base case shaft and shaft seal parameters (i.e. all cases except for NE-EDZ) showed very good performance, with low rates of mass transport to the biosphere. All the cases conservatively assumed instant resaturation of the repository and instant dissolution of the CI-36 inventory in this water. Cases based on the lower-permeability UG geosphere showed excellent performance with extremely low levels of transport. The implications of these release rates are not evaluated here, but are presented in the Normal Evolution Scenario Analysis report (Walke et al. 2009a) and the Human Intrusion and Other Disruptive Scenarios Analysis report (Penfold and Little 2009).

In all cases the Ordovician and Silurian units serve as a highly effective barrier, preventing radionuclide migration into the accessible biosphere. Horizontal flow in the permeable Silurian units, as suggested by current Geosynthesis modelling and incorporated in most 3DS modelling cases presented in this report, is effective in diluting any contaminants released, and preventing them from reaching the shallow bedrock groundwater zone above the repository.

The advective flow in the permeable shallow bedrock groundwater zone would provide further dilution. A well in these units, located directly downgradient of the shaft, would only be able to capture a small fraction of any contaminated water released into this zone. Most contaminated groundwater would be transported through the lower Devonian units, below the capture zone of any likely well.

For all cases, the primary pathway for mass flow from the repository is through the shaft/EDZ system. The shaft/EDZ collects groundwater flow at the repository horizon, and then transports it vertically towards ground surface if there is a net driving force of the Cambrian pressure gradient (i.e., the current Ordovician underpressure has dissipated). A system of shaft seals is designed to intercept flow. However, if the shaft EDZ is particularly permeable, and if there is a net Cambrian pressures upward, then the shaft system provides a path for steady release from the repository, with the potential for half the initial mass (no decay) to be released over 1 000 000 years. This effect is of lower significance for the reduced permeability geosphere.

Backfilling the access tunnels with concrete was not found to be particularly useful in base case, although it might be more useful if the shaft seals were degraded.

Results for the Disruptive Scenarios are consistent with the base case results for the Normal Evolution Scenario in that man-made, comparatively high-permeability features have the largest impact on performance. For the Human Intrusion Scenario (HI-GR) a borehole intercepts the facility and is subsequently improperly abandoned. The borehole acts as an enhanced permeability pathway, channelling flow into the repository from the rock mass upwards to surface. The results indicate that nearly the entire CI-36 inventory will have been transported from the facility by 10 000 years. The Severe Shaft Seal Failure Scenario (case SF-ES1) assumes that the shaft seals degrade to enhanced-permeability media. Results for this case also indicate higher rates of mass flow than for the Normal Evolution Scenario.

An open site characterization borehole which is located adjacent to, but does not penetrate the repository (OB-BC), has only a minor impact, with an approximate doubling of mass flow to the shallow bedrock groundwater zone. An enhanced permeability full vertical fault downgradient of the repository (EE-BC) also indicated only small impact, with total mass flow to the shallow bedrock groundwater zone a factor of approximately 20 higher than the base (NE-RS1-F3) case.

Uncertainties with simulation results are related primarily to uncertainty associated with the geosphere hydraulic conductivity and with shaft and EDZ parameterization. The primary uncertainty in EDZ parameterization is the characterization of the shaft EDZ hydraulic conductivities. Additional significant geosphere uncertainties relate to gradients in the Silurian, the time dependence of the Cambrian overpressure, and the causal mechanism and characterization of the measured Ordovician underpressures. Further geosphere uncertainties relate to the hydromechanical response of the repository and geosphere system to glaciation events. These uncertainties have been tested here by use of sensitivity cases or conservative representations.

The cases analysed in this report are complemented by gas transport modelling and assessment model results presented in companion reports. The results presented in this groundwater modelling report provide insight into the behaviour of the repository system over 1 Ma timeframes to support the assessment of potential impacts presented in the Postclosure Safety Assessment Report (Quintessa et al. 2009).

REFERENCES

- Calder, N., J. Avis, P. Humphreys, F. King, P. Suckling and R. Walsh. 2009. Postclosure Safety Assessment (V1): Gas Modelling. Nuclear Waste Management Organization (NWMO) Report DGR-TR-2009-07-R0. Toronto, Canada.
- DGR. 2009. Estimated Low Hydraulic Conductivity Values from Preliminary DGR-3 & DGR-4 Test Results. DGR Project Data Release 5/3/09. NWMO Records: 00216N-01900-T7. Nuclear Waste Management Organization. Toronto, Canada.
- Garisto, N., J. Avis, S. Fernandes, R. Jackson, R. Little, J. Rees, G. Towler, and R. Walke. 2009. Postclosure Safety Assessment (V1): Features, Events and Processes. Nuclear Waste Management Organization (NWMO) Report DGR-TR-2009-05-R0. Toronto, Canada.
- Gartner Lee Limited. 2008a. OPG's Deep Geologic Repository for Low and Intermediate Level Waste. Phase 1 Geosynthesis. Ontario Power Generation Report OPG 00216-REP-01300-00010-R00. Toronto, Canada.
- Gartner Lee Limited. 2008b. OPG's Deep Geologic Repository for Low and Intermediate Level Waste. Phase 1 Regional Geology, Southern Ontario. Ontario Power Generation Report OPG 00216-REP-01300-00007-R00. Toronto, Canada.
- Hatch. 2008. OPG's Deep Geological Repository For Low and Intermediate Level Waste: Conceptual Design Report. Hatch 323874DGR-RPT-CDR200-Rev01. OPG 00216-REP-03902-00004-R01. Toronto, Canada.
- Little, R., A. Bath, P. Humphreys, F. King, R. Metcalfe, J. Penfold, D. Savage, G. Towler and R. Walke. 2009. Postclosure Safety Assessment (V1): System and Its Evolution. Nuclear Waste Management Organization (NWMO) Report DGR-TR-2009-04-R0. Toronto, Canada.
- Penfold, J. and R. Little. 2009. Postclosure Safety Assessment (V1): Analysis of Human Intrusion and Other Disruptive Scenarios. Nuclear Waste Management Organization (NWMO) Report DGR-TR-2009-03-R0. Toronto, Canada.
- Penfold, J.S.S., R.H. Little, R.A. Bowden and M.J. Egan. 2003. Preliminary Safety Assessment of Concepts for a Permanent Waste Repository at the Western Waste Management Facility Bruce Site. Quintessa Report QRS-1027B-1 v1.0. Henley-on-Thames, UK.
- Quintessa, Intera and SENES. 2009. Postclosure Safety Assessment (V1) Report. Nuclear Waste Management Organization (NWMO) Report DGR-TR-2009-01-R0. Toronto, Canada.
- Sykes, J.F., E.A. Sykes, S.D. Normani, Y. Yin and Y.-J. Park, University of Waterloo. 2008. OPG's Deep Geologic Repository for Low and Intermediate Level Waste. Phase I Hydrogeologic Modelling. Ontario Power Generation Report OPG 00216-REP-01300-00009-R00. Toronto, Canada

- Therrien, R. and E.A. Sudicky. 1996. Three-dimensional Analysis of Variably-saturated Flow and Solute Transport in Discretely-fractured Porous Media. *J. Contaminant Hydrology* 23, 1-44.
- Walke, R, L. Limer, R Little and G. Towler. 2009a. Postclosure Safety Assessment (V1): Analysis of the Normal Evolution Scenario. Nuclear Waste Management Organization (NWMO) Report DGR-TR-2009-02-R0. Toronto, Canada.
- Walke, R, A. Bath, A. Bond, N. Calder, P. Humphreys, F. King, R. Little, R. Metcalfe, J. Penfold, J. Rees, D. Savage, G. Towler and R. Walsh. 2009b. Postclosure Safety Assessment (V1): Data. Nuclear Waste Management Organization (NWMO) Report DGR-TR-2009-08-R0. Toronto, Canada.

APPENDIX A: FRAC3DVS

FRAC3DVS is a code developed and maintained by Groundwater Simulations Group (Waterloo, Canada). Code development and use has been supported by OPG and NWMO as part of its used fuel technology programme, as well as by other commercial and academic users.

FRAC3DVS is currently undergoing qualification to NWMO requirements under control of another NWMO project. Software quality assurance documentation is currently being produced on that project. Currently available references are described in this appendix.

FRAC3DVS is also known as FRAC3DVS_OPG and F3DOPG. The numeric engine is also incorporated into the HydroSphere model.

A.1 PROBLEM DESCRIPTION

FRAC3DVS provides transient groundwater modelling and contaminant transport in 2D and 3D geometry for saturated variable-density systems, including both equivalent porous medium and discrete fracture networks.

A.2 SOFTWARE PLAN

FRAC3DVS was used to simulate 2D and 3D transient groundwater flow and contaminant transport for the Version 1 postclosure assessment of the DGR. It was used for the following scenarios:

- Normal Evolution;
- Human Intrusion;
- Open Borehole;
- Severe Shaft Seal Failure; and
- Extreme Earthquake.

The site and repository was represented using an equivalent porous medium model. The current application did not use the variable-density, 1-D hydromechanical, or discrete-fracture capabilities of the code.

A.3 THEORY MANUAL

FRAC3DVS theory is described in Therrien et al. (2007) and Therrien and Sudicky (1996).

A.4 REQUIREMENTS SPECIFICATION

A formal requirements document is not available. Basic capabilities are described in Therrien et al. (2007).

A.5 DESIGN DESCRIPTION

Numeric implementation is described in Therrien et al. (2007). Details on overall software development practices and approaches are not described.

A.6 SOURCE CODE

FRAC3DVS source code is maintained by Groundwater Simulation Group:

Groundwater Simulations Group
574 Sprucehill Avenue
Waterloo, Ontario
N2L 4V9

Source code is not distributed with the model.

A.7 VERIFICATION REPORTS FOR THEORY, REQUIREMENTS, DESIGN AND CODE

Verification reports for theory, requirements, design, and code are not available.

A.8 VALIDATION REPORT(S)

FRAC3DVS validation test cases are described in Therrien et al. (2007).

A.9 COMPUTER PROGRAM ABSTRACT

A.9.1 Purpose

FRAC3DVS is a commercially available software tool that performs numeric simulations of groundwater flow and radionuclide transport in three-dimensional flow regimes. FRAC3DVS is designed for expert users and assumes a high degree of modelling proficiency and access to supporting pre- and post-processing software.

A.9.2 Code History

FRAC3DVS has been under continuous development since 1996 by the Groundwater Simulations Group, Waterloo. It is available as a standalone code, and also integrated into HydroSphere.

A.9.3 Operating Requirements

FRAC3DVS is a FORTRAN code and can be compiled to run on 32-bit and 64-bit Windows and Linux operating systems. Specific computational requirements (RAM, processor speed, disc storage) are entirely problem dependent. The current postclosure 2DR models will run satisfactorily on 32-bit systems with 512 MB of RAM, while the 3DS models required 64-bit systems with 4 GB of RAM.

A.9.4 Components

FRAC3DVS is distributed as a single executable file.

A.9.5 Capabilities

A full description is provided in Therrien et al. (2007).

A.9.6 Limitations

FRAC3DVS is subject to spatial and temporal discretisation requirements similar to most Finite-Element and Finite-Difference models. End users of the application are responsible for ensuring that suitable discretizations are specified.

A.9.7 Documentation

As described in this Appendix.

A.10 USER MANUAL

The FRAC3DVS User Manual is contained within Therrien et al. (2007).

A.11 PROGRAMMER MANUAL

There is no programmer's manual for FRAC3DVS.

A.12 VERSION TRACKING RECORD

FRAC3DVS_OPG (Version R622, Build Date 2008 04 28 - 64-bit)

REFERENCES FOR APPENDIX A

- Therrien, R., R.G. McLaren, E.A. Sudicky, S.M. Panday, V. Guvanasen, 2007. FRAC3DVS_OPG - A Three Dimensional Numeric Model Describing Subsurface Flow and Solute Transport. Draft. Groundwater Simulations Group, Waterloo, Ontario.
- Therrien, R. and E.A. Sudicky. 1996. Three-dimensional Analysis of Variably-saturated Flow and Solute Transport in Discretely-fractured Porous Media. *J. Contaminant Hydrology* 23, 1-44.